Analysis and design of nonlinear systems in the frequency domain

By:

Yun-Peng Zhu
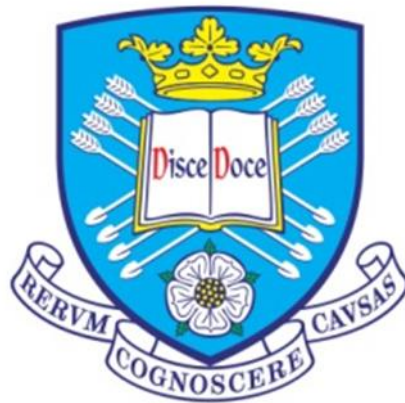
A thesis submitted in partial fulfilment of the requirements for the degree of
Doctor of Philosophy

The University of Sheffield

Faculty of Engineering

Department of Automatic Control and Systems Engineering

August 2019

Abstract

Nonlinear system analyses have been widely applied in engineering practice, where the frequency domain approaches have been developed to satisfy the requirement of the analysis and design of nonlinear systems. However, there exist many problems with current techniques including the challenges with the nonlinear system representation using physically meaningful models, and difficulties with the evaluation of the frequency properties of nonlinear systems. In the present work, some new approaches, that have potential to be used to systematically address these problems, are developed based on the NDE (Nonlinear Differential Equation) model and the NARX (Nonlinear Auto Regressive with eXegenous input) model of nonlinear systems.

In this thesis, the background of the frequency domain analysis and design of nonlinear systems is introduced in Chapter 1, and the existing approaches are reviewed in Chapter 2. In general, the frequency analysis of nonlinear systems is conducted based on the Volterra series representation of nonlinear systems, and as basic issues, the evaluation of the Volterra series representation and its convergence are discussed in Chapters 3 and 4, respectively. An extension of the existing frequecncy analysis and design techniques is discussed in Chapter 5 to facilitate the analysis of the effects of both linear and nonlinear characteristic parameters on the output frequency responses of nonlinear systems. An experimental study is conducted in Chapter 6 to show how a nonlinear component can benefit the engineering system, such to empahasis the significance of developing the analysis and design approaches of nonlinear systems. The main contributions are summarized as below.

(1) The GALEs is proposed that can accurately evaluate the system Volterra series representation. By using the GALEs, the solution to the NDE model or the NARX model of nonlinear systems can be obtained by simply dealing with a series of linear differential or difference equations, which can facilitate a wide range of nonlinear system analyses and associated practical applications.

(2) A new criterion is derived to determine the convergence of the Volterra series representation of nonlinear systems described by a NARX model. The analysis is performed based on a new function known as Generalized Output Bound Characteristic Function (GOBCF), which is defined in terms of the input, output and parameters of the NARX model of nonlinear systems. Compared to the existing results, the new criterion provides a much more rigorous and effective approach to the analysis of the convergence conditions and properties of the Volterra series representation of nonlinear systems.

(3) The Output Frequency Response Function (OFRF) in terms of physical parameters of concern is introduced for the NARX Model with parameters of interest for Design (NARX-M-for-D). Moreover, a new concept known as the Associated Output Frequency Response Function (AOFRF) is introduced to facilitate the analysis of the effects of both linear and nonlinear characteristic parameters on the output frequency responses of nonlinear systems.

(4) Nonlinear damping can achieve desired isolation performance of a system over both low and high frequency regions and the optimal nonlinear damping force can be realized by closed loop controlled semi-active dampers. Both simulation and laboratory experiments are studied, demonstrating the advantages of the proposed nonlinear damping technologies over both traditional linear damping and more advanced Linear-Quadratic Gaussian (LQG) feedback control which have been used in practice to address building isolation system design and implementation problems.

Acknowledgements

I would like to thank Prof. Z Q Lang, my supervisor, for his great support and supervision on my PhD study. He has provided a lot of suggestions on my research and writing so that I can complete the project and this PhD thesis.

I also want to express my thankfulness to the research and work staffs of the department for their kind help on my study, and also would like to acknowledge the support of Engineering Faculty Scholarship for my PhD study at Sheffield.

Moreover, I would like to acknowledge my friends and colleagues for their help on my research and living in Sheffield. Particular thanks to Dr. Sikai Zhang and Dr. Yuzhu Guo from Sheffield, Prof. Hui Ma, Prof. Zhong Luo, and Prof. Xueliang Zhang from Northeastern University, China.

Special thankfulness to the comprehensive social and academic environment in UK, which made me see a rainbow colour life and learn to be myself.

Finally, I would like to dedicate this thesis to my mother for her great love and support in my life.

Catalogue

Chapter 1. Introduction

1.1 Background

In engineering practice, the analysis and design of a nonlinear system is often conducted in both the time and frequency domain, including, for example, identifying a mathematic model to represent the system [1-3], and studying and designing the system's output frequency response [4-6].

Compared with the time domain analyses and design methods for nonlinear systems such as, e.g., the harmonic balance method and the multi-scale method [7,8], etc., the nonlinear system design in the frequency domain does not need a specific model description and can therefore deal with a more general class of nonlinear systems [9,10].

In this Chapter, the frequency domain analysis and design of nonlinear systems are reviewed, both the development and existing issues are covered in deteils.

1.1.1 Modelling of nonlinear systems

Basically, the modelling of nonlinear systems is to determine a mathematical model in order to describe the behaviour of the systems under certain input or working conditions [11]. There are varies model structures that have been studied to describe a wide class of nonlinear systems, i.e., the NDE (Nonlinear Differential Equation) model [12], the NARX (Nonlinear Auto Regressive with eXegenous input) model [13,14], the W-H (Wiener-Hammerstein) [15,16], etc.. The analysis and design of nonlinear systems are usually studied based on the NDE model due to its clear physical meanings [17-20]. For example, Hwang and Lin [18] studied the sliding mode control of NDE systems by the application of fuzzy set theory; Barton et al. [19] investigated the nonlinear energy harvester represented by an NDE model.

However, in most cases of engineering designs, such as, e.g., vibration isolators made of viscoelastic and composite materials [21] and bladed disks of aero-engines [22], it is difficult or impossible to find such a physical model for the systems. But, it is possible to find, via a nonlinear system identification approach [23-26], a data driven model, i.e. the NARX model and the W-H model, representing the relationship between the input excitation and corresponding system response. For example, by using the FROLS (Forward Regression Orthogonal Least Squares) algorithm, the NARX model can be identified by using the input and output data of a system [23]. Many algorithms have been proposed for this purpose, which include,

for example, the PRESS (Predicted REsidual Sums of Squares) algorithm [24], the iterative FROLS algorithm [25], and block-oriented nonlinear system identification approaches [26].

These data driven models are basically data fitting solutions and their physical meanings are often not transparent to engineers [11]. Considering the discretization relationship between a system NDE model and its corresponding NARX model, it is possible to identify a NARX model such that the physically meaningful parameters appear explicitly as coefficients in the model. For example, Wei et al. [27] identified the NARX models with coefficients explicitly representing the design parameters for particle dampers and thermoplastic auxetic foams. Liu et al. [28] developed an identification algorithm that can produce the parametrical NARX model of a cantilever beam.

In the present study, the NDE and the polynomial NARX models of nonlinear systems will be used for the analysis and design of nonlinear systems in the frequency domain.

1.1.2 Frequency domain analysis and design of nonlinear systems

The frequency domain design of linear systems [29-31] based on the traditional concept of Frequency Response Function (FRF) has been widely applied in engineering system designs such as, e.g., the design of the dynamic properties of vibration absorbers [32], vehicle suspensions [33], and aero engine blades [34]. However, many systems in practice cannot be simply described by a linear model [35]. In this case, nonlinear system analysis and design methods in either the time or the frequency domain have to be applied to study these systems.

(A) The GFRFs of nonlinear systems

The frequency domain analyses of nonlinear systems were originally studied by using the Generalized Frequency Response Functions (GFRFs) [36], which is developed based on the Volterra series representation of nonlinear systems. The characteristics of the GFRFs have been studied by researchers. For example, Han et al. [37] discussed the non-parametric identification of GFRFs for Multiple-Input-Multiple-Output (MIMO) systems. Zhang and Billings [38] investigated the gain bound properties of the GFRFs. Yue et al. [39,40] studied the properties of GFRFs by using a graphic method, where only lower order GFRFs can be displayed but higher order GFRFs are difficult to investigate due to the multi-dimensional nature of the GFRFs. Moreover, based on the NDE and NARX model, recursive algorithms were proposed to evaluate the GFRFs by using the probing method [13,41,42].

The GFRFs have played an important role in nonlinear system analyses [43-51]. For example, the output frequency combination characteristics were theoretically explained using GFRFs [43], and algorithms have

been proposed to determine the nonlinear output frequency components [44-46]. The NDE model was reconstructed from a NARX model of a nonlinear system, based on the observation that the GFRFs of the NDE and NARX model of the same system are invariant [47-49]. Chatterjee et al. [50,51] studied the parameter estimation approaches of nonlinear systems using the high order GFRFs, where both single and multi-tone harmonic excitations were applied for the parameter estimation. The parameter characteristics of nonlinear systems were also discussed by Jing et al. using the GFRFs in [52-54].

However, the higher order GFRFs are very complex due to the multi-dimensional nature, and difficult to be used in practice. To address this and related issues, many new concepts such as Nonlinear Output Frequency Response Functions (NOFRFs) [55], Output Frequency Response Function (OFRF) [56], and Higher Order Sinusoidal Input Describing Functions (HOSIDF) [57] have been proposed.

(B) The NOFRFs based analysis of nonlinear systems

The concept of NOFRFs [55] is a new extension of the FRF to the nonlinear case. One of its most attractive features is its one-dimensional nature, which has many advantages, as has been demonstrated by a wide range of studies [58-64]. For example, The NOFRFs have been used for the damage detection and fault diagnosis in many engineering systems. Peng et al. [58] studied the NOFRFs based fault detection of cracked beams. The concept of transmissibility of nonlinear systems was introduced using the NOFRFs concept and applied to find the location of fault in a MDOF system [61]. Chu et al. [62] applied the NOFRFs approach in the condition monitoring of rotor systems. Moreover, the NOFRFs have also been applied for system identification, where both the linear and nonlinear parameters of a MDOF structure have been determined [63,64].

However, current applications of the NOFRFs use a Least Squares (LS) based evaluation method [55,58]. This requires an appropriate selection of the maximum order of the system nonlinearity, which is sometimes difficult and may suffer from numerical issues. In addition, the method requires the system response data from several simulation or experimental tests, which may not be convenient for implementation. This issue is partly addressed by using the Associated Linear Equations (ALEs) of nonlinear systems [65-68], but the existing methods can only deal with systems represented by simple NDE models such as Duffing systems [65], etc.. More effective approaches are required to systematically address the issues associated with more general NDE/NARX models of nonlinear systems.

(C) The OFRF based design of nonlinear systems

The OFRF reveals an analytical relationship between the output frequency response of nonlinear systems

and the parameters which define the system nonlinearities and can be used to facilitate both the analysis and design of nonlinear systems in the frequency domain [69,70]. The HOSIDF can be considered to be a special case of the OFRF of a static polynomial nonlinear system [71,72] and has been applied to the detection and optimal compensation of degrading nonlinear effects in Lur'e-type systems [73].

Since the introduction of the OFRF in 2007 [56], many studies on the application of this concept to the nonlinear system analysis and design have been conducted. For example, Peng and Lang [74] have derived a recursive algorithm to determine the structure of the OFRF for the system described by a nonlinear differential equation model. More recently, the OFRF based approach has been applied in the analysis and design of nonlinear vibration isolators [75-77]. For example, by using the OFRF, Lang et al. [75] and Peng et al. [76] have rigorously proved significant beneficial effects of nonlinear damping on vibration isolation systems. Recently, Lv and Yao [77] have applied the OFRF to study the effect of damping coefficients on both the force and displacement transmissibility, showing that the nonlinear isolators can perform better than linear isolators over certain frequency ranges.

It is well known that the output frequency responses of nonlinear systems are affected by both the linear and nonlinear characteristic parameters of the system. The OFRF shows an analytical relationship between the output spectra of nonlinear systems and the system's nonlinear characteristic parameters, but this relationship is only valid under the condition that the system linear characteristic parameters are fixed. Very recently, the issue associated with the effect of linear characteristic parameters on the nonlinear system output frequency responses have been studied [78-80]. However, the result is, so far, only a conceptual polynomial approximation for the system output spectrum, and there are still no results that can systematically relate the output frequency response of nonlinear systems to both system linear and nonlinear characteristic parameters so as to facilitate the system analysis and design.

1.1.3 LS methods in nonlinear system analyses

It can be seen from the above discussion that, Least Squares (LS) methods including the ordinary LS algorithm, FROLS algorithm, PRESS algorithm, etc. are widely applied in the identification of system models and the evaluation of NOFRFs and OFRF. On the other hand, algorithms based on other approximation criteria such as the Orthogonal Matching Pursuit (OMP) [81-83], convex optimization [84-86], etc. can also be applied to solve these issues. Basically, LS methods are used to solve over-determined problems, where the number of the unknown parameters to be evaluated is less than the functions to be solved, while OMP and convex optimization are developed for the aim of solving under-determination

problems, where the number of the unknown parameters to be evaluated is more than the functions to be solved [86]. For example, in order to solve the signal recovery issue, Herzet et al. [82] conducted the evaluation of frequency components of periodical signals by using the OMP. Needell and Tropp [85] developed the CoSaMP algorithm and related toolbox to solve the under-determination problem by using the convex optimization.

Both OMP and convex optimization can also be applied to solve over-determined problems, but compared to LS methods, convex optimization is much more complex [86], and although OMP has less computational cost, the accuracy is worse than the LS methods [83]. Consequently, in the analysis and design of nonlinear systems, the LS methods are used to solve related problems.

1.1.4 Convergence issues with the frequency analysis of nonlinear systems

Because of having a structure similar to the power series, the Volterra series based nonlinear system representation has played an important role in the system identification [87,88], nonlinear circuits [89,90] and nonlinear signal processing [91,92]. The frequency analysis of nonlinear systems including the analysis using GFRF, NOFRFs and OFRFs, etc. was all developed based on the Volterra series representation of nonlinear systems.

However, all of these existing approaches require that the Volterra series representation for a nonlinear system is convergent. Generally, the condition of convergence is complicated and the assessment can often only be done via numerical analyses to see whether the higher order terms of the Volterra series are degressive or not [93]. In addition, some analytical methods have been derived to study the convergence problem of the Volterra series representation of relatively simple nonlinear systems [94,95]. For example, Barrett [90] proposed a simple convergence criterion that can be used for the convergence analysis of the Volterra series representation of the Duffing oscillator. The convergence of the Volterra type output of the Duffing oscillator and quadratic nonlinear systems were discussed by using the convergence ratio $|\sigma_{n+1}|/|\sigma_n| < 1$, where $|\sigma_n|$ represents the magnitude of the n th order nonlinear output spectrum [97-99]. The convergence ratio of the Duffing oscillator under harmonic input was investigated by studying the convergence ratio of a power series in [100].

Recently, by using the mathematical tools of analytic combinatorics, the Singular Inversion Theorem was introduced to compute the convergence ratio of a general Volterra series in the time domain [101,102]. The Analytic Inversion Theorem was also employed to solve the parameter convergence bound of a NARX model's Volterra series representation in the frequency domain [103,104].

However, by using these available methods, the convergence criteria can either only consider specific nonlinear systems [97-100] and harmonic input signals [97-102] or produce an over estimated bound on the system input which can ensure the convergence of the system's Volterra series representation [99,101-104]. In addition, although some approaches such as, for example, the Hélie's and Xiao's criteria [101-104] can be used for the convergent analysis of general nonlinear systems, complex mathematical operations are required to obtain the analysis results. Therefore, it is necessary to develop a simpler and more efficient criterion for the analysis of the convergence of the Volterra series representation of a general class of nonlinear systems subject to either harmonic or general input excitations.

1.2 Aim, objectives and Contributions

This research aims to resolve the existing issues in the frequency domain analyses and design of nonlinear systems. The main achievements are listed as follows.

(1) A general representation of the NARX model with physically meaningful parameters appear explicitly as coefficients in the model is introduced, referred to as the NARX Model with parameters of interest for Design (NARX-M-for-D). The NARX-M-for-D is significant especially for the design of nonlinear systems.

(2) A new concept known as the Generalized Associated Linear Equations (GALEs) is proposed to evaluate the output components in the Volterra series representation of a wide class of nonlinear systems up to an arbitrary order of nonlinearity of interest. The GALEs and associated techniques can significantly facilitate the analysis of nonlinear systems in both the time and frequency domain, and enable the development of a more effective technique for the identification of the NDE model of nonlinear systems, producing a physically meaningful representation for nonlinear systems.

(3) A new convergence criterion for the Volterra series representation of the NARX model of nonlinear systems is derived to address the problems with existing methods. The derivation is based on the frequency domain representation of the NARX model. The new criterion has the advantages of being independent of sampling frequency with the NARX model, applicable to nonlinear systems under general inputs, and having no need of carrying out complex mathematical computations.

(4) An OFRF representation that takes the effect of both the system linear and nonlinear characteristic parameters on the system output response into account is proposed based on the NARX-M-for-D. A recursive algorithm for the determination of the structure of the OFRF for a class of nonlinear systems described by a NARX-M-for-D is derived, which can directly produce the OFRF representation

without involving any complicated mathematical derivations/operations.

(5) A new concept known as Associated Output Frequency Response Function (AOFRF) is introduced for the NARX model of nonlinear systems and, based on the AOFRF, it is rigorously shown that the output frequency response of nonlinear systems can be represented by a polynomial function of both the system linear and non-linear characteristic parameters. Effective algorithms are derived to determine the structure and coefficients of the AOFRF based representation of the output frequency response of nonlinear systems.

(6) The practical application of nonlinear system designs in the frequency domain is investigated by studying a nonlinear building base-isolation system, where a nonlinear damper is implemented by using a semi-active control method. The laboratory experimental studies on a two storey physical building model are also conducted. The experimental results confirm the results of the analysis and numerical simulation studies and demonstrate the advantages of the proposed nonlinear damping technologies over traditional linear damping as well as currently used LQG feedback control.

1.3 Thesis layout

This thesis includes seven chapters covering background introduction, literature review, development of new frequency domain analysis approaches, and the experimental study of a nonlinear damping based building base-isolation system. The flow of the thesis contents are illustrated in Fig.1.1.
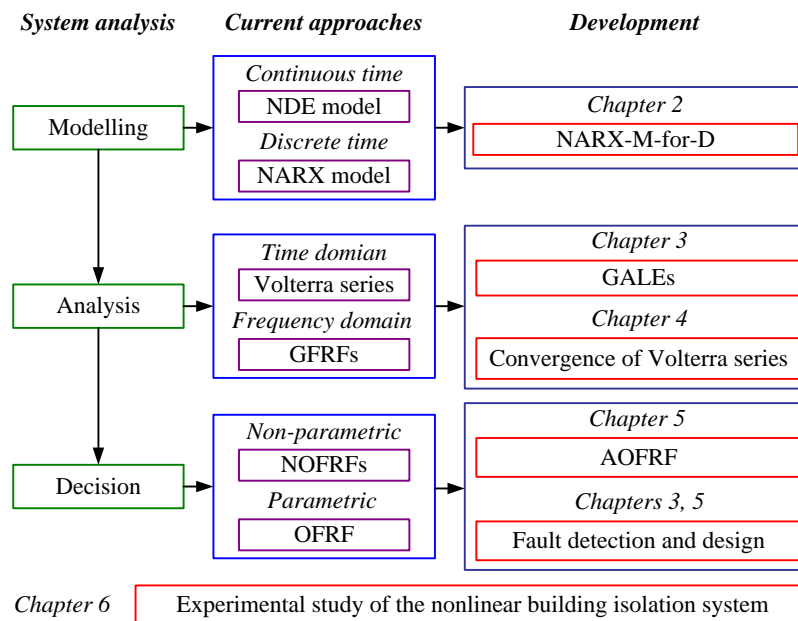
Fig.1.1 The flow of the thesis contents

In the analysis of dynamic systems, basically there are three levels which are the modelling of the system,

the analysis of the system and the decision of the system. For each level in the frequency analysis of nonlinear systems, the current thesis proposed some novel approaches to solve the existing issues of the current methods, which are discussed in Chapaters 2-5. A practical experiment was discussed in Chapter 6, demonstrating why the current study on nonlinear systems is significant and how nonlinearities can affect the system dynamics in engineering practice. The contents of each chapter are summarised as follows:

Chapter 1 is concerned with the introduction of the frequency analyses of nonlinear systems.

Chapter 2 reviews the state of the art of the current frequency domain analysis and design approaches, such as the GFRFs, the NOFRFs and the OFRF.

Chapter 3 introduces the concept of GALEs, and proposed a recursive algorithm for determining the GALEs. Three case studies on the application of the GALEs for nonlinear system analyses are provided to demonstrate the significance of the new GALEs concept. These include the application of the GALEs for the evaluation of the time domain output response of a nonlinear system, the determination of the NOFRFs using the GALEs for nonlinear system frequency analyses, and the use of the GALEs in the identification of the NDE model of a nonlinear system.

Chapter 4 introduces a new approach of analysing the convergence of the system Volterra series representation. The Generalized Output Bound Characteristic Function (GOBCF) is derived based on the NARX model of nonlinear systems, and the new convergence criterion of Volterra series is derived based on the GOBCF. Two Case studies are used to demonstrate the efficiency and advantages of the new criterion.

Chapter 5 provides a systematic nonlinear system design approach based on the OFRF of the NARX-M-for-D. Moreover, the AOFRF representation of nonlinear systems is determined by a newly derived algorithm, where both the linear and nonlinear parameters of the systems are taken into account.

In **Chapter 6**, a nonlinear building base isolation system is investigated, where a nonlinear damping is implemented by using a semi-active control method. Both the simulation and experimental studies are conducted, showing the significance and promising advantages of application of nonlinear systems frequency design in engineering practice.

Finally, conclusions are summarized in **Chapter 7**.

Chapter 2. Nonlinear systems and the frequency domain representations

2.1 Introduction

It is well known that a large class of nonlinear systems can be represented by a NDE model, or in discrete time, a NARX. Frequency domain analysis and design of these nonlinear systems are usually conducted based on the Volterra series representation, where many effective approaches such as the GFRFs, the NOFRFs, the OFRF, etc. have been developed and applied in engineering practice.

In this Chapter, different nonlinear models and the approaches for the frequency domain analysis of these nonlinear models are reviewed. Then a NARX model of nonlinear systems, where the physical parameters of interest for the system design appear explicitly as coefficients in the model, is introduced. The model is referred to as the NARX-M-for-D, which has the potential to be applied to represent a wide range of engineering systems and structures. The frequency domain representation of the NARX-M-for-D is then studied, and the application of this representation will be discussed in details in Chapter 5. The contents of this chapter are illustrated as below in Fig.2.1.
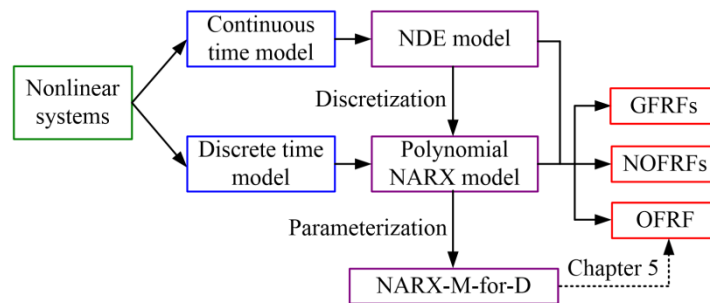
Fig.2.1 The contents of Chapter 2

2.2 Polynomial models of nonlinear systems

2.2.1 The NDE model of nonlinear systems

Many nonlinear systems can be described by differential equations, known as the NDE model, according to the study of their physical characteristics. The NDE model of a nonlinear system can be expressed as [41]

$$\sum_{m=1}^{M}\sum_{p=0}^{m}\sum_{l_1,l_{p+q}=0}^{L}\left[c_{p,q}\left(l_1,\cdots,l_{p+q}\right)\prod_{i=1}^{p}D^{l_i}y(t)\prod_{i=p+1}^{p+q}D^{l_i}u(t)\right]=0 \qquad (2.1)$$

where $y(t)$ and $u(t)$ are the system output and input, respectively; $p+q=m$, $\displaystyle\sum_{l_1,l_{p+q}=0}^{L}=\sum_{l_1=0}^{L}\cdots\sum_{l_{p+q}=0}^{L}$, M

and L are integers; $c_{p,q}\left(l_1,\cdots,l_{p+q}\right)$ are coefficients of the nonlinear model; The operator D in (2.1) is

defined by

$$D^l x(t)=\frac{d^l x(t)}{dt^l} \qquad (2.2)$$

In order to illustrate the NDE model (2.1), a Duffing equation

$$\ddot{y}(t)+c_l\dot{y}(t)+k_l y(t)+k_{n3}y(t)^3=u(t) \qquad (2.3)$$

is considered where c_l and k_l represent the linear damping and stiffness of the system, respectively; k_{n3}

is the nonlinear stiffness of the system.

In (2.3), by referring to the general form of the NDE model (2.1), it is known that

$$c_{1,0}(2)=1;\ \ c_{1,0}(1)=c_l;\ \ c_{1,0}(0)=k_l;\ \ c_{3,0}(0,0,0)=k_{n3}\ \ \text{and}\ \ c_{0,1}(0)=-1 \qquad (2.4)$$

However, in most practical cases, such as, e.g., vibration isolators made of viscoelastic and composite

materials [105] and bladed disks of aero-engines [106], it is difficult or impossible to find such a physical

model for the systems. But, it is possible to find, via a nonlinear system identification approach, a data driven

NARX model representing the relationship between the input excitation and corresponding system response

[107]. The general structure of the polynomial type NARX model is introduced in the next section.

2.2.2 The polynomial NARX model of nonlinear systems

In the discrete time domain, a nonlinear system output can always be represented by a relationship

between the system input and output as

$$y(t)=f\left(y(t-1),\ldots,y\left(t-n_y\right),u(t-1),\ldots,u\left(t-n_u\right)\right) \qquad (2.5)$$

where n_y and n_u are the maximum time delay of the output and input, respectively; $f(.)$ is a nonlinear

function. Equation (2.9) is defined as the NARX model of the system.

When $f(.)$ is a polynomial type function, the NARX model can be written in a polynomial form as [13]

$$y(k)=\sum_{m=1}^{M}\sum_{p=0}^{m}\sum_{k_1,k_{p+q}=1}^{K}\left[c_{p,q}(k_1,\cdots,k_{p+q})\prod_{i=1}^{p}y(k-k_i)\prod_{i=p+1}^{p+q}u(k-k_i)\right] \qquad (2.6)$$

where k represents the discrete time; $c_{p,q}\left(k_1,\cdots,k_{p+q}\right)$ with $p+q=m$ represents the model coefficients

of the NARX model; M and K are integers.

A polynomial NARX model can usually be determined by using NARMAX modelling method proposed in [11], or directly discretized from an NDE model [8]. For example, consider the first and the second derivatives in (2.3) that can be approximated by:

$$\dot{y}(t) = \frac{y(k) - y(k-1)}{\Delta t}, \ \ddot{y}(t) = \frac{y(k+1) - 2y(k) + y(k-1)}{\Delta t^2} \tag{2.7}$$

respectively, where Δt is the sampling period, the NDE model (2.3) can be discretized as

$$y(k) = \Delta t^2 u(k-1) + (2 - c_l \Delta t - k_l \Delta t^2) y(k-1) + (c_l \Delta t - 1) y(k-2) - k_{n3} \Delta t^2 y(k-1)^3 \tag{2.8}$$

which can be obtained from the general polynomial NARX model by choosing

$$c_{1,0}(2) = c_l \Delta t - 1; \ c_{1,0}(1) = 2 - c_l \Delta t - k_l \Delta t^2; \ c_{3,0}(1,1,1) = -k_{n3} \Delta t^2 \ \text{and} \ c_{0,1}(1) = \Delta t^2 \tag{2.9}$$

and zeros for other coefficients

It is worth pointing out that in order to obtain an effective discretized model, the sampling frequency $f_s = 1/\Delta t$ is required to be large enough to cover all system behaviors of interest to ensure the discretized model can sufficiently represent the original nonlinear system.

The NARX model is usually applied to study complex nonlinear systems where the NDE model cannot be obtained. However, an identified NARX model by using the NARMAX method doesn't have any physical meaning so that the model is difficult to be applied for the analysis and design of practical nonlinear systems. Ideally, an NARX model like (2.8) where that the physically meaningful parameters, i.e. c_l and k_{n3} appear explicitly as coefficients in the model should be produced to facilitate the system design. Such an NARX model is referred to as the NARX Model with parameters of interest for Design (NARX-M-for-D), which will be introduced next.

2.2.3 The NARX-M-for-D of nonlinear systems

The NARX-M-for-D is a NARX model where the physical parameters of interest for the system design appear explicitly as model coefficients. A general form of the single input single output NARX-M-for-D of nonlinear systems can be given as:

$$y(t) = f\left(y(t-1),\ldots,y(t-n_y),u(t-1),\ldots,u(t-n_u),\boldsymbol{\theta}(\boldsymbol{\xi})\right) \tag{2.10}$$

where $\boldsymbol{\theta}(\boldsymbol{\xi})$ is a vector representing a set of functions of the parameter vector $\boldsymbol{\xi} = [\xi_1,\ldots,\xi_S]$, where $\xi_1,\ldots,\xi_S$ are the physical parameters of interest for the system design, and S is the number of these design parameters.

Considering $f(.)$ can be approximated by a polynomial function of the delayed system input and output as in model (2.10), the NARX-M-for-D can further be expressed as:

$$y(k) = \sum_{m=1}^{M} \sum_{p=0}^{m} \sum_{k_1, k_{p+q}=1}^{K} \left[\theta_{p,q}^{(k_1, k_2, \cdots, k_{p+q})}(\xi) \prod_{i=1}^{p} y(k-k_i) \prod_{i=p+1}^{p+q} u(k-k_i) \right] \tag{2.11}$$

where $\theta_{p,q}^{(k_1, \cdots, k_{p+q})}(\xi)$ with $p+q=m$ representing the coefficients of the NARX-M-for-D (2.11) belongs to vector $\theta(\xi)$.

For example, the NARX model (2.8) is also a NARX-M-for-D, where $\xi = [c_l, k_l, k_{n3}]$ and

$$\theta_{1,0}^{(2)}(\xi) = c_l \Delta t - 1; \quad \theta_{1,0}^{(1)}(\xi) = 2 - c_l \Delta t - k_l \Delta t^2; \quad \theta_{3,0}^{(1,1,1)}(\xi) = -k_{n3} \Delta t^2 \quad \text{and} \quad \theta_{0,1}^{(1)}(\xi) = \Delta t^2 \tag{2.12}$$

The design of the parameters k_l, c_l and k_{n3} of the Duffing system (2.3) can therefore be transformed to the design of the same parameters but for the NARX-M-for-D (2.8).

It can be concluded from the above discussion that, the analysis and design of a nonlinear NDE model is covered by the study of a NARX model or a NARX-M-for-D. Consequently, in the following studies, most of the results are proposed based on the NARX model or NARX-M-for-D of nonlinear systems.

2.3 The frequency domain representations of nonlinear systems

2.3.1 The Volterra series representation

The output of continuous time nonlinear systems, such as the NDE model (2.1), when it is stable at the zero equilibrium, can be represented by using a Volterra series as [36]:

$$y(t) = \sum_{n=1}^{+\infty} y_n(t) \approx \sum_{n=1}^{N} \int_{-\infty}^{+\infty} \cdots \int_{-\infty}^{+\infty} h_n(\tau_1, \ldots, \tau_n) \prod_{i=1}^{n} u(t-\tau_i) d\tau_i \tag{2.13}$$

where the order of the Volterra series is usually truncated at order N, which represents the maximum order of the series expansion, $h_n(\tau_1, \ldots, \tau_n)$ is known as the nth order kernel of the system output.

The output of discrete time nonlinear systems, such as the NARX model (2.6), when it is stable at the zero equilibrium, can be described by the discrete time Volterra series as [108]

$$y(k) = \sum_{n=1}^{+\infty} y_n(k) \approx \sum_{n=1}^{N} \sum_{\tau_1=-\infty}^{+\infty} \cdots \sum_{\tau_n=-\infty}^{+\infty} h_n(\tau_1, \ldots, \tau_n) \prod_{i=1}^{n} u(k-\tau_i) \tag{2.14}$$

In the frequency domain, the output spectrum of the system $Y(j\omega)$ can be represented as [43]

$$Y(j\omega) = \sum_{n=1}^{N} Y_n(j\omega) = \sum_{n=1}^{N} \frac{1}{\sqrt{n}(2\pi)^{n-1}} \int_{\omega_1+\cdots+\omega_n=\omega} H_n(\omega_1, \ldots, \omega_n) \prod_{i=1}^{n} U(j\omega_i) d\sigma_\omega \tag{2.15}$$

where $U(j\omega)$ and $Y(j\omega)$ are the spectra of the system input and output, respectively; ω and $\omega_1,\ldots,\omega_n$ are physical frequencies, and for discrete time Volterra series (2.14), $-\pi f_s \le \omega \le \pi f_s$; $H_n(\omega_1,\ldots,\omega_n)$ is the n th order GFRFs of the nonlinear system defined as

$$H_n(\omega_1,\ldots,\omega_n) = \int_{-\infty}^{+\infty}\cdots\int_{-\infty}^{+\infty} h_n(\tau_1,\ldots,\tau_n)\exp\big(-j(\omega_1\tau_1+\cdots+\omega_n\tau_n)\big)d\tau_1\cdots d\tau_n \tag{2.16a}$$

for continuous time systems and as

$$H_n(\omega_1,\ldots,\omega_n) = \Delta t \sum_{\tau_1=-\infty}^{+\infty}\cdots\sum_{\tau_n=-\infty}^{+\infty} h_n(\tau_1,\ldots,\tau_n)\exp\big(-j(\omega_1\tau_1+\cdots+\omega_n\tau_n)\Delta t\big) \tag{2.16b}$$

for discrete time systems.

It is worth noting that when the system is linear, $H_1(\omega)$ is the Frequency Response Function (FRF) of the system. There are many approaches to determine the GFRFs [36-38], and the most commonly used method is the recursive algorithm proposed in [13,41] as introduced below.

2.3.2 The Generalised Frequency Response Functions (GFRFs) of nonlinear systems

The recursive algorithm of determining the n th order GFRFs $H_n(\omega_1,\ldots,\omega_n)$ was derived by using the probing method [13,41,109]. The n th order GFRFs of the system NDE model (2.1) can be calculated by using the following recursive algorithm [41,42]:

$$\left\{\begin{array}{l}
-\left[\displaystyle\sum_{l_1=0}^{L} c_{1,0}(l_1)(j\omega_1+\cdots+j\omega_n)^{l_1}\right]H_n(\omega_1,\cdots,\omega_n) = \displaystyle\sum_{l_1,l_n=0}^{L} c_{0,n}(l_1,\cdots,l_n)(j\omega_1)^{l_1}\cdots(j\omega_n)^{l_n} \\[6pt]
\quad +\displaystyle\sum_{q=1}^{n-1}\sum_{p=1}^{n-q}\sum_{l_1,l_{p+q}=0}^{L}\left[c_{p,q}(l_1,\cdots,l_{p+q})H_{n-q,p}(\omega_1,\cdots,\omega_{n-q})(j\omega_{n-q+1})^{l_{p+1}}\cdots(j\omega_n)^{l_{p+q}}\right] \\[6pt]
\quad +\displaystyle\sum_{p=2}^{n}\sum_{l_1,l_p=0}^{L}\left[c_{p,0}(l_1,\cdots,l_p)H_{n,p}(\omega_1,\cdots,\omega_n)\right] \\[6pt]
H_{n,p}(\omega_1,\cdots,\omega_n) = \displaystyle\sum_{i=1}^{n-(p-1)} H_i(\omega_1,\cdots,\omega_i)H_{n-i,p-1}(\omega_{i+1},\cdots,\omega_n)(j\omega_1+\cdots+j\omega_i)^{l_p} \\[6pt]
H_{n,1}(\omega_1,\cdots,\omega_n) = H_n(\omega_1,\cdots,\omega_n)(j\omega_1+\cdots+j\omega_n)^{l_1}
\end{array}\right. \tag{2.17}$$

Similarly, the n th order GFRFs of the system NARX model (2.6) can be calculated by using the following recursive algorithm [13]:

$$\left\{\begin{array}{l}
\left[1-\displaystyle\sum_{k_1=1}^{K} c_{1,0}(k_1)\exp\big(-j(\omega_1+\cdots+\omega_n)k_1\Delta t\big)\right]H_n(\omega_1,\cdots,\omega_n) = \displaystyle\sum_{k_1,k_n=1}^{K} c_{0,n}(k_1,\cdots,k_n) \\[6pt]
\quad \times\exp\big(-j(\omega_1 k_1+\cdots+\omega_n k_n)\Delta t\big)+\displaystyle\sum_{q=1}^{n-1}\sum_{p=1}^{n-q}\sum_{k_1,k_{p+q}=1}^{K}\left[c_{p,q}(k_1,\cdots,k_{p+q})H_{n-q,p}(\omega_1,\cdots,\omega_{n-q})\right. \\[6pt]
\quad \left.\times\exp\big(-j(\omega_{n-q+1}k_{p+1}+\cdots+\omega_n k_{p+q})\Delta t\big)\right]+\displaystyle\sum_{p=2}^{n}\sum_{k_1,k_p=1}^{K}\left[c_{p,0}(k_1,\cdots,k_p)H_{n,p}(\omega_1,\cdots,\omega_n)\right] \\[6pt]
H_{n,p}(\omega_1,\cdots,\omega_n) = \displaystyle\sum_{i=1}^{n-(p-1)} H_i(\omega_1,\cdots,\omega_i)H_{n-i,p-1}(\omega_{i+1},\cdots,\omega_n)\exp\left(-j\left(\displaystyle\sum_{l=1}^{i}\omega_l\right)k_p\Delta t\right) \\[6pt]
H_{n,1}(\omega_1,\cdots,\omega_n) = H_n(\omega_1,\cdots,\omega_n)\exp\big(-j(\omega_1+\cdots+\omega_n)k_1\Delta t\big)
\end{array}\right. \tag{2.18}$$

It can be observed that the recursive algorithms of the n th order GFRFs for the continuous and discrete time models have a similar structure.

For example, the first three orders' GFRFs of the Duffing equation (2.3) can be determined as follows

For $n = 1$,

$$H_1(\omega_1) = \frac{-1}{\omega_1^2 - \mathrm{j}c_l\omega_1 - k_l} \tag{2.19}$$

For $n = 2$,

$$H_2(\omega_1, \omega_2) = 0 \tag{2.20}$$

For $n = 3$,

$$
\begin{aligned}
H_3(\omega_1, \omega_2, \omega_3) &= \frac{c_{3,0}(0,0,0)H_{3,3}(\omega_1, \omega_2, \omega_3)}{m(\omega_1 + \omega_2 + \omega_3)^2 - \mathrm{j}c(\omega_1 + \omega_2 + \omega_3) - k} \\
&= \frac{c_{3,0}(0,0,0)\big(H_1(\omega_1)H_{2,2}(\omega_2, \omega_3) + H_2(\omega_1, \omega_2)H_{1,1}(\omega_3)\big)}{m(\omega_1 + \omega_2 + \omega_3)^2 - \mathrm{j}c(\omega_1 + \omega_2 + \omega_3) - k} \\
&= \frac{k_{n3}H_1(\omega_1)H_1(\omega_2)H_1(\omega_3)}{m(\omega_1 + \omega_2 + \omega_3)^2 - \mathrm{j}c(\omega_1 + \omega_2 + \omega_3) - k}
\end{aligned}
\tag{2.21}
$$

It can be seen that, the GFRFs are a series of multi-dimensional functions which, although the graphic presentation approaches have been introduced in [39,40] for low order GFRFs, it is are often difficult to measure, display and interpret higher order GFRFs in practice.

To address this issue, many new concepts such as the NOFRF [55], the OFRF [56] etc. have been proposed to replace the GFRFs with one dimensional functions of frequencies. For example, the NOFRF is a significant extension of the FRF for linear systems to the nonlinear case, which are one-dimensional functions that enable an exploration of the system frequency domain characteristics by means of a series of Bode diagram like plots; The OFRF represents the polynomial relationship between the system output and nonlinear characteristic parameters which have been widely applied in the analysis and design of nonlinear systems. The details of the NOFRFs and OFRF are introduced as follows.

2.3.3 The Nonlinear Output Frequency Response Funtions (NOFRFs) of nonlinear systems

The n th order NOFRF is defined as

$$G_n(\mathrm{j}\omega) = \frac{Y_n(\mathrm{j}\omega)}{U_n(\mathrm{j}\omega)}; \, \omega \in \Omega \tag{2.22}$$

where $Y_n(\mathrm{j}\omega)$ and $U_n(\mathrm{j}\omega)$ are the n th order output spectrum and the n th order generalized input spectrum that obtained by the Fourier Transform of $y_n(t)$ and $u^n(t)$, respectively, for continuous time system where

$$U_n(j\omega) = F\left\{u(t)^n\right\} = \frac{1}{\sqrt{n}(2\pi)^{n-1}}\int_{\omega_1+\cdots+\omega_n=\omega}\prod_{i=1}^{n}U(j\omega_i)\,d\sigma_{n,\omega} \tag{2.23}$$

$\sigma_{n,\omega}$ represents the hyperplane $\omega_1+\cdots+\omega_n=\omega$, $F\{.\}$ denotes the Fourier Transform, Ω is the frequency support of $|U_n(j\omega)|$, which can be determined using the results about the output frequencies of nonlinear systems [43].

For discrete time nonlinear systems, the NOFRFs defined by $Y_n(j\omega)$ and $U_n(j\omega)$ in (2.22) are determined by using the normalised Discrete Time Fourier Transform (the Discrete Time Fourier Transform times Δt) of $y_n(k)$ and $u^n(k)$, respectively, where

$$U_n(j\omega) = DF\left\{u(k)^n\right\}\Delta t = \frac{1}{\sqrt{n}(2\pi)^{n-1}}\int_{\omega_1+\cdots+\omega_n=\omega}\prod_{i=1}^{n}U(j\omega_i)\,d\sigma_{n,\omega} \tag{2.24}$$

where $DF\{.\}$ denotes the Discrete Time Fourier Transform and $\Omega\subseteq[-\pi f_s,\pi f_s]$.

Therefore, the output spectrum of nonlinear systems can be represented as

$$Y(j\omega) = \sum_{n=1}^{N}Y_n(j\omega) = \sum_{n=1}^{N}G_n(j\omega)U_n(j\omega) \tag{2.25}$$

which is illustrated in Fig.2.2, where $u(.)$ represents either the continuous or discrete time input signal.
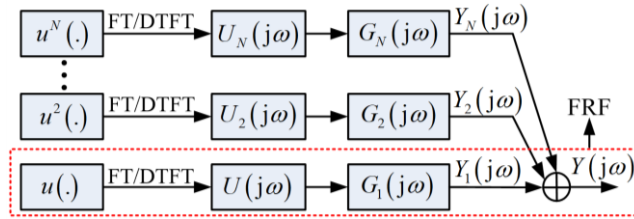
Fig.2.2 The NOFRFs based analysis of a nonlinear system

Fig.2.2 indicates that, when $n=N=1$, $G_n(j\omega)=G_1(j\omega)$ reduceing to the FRF of a linear system.

Notice that when the input signal is zoomed by a factor α as $\hat{u}(.)=\alpha u(.)$, where the corresponding output and input spectrum are denoted as $\hat{Y}_n(j\omega)$ and $\hat{U}_n(j\omega)$, respectively, the NOFRFs will have no change according to (2.15) and (2.24),

$$\begin{aligned}G_n(j\omega) &= \frac{\hat{Y}_n(j\omega)}{\hat{U}_n(j\omega)} = \frac{\dfrac{1}{\sqrt{n}(2\pi)^{n-1}}\displaystyle\int_{\omega_1+\cdots+\omega_n=\omega}H_n(\omega_1,\ldots,\omega_n)\prod_{i=1}^{n}\alpha U(j\omega_i)\,d\sigma_\omega}{\dfrac{1}{\sqrt{n}(2\pi)^{n-1}}\displaystyle\int_{\omega_1+\cdots+\omega_n=\omega}\prod_{i=1}^{n}\alpha U(j\omega_i)\,d\sigma_\omega} \\[2mm] &= \frac{\displaystyle\int_{\omega_1+\cdots+\omega_n=\omega}H_n(\omega_1,\ldots,\omega_n)\prod_{i=1}^{n}U(j\omega_i)\,d\sigma_\omega}{\displaystyle\int_{\omega_1+\cdots+\omega_n=\omega}\prod_{i=1}^{n}U(j\omega_i)\,d\sigma_\omega} = \frac{Y_n(j\omega)}{U_n(j\omega)}\end{aligned} \tag{2.26}$$

and the output spectrum can be represented as

$$Y(j\omega) = \sum_{n=1}^{N} \hat{Y}_n(j\omega) = \sum_{n=1}^{N} G_n(j\omega)\hat{U}_n(j\omega) = \sum_{n=1}^{N} \alpha^n G_n(j\omega) U_n(j\omega) \qquad (2.27)$$

Consequently, the following properties of the NOFRFs can be concluded

Property 1. [55] Let α be an arbitrary constant and $G_n(j\omega)$ the nth order NOFRF evaluated for

$U(j\omega)$. Then, the NOFRF corresponding to $\alpha U(j\omega)$ are also $G_n(j\omega)$.

Property 2. [55] The frequency support of $G_n(j\omega)$, $Y_n(j\omega)$ and $U_n(j\omega)$, i.e., the frequency range

where these functions of frequency are well defined, are the same.

The NOFRFs can be evaluated by using the Least Squares (LS) method as [55]

$$G = \left[\hat{U}^{\mathrm{T}}\hat{U}\right]^{-1}\hat{U}^{\mathrm{T}}Y \qquad (2.28)$$

where

$$Y = \begin{bmatrix} Y^{(1)}(j\omega) \\ \vdots \\ Y^{(\bar{N})}(j\omega) \end{bmatrix}, \quad \hat{U} = \begin{bmatrix} \alpha_1 U_1(j\omega) & \cdots & \alpha_1^N U_N(j\omega) \\ \vdots & \ddots & \vdots \\ \alpha_{\bar{N}} U_1(j\omega) & \cdots & \alpha_{\bar{N}}^N U_N(j\omega) \end{bmatrix}_{\bar{N}\times N}, \quad G = \begin{bmatrix} G_1(j\omega) \\ \vdots \\ G_N(j\omega) \end{bmatrix}$$

and $\alpha_1, \ldots, \alpha_{\bar{N}}$ are $\bar{N} \geq N$ numbers of testing input magnitude for the LS evaluation,

$Y^{(1)}(j\omega), \ldots, Y^{(\bar{N})}(j\omega)$ are the $\bar{N}$ output spectra under $\bar{N}$ different inputs, respectively.

The example of Duffing equation (2.3) is discussed here to illustrate the LS evaluation of the NOFRFs.

Given $c_l = 40$ N/ms^{-1} and $k_l = 1\times10^4$ N/m and $k_{n3} = 5\times10^8$ N/m^3, the input of the system (2.3) is

assumed as

$$u(t) = A\cos(\omega_F t) \qquad (2.29)$$

where the A is the input magnitude, and $\omega_F \in [0, 300]$ rad/s.

The NOFRFs up to the 5th order $G_1(j\omega_F)$, $G_3(j\omega_F)$ and $G_5(j\omega_F)$ are shown in Fig.2.3 which were

obtained by using the LS method and the system output responses to the testing inputs (2.29) with 5 different

magnitudes of $A = \{0.8, 0.9, 1.0, 1.1, 1.2\}$.

The output spectra subject to $u(t) = 2\cos(\omega_F t)$ are predicted by using the NOFRFs based representation

$$Y(j\omega_F) = G_1(j\omega_F)U_1(j\omega_F) + G_3(j\omega_F)U_3(j\omega_F) + \cdots + G_N(j\omega_F)U_N(j\omega_F) \qquad (2.30)$$

with results shown in Fig.2.4 for the cases of $N = 1, 3, 5, 7$, respectvely. The results show that a higher order

NOFRFs based representation can provide a more accurate output prediction, where the true output spectra in

Fig.2.4 are obtained by using the Runge-Kutta numerical method.
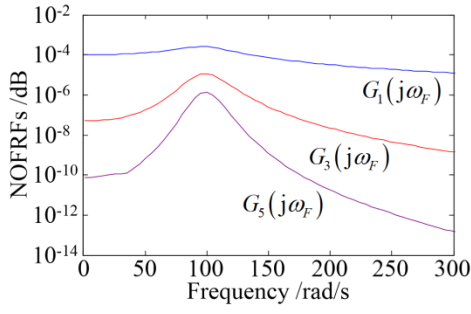
Fig.2.3 The GALEs evaluated NOFRFs   **Fig.2.4** Outputs under the NOFRFs based representation
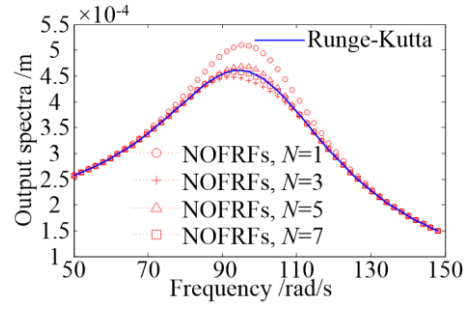
The NOFRFs represent the frequency domain properties of nonlinear systems. In the next section, the OFRF of nonlinear systems is introduced, which shows the relationship between the system output frequency response and the nonlinear parameters of interest. It is worth noting that, the peaks of the NOFRFs representations in Fig.2.4 are not reached. The results are only aproximations of the truncated Volterra series representation of the system. When the Volterra series is convergent, higher truncation order N can provide more accurate approximation results.

2.3.4 The Output Frequency Response Function (OFRF) of nonlinear systems

The OFRF of nonlinear systems can be represented by a polynomial function in terms of system nonlinear characteristic parameters as [56]

$$Y(j\omega) = \sum_{(j_1,\ldots,j_s)\in \boldsymbol{J}} \lambda_{(j_1,\ldots,j_s)}(j\omega) x_1^{j_1} \cdots x_s^{j_s} = \boldsymbol{C}\boldsymbol{\Lambda} \tag{2.31}$$

where $\boldsymbol{J}$ is the set of all available index $j_1,\ldots,j_s$; $\boldsymbol{C}$ is the monomial vector consisting of nonlinear characteristic parameters $c_{p,q}(.)$, $p+q \geq 2$ represented by $x_1,\ldots,x_s$; $\boldsymbol{\Lambda}$ is the column vector with elements $\lambda_{j_1,\ldots,j_s}(j\omega)$, which are determined the frequency variable ω and system linear parameters $c_{1,0}(.)$ and $c_{0,1}(.)$.

In order to use the OFRF to perform the system analysis and design, it is very important that the "structure" and "coefficients" of the OFRF representation have to be determined. The OFRF "structure" basically refers to the monomials that need to be included in the OFRF representation, whilst the "coefficients" are the value of $\lambda_{(j_1,\cdots,j_S)}(j\omega)$ associated with each monomial in the OFRF.

Given the order N of the system Volterra series representation, the structure of the OFRF of the NDE model (2.1) defined by the vector $\boldsymbol{C}$ in (2.31) can be determined by using the recursive algorithm as [74]

$$C = \bigcup_{n=1}^{N} C_n \tag{2.32}$$

where

$$C_n = \left[\bigcup_{l_1,\dots,l_n=0}^{L} c_{0,n}(l_1,\dots,l_n) \right] \cup \left[\bigcup_{q=1}^{n-1} \bigcup_{p=1}^{n-q} \bigcup_{l_1,\dots,l_n=0}^{L} \left(c_{p,q}(l_1,\dots,l_{p+q}) \otimes C_{n-q,p} \right) \right]$$
$$\cup \left[\bigcup_{p=2}^{n} \bigcup_{l_1,\dots,l_n=0}^{L} \left(c_{p,0}(l_1,\dots,l_p) \otimes C_{n,p} \right) \right] \tag{2.33}$$

with $C_1 = [1]$, where $\otimes$ is the Kronecker product, and

$$C_{n,p} = \bigcup_{i=1}^{n-p+1} C_i \otimes C_{n-i,p-1} \quad \text{and} \quad C_{n,1} = C_n \tag{2.34}$$

For a NARX model (2.6), the OFRF structure can be determined by using the same algorithm by replacing $c_{p,q}(l_1,\dots,l_{p+q})$ with $c_{p,q}(k_1,\dots,k_{p+q})$.

The evaluation of the OFRF coefficients can be conducted by using the LS algorithm. It can be seen that the OFRF (2.31) is a polynomial function, where assuming there are N terms in the OFRF representation, and $\bar{N} \geq N$ sets of testing parameter values are used for the LS evaluation. $Y^{(1)}(j\omega),\dots, Y^{(\bar{N})}(j\omega)$ are the $\bar{N}$ output spectra under $\bar{N}$ different sets of parameter values, respectively. Consequently, the OFRF coefficients can be evaluated as

$$\Lambda = \left(C_v^{\mathrm{T}} C_v \right)^{-1} C_v^{\mathrm{T}} Y \tag{2.35}$$

where

$$Y = \begin{bmatrix} Y^{(1)}(j\omega) \\ \vdots \\ Y^{(\bar{N})}(j\omega) \end{bmatrix}, \quad C_v = \begin{bmatrix} C_{(1)}(1) & \cdots & C_{(1)}(N) \\ \vdots & \ddots & \vdots \\ C_{(\bar{N})}(1) & \cdots & C_{(\bar{N})}(N) \end{bmatrix}_{\bar{N} \times N}, \quad \Lambda = \begin{bmatrix} \vdots \\ \lambda_{(j_1,\dots,j_s)}(j\omega) \\ \vdots \end{bmatrix}_{(j_1,\dots,j_s) \in J}$$

and $C_{(i)}(j)$ represents the j th element of the monomial vector C under the i th set of nonlinear parameter values.

For example, the monomials of the OFRF of the Duffing equation (2.3) can be determined as

$$C_1 = [1]; C_2 = [\text{NULL}]; C_3 = [a_3]; C_4 = [\text{NULL}];$$
$$C_5 = [k_{n3} \otimes C_{5,3}] = [k_{n3} \otimes C_3] = [k_{n3}^2]; \cdots \tag{2.36}$$

and the OFRF of the system (2.3) is written as

$$Y(j\omega) = \lambda_{(0)}(j\omega) + \lambda_{(1)}(j\omega)k_{n3} + \lambda_{(2)}(j\omega)k_{n3}^2 + \cdots \tag{2.37}$$

Given $c_l = 40\ \text{N/ms}^{-1}$ and $k_l = 1 \times 10^4\ \text{N/m}$, the OFRF up to $N = 7$ of the system (2.3) can be evaluated as follows.

The structure of the OFRF representation up to $N = 7$ of the system (2.3) can be obtained as

$$Y(\mathrm{j}\omega) = \lambda_{(0)}(\mathrm{j}\omega) + \lambda_{(1)}(\mathrm{j}\omega)k_{n3} + \lambda_{(2)}(\mathrm{j}\omega)k_{n3}^{2} + \lambda_{(3)}(\mathrm{j}\omega)k_{n3}^{3} \tag{2.38}$$

Under harmonic input (2.29) with $A = 2$ and $\omega_F = 80\ \text{rad/s}$ by testing the system over 8 parameter values of $k_{n3} \in \{0:0.5:3.5\} \times 10^9\ \text{N/m}^3$, there is

$$\begin{cases} Y^{(1)}(\mathrm{j}\omega) = \lambda_{(0)}(\mathrm{j}\omega) + \lambda_{(1)}(\mathrm{j}\omega)k_{n3,1} + \lambda_{(2)}(\mathrm{j}\omega)k_{n3,1}^{2} + \lambda_{(3)}(\mathrm{j}\omega)k_{n3,1}^{3} \\ \qquad\qquad\qquad\qquad\vdots \\ Y^{(8)}(\mathrm{j}\omega) = \lambda_{(0)}(\mathrm{j}\omega) + \lambda_{(1)}(\mathrm{j}\omega)k_{n3,8} + \lambda_{(2)}(\mathrm{j}\omega)k_{n3,8}^{2} + \lambda_{(3)}(\mathrm{j}\omega)k_{n3,8}^{3} \end{cases} \tag{2.39}$$

where $k_{n3,i}, i = 1,\ldots,8$ are the 8 different parameter values.

Therefore, the cofficients of the OFRF representation can be evaluated by using (2.35) with

$$\mathbf{Y} = \begin{bmatrix} Y^{(1)}(\mathrm{j}\omega) \\ \vdots \\ Y^{(8)}(\mathrm{j}\omega) \end{bmatrix}, \quad \mathbf{C}_v = \begin{bmatrix} 1 & k_{n3,1} & k_{n3,1}^{2} & k_{n3,1}^{3} \\ \vdots & \vdots & \vdots & \vdots \\ 1 & k_{n3,8} & k_{n3,8}^{2} & k_{n3,8}^{3} \end{bmatrix}, \text{ and } \mathbf{\Lambda} = \begin{bmatrix} \lambda_{(0)}(\mathrm{j}\omega) \\ \lambda_{(1)}(\mathrm{j}\omega) \\ \lambda_{(2)}(\mathrm{j}\omega) \\ \lambda_{(3)}(\mathrm{j}\omega) \end{bmatrix}$$

yields

$$\begin{aligned} Y(\mathrm{j}\omega) &= (-0.0901 - 0.3218\mathrm{i}) \times 10^{-3} + (0.7485 + 0.477\mathrm{i}) \times 10^{-5} k_{n3} \\ &\quad + (-0.4882 - 0.1313\mathrm{i}) \times 10^{-6} k_{n3}^{2} + (0.2273 + 0.1313\mathrm{i}) \times 10^{-6} k_{n3}^{3} \end{aligned} \tag{2.38}$$

The OFRF results are shown in Fig.2.5. The results indicate that the OFRF can be used to represent and predict the output response of a nonlinear system under different nonlinear characteristic parameters.
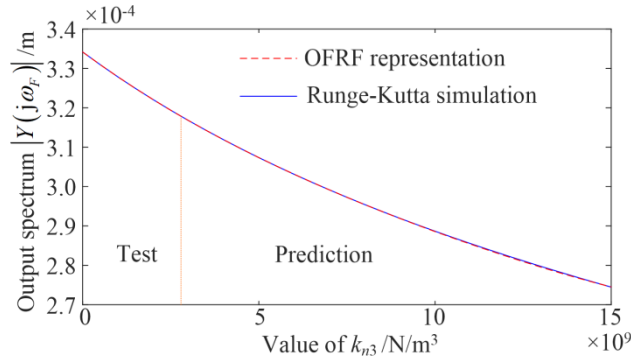
Fig.2.5 The OFRF representation of the Duffing system (2.3)

It is worth noting that, the OFRF of a NDE/NARX model is unique when the order of system nonlinearity

that has been taken into account is sufficiently high [56]. The increase of the system design parameters may increase the complexity of the OFRF. But, different from numerical approximation or curve fitting, there is no overfitting issue because of the OFRF's uniqueness.

2.4 Conclusions

This chapter prepare presents the basic results about the frequency domain analysis and design of nonlinear systems. In general, the discrete or continuous time model of the system can be established by using either data driven modelling or physical analyses. After that, the frequency domain analysis and design can be conducted by using the NOFRFs and OFRF approaches of nonlinear systems, respectively.

However, there are many fundamental issues need to be solved in order to widely apply the frequency domain analysis and design in engineering practice. For example, an appropriate expansion order for the NOFRFs and the OFRF based results are difficult to determine, and the LS based evaluation for both NOFRFs and OFRF may suffer significant numerical errors due to an inappropriate choice of order N. In existing studies, the order N is often empirically chosen as 3 or 5 [74]. On the other hand, before using the NOFRFs and OFRF, the convergence of the system Volterra series representation should be guaranteed, but in the previous studies, the convergent condition is only an assumption. Moreover, the system OFRF representation only shows an analytical relationship between the output spectra of nonlinear systems and the system's nonlinear characteristic parameters, but this relationship is only valid under the condition that the system linear characteristic parameters are fixed.

In the following Chapters, these issues are fundamentally addressed by using a series of new concepts known as the Generalized Associated Linear Equations (GLAEs), the Generalized Output Bound Characteristic Function (GOBCF), and the Associated Output Frequency Response Function (AOFRF), respectively. Finally, an experimental study is conducted to demonstrate the application of the newly proposed nonlinear ystem frequency analysis and designs in engineering practice.

Chapter 3. Generalized Associated Linear Equations (GALEs) with applications to nonlinear system analyses

3.1 Introduction

The Volterra series theory is the fundamental basis of the frequency domain analysis of nonlinear systems. According to this theory, the output of a wide class of nonlinear systems can be represented by a truncated functional series consisting of a summation of the system output components contributed by the first, second, and higher order system nonlinearities. An effective determination of these system output components has significant implications for further development and practical application of nonlinear system frequency domain theories and methods. Available approaches that could be applied to address this issue is known as Associated Linear Equations (ALEs) which, however, can only resolve this significant problem for a very special class of nonlinear systems [65,66,111].

In this Chapter, motivated by the need of addressing these problems, the ALEs are extended to polynomial type NARX models such that the Volterra series representation of a NARX model can be determined up to an arbitrary order of interest by solving a series of linear difference equations. Moreover, a new concept known as the Generalized Associated Linear Equations (GALEs) is proposed to systematically determine the structure of these linear equations for both the NARX and NDE models of nonlinear systems.

The GALEs and associated techniques can significantly facilitate the analysis of nonlinear systems in the time and frequency domain. The GALEs can also enable the development of a more effective technique for the identification of the NDE model of nonlinear systems, producing a physically meaningful representation for nonlinear systems. Four case studies on the application of the GALEs for nonlinear system analyses are provided to demonstrate the significance of the new GALEs concept. These include the application of the GALEs for the evaluation of the time domain output response of a nonlinear system, the determination of the NOFRFs and OFRFs using the GALEs for nonlinear system frequency analyses, and the use of the GALEs in the identification of the NDE model of a nonlinear system. The structure of this chapter is illustrated as below
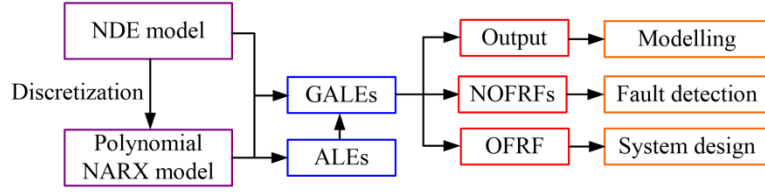
Fig.3.1 The contents of Chapter 3

3.2 The Associated Linear Equations (ALEs) of nonlinear systems

3.2.1 The ALEs of Duffing equations

Consider the Duffing equation (2.3) where the output can be represented by a Volterra series as

$$y(t) = \sum_{n=1}^{+\infty} y_n(t) \tag{3.1}$$

Substituting (3.1) into (2.3), yields

$$\sum_{n=1}^{\infty} \ddot{y}_n(t) + c_l \sum_{n=1}^{\infty} \dot{y}_n(t) + k_l \sum_{n=1}^{\infty} y_n(t) + k_{n3} \left[\sum_{n=1}^{\infty} y_n(t) \right]^3 = u(t) \tag{3.2}$$

which can be rearrange the equation (3.2) as

$$\begin{aligned}
\ddot{y}_1(t) + c_l \dot{y}_1(t) + k_l y_1(t) &= u(t) \\
\ddot{y}_3(t) + c_l \dot{y}_3(t) + k_l y_3(t) &= -k_{n3} y_1^3(t) \\
\ddot{y}_5(t) + c_l \dot{y}_5(t) + k_l y_5(t) &= -3k_{n3} y_1^2(t) y_3(t) \\
&\vdots
\end{aligned} \tag{3.3}$$

Therefore, it is known that

$$\begin{cases}
\ddot{y}_1(t) + c_l \dot{y}_1(t) + k_l y_1(t) = u(t), \, n = 1 \\
\ddot{y}_n(t) + c_l \dot{y}_n(t) + k_l y_n(t) = -\sum_{j_1=1}^{n-2} \sum_{j_2=1}^{n-j_1-1} \sum_{j_3=1}^{n-j_1-j_2} k_{n3} \prod_{i=1}^{3} y_{j_i}(t), \, n \geq 2
\end{cases} \tag{3.4}$$

which is known as the ALEs of the Duffing equation (2.3).

The ALEs of a general Duffing type equation have been proposed by Feijoo et al [111], but there is still no a systematic approach that can be applied to determine the ALEs for much more general nonlinear systems.

In the following sections, the ALEs of the NARX model (2.6) for nonlinear systems [108] are derived. Moreover, a recursive algorithm is proposed for the determination of ALEs of the NDE model (2.1) of nonlinear systems. These general ALEs are known as the GALEs of nonlinear systems.

3.2.2 The ALEs of the NARX model

For the convenience of discussion, the polynomial NARX model (2.6) is rearranged as

$$Ay(k) = Bu(k) + \sum_{m=1}^{M} c_m F_m(k) \tag{3.5}$$

where c_m are coefficients

$$F_m(k) = \prod_{l=1}^{L} y(k-l)^{p(m,l)} u(k-l)^{q(m,l)} \tag{3.6}$$

$p(m,l)$ and $q(m,l)$ represent the non-negative integers such that $q(m,l) + p(m,l) > 1$, and A and B

denote linear time shifting operators such that

$$Ay(k) = y(k) + \sum_{l=1}^{L} a_l y(k-l) \tag{3.7}$$

$$Bu(k) = \sum_{l=1}^{L} b_l u(k-l) \tag{3.8}$$

where a_l and b_l are coefficients.

The ALEs of system (3.5)-(3.8) can be obtained as described in Proposition 3.1 below.

Proposition 3.1: *The ALEs of the NARX model (3.5)-(3.8) are a series of linear difference equations*

described by:

$$Ay_1(k) = Bu(k) \tag{3.9}$$

$$Ay_n(k) = \upsilon_n(k); n \geq 2 \tag{3.10}$$

where

$$\upsilon_n(k) = \sum_{m=1}^{M} c_m \psi_m(k) \sum_{S_m} \rho_m \phi_m(k) \tag{3.11}$$

$$\rho_m = \frac{\prod_{l=1}^{L} p(m,l)!}{\prod_{l=1}^{L} \prod_{j=1}^{J_m} r(m,l,j)!} \tag{3.12}$$

$$\psi_m(k) = \prod_{l=1}^{L} u(k-l)^{q(m,l)} \tag{3.13}$$

$$\phi_m(k) = \prod_{l=1}^{L} \prod_{j=1}^{J_m} y_k(k-l)^{r(m,l,j)} \tag{3.14}$$

$$J_m = n - \sum_{l=1}^{L} [q(m,l) + p(m,l)] + 1 \tag{3.15}$$

and S_m *is the set of all non-negative integer solutions of the linear Diophantine system*

$$\sum_{j=1}^{J_m} r(m,l,j) = p(m,l) \quad \forall l \tag{3.16}$$

$$\sum_{l=1}^{L}\sum_{j=2}^{J_m}(j-1)r(m,l,j)=J_m-1 \tag{3.17}$$

Proof of Proposition 3.1: Substituting the Volterra series representation (2.14) of the NARX model into (3.6)-(3.8), yields:

$$\sum_{j=1}^{+\infty}Ay_j(k)=Bu(k)+\sum_{m=1}^{M}c_mF_m(k) \tag{3.18}$$

where

$$F_m(k)=\psi_m(k)\alpha_m(k) \tag{3.19}$$

$$\psi_m(k)=\prod_{l=1}^{L}u(k-l)^{q(m,l)} \tag{3.20}$$

$$\alpha_m(k)=\prod_{l=1}^{L}\left(\sum_{j=1}^{+\infty}y_j(k-l)\right)^{p(m,l)} \tag{3.21}$$

In order to determine the n th order ALE, it is necessary to expand (3.19), identify all n th order terms and equate them to those of the same order on the left-hand side of (3.18). The n th order terms on the left hand side of (3.18) can be found by noticing that the linear operator A does not change the order of any functional component. Therefore, the n th order component on the left-hand side of (3.18) is $Ay_n(k)$.

On the other hand, the products in (3.19) produce an expansion in terms of each $y_n(k)$, spanning functionals of many different orders. The order of $\psi_m(n)$ is found as:

$$\sum_{l=1}^{L}q(m,l) \tag{3.22}$$

Therefore, the n th order terms in (3.19) can be found by identifying terms of $\alpha_m(k)$ of order

$$n-\sum_{l=1}^{L}q(m,l) \tag{3.23}$$

Consider the multinomial expansion with respect to $y_n(k), n\geq 1$:

$$\gamma(m,l)=\left(\sum_{j=1}^{+\infty}y_j(k-l)\right)^{p(m,l)}=\sum\beta(m,l)\prod_{j=1}^{+\infty}y_j(k-l)^{r(m,l,j)} \tag{3.24}$$

where

$$\beta(m,l)=\frac{p(m,l)!}{\prod_{j=1}^{+\infty}r(m,l,j)!} \tag{3.25}$$

and the sum in (3,24) is computed over all nonnegative integers $r(m,l,j)$ that satisfy

$$\sum_{j=1}^{+\infty} r(m,l,j) = p(m,l) \tag{3.26}$$

Using (3.24), $\alpha_m(k)$ can be expanded as:

$$\alpha_m(k) = \sum \prod_{l=1}^{L} \beta(m,l) \prod_{j=1}^{+\infty} y_j (k-l)^{r(m,l,j)} \tag{3.27}$$

where the order of the general term of (3.27) is

$$\sum_{l=1}^{L} \sum_{j=1}^{+\infty} jr(m,l,j) \tag{3.28}$$

Therefore, for finding terms of order (3.23), it is necessary to find all integers $r(m,l,j)$ that simultaneously satisfy:

$$\sum_{j=1}^{+\infty} r(m,l,j) = p(m,l); 1 \le l \le L \tag{3.29}$$

and

$$\sum_{l=1}^{L} \sum_{j=1}^{+\infty} jr(m,l,j) = n - \sum_{l=1}^{L} q(m,l) \tag{3.30}$$

System (3.29)-(3.30) is known as a Diophantine system, because all unknowns are integers. The particular form of these equations allow them to be further simplified by subtracting (3.30) from (3.29), for every possible l, yielding:

$$\sum_{l=1}^{L} \sum_{j=2}^{+\infty} (j-1)r(m,l,j) = J_m - 1 \tag{3.31}$$

where

$$J_m = 1 + n - \sum_{l=1}^{L} q(m,l) + p(m,l) \tag{3.32}$$

Notice that, since $r(m,l,j) \ge 0$, we must have $j \le J_m$, so that J_m can be used as upper limit to all summations and products in j, allowing system (3.29)-(3.30) to be rewritten as (3.16)-(3.17).

Let S_m denote the set of all nonnegative solutions of (3.16)-(3.17). By taking only the n th order terms from the expansion of (3.19), the n th order ALE can be written as:

$$Ay_n(k) = \sum_{m=1}^{M} c_m \psi_m(k) \alpha_m(k) \tag{3.33}$$

$$\alpha_m(k) = \sum_{S_m} \prod_{l=1}^{L} \beta(m,l) \prod_{j=1}^{J_m} y_j(k-l)^{r(m,l,j)} \tag{3.34}$$

Finally, by splitting the products in $\alpha_m(k)$ with respect to l and defining

$$\rho_m = \prod_{l=1}^{L} \beta(m,l) = \frac{\prod_{l=1}^{L} p(m,l)!}{\prod_{l=1}^{L} \prod_{j=1}^{J_m} r(m,l,j)!} \tag{3.35}$$

$$\phi_m(k) = \prod_{l=1}^{L} \prod_{j=1}^{J_m} y_j(k-l)^{r(m,l,j)} \tag{3.36}$$

we obtain the n th order ALE, equation (3.10).

A simple example is given below to illustrate how to obtain the ALEs of the NARX model using Proposition 3.1.

Consider a identified NARX model under the sampling frequency of $f_s = 1024$ Hz

$$Ay(k) = Bu(k) + c_1 y^2(k-1) + c_2 y^4(k-1) \tag{3.37}$$

with

$$\begin{cases} Ay(k) = y(k) + a_1 y(k-1) + a_2 y(k-2) \\ Bu(k) = b_1 u(k-1) \end{cases} \tag{3.38}$$

The ALEs of the system up to the 4th order are obtained as follows. For $n=1$:

$$Ay_1(k) = b_1 u(k-1) \tag{3.39}$$

For $n=2$, $J_1 = 2-2+1 = 1$ and $J_2 = 2-4+1 = -1$, yielding the Diophantine system:

$$\begin{cases} r(1,1,1) = 2 \\ 0 = 0 \end{cases} \text{ and } \begin{cases} 0 = 4 \\ 0 = -2 \end{cases} \tag{3.40}$$

The first Diophantine system has only one solution which is $r(1,1,1) = 2$, and the second Diophantine system is inconsistent so that can be ignored. Consequently, the second order ALE can be obtained as

$$Ay_2(k) = c_1 y_1^2(k-1) \tag{3.41}$$

For $n=3, 4$, a similar procedure can be followed to produce the 3rd and 4th order ALEs as

$$Ay_3(k) = 2c_1 y_1(k-1) y_2(k-1) \tag{3.42}$$

and

$$Ay_4(k) = c_1 y_2^2(k-1) + 2c_1 y_1(k-1) y_3(k-1) + c_2 y_1^4(k-1) \tag{3.43}$$

respectively.

It can be seen that, although the ALEs of a NARX model can be determined by solving a series of Diophantine equations as illustrated above, the procedure is generally still very complicated. In the next section, a more effective recursive algorithm is derived to determine the ALEs for the NARX or NDE model

of nonlinear systems, which is known as the GALEs.

3.3 The Generalized Associated Linear Equations (GALEs)

3.3.1 The concept of the GALEs

By multiplying each side of equations (2.17)/(2.18) with $\prod_{i=1}^{n} U(j\omega_i)$ and evaluating the integration of the

result over the hyperplane $\omega_1 + \cdots + \omega_n = \omega$, it can be shown that

$$Y_n(j\omega) = \bar{H}(j\omega)V_n(j\omega); n = 1,\ldots,N \tag{3.44}$$

where for the NDE model,

$$\begin{cases} \bar{H}(j\omega) = -\left[\sum_{l_1=0}^{L} c_{1,0}(l_1)(j\omega)^{l_1}\right]^{-1} \\ V_n(j\omega) = \frac{1}{\sqrt{n}(2\pi)^{n-1}} \int_{\omega_1+\cdots+\omega_n=\omega} \left(\Psi_{n,u} + \Psi_{n,uy} + \Psi_{n,y}\right) \prod_{i=1}^{n} U(j\omega_i) d\sigma_\omega \end{cases} \tag{3.45}$$

with

$$\begin{cases} \Psi_{n,u} = \sum_{l_1,l_n=0}^{L} c_{0,n}(l_1,\cdots,l_n)(j\omega_1)^{l_1}\cdots(j\omega_n)^{l_n} \\ \Psi_{n,uy} = \sum_{q=1}^{n-1}\sum_{p=1}^{n-q}\sum_{l_1,l_{p+q}=0}^{L}\left[c_{p,q}(l_1,\cdots,l_{p+q})H_{n-q,p}(\omega_1,\cdots,\omega_{n-q})(j\omega_{n-q+1})^{l_{p+1}}\cdots(j\omega_n)^{l_{p+q}}\right] \\ \Psi_{n,y} = \sum_{p=2}^{n}\sum_{l_1,l_p=0}^{L}\left[c_{p,0}(l_1,\cdots,l_p)H_{n,p}(\omega_1,\cdots,\omega_n)\right] \end{cases} \tag{3.46}$$

and for the NARX model,

$$\begin{cases} \bar{H}(j\omega) = \left[1-\sum_{k_1=1}^{K} c_{1,0}(k_1)\exp(-j\omega k_1 \Delta t)\right]^{-1} \\ V_n(j\omega) = \frac{1}{\sqrt{n}(2\pi)^{n-1}} \int_{\omega_1+\cdots+\omega_n=\omega} \left(\Psi_{n,u} + \Psi_{n,uy} + \Psi_{n,y}\right) \prod_{i=1}^{n} U(j\omega_i) d\sigma_\omega \end{cases} \tag{3.47}$$

with

$$\begin{cases} \Psi_{n,u} = \sum_{k_1,k_n=1}^{K} c_{0,n}(k_1,\cdots,k_n)\exp(-j(\omega_1 k_1 + \cdots + \omega_n k_n)\Delta t) \\ \Psi_{n,uy} = \sum_{q=1}^{n-1}\sum_{p=1}^{n-q}\sum_{k_1,k_{p+q}=1}^{K}\left[c_{p,q}(k_1,\cdots,k_{p+q})H_{n-q,p}(\omega_1,\cdots,\omega_{n-q})\exp(-j(\omega_{n-q+1}k_{p+1}+\cdots+\omega_n k_{p+q})\Delta t)\right] \\ \Psi_{n,y} = \sum_{p=2}^{n}\sum_{k_1,k_p=1}^{K}\left[c_{p,0}(k_1,\cdots,k_p)H_{n,p}(\omega_1,\cdots,\omega_n)\right] \end{cases} \tag{3.48}$$

It is obvious that (3.44) is the frequency domain representation of a linear system, where $\bar{H}(j\omega)$ is the

frequency response function and $V_n(j\omega)$ is the input spectrum of this linear system. By applying the

inverse Fourier Transform/ inverse Discrete Time Fourier Transform on both sides of equation (3.44), this linear system can be described in the time domain as

$$f_{\text{lin}}\left[y_n\left(t \right) \right] = v_n\left(t \right), n = 1, \ldots, N \tag{3.49}$$

for the continuous time case and

$$f_{\text{lin}}\left[y_n\left(k \right) \right] = v_n\left(k \right), n = 1, \ldots, N \tag{3.50}$$

for the discrete time case, respectively, where $v_n\left(t \right)$ is the inverse Fourier Transform of $V_n\left(j\omega \right)$, $v_n\left(k \right)$ is the inverse Discrete Time Fourier Transform of $V_n\left(j\omega \right)$, and $f_{\text{lin}}\left[. \right]$ denotes a linear differential or difference operator.

Equations (3.49) and (3,50) are referred to as the Generalized Associated Linear Equations (GALEs) of the system NDE model (2.1) and NARX model (2.6), respectively, where $y_n\left(t \right)$ and $y_n\left(k \right)$ are the n th order output in the continuous and discrete time Volterra series representations of a nonlinear system, respectively, with $n = 1, \ldots, N$. Based on GALEs, $y_n\left(t \right)$ and $y_n\left(k \right)$, $n = 1, \ldots, N$, can be readily be determined by solving N simple linear differential and difference equations, respectively. This can significantly facilitate the analysis of nonlinear systems in many applications.

It can be seen that for a Duffing equation, the GALEs are the same as the ALEs (3.3) that can also be obtained by using the perturbation method [111]. In the next section, an effective approach will be derived to determine the GALEs for the NARX model (2.6) of nonlinear systems. The approach will then be extended to continuous time nonlinear systems to derive an approach for the determination of the GALEs of the NDE model (2.1) of nonlinear systems.

3.3.2 Determination of the GALEs

For the convenience of derivation, an integration operator is first introduced as

$$\mathop{\aleph}_{\omega_1 + \cdots + \omega_n = \omega}\left[. \right] = \frac{1}{\sqrt{n}\left(2\pi \right)^{n-1}} \int_{\omega_1 + \cdots + \omega_n = \omega}\left[. \right] \mathrm{d}\sigma_\omega \tag{3.51}$$

In order to determine the GALEs of nonlinear systems, two Lemmas are proposed as follows.

Lemma 3.1. *The derivative property of the Discrete Time Fourier Transform is given as*

$$DF\left[D^n w\left(t \right) \right] = \left(j\omega \right)^n W\left(j\omega \right) \tag{3.52}$$

where $DF\left[. \right]$ represents the normalised Discrete Time Fourier Transform, $-\pi f_s \le \omega \le \pi f_s$ and $W\left(j\omega \right)$ is the spectrum of the time domain signal $w\left(t \right)$.

Proof of Lemma 3.1. The result can be obtained by referring to Section 2.2 in [112].

Lemma 3.2. *The Fourier Transform of the production of n time domain signals $w_i(t), i = 1,..,n$ can be calculated as*

$$DF\left[\prod_{i=1}^{n} w_i(t)\right] = \underset{\omega_1 + \cdots + \omega_n = \omega}{\aleph}\left[\prod_{i=1}^{n} W_i(j\omega_i)\right] \tag{3.53}$$

where $W_i(j\omega_i) = DF\left[w_i(t)\right]_{\omega = \omega_i}$ is the spectrum of the time domain signal $w_i(t)$.

Proof of Lemma 3.2. The result can be obtained by referring to Section 2.4 in [112].

From Lemmas 3.1 and 3.2 and using the operators defined in (3.51), it can be shown that the GALEs of the NARX model (2.6) of nonlinear systems can be obtained by using Proposition 3.2 as follows.

Proposition 3.2. *The GALEs of the NARX model (2.6) of nonlinear systems can be determined as*

$$\begin{aligned}
y_n(k) &= \sum_{k_1=1}^{K} c_{1,0}(k_1) y_n(k-k_1) + \sum_{k_1,k_n=1}^{K} c_{0,n}(k_1,\cdots,k_n) \prod_{i=1}^{n} u(k-k_i) \\
&+ \sum_{q=1}^{n-1}\sum_{p=1}^{n-q}\sum_{k_1,k_{p+q}=1}^{K} c_{p,q}(k_1,\cdots,k_{p+q}) y_{n-q,p}(k) \prod_{i=p+1}^{p+q} u(k-k_i) \\
&+ \sum_{p=2}^{n}\sum_{k_1,k_p=1}^{K} c_{p,0}(k_1,\cdots,k_p) y_{n,p}(k)
\end{aligned} \tag{3.54}$$

where $n \geq 1$ and

$$y_{n,p}(k) = \sum_{i=1}^{n-(p-1)} y_i(k-k_p) \times y_{n-i,p-1}(k) \quad and \quad y_{n,1}(k) = y_n(k-k_1) \tag{3.55}$$

Proof of Proposition 3.2: The n th order GFRFs (2.18) can symbolically be represented as

$$\Psi_n = \Psi_{n,u} + \Psi_{n,uy} + \Psi_{n,y} \tag{3.56}$$

where $\Psi_{n,u}, \Psi_{n,uy}$ and $\Psi_{n,y}$ are shown in (3.48) and

$$\Psi_n = \left[1 - \sum_{k_1=1}^{K} c_{1,0}(k_1)\exp\left(-j(\omega_1 + \cdots + \omega_n)k_1\Delta t\right)\right] H_n(\omega_1,\cdots,\omega_n) \tag{3.57}$$

Consider the hyperplane integration

$$\begin{aligned}
\underset{\omega_1 + \cdots + \omega_n = \omega}{\aleph}\left[\Psi_n \prod_{i=1}^{n} U(j\omega_i)\right] &= \underset{\omega_1 + \cdots + \omega_n = \omega}{\aleph}\left[\Psi_{n,u} \prod_{i=1}^{n} U(j\omega_i)\right] \\
&+ \underset{\omega_1 + \cdots + \omega_n = \omega}{\aleph}\left[\Psi_{n,uy} \prod_{i=1}^{n} U(j\omega_i)\right] + \underset{\omega_1 + \cdots + \omega_n = \omega}{\aleph}\left[\Psi_{n,y} \prod_{i=1}^{n} U(j\omega_i)\right]
\end{aligned} \tag{3.58}$$

The left hand side of (3.58) can be arranged as

$$\underset{\omega_1+\cdots+\omega_n=\omega}{\aleph}\left[\Psi_n\prod_{i=1}^{n}U\left(j\omega_i\right)\right]=\left[1-\sum_{k_1=1}^{K}c_{1,0}(k_1)\exp\left(-j\omega k_1\Delta t\right)\right]$$

$$\times\underset{\omega_1+\cdots+\omega_n=\omega}{\aleph}\left[H_n\left(\omega_1,\ldots,\omega_n\right)\prod_{i=1}^{n}U\left(j\omega_i\right)\right]=DF\left[y_n(k)\right]-\sum_{k_1=1}^{K}c_{1,0}(k_1)DF\left[y_n(k-k_1)\right]$$

(3.59)

and the right hand side of (3.58) are separately discussed as below.

(A) Hyperplane integration of $\Psi_{n,u}$

The first term on the right hand side of (3.58) can be arranged as

$$\underset{\omega_1+\cdots+\omega_n=\omega}{\aleph}\left[\Psi_{n,u}\prod_{i=1}^{n}U\left(j\omega_i\right)\right]=\sum_{k_1,\,k_n=1}^{K}c_{0,n}\left(k_1,\cdots,k_n\right)\underset{\omega_1+\cdots+\omega_n=\omega}{\aleph}\left[\prod_{i=1}^{n}U\left(j\omega_i\right)\exp\left(-j\omega_i k_i\Delta t\right)\right]$$

$$=\sum_{k_1,\,k_n=1}^{K}c_{0,n}\left(k_1,\cdots,k_n\right)DF\left[\prod_{i=1}^{n}u\left(k-k_i\right)\right]$$

(3.60)

(B) Hyperplane integration of $\Psi_{n,y}$

Denote

$$\underset{\omega_1+\cdots+\omega_n=\omega}{\aleph}\left[H_{n,p}\left(\omega_1,\cdots,\omega_n\right)\prod_{i=1}^{n}U\left(j\omega_i\right)\right]=Y_{n,p}\left(j\omega\right)=DF\left[y_{n,p}(k)\right]$$

(3.61)

where $p=2,\ldots,n$, and according to (2.14) and (2.18), it is known that

$$\underset{\omega_1+\cdots+\omega_n=\omega}{\aleph}\left[H_{n,1}\left(\omega_1,\cdots,\omega_n\right)\prod_{i=1}^{n}U\left(j\omega_i\right)\right]=DF\left[y_{n,1}(k)\right]$$

$$=\underset{\omega_1+\cdots+\omega_n=\omega}{\aleph}\left[H_n\left(\omega_1,\cdots,\omega_n\right)\exp\left(-j\omega k_1\Delta t\right)\prod_{i=1}^{n}U\left(j\omega_i\right)\right]=DF\left[y_n\left(k-k_1\right)\right]$$

(3.62)

Therefore, the third term on the right hand side of (3.58) can be arranged as

$$\underset{\omega_1+\cdots+\omega_n=\omega}{\aleph}\left[\Psi_{n,y}\prod_{i=1}^{n}U\left(j\omega_i\right)\right]=\sum_{p=2}^{n}\sum_{k_1,\,k_p=1}^{K}c_{p,0}\left(k_1,\cdots,k_p\right)\underset{\omega_1+\cdots+\omega_n=\omega}{\aleph}\left[H_{n,p}\left(\omega_1,\cdots,\omega_n\right)\prod_{i=1}^{n}U\left(j\omega_i\right)\right]$$

$$=\sum_{p=2}^{n}\sum_{k_1,\,k_p=1}^{K}c_{p,0}\left(k_1,\cdots,k_p\right)DF\left[y_{n,p}(k)\right]$$

(3.63)

Substituting the n th order GFRF (2.18) into (3.63), yields

$$\underset{\omega_1+\cdots+\omega_n=\omega}{\aleph}\left[H_{n,p}\left(\omega_1,\cdots,\omega_n\right)\prod_{i=1}^{n}U\left(j\omega_i\right)\right]=\sum_{i=1}^{n-(p-1)}\underset{\omega_1+\cdots+\omega_n=\omega}{\aleph}\left[\left(H_i\left(\omega_1,\cdots,\omega_i\right)\exp\left(-j\bar{\omega}k_p\Delta t\right)\prod_{j=1}^{i}U\left(j\omega_j\right)\right)\right.$$

$$\left.\times\left(H_{n-i,p-1}\left(\omega_{i+1},\cdots,\omega_n\right)\prod_{j=i+1}^{n}U\left(j\omega_j\right)\right)\right]=\sum_{i=1}^{n-(p-1)}DF\left[y_i\left(k-k_p\right)\times y_{n-i,p-1}(k)\right]$$

(3.64)

with $\omega_1+\cdots+\omega_i=\bar{\omega}$ and $\omega_{i+1}+\cdots+\omega_n=\omega-\bar{\omega}$.

Consequently,

$$\sum_{p=2}^{n}\sum_{k_1,\,k_p=1}^{K}c_{p,0}\left(k_1,\cdots,k_p\right)DF\left[y_{n,p}(k)\right]=\sum_{p=2}^{n}\sum_{k_1,\,k_p=1}^{K}c_{p,0}\left(k_1,\cdots,k_p\right)DF\left[\sum_{i=1}^{n-(p-1)}y_i\left(k-k_p\right)\times y_{n-i,p-1}(k)\right]$$ (3.65)

(C) Hyperplane integration of $\Psi_{n,uy}$

The second term on the right hand side of (3.58) can be arranged as

$$\underset{\omega_1+\cdots+\omega_n=\omega}{\aleph}\left[\Psi_{n,uy}\prod_{i=1}^{n}U(j\omega_i)\right]=\sum_{q=1}^{n-1}\sum_{p=1}^{n-q}\sum_{k_1,\,k_{p+q}=1}^{K}c_{p,q}\left(k_1,\cdots,k_{p+q}\right)$$
$$\times\underset{\omega_1+\cdots+\omega_n=\omega}{\aleph}\left[\left(H_{n-q,p}\left(\omega_1,\cdots,\omega_{n-q}\right)\prod_{i=1}^{n-q}U(j\omega_i)\right)\left(\prod_{i=p+1}^{p+q}U\left(j\omega_{n-q+i-p}\right)\exp\left(-j\omega_{n-q+i-p}k_i\Delta t\right)\right)\right] \quad (3.66)$$
$$=\sum_{q=1}^{n-1}\sum_{p=1}^{n-q}\sum_{k_1,\,k_{p+q}=1}^{K}c_{p,q}\left(k_1,\cdots,k_{p+q}\right)DF\left[y_{n-q,p}(k)\prod_{i=p+1}^{p+q}u(k-k_i)\right]$$

Consequently, by substituting (3.59), (3.60), (3.63) and (3.66) into (3.58), yields

$$-\sum_{l_1=0}^{L}c_{1,0}(l_1)F\left[D^{l_1}y_n(t)\right]=\sum_{l_1,l_n=0}^{L}c_{0,n}(l_1,\cdots,l_n)F\left[\prod_{i=1}^{n}D^{l_i}u(t)\right]$$
$$+\sum_{q=1}^{n-1}\sum_{p=1}^{n-q}\sum_{l_1,\,l_{p+q}=0}^{L}c_{p,q}(l_1,\cdots,l_{p+q})F\left[y_{n-q,p}(t)\prod_{i=p+1}^{p+q}D^{l_i}u(t)\right] \quad (3.67)$$
$$+\sum_{p=2}^{n}\sum_{l_1,\,l_p=0}^{L}c_{p,0}(l_1,\cdots,l_p)F\left[y_{n,p}(t)\right]$$

where according to (3.65)

$$DF\left[y_{n,p}(k)\right]=DF\left[\sum_{i=1}^{n-(p-1)}y_i(k-k_p)\times y_{n-i,p-1}(k)\right] \quad \text{and} \quad DF\left[y_{n,1}(k)\right]=DF\left[D^{l_1}y_n(k)\right] \quad (3.68)$$

Proposition 3.2 can then be proven by applying the inverse Discrete Time Fourier Transform on both sides of (3.67) and (3.68).

For example, for the NARX model:

$$y(k)=c_{0,1}(1)u(k-1)+c_{1,0}(1)y(k-1)+c_{1,0}(2)y(k-2)+c_{3,0}(1,1,1)y^3(k-1) \quad (3.69)$$

the GALEs can be determined using proposition 3.2 as follows

For $n=1$

$$y_1(k)=c_{0,1}(1)u(k-1)+c_{1,0}(1)y_1(k-1)+c_{1,0}(2)y_1(k-2) \quad (3.70)$$

For $n=2$

$$y_2(k)=c_{1,0}(1)y_2(k-1)+c_{1,0}(2)y_2(k-2)=0 \quad (3.71)$$

For $n=3$

$$y_3(k)=c_{1,0}(1)y_3(k-1)+c_{1,0}(2)y_3(k-2)+c_{3,0}(1,1,1)y_1^3(k-1) \quad (3.72a)$$

where

$$y_{3,3}(k-1)=y_1(k-1)y_{2,2}(k-1)=y_1^2(k-1)y_{1,1}(k-1)=y_1^3(k-1) \quad (3.72b)$$

For $n=4$

$$y_4(k) = c_{1,0}(1)y_4(k-1) + c_{1,0}(2)y_4(k-2) = 0 \tag{3.73a}$$

where

$$y_{4,3}(k-1) = y_1(k-1)y_{3,2}(k-1) + y_2(k-1)y_{2,2}(k-1) = 2y_1^2(k-1)y_2(k-1) = 0 \tag{3.73b}$$

For $n = 5$

$$y_5(k) = c_{1,0}(1)y_5(k-1) + c_{1,0}(2)y_5(k-2) + 3c_{3,0}(1,1,1)y_1^2(k-1)y_3(k-1) \tag{3.74a}$$

where

$$\begin{aligned}
y_{5,3}(k-1) &= y_1(k-1)y_{4,2}(k-1) + y_3(k-1)y_{2,2}(k-1) \\
&= y_1^2(k-1)y_{3,1}(k-1) + y_1(k-1)y_3(k-1)y_{1,1}(k-1) \\
&+ y_3(k-1)y_1(k-1)y_{1,1}(k-1) = 3y_1^2(k-1)y_3(k-1)
\end{aligned} \tag{3.74b}$$

Clearly, by following Proposition 3.2, one can proceed to produce the GALEs associated with a NARX model of nonlinear systems up to any order n of system nonlinearity of interest. The GALEs of the NDE model (2.1) can be obtained in a similar way in Proposition 3.3 as below.

Proposition 3.3. *The GALEs of the NDE model (2.1) of nonlinear systems can be obtained as*

$$\begin{aligned}
-\sum_{l_1=0}^{L}c_{1,0}(l_1)D^{l_1}y_n(t) &= \sum_{l_1,l_n=0}^{L}c_{0,n}(l_1,\cdots,l_n)\prod_{i=1}^{n}D^{l_i}u(t) \\
&+ \sum_{q=1}^{n-1}\sum_{p=1}^{n-q}\sum_{l_1,l_{p+q}=0}^{L}c_{p,q}(l_1,\cdots,l_{p+q})y_{n-q,p}(t)\prod_{i=p+1}^{p+q}D^{l_i}u(t) \\
&+ \sum_{p=2}^{n}\sum_{l_1,l_p=0}^{L}c_{p,0}(l_1,\cdots,l_p)y_{n,p}(t)
\end{aligned} \tag{3.75}$$

where $n \geq 1$ and

$$y_{n-q,p}(t) = \sum_{i=1}^{n-(p-1)}D^{l_p}y_i(t)\times y_{n-i,p-1}(t) \quad and \quad y_{n,1}(t) = D^{l_1}y_n(t) \tag{3.76}$$

Proof of Proposition 3.3. The proof can be done in a way similar to the proof of Proposition 3.2.

For example, the GALEs of the Duffing model (2.3) can be determined using Proposition 3.3 as follows.

For $n = 1$

$$m\ddot{y}_1(t) + c\dot{y}_1(t) + ky_1(t) = u(t) \tag{3.77}$$

For $n = 2$

$$m\ddot{y}_2(t) + c\dot{y}_2(t) + ky_2(t) = 0 \tag{3.78}$$

For $n = 3$

$$m\ddot{y}_3(t) + c\dot{y}_3(t) + ky_3(t) = -k_{n3}y_{3,3}(t) \tag{3.79a}$$

where

$$y_{3,3}(t) = y_1(t) y_{2,2}(t) = y_1^2(t) y_{1,1}(t) = y_1^3(t) \tag{3.79b}$$

For $n = 4$

$$m\ddot{y}_4(t) + c\dot{y}_4(t) + ky_4(t) = 0 \tag{3.80a}$$

where

$$y_{4,3}(t) = y_1(t) y_{3,2}(t) + y_2(t) y_{2,2}(t) = 2y_1^2(t) y_2(t) = 0 \tag{3.80b}$$

For $n = 5$

$$m\ddot{y}_5(t) + c\dot{y}_5(t) + ky_5(t) = -k_{n3} y_{5,3}(t) \tag{3.81a}$$

where

$$\begin{aligned} y_{5,3}(t) &= y_1(t) y_{4,2}(t) + y_3(t) y_{2,2}(t) = y_1^2(t) y_{3,1}(t) \\ &+ y_1(t) y_3(t) y_{1,1}(t) + y_3(t) y_1(t) y_{1,1}(t) = 3y_1^2(t) y_3(t) \end{aligned} \tag{3.81b}$$

The GALEs that can readily be determined using Propositions 3.2 and 3.3 from the NARX and NDE models of nonlinear systems, respectively, are a group of linear difference equations with regard to the nth order nonlinear output $y_n(k), n = 1, \ldots, N$, and a group of linear differential equations with regard to the nth order discrete time nonlinear output $y_n(t), n = 1, \ldots, N$. From the GALEs, the output components contributed by any order of system nonlinearity in the Volterra series representation of nonlinear systems can easily be evaluated, and this has never been achieved before. Different applications of the GALEs to the analysis of nonlinear systems will be studied in the next section to demonstrate the practical significance of these new results.

3.4 System analyses using the GALEs

3.4.1 Evaluation of the output response of nonlinear systems

It is a common practice to evaluate the output response for the analysis of the behaviours of nonlinear systems in the time domain, and this is frequently conducted by numerical simulations using numerical integration techniques such as Runge-Kutta method. But, for systems which are described by more complicated NDEs, the numerical solutions can be inaccurate and even unstable [113]. In these cases, the GALEs have potential to be used to produce more accurate and stable solutions. This is because the GALEs enable the numerical simulation to be conducted by only dealing with a series of linear differential equations. This potential application of the GALEs will be demonstrated in a case study in the following.

Consider the NDE model of a nonlinear system

$$\dot{y}(t) + u(t) y(t) = u(t) \tag{3.82}$$

where $u(t) = 10\cos(\omega t)$ and $\omega = 100 \text{ rad/s}$.

The output response of system (3.82) can be analytically determined as

$$y(t) = -\exp\left(-\int u(t)\,dt\right) + \exp\left(-\int u(t)\,dt\right) \times \int u(t)\exp\left(\int u(t)\,dt\right)dt$$
$$= 1 - \exp\left(\frac{-\sin(100t)}{10}\right) \tag{3.83}$$

when $y(0) = 0$.

According to Proposition 3.3, the GALEs of system (3.82) can be obtained as

$$\begin{cases} \dot{y}_1(t) = u(t) \\ \dot{y}_n(t) = -u(t) y_{n-1}(t), n \geq 2 \end{cases} \tag{3.84}$$

Therefore, the output response of system (3.82) can also be obtained by numerically solving N simple linear differential equations as given by (3.84) to produce the components in the system's Volterra series representation $y_1(t), \cdots, y_N(t)$ up to an arbitrary order N of interest, and then find

$$y(t) \approx y_1(t) + \cdots + y_5(t) \tag{3.85}$$

The output response of system (3.82) obtained by solving the GALEs with $N = 5$ using a Runge-Kutta method (ode45 in MATLAB) under the sampling frequency $f_s = 512 \text{ Hz}$ and $f_s = 1024 \text{ Hz}$, respectively, is shown in Fig.1. It is worth pointing out that both sampling frequencies are generally applied in engineering practice for either simulation analysis or experiments due to the requirement of conducting Fast Fourier Transform (FFT) [11, 35]. The analytic result of (3.83) as well as the result obtained by directly solving nonlinear differential equation (3.84) using the Runge-Kutta method are also provided for a comparison in Fig.3.2.
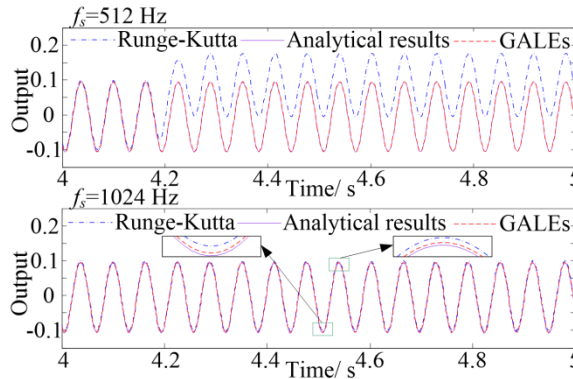

Fig.3.2 The output response of system (3.82) obtained by using different methods

It can be observed from the results in Fig.3.2 that the solution obtained by using the GALEs is much more accurate than the result obtained by directly solving nonlinear differential equation (3.84) using the Runge-Kutta method based numerical integration.

3.4.2 Evaluation of the NOFRFs of nonlinear systems

The NOFRFs is a significant extension of the FRF for linear systems to the nonlinear case as defined in (2.22). Although the NOFRFs have been proposed for many years, currently, the determination of NOFRFs can only be done by using a LS based algorithm [55]. This algorithm requires an appropriate selection of the maximum order N of the system nonlinearity, needs the system response data from several simulation or experimental tests, and sometimes suffer from numerical problems.

Motivated by the need of solving this issue, the GALEs proposed in Propositions 3.2 and 3.3 are applied to accurately determine the NOFRFs. The idea of the GALEs based method is simply summarized in two steps: (i) Determine the n th order system output $y_n(t)$ by solving the GALEs of the system model; (ii) Evaluate the n th order NOFRF by computing the ratio of $Y_n(j\omega)$ and $U_n(j\omega)$. A case study will be used in following to demonstrate the application of the GALEs to the determination of the NOFRFs.

Duffing system with nonlinear damping described by the NDE model

$$\ddot{y}(t) + c_l \dot{y}(t) + k_l y(t) + k_{n3} y^3(t) + c_{n3} \dot{y}^3(t) = u(t) \tag{3.86}$$

will be used to demonstrate the novel GALEs based method for the evaluation of the NOFRFs.
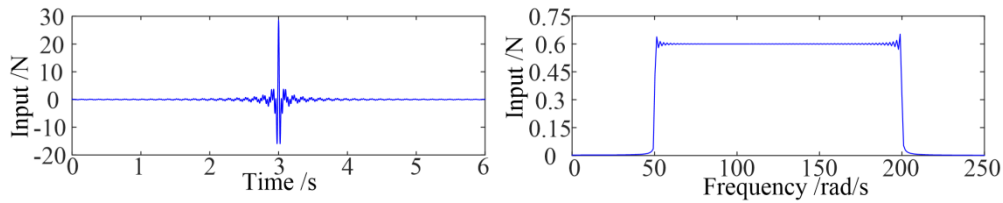
Fig.3.3 The band width input signal

Consider the case where system (34) is subject to the band limited input

$$u(t) = \frac{0.6}{\pi} \frac{\sin(200(t-3)) - \sin(50(t-3))}{t-3}; t \in [0, 6] \sec \tag{3.87}$$

as shown in Fig.3.3 in both the time and the frequency domain.

The NOFRFs of system (3.86) can be evaluated by using the GALEs based approach following three steps as below.

Step 1: Determine the GALEs.

According to Proposition 3.3, the GALEs of the system associated with the system nonlinear outputs up to the 5th order can be formulated as

$$\begin{cases} m\ddot{y}_1(t) + c_l\dot{y}_1(t) + k_l y_1(t) = u(t) \\ m\ddot{y}_3(t) + c_l\dot{y}_3(t) + k_l y_3(t) = -k_{n3}y_1^{\,3}(t) - c_{n3}\dot{y}_1^{\,3}(t) \\ m\ddot{y}_5(t) + c_l\dot{y}_5(t) + k_l y_5(t) = -3k_{n3}y_1^{\,2}(t)y_3(t) - 3c_{n3}\dot{y}_1^{\,2}(t)\dot{y}_3(t) \end{cases} \tag{3.88}$$

Step 2: Solve the GALEs numerically and find the spectrum of the solution.

This is to determine $y_n(t)$ for $n = 1,3,5$ by numerically solving differential equations (3.88) and then

evaluate the Fourier Transform of the results to get $Y_n(j\omega)$, $n = 1,3,5$.

Step 3: Evaluate the NOFRFs

Compute the system NOFRFs as

$$G_n(j\omega) = \frac{Y_n(j\omega)}{U_n(j\omega)}, \; n = 1,3,5 \tag{3.89}$$

using $Y_n(j\omega)$ obtained in Step 2 and $U_n(j\omega)$, the Fourier Transform of $u^n(t)$, for $n = 1,3,5$.

Fig.3.4 shows the NOFRFs $G_1(j\omega), G_3(j\omega)$ and $G_5(j\omega)$ evaluated for the case where the values of

the parameters in the NDE model (3.86) are $c_l = 40 \text{ N/ms}^{-1}$, $k_l = 1 \times 10^4 \text{ N/m}$, $c_{n3} = 3 \times 10^3 \text{ Ns}^3/\text{m}^3$ and

$k_{n3} = 5 \times 10^8 \text{ N/m}^3$, showing three Bode diagram like plots representing the first, third and fifth order

nonlinear characteristics of the system, respectively.
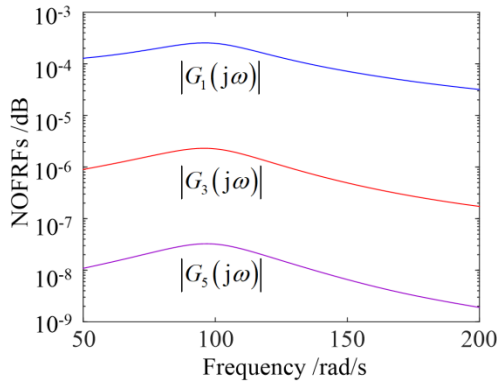
Fig.3.4 The NOFRFs evaluated using the GALEs based method
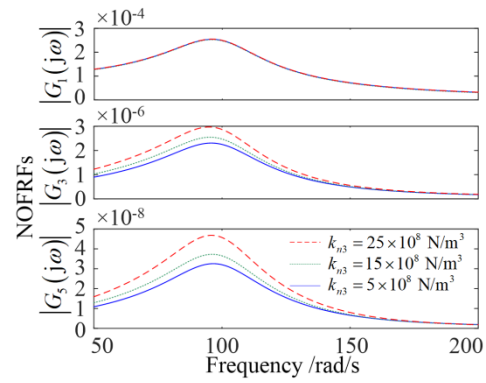
Fig.3.5 The changes of the NOFRFs with the changes in the nonlinear stiffness parameter k_{n3} of system (34)

One practical significance of the NOFRFs is that the concept can be exploited to not only represent the

system characteristics associated with different order system nonlinearities but also indicate how these

system properties change with the changes in the system characteristic parameters.

Fig.3.5 shows how the NOFRFs of system (3.87) evaluated using the GALEs based method can be used to

represent the changes of the nonlinear stiffness parameter k_{n3} in system (3.87). This observation is the basis

of the application of the NOFRFs based analysis to the condition monitoring and fault diagnosis of

engineering systems and structures. In this application, the NDE model of the engineering system under study is often not available. Therefore, a data driven NARX model of the system needs to be established first using a nonlinear system identification method. Then, Proposition 3.2 can be applied to evaluate the NOFRFs of the system. After that, a comparison of the obtained NOFRFs with a base line can be used to monitor any changes in the system characteristic parameters for the purpose of the system condition monitoring and fault diagnosis.

3.4.3 Evaluation of the OFRF of nonlinear systems

The OFRF of nonlinear systems reveals a significant link between the system output frequency response and the parameters as defined in (2.31), and can therefore facilitate a systematic design of nonlinear systems. It has been introduced in Section 2 that, in order to determine the OFRF represention of nonlinear systems, the structure of the OFRF representation should be first determined by using the recursive algorithm in (2.32), then the LS method (2.35) is applied to evaluate the coefficients of the OFRF representation. However, such method requires an appropriate selection of the maximum order N of the OFRF representation, and a significant number of numerical simulations are needed to generate the system responses under different values of the system design parameters.

Noticing that by using the GALEs of nonlinear systems, the n th order nonlinearity of nonlienar systems can be separately discussed, it is then applied in the evaluation of the system OFRF representation, where the number of numerical simulations for determining the OFRF is significantly reduced. Moreover, the OFRF representation can be accurately determined from the low order to an arbitrary high order to avoid the truncation error in the traditional evaluation method in Section 2. The case study in 3.4.2 above is used in this section to illustrate the evaluation of the OFRF using the GALEs.

System (3.86) is considered under the harmonic input

$$u(t) = A\cos(\omega_F t) \tag{3.90}$$

where the $A = 1$ is the input magnitude, and $\omega_F = 100 \text{ rad/s}$.

The OFRF of the system (3.86) up to $N = 5$ are determined by using GALEs with following steps.

Step 1: Determine the structure of the OFRF

The monomial vectors of each order's OFRF representation C_n can be determined by using (2.33) as

$$C_1 = [1], C_3 = [c_{n3}, k_{n3}], C_5 = \left[c_{n3}{}^2, c_{n3}k_{n3}, k_{n3}{}^2 \right] \tag{3.91}$$

such that the OFRF of the system (3.86) up to $N = 5$ can be written as

$$Y\left(j\omega_F\right) = Y_1\left(j\omega_F\right) + Y_3\left(j\omega_F\right) + Y_5\left(j\omega_F\right) \qquad (3.92)$$

where

$$\begin{cases} Y_1\left(j\omega_F\right) = \lambda_{(0,0)}\left(j\omega_F\right) \\ Y_3\left(j\omega_F\right) = \lambda_{(1,0)}\left(j\omega_F\right)c_{n3} + \lambda_{(0,1)}\left(j\omega_F\right)k_{n3} \\ Y_5\left(j\omega_F\right) = \lambda_{(2,0)}\left(j\omega_F\right)c_{n3}^{\ 2} + \lambda_{(1,1)}\left(j\omega_F\right)c_{n3}k_{n3} + \lambda_{(0,2)}\left(j\omega_F\right)k_{n3}^{\ 2} \end{cases} \qquad (3.93)$$

and $\lambda_{(j_1,j_2)}\left(j\omega_F\right)$, $j_1, j_2 = 0, 1, \ldots$ are OFRF coefficients with respect to the frequency variable ω_F.

Step 2: Solve the GALEs of the nonlinear system

Solve the GALEs (3.75) of the system (3.86) under 3 pairs of different nonlinear characteristic parameters

$$\left\{c_{n3,1}, k_{n3,1}\right\} = \left\{0.1\times10^3, 1\times10^8\right\}, \ \left\{c_{n3,2}, k_{n3,2}\right\} = \left\{1.5\times10^3, 2\times10^8\right\}, \ \text{and} \ \left\{c_{n3,3}, k_{n3,3}\right\} = \left\{2\times10^3, 3\times10^8\right\} (3.94)$$

yield 3 sets of $y_1(t)$, $y_3(t)$ and $y_5(t)$ and their spectra, which are combined in vectors

$$\begin{cases} \mathbf{Y}_1 = \left[Y_1\left(j\omega_F\right)\right] \\ \mathbf{Y}_n = \left[Y_{n,(1)}\left(j\omega_F\right),\ldots,Y_{n,(3)}\left(j\omega_F\right)\right]^T, n = 3,5 \end{cases} \qquad (3.95)$$

Step 3: Compute the OFRF coefficients by using the LS method

Compute the third and the fifth order coefficients by using the LS method as

$$\Lambda_n = \left(\mathbf{C}_{n,v}^{\ T}\mathbf{C}_{n,v}\right)^{-1}\mathbf{C}_{n,v}^{\ T}\mathbf{Y}_n, n = 1,3,5 \qquad (3.96)$$

where

$$\mathbf{C}_{1,v} = [1], \mathbf{C}_{3,v} = \begin{bmatrix} c_{n3,1} & k_{n3,1} \\ c_{n3,2} & k_{n3,2} \end{bmatrix}, \mathbf{C}_{5,v} = \begin{bmatrix} c_{n3,1}^{\ 2} & c_{n3,1}k_{n3,1} & k_{n3,1}^{\ 2} \\ c_{n3,2}^{\ 2} & c_{n3,2}k_{n3,2} & k_{n3,2}^{\ 2} \\ c_{n3,3}^{\ 2} & c_{n3,2}k_{n3,3} & k_{n3,3}^{\ 2} \end{bmatrix} \qquad (3.97)$$

The output spectra predicted by the evaluated OFRF are plotted in Fig.3.6, comparing with the true output

spectrum obtained by using the Runge-Kutta simulation.
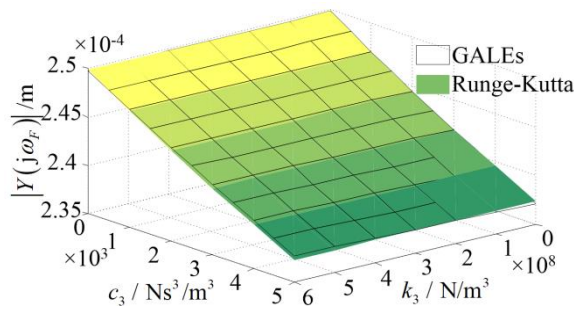


Fig.3.6 The GALEs evaluated OFRF

Fig.3.6 indicates that the GALEs base evaluation of the system OFRF is accurate. More important, only 3

pairs of testing parameters (3.94) are needed to determine the OFRF by using the GALEs, comparing with

that at least the 7 pairs testing parameters are required in the traditional LS evaluation method. Moreover, the LS algorithm used for each order's GALEs can evaluate the OFRF coefficients accurately because the structure of the GALEs is unique without truncation errors.

Tab.3.1 provides a comprehensive comparison of the newly proposed GALEs based system analysis with the existing techniques. The conclusions are reached based on the discussion above, indicating the GALEs analysis has significant advantages over the existing methods.

Tab.3.1 Comparison of the GALEs and existing techniques

Nonlienar system simulation	
GALEs	*Runge-Kutta*
Stable	Unstable under certain conditions
NOFRF based condition monitoring	
GALEs	*LS*
Conducted online/ offline	Conducted offline only
OFRF based design	
GALEs	*LS*
Less training parameters required	More training parameters required

In the next section, the application of the GALEs to nonlinear system modelling, fault diagnosis, and design will be further discussed.

3.5 Application of the GALEs to nonlinear system modelling, fault diagnosis, and design

3.5.1 Application to the identification of the NDE model of a nonlinear system

The GALEs based NDE model identification basically exploits the equivalence of the nonlinear output spectra of the NDE and NARX models of the same system, known as Nonlinear Spectrum Invariance Method (NSIM). The NARX model can be identified by using a nonlinear system identification method from the input and output data of the system under study, thus, the nonlinear output spectra up to an arbitrary order of system nonlinearity can be obtained by determining and solving the GALEs for the NARX model following Proposition 3.2. Then, from the GALEs formulation of the NDE model of the same system, and the having obtained nonlinear output spectra, the physically meaningful parameters in the NDE model of the system can be obtained so as to find the NDE model of the system. Compared to available techniques which

are based on the equivalence of the GFRFs of the NDE and NARX models of the same system, known as the Kernel Invariant Method (KIM) [48,114], the new NSIM based approach only deals with one-dimensional functions and can fundamentally resolve the difficulties associated with the KIM when dealing with higher order system nonlinearities. In the following, a case study will be provided to demonstrate how to apply the GALEs and NSIM to the identification of the NDE model of a nonlinear system.

Consider the unplugged van der Pol system [115]:

$$m\ddot{y}(t) + c_l \dot{y}(t) + k_l y(t) + c_E y^2(t) \dot{y}(t) = u(t) \tag{3.98}$$

where $m = 1\,\text{Kg}$, $c_l = 50\,\text{Ns/m}$, $k_l = 10^4\,\text{N/m}$ and $c_E = 3 \times 10^6\,\text{Ns/m}^3$.

Assume that parameters m, c_l, k_l and c_E with the system are unknown but the structure of the NDE model is known a priori. Consequently, the identification of the NDE model (3.98) becomes the problem of the estimation of parameters m, c, k and c_E of the system, which can be addressed by using the following 4 steps.

Step 1: Identify the NARX model of the system.

From the sampled data of the response of system (3.98) to the random input

$$u(t) = 20 \times \text{rand}(t)\,\text{N} \tag{3.99}$$

under the sampling frequency of $f_s = 512\,\text{Hz}$, where $\text{rand}(t)$ is a random signal uniformly distributed in $[-1,1]$, a NARX model of the system was identified using the NARMAX approach [11] as

$$\begin{aligned} y(k) &= 1.871 y(k-1) - 0.907 y(k-2) + 3.590 \times 10^{-6} u(k-1) \\ &\quad + 5.271 \times 10^3 y^2(k-1) y(k-2) - 5.202 \times 10^3 y^3(k-1) \end{aligned} \tag{3.100}$$
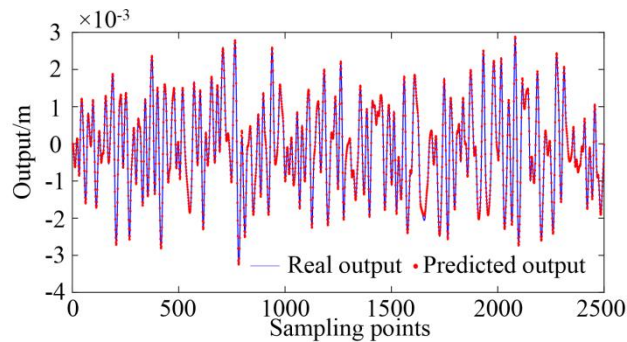

Fig.3.7 The NARX model of the system

Fig.3.7 shows a comparison between the real and the NARX model predicted outputs of the system, indicating an excellent performance of the identified NARX model (3.100).

Step 2: Determine the GALEs of the nonlinear NDE model

The GALEs of the unplugged van der Pol system (3.98) up to the third order was obtained using Proposition 3.3 as

$$
\begin{cases}
m\ddot{y}_1(t) + c_l\dot{y}_1(t) + k_l y_1(t) = u(t) \\
m\ddot{y}_3(t) + c_l\dot{y}_3(t) + k_l y_3(t) = -c_E y_1^2(t)\dot{y}_1(t)
\end{cases}
\tag{3.101}
$$

Step 3: Estimate the unknown parameters m, c_l, k_l in the NDE model

(a): Taking the Fourier Transform on both sides of the first order GALE, yields

$$
\frac{c_l}{k_l}Y_1(j\omega)(j\omega) + \frac{m}{k_l}Y_1(j\omega)(j\omega)^2 + \frac{1}{k_l}U(j\omega) = -Y_1(j\omega)
\tag{3.102}
$$

where

$$
\bar{C}_1 = \left[\frac{c_l}{k_l}, \frac{m}{k_l}, \frac{1}{k_l}\right]^{\mathrm{T}}
\tag{3.103}
$$

are normalized linear parameters to be estimated.

Evaluating the first order output $y_1(k)$ and its spectrum $Y_1(j\omega)$ under the band limited input (3.87) using the GALEs of the NARX model (3.54)-(3.55) at the frequencies of $\bar{\omega}_1 = 50 \text{ rad/s}$, $\bar{\omega}_2 = 100 \text{ rad/s}$ and $\bar{\omega}_3 = 200 \text{ rad/s}$, repectively, yields the results shown in Tab.3.2.

Tab.3.2 The first order nonlinear output spectrum at three frequencies evaluated using the GALEs of NARX model

(3.55)

	$\bar{\omega}_1 = 50 \text{ rad/s}$	$\bar{\omega}_2 = 100 \text{ rad/s}$	$\bar{\omega}_3 = 200 \text{ rad/s}$
$Y_1(j\bar{\omega}_i)$	$0.1389 \times 10^{-5} - 0.3969 \times 10^{-6}\mathrm{i}$	$-0.4489 \times 10^{-5} + 0.3978 \times 10^{-4}\mathrm{i}$	$-0.6088 \times 10^{-5} - 0.3427 \times 10^{-5}\mathrm{i}$

(b): Estimate the values of the three parameters in (3.103) by using the LS method as

$$
\bar{C}_1 = \left(\bar{P}_1^{\mathrm{T}}\bar{P}_1\right)^{-1}\bar{P}_1^{\mathrm{T}}\bar{Y}_1
\tag{3.104}
$$

where

$$
\bar{Y}_1 = \begin{bmatrix} \mathrm{Re}[Y_1] \\ \cdots \\ \mathrm{Im}[Y_1] \end{bmatrix} \quad \text{and} \quad \bar{P}_1 = \begin{bmatrix} \mathrm{Re}[P_1] \\ \cdots \\ \mathrm{Im}[P_1] \end{bmatrix}
\tag{3.105}
$$

with

$$
Y_1 = \left[Y_1(j\bar{\omega}_1), Y_1(j\bar{\omega}_2), Y_1(j\bar{\omega}_3)\right]^{\mathrm{T}}
\tag{3.106}
$$

and

$$P_1 = \begin{bmatrix} Y_1(j\bar{\omega}_1)(j\bar{\omega}_1) & Y_1(j\bar{\omega}_1)(j\bar{\omega}_1)^2 & U(j\bar{\omega}_1) \\ Y_1(j\bar{\omega}_2)(j\bar{\omega}_2) & Y_1(j\bar{\omega}_2)(j\bar{\omega}_2)^2 & U(j\bar{\omega}_2) \\ Y_1(j\bar{\omega}_3)(j\bar{\omega}_3) & Y_1(j\bar{\omega}_3)(j\bar{\omega}_3)^2 & U(j\bar{\omega}_3) \end{bmatrix} \tag{3.107}$$

yielding

$$\bar{C}_1 = [-49.1012, -0.9826, 0.9901] \times 10^{-4} \tag{3.108}$$

Step 4: Estimate the unknown parameter c_E in the NDE model

(a): Taking the Fourier Transform on both sides of the third order GALE in (3.101) yields

$$\frac{1}{k_l} Y_3(j\omega) + \frac{c_l}{k_l} Y_3(j\omega)(j\omega) + \frac{m}{k_l} Y_3(j\omega)(j\omega)^2 = \frac{c_E}{k_l} F\left[y_1^2(t)\dot{y}_1(t)\right] \tag{3.109}$$

where

$$\bar{C}_3 = \left[\frac{c_E}{k}\right] \tag{3.110}$$

are normalized nonlinear parameters to be estimated.

Evaluating the third order output $y_3(k)$ and then its spectrum $Y_3(j\omega)$ under the band limited input (3.87) using the GALEs of the NARX model (3.54)-(3.55) at the frequency $\bar{\omega}_2 = 100$ rad/s yields

$$Y_3(j\bar{\omega}_2) = 0.2572 \times 10^{-6} - 0.3277 \times 10^{-5}i \tag{3.111}$$

Moreover, using $y_1(t)$ obtained in Step 3 (a), $F\left[y_1^2(t)\dot{y}_1(t)\right]$ is evaluated producing

$$F\left[y_1^2(t)\dot{y}_1(t)\right]_{\omega=\bar{\omega}_2} = -5.6466 \times 10^{-9} - 1.1824 \times 10^{-9}i \tag{3.112}$$

(b): Substituting $Y_3(j\bar{\omega}_2)$ and $F\left[y_1^2(t)\dot{y}_1(t)\right]_{\omega=\bar{\omega}_2}$ into (3.109), the value of parameter c_E can be found as

$$c_E = k_l\bar{C}_3 = \left[2.8105 \times 10^6\right] \tag{3.113}$$

Consequently, the estimated model of system (3.98) is

$$0.9924\ddot{y}(t) + 49.5922\dot{y}(t) + 2.8105 \times 10^6 y^2(t)\dot{y}(t) + 1.0100 \times 10^4 y(t) = u(t) \tag{3.114}$$

A comparison of the output frequency responses of the estimated model (3.114) under the harmonic input

$$u(t) = 10\cos(\omega t), \ \omega \in [0, 300] \text{ rad/s} \tag{3.115}$$

and the band limited random input

$$u(t) = 10 \times \text{rand}(t), \ \text{rand}(t) \in [-1,1] \tag{3.116}$$

respectively with the corresponding responses of the real system (3.98) is shown in Fig.3.8, indicating a very good match of the estimated model's frequency response to the accurate result.
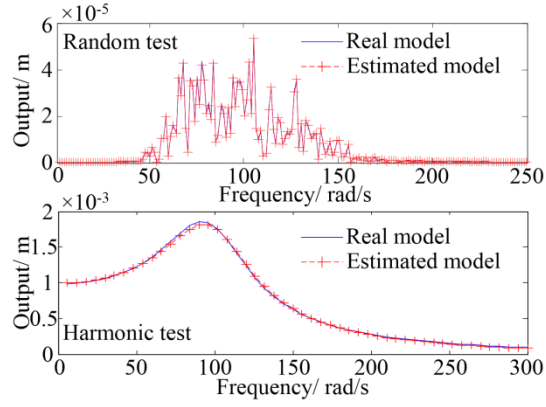
Fig.3.8 Validation of the estimated NDE model

3.5.2 Application to the NOFRFs based fault diagnosis

Beam like structures are widely applied in engineering practice and the fault detection of such structures has been widely studied by researchers [58,116]. A simple cantilever beam with crack is illustrated in Fig.3.9.
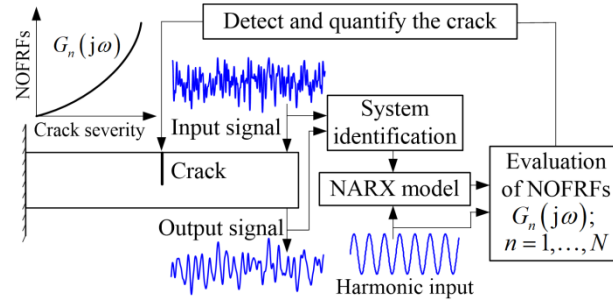
Fig.3.9 The NOFRFs based fault detection of cracked beams

Cracks in beam like structures can often be detected by analyzing the output spectra under a harmonic excitation [116], and the higher order super-harmonic output spectrum is expected to be monotonously increase/ decrease along the increase of the severity of a crack. However, there are many cracks that can generate more complex output responses, making the output spectrum analysis based detection of cracks not applicable in these situations [117,118].

This issue will now be addressed by using the NOFRFs which are more sensitive to variations in nonlinear characteristics in structural systems [58]. The basic idea of the NOFRFs based fault detection is illustrated in Fig.3.9 and the details will be explained below.

Step 1: The NARX model of cracked cantilever beams

In practice, the dynamic properties of a cantilever beam with cracks can often be investigated by using a nonlinear differential equation model with second and forth order nonlinearities such as [117,118]

$$\ddot{y}(t) + c_l \dot{y}(t) + k_l y(t) + k_{n2} y^2(t) - k_{n4} y^4(t) = u(t) \tag{3.117}$$

In this case study, $c_l = 20 \text{ N}/\text{ms}^{-1}$, $k_l = 1 \times 10^3 \text{ N}/\text{m}$, k_{n2} and k_{n4} are the model nonlinear parameters

determined by crack characteristics.

According to the NOFRFs based approach for nonlinear system analysis introduced above, the NARX models of the cracked cantilever beam, under different values of nonlinear parameter k_{n4}, are identified using the input and the output data generated using model (3.117) and the nonlinear system identification method in [11].

For the specific cases of

$$k_{n2} = 1 \times 10^5 \ \text{N/m}^2 \ , \quad k_{n4} = [0, 2, 3.5, 5, 7] \times 10^{10} \ \text{N/m}^4 \ ,$$

and the sampling frequency of $f_s = 1024 \ \text{Hz}$ the identified NARX model are

$$y(k) = a_1 y(k-1) + a_2 y(k-2) + b_1 u(k-1) + c_1 y^2(k-1) + c_2 y^4(k-1) \tag{3.118}$$

where the model coefficients are shown in Tab.3.3.

Tab.3.3 NARX model coefficients under $k_2 = 1 \times 10^5 \ \text{N/m}^2$

$k_4 \times 10^{10}$ N/m⁴	$a_1 \times 10^{-6}$	a_2	b_1	c_1	$c_2 \times 10^4$
0	-0.9436	-1.9797	-0.9807	-0.0938	-
2.0	-0.9438	-1.9797	-0.9807	-0.0935	1.7690
3.5	-0.9437	-1.9797	-0.9807	-0.0935	3.1558
5.0	-0.9436	-1.9797	-0.9807	-0.0930	4.3261
7.0	-0.9435	-1.9797	-0.9807	-0.0940	6.4804

In the next, the newly proposed GALEs based NOFRFs analysis will be applied to the NARX models (3.118) to demonstrate how the novel analysis can reveal the changes of the system nonlinear parameter k_{n4} so as to enable the detection and quantification of cracks in cantilever beams.

Step 2: Determination of the GALEs

Given the NARX model (3.118), the GALEs of the system up to 4th order are obtained as

$$\begin{cases} y_1(k) = a_1 y_1(k-1) + a_2 y_1(k-2) + b_1 u(k-1) \\ y_2(k) = a_1 y_2(k-1) + a_2 y_2(k-2) + c_1 y_1^2(k-1) \\ y_3(k) = a_1 y_3(k-1) + a_2 y_3(k-2) + 2c_1 y_1(k-1) y_2(k-1) \\ y_4(k) = a_1 y_{43}(k-1) + a_2 y_4(k-2) + c_1 y_2^2(k-1) \\ \quad + 2c_1 y_1(k-1) y_3(k-1) + c_2 y_1^4(k-1) \end{cases} \tag{3.119}$$

Step 3: Evaluation of the NOFRFs

Consider the case where system (3.118) is subject to the sinusoidal input $u(t) = A \sin(\omega_F t)$. From the GALEs of system (3.118) determined above, the nonlinear output responses $y_1(k), \ldots, y_N(k)$ of the system

are obtained. Then, the system output spectra contributed by up to the 4th order system nonlinearity, namely,

$Y_1(j\omega_F)$, $Y_2(j2\omega_F)$, $Y_3(j\omega_F)$, $Y_3(j3\omega_F)$, $Y_4(j2\omega_F)$, $Y_4(j4\omega_F)$ are obtained by evaluating the

normalised Discrete Time Fourier Transform of $y_1(k),...,y_4(k)$. Consequently, the NOFRFs $G_1(j\omega_F)$,

$G_2(j2\omega_F)$, $G_3(j\omega_F)$ and $G_4(j2\omega_F)$ are evaluated as

$$G_1(j\omega_F) = \frac{Y_1(j\omega_F)}{U(j\omega_F)}; G_3(j\omega_F) = \frac{Y_3(j\omega_F)}{U_3(j\omega_F)}; G_2(j2\omega_F) = \frac{Y_2(j2\omega_F)}{U_2(j2\omega_F)}; G_4(j2\omega_F) = \frac{Y_4(j2\omega_F)}{U_4(j2\omega_F)} \quad (3.120)$$

where $U(j\omega_F)$, $U_2(j2\omega_F)$, $U_3(j\omega_F)$, $U_4(j2\omega_F)$ are obtained from evaluating the normalised Discrete

Time Fourier Transform of $u(k), u^2(k), u^3(k)$ and $u^4(k)$, respectively.

Moreover, for a specific ω_F, the NOFRFs in (3.120) are evaluated, which is expected to produce an

effective index whose value increases/decreases monotonically with the severity of cracks so as to be able to

be used to detect and quantify the cracks in beam structures.

Step 4: The NOFRF based crack detection

The sinusoidal input with the magnitude of $A = 1 \text{ N}$ and the frequency of $\omega_F = 30 \text{ rad/s}$, which is close

to the resonant frequency of the system, is applied to the NARX model of (3.118) to evaluate $G_2(j2\omega_F)$,

$G_3(j\omega_F)$ and $G_4(j2\omega_F)$ under the five different values of $k_{n4} = [0, 2, 3.5, 5, 7] \times 10^{10} \text{ N/m}^4$.

The results are given in Fig.3.10, showing that $G_4(j2\omega_F)$ monotonously increases with the increase of

k_{n4}, while $G_2(j2\omega_F)$ and $G_3(j\omega_F)$ have no change with the increase of k_{n4}, indicating that the

severity of cracks in the beam can be detected and quantified using the NOFRF $G_4(j2\omega_F)$.
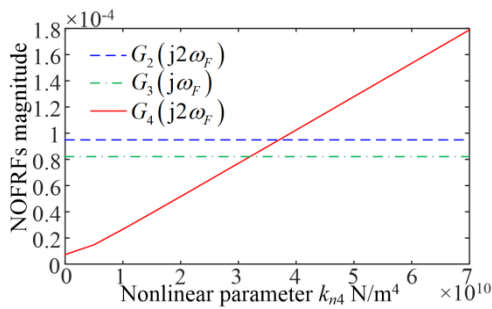
**Fig.3.10** The change of the NOFRFs with respect to k_{n4} at $\omega_F = 30 \text{ rad/s}$
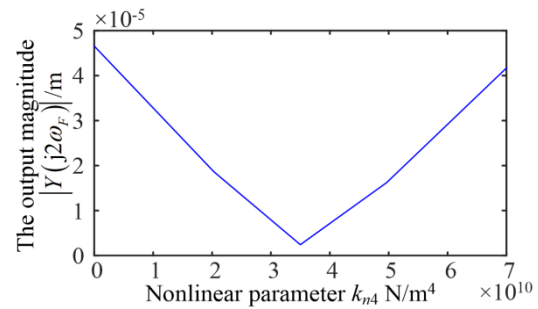
Fig.3.11 The change of $|Y(j2\omega_F)|$ with respect to k_{n4} at $\omega_F = 30 \text{ rad/s}$

For a comparison, the traditional frequency response method introduced in Zhang et al. [118] is also

applied to quantify the increase of parameter k_{n4}. The results are illustrated in Fig.3.11, indicating the

second order super-harmonic magnitudes $\left| Y\left(j2\omega_F \right) \right|$ of the system varies non-monotonically with the increase of the value of k_{n4} and is therefore not suitable for use to detect cracks in this case.

3.5.3 Application to the OFRFs based design of nonlinear energy harvester systems

Consider a SDOF vibration-based energy (VBE) harvester as illustrated in Fig. 3.12 having an isolated mass m and a vibrating base with displacement $y(t)$. The mass is isolated from the base by an isolation system modeled as a nonlinear (electromagnetic) damper connected in parallel to a nonlinear spring. The linear and cubic stiffness coefficients are k_l and k_{n3} respectively while the linear and cubic damping coefficients are c_l and c_{n3} respectively.
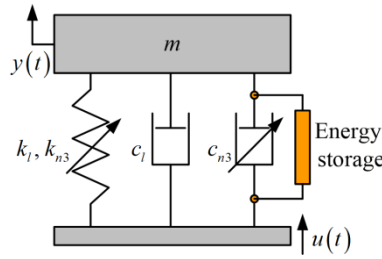
Fig.3.12. SDOF base excited VBE harvester with nonlinear cubic damping

The model of the SDOF VBE harvester is an NDE and the equation of motion of the mass with respect to the relative displacement $y(t)$ is given as [119]

$$m\ddot{y}(t) + c_l\dot{y}(t) + c_{n3}\dot{y}(t)^3 + k_l y(t) + k_{n3} y(t)^3 = -m\ddot{u}(t) \tag{3.121}$$

For a harmonic base displacement with amplitude A, frequency ω_F and zero phase shift, the base displacement is given by

$$u(t) = A\sin\left(\omega_F t\right) \tag{3.122}$$

Therefore,

$$m\ddot{y}(t) + c_l\dot{y}(t) + c_{n3}\dot{y}(t)^3 + k_l y(t) + k_{n3} y(t)^3 = m\omega^2 A\sin\left(\omega_F t\right) \tag{3.123}$$

The nonlinear damping device absorbs an instantaneous power equal to the product of the instantaneous damper force and the relative velocity of the VBE harvester [119]. producing an average power given by

$$P_{av} = \frac{1}{T}\int_0^T \left(c_{n3}\dot{y}(t)^3 \right)\dot{y}(t)\,dt \tag{3.124}$$

For a single-frequency harmonic oscillation where $y(t) = Y\sin\left(\omega_F t\right)$, this yields,

$$P_{av} = \frac{3}{8} c_{n3} \omega_F^{\ 4} Y^4 \tag{3.125}$$

It should be noted that while the cubic damping term in (3.123) is considered to provide harvested energy, c_l is considered a loss. In addition, it can be deduced that since the output frequency response, Y of model (3.123) is a function of ω_F and the nonlinear parameters, c_{n3} and k_{n3}. Therefore P_{av} in (3.125) is a function of c_{n3}, k_{n3} and ω_F. The frequency of interest here is the resonance frequency which is the frequency where maximum power absorption occurs.

The OFRF of the system (3.123) up to $N = 7$ can be determined by using the GALEs based evaluation process in 3.4.3.

The design of the VBE harvester can be conducted following the steps as below.

Step 1: Determine the structure of the OFRF

The monomial vectors of each order's OFRF representation C_n can be determined as

$$\boldsymbol{C}_1 = [1], \boldsymbol{C}_3 = [c_{n3}, k_{n3}], \boldsymbol{C}_5 = \left[c_{n3}^{\ 2}, c_{n3}k_{n3}, k_{n3}^{\ 2} \right], \boldsymbol{C}_7 = \left[c_{n3}^{\ 3}, c_{n3}^{\ 2}k_{n3}, c_{n3}k_{n3}^{\ 2}, k_{n3}^{\ 3} \right] \tag{3.126}$$

such that the OFRF of the system up to $N = 7$ can be written as

$$Y(\mathrm{j}\omega_F) = Y_1(\mathrm{j}\omega_F) + Y_3(\mathrm{j}\omega_F) + Y_5(\mathrm{j}\omega_F) + Y_7(\mathrm{j}\omega_F) \tag{3.127}$$

where

$$\begin{cases} Y_1(\mathrm{j}\omega_F) = \lambda_{(0,0)}(\mathrm{j}\omega_F) \\ Y_3(\mathrm{j}\omega_F) = \lambda_{(1,0)}(\mathrm{j}\omega_F)c_{n3} + \lambda_{(0,1)}(\mathrm{j}\omega_F)k_{n3} \\ Y_5(\mathrm{j}\omega_F) = \lambda_{(2,0)}(\mathrm{j}\omega_F)c_{n3}^{\ 2} + \lambda_{(1,1)}(\mathrm{j}\omega_F)c_{n3}k_{n3} + \lambda_{(0,2)}(\mathrm{j}\omega_F)k_{n3}^{\ 2} \\ Y_7(\mathrm{j}\omega_F) = \lambda_{(3,0)}(\mathrm{j}\omega_F)c_{n3}^{\ 3} + \lambda_{(2,1)}(\mathrm{j}\omega_F)c_{n3}^{\ 2}k_{n3} + \lambda_{(1,2)}(\mathrm{j}\omega_F)c_{n3}k_{n3}^{\ 2} + \lambda_{(0,3)}(\mathrm{j}\omega_F)k_{n3}^{\ 3} \end{cases} \tag{3.128}$$

and $\lambda_{(j_1,j_2)}(\mathrm{j}\omega_F)$, $j_1, j_2 = 0, 1, \ldots$ are the OFRF coefficients with respect to the frequency variable ω_F.

Step 2: Solve the GALEs of the nonlinear system

Subsequent analysis in this study has been done using the following model parameter values; $m = 1\,\mathrm{kg}$, $k_l = 25\,\mathrm{N/m}$, $c_l = 2\,\mathrm{Ns/m}$, $A = 0.05\,\mathrm{m}$, $\omega_n = 5\,\mathrm{rad/s}$, $\Omega = \omega/\omega_n$.

To obtain the OFRF coefficients up to the 7th order, four simulations are required using four different values of $c_{n3,r}$ and $k_{n3,r}$ (where $r = 1, 2, 3, 4$) as given in Tab.3.4.

Tab.3.4. Simulation (Training) values of model parameters

Model nonlinear parameter	Sim1 value	Sim2 value	Sim3 value	Sim4 value
$c_{n3}\left(\mathrm{Ns}^3/\mathrm{m}^3\right)$	0.300	0.325	0.350	0.375
$k_{n3}\left(\mathrm{N}/\mathrm{m}^3\right)$	0	55	110	165

Four sets of spectra are combined in vectors as

$$Y_n = \left[\, Y_{n,(1)}\left(\mathrm{j}\omega_F\right),\ldots,Y_{n,(4)}\left(\mathrm{j}\omega_F\right)\,\right]^{\mathrm{T}},\, n=1,3,5,7 \tag{3.129}$$

Step 3: Compute the OFRF coefficients by using the LS method

The OFRF coefficients are obtained for all frequencies by solving

$$\lambda_{(0,0)}\left(\mathrm{j}\omega_F\right) = Y_{1,(1)}\left(\mathrm{j}\omega_F\right)$$

$$\begin{bmatrix} \lambda_{(1,0)}\left(\mathrm{j}\omega_F\right) \\ \lambda_{(0,1)}\left(\mathrm{j}\omega_F\right) \end{bmatrix} = \begin{bmatrix} c_{n3,1} & k_{n3,1} \\ c_{n3,2} & k_{n3,2} \end{bmatrix}^{-1} \begin{bmatrix} Y_{3,(1)}\left(\mathrm{j}\omega_F\right) \\ Y_{3,(2)}\left(\mathrm{j}\omega_F\right) \end{bmatrix}$$

$$\begin{bmatrix} \lambda_{(2,0)}\left(\mathrm{j}\omega_F\right) \\ \lambda_{(1,1)}\left(\mathrm{j}\omega_F\right) \\ \lambda_{(0,2)}\left(\mathrm{j}\omega_F\right) \end{bmatrix} = \begin{bmatrix} c_{n3,1}{}^2 & c_{n3,1}k_{n3,1} & k_{n3,1}{}^2 \\ c_{n3,2}{}^2 & c_{n3,2}k_{n3,2} & k_{n3,2}{}^2 \\ c_{n3,3}{}^2 & c_{n3,3}k_{n3,3} & k_{n3,3}{}^2 \end{bmatrix}^{-1} \begin{bmatrix} Y_{5,(1)}\left(\mathrm{j}\omega_F\right) \\ Y_{5,(2)}\left(\mathrm{j}\omega_F\right) \\ Y_{5,(3)}\left(\mathrm{j}\omega_F\right) \end{bmatrix} \tag{3.130}$$

$$\begin{bmatrix} \lambda_{(3,0)}\left(\mathrm{j}\omega_F\right) \\ \lambda_{(2,1)}\left(\mathrm{j}\omega_F\right) \\ \lambda_{(1,2)}\left(\mathrm{j}\omega_F\right) \\ \lambda_{(0,3)}\left(\mathrm{j}\omega_F\right) \end{bmatrix} = \begin{bmatrix} c_{n3,1}{}^3 & c_{n3,1}{}^2 k_{n3,1} & c_{n3,1}k_{n3,1}{}^2 & k_{n3,1}{}^3 \\ c_{n3,2}{}^3 & c_{n3,2}{}^2 k_{n3,2} & c_{n3,2}k_{n3,2}{}^2 & k_{n3,2}{}^3 \\ c_{n3,3}{}^3 & c_{n3,3}{}^2 k_{n3,3} & c_{n3,3}k_{n3,3}{}^2 & k_{n3,3}{}^3 \\ c_{n3,4}{}^3 & c_{n3,4}{}^2 k_{n3,4} & c_{n3,4}k_{n3,4}{}^2 & k_{n3,4}{}^3 \end{bmatrix}^{-1} \begin{bmatrix} Y_{7,(1)}\left(\mathrm{j}\omega_F\right) \\ Y_{7,(2)}\left(\mathrm{j}\omega_F\right) \\ Y_{7,(3)}\left(\mathrm{j}\omega_F\right) \\ Y_{7,(4)}\left(\mathrm{j}\omega_F\right) \end{bmatrix}$$

The OFRF generated output spectrum is obtained as

$$\begin{aligned} Y\left(\mathrm{j}\omega_F\right) = {}& \lambda_{(0,0)}\left(\mathrm{j}\omega_F\right) + \lambda_{(1,0)}\left(\mathrm{j}\omega_F\right)c_{n3} + \lambda_{(0,1)}\left(\mathrm{j}\omega_F\right)k_{n3} + \lambda_{(2,0)}\left(\mathrm{j}\omega_F\right)c_{n3}{}^2 \\ & + \lambda_{(1,1)}\left(\mathrm{j}\omega_F\right)c_{n3}k_{n3} + \lambda_{(0,2)}\left(\mathrm{j}\omega_F\right)k_{n3}{}^2 + \lambda_{(3,0)}\left(\mathrm{j}\omega_F\right)c_{n3}{}^3 + \lambda_{(2,1)}\left(\mathrm{j}\omega_F\right)c_{n3}{}^2 k_{n3} \\ & + \lambda_{(1,2)}\left(\mathrm{j}\omega_F\right)c_{n3}k_{n3}{}^2 + \lambda_{(0,3)}\left(\mathrm{j}\omega_F\right)k_{n3}{}^3 \end{aligned} \tag{3.128}$$

To obtain the OFRF of the average power absorbed by the VBE harvester through the nonlinear cubic damper, the OFRF approximation of the output spectrum in (3.128) is substituted in (3.125) which yields

$$P_{av}\left(\mathrm{j}\omega_F\right) = \frac{3}{8}c_{n3}\omega_F{}^4 \left|Y\left(\mathrm{j}\omega_F\right)\right|^4 \tag{3.129}$$

Consequently, the average power absorbed by the electromagnetic damper for a combination of the nonlinear parameter values (c_{n3} and k_{n3}), within and beyond the training range, is estimated and shown in Figs.3.13 and 3.14, respectively, where the relative frequency is defined as the ratio of the output frequency over the natural frequeny of the system $\omega_0 = \sqrt{k_l/m}$. The results shown that the GALEs generated OFRF (GALEs-OFRF) can estimate, accurately, the output spectrum of the VBE harvester system and the average

power it absorbs when the damper parameter values are either within or outside the training range.


|(a)|(b)|
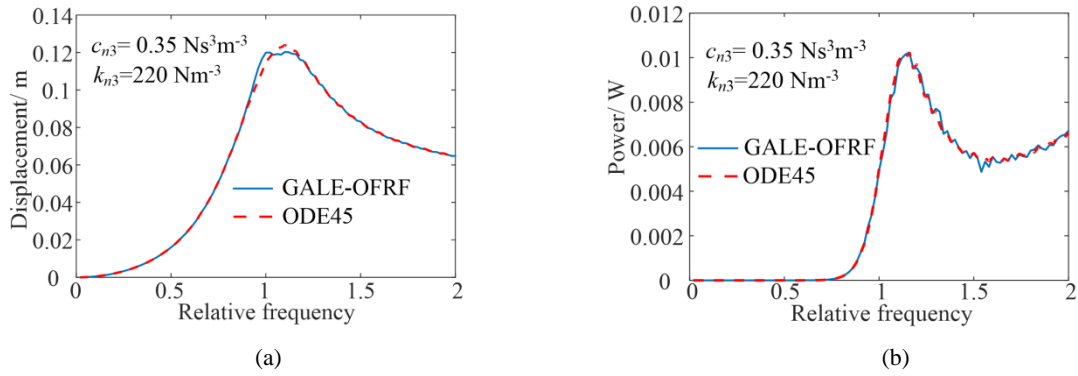
Fig.3.13. GALEs-OFRF evaluated against ODE45 result within the training range of damper parameters

|(a)|(b)|
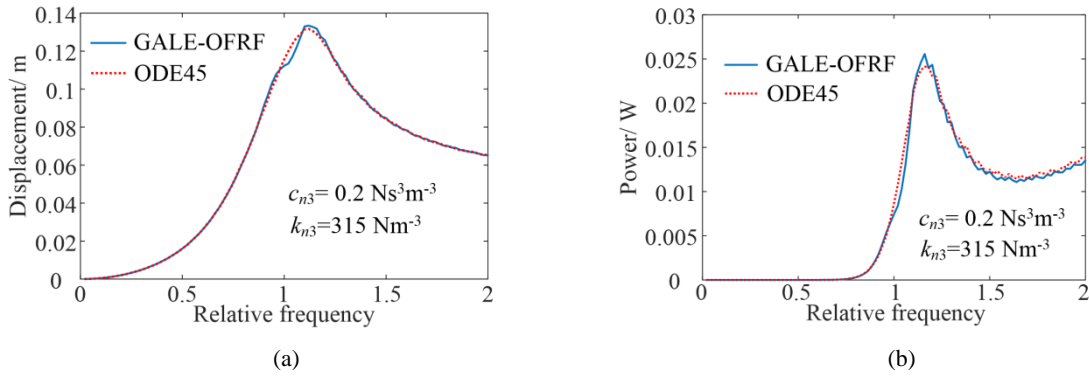
Fig.3.14. GALEs-OFRF evaluated against ODE45 result outside the training range of damper parameters

The effect of the hardening stiffness, k_{n3} can be observed in Fig.3.15 as it clearly extends the operational bandwidth of the VBE harvester system by increasing the resonance frequency (frequency of interest). The GALE-OFRF approximation will then be used for the system analysis/design to determine the appropriate nonlinear parameter k_{n3} of the VBE harvester.

Fig.3.16 shows the relationship between the VBE harvester system nonlinear design parameters against (a) the output spectrum and (b) the average power absorbable by the VBE harvester system at the resonant frequency, which are obtained from the OFRF representation (3.128). Therefore, the desired output performance of the VBE harvester can be designed according to the Fig.3.16.


|(a)|(b)|
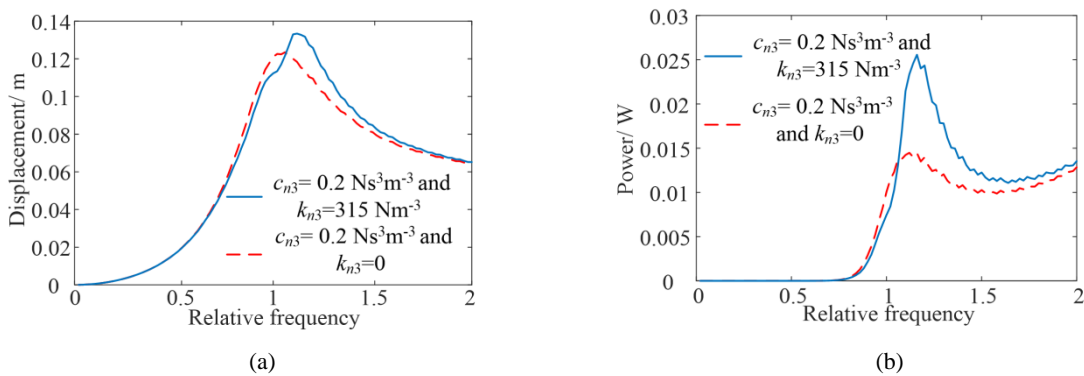
Fig.3.15. Effect of hardening stiffness on the output spectrum and average power absorbed by the vibration-based energy harvester system
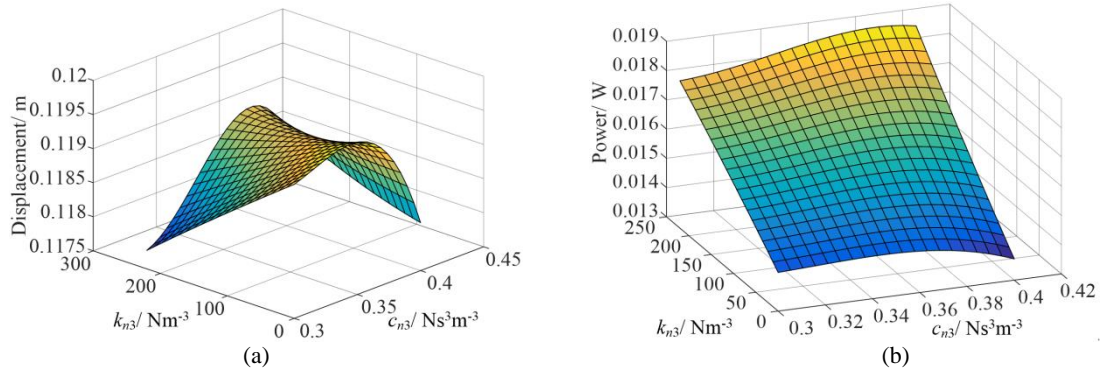
Fig.3.16. Relationship between nonlinear parameters

3.6 Conclusions

Nonlinear system analyses have been studied for decades and widely applied in engineering practice. Nonlinear systems can be investigated by using either analytical or numerical approaches in both the time and the frequency domain, if the mathematical model of the systems is available, and if not, the system identification can be conducted to produce a data driven model to facilitate the system analysis.

In this chapter, a new concept known as the GALEs is proposed for nonlinear system analyses based on the Volterra series representation of the system's NARX/NDE model. The output of nonlinear systems can be determined by solving a series of linear equations derived from the system's GALEs. This can facilitate a more efficient evaluation of the output response of nonlinear systems as well as the determination of the NOFRFs and OFRF of nonlinear systems up to an arbitrarily high order of nonlinearity of interest that has never been able to be achieved before.

Three case studies are used to demonstrate the application of the GALEs to the nonlinear system modelling, analyses and designs including the NOFRFs based nonlinear structural system fault diagnosis, nonlinear structural system fault diagnosis, nonlinear vibration energy harvester design, and the identification of the NDE model of nonlinear systems

Chapter 4. The convergence of the Volterra series representation of nonlinear systems

4.1 Introduction

The Volterra series based frequency domain analysis has been investigated in the previous chapters. It has been notated that two important issues are required to be resolved. One of these issues is how to accurately evaluate the nonlinear outputs up to an arbitrarily high order, which has been addressed in Chapter 3 by using the GALEs. The other is to guarantee the convergence of the Volterra series.

Many approaches have been developed for the convergence analysis of Volterra series, which has been reviewed in Chapter 1. However, available approaches only consider specific nonlinear systems or system subject to harmonic input signals and are often difficult to apply in practice. Therefore, it is necessary to develop a simpler and more efficient criterion for the analysis of the convergence of the Volterra series representation of a general class of nonlinear systems subject to either harmonic or general input excitations.

In this chapter, a new convergence criterion for the Volterra series representation of the NARX model of nonlinear systems is derived to address the problems with existing methods. The derivation is based on the frequency domain representation of the NARX model. A new bound characterisation function known as the Generalized Output Bound Characteristic Function (GOBCF) is proposed to determine a new criterion for the convergence analysis. The new criterion has the advantages of being independent of sampling frequency with the NARX model, applicable to nonlinear systems under general inputs, and having no need of carrying out complex mathematical computations. Two case studies including the unplugged Van der Pol equation, and the Duffing equation with nonlinear damping are used to demonstrate the effectiveness of the new criterion and its advantages over existing methods. This Chapter is organized as below
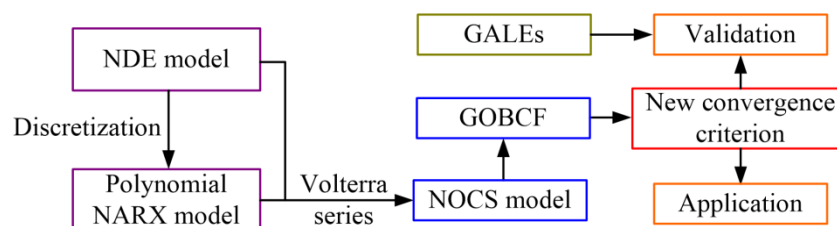

Fig.4.1 The contents of Chapter 4

4.2 The NARX model in the frequency domain: Nonlinear Output Characteristic Spectra (NOCS) model

According to the condition of the existence of the Volterra series representation of a nonlinear system, it has been shown that if the system output spectrum is bounded and this bound is continuous and smoothly changes against the input magnitude over the whole frequency range, then the system is stable at the zero equilibrium and can be represented by a Volterra series [101,102]. In order to obtain the output bound for a nonlinear system, the NARX model (2.6) will be transformed into the frequency domain as described in Proposition 4.1 below using Lemma 3.2 in Chapter 3.

Proposition 4.1: *The NARX model (2.6) can be described in the frequency domain as*

$$Y(j\omega) = \sum_{m=1}^{M} \widehat{Y}_m(j\omega) \tag{4.1}$$

where

$$\begin{cases} \widehat{Y}_1(j\omega) = L(j\omega)C_{0,1}(\omega)U(j\omega) & m = 1 \\ \widehat{Y}_m(j\omega) = \dfrac{L(j\omega)}{\sqrt{m}(2\pi)^{m-1}} \displaystyle\sum_{p=0}^{m} \int_{\omega_1+\cdots+\omega_m=\omega} C_{p,m-p}(\omega_1,\ldots,\omega_m) \\ \qquad \times \displaystyle\prod_{i=1}^{p} Y(j\omega_i) \prod_{i=p+1}^{m} U(j\omega_i) \, d\sigma_{\omega} & m \geq 2 \end{cases} \tag{4.2}$$

and

$$L(j\omega) = \left[1 - \sum_{k_1=1}^{K} c_{1,0}(k_1)\exp(-jk_1\omega\Delta t)\right]^{-1} \tag{4.3}$$

$$C_{p,m-p}(\omega_1,\ldots,\omega_m) = \sum_{k_1,\,k_m=1}^{K} c_{p,m-p}(k_1,\cdots,k_m)\exp\left(-j(k_1\omega_1+\cdots+k_m\omega_m)\Delta t\right) \tag{4.4}$$

Proof of Proposition 4.1: Let $p+q=m$ and rearrange the NARX model (2.6) as

$$y(k) - \sum_{k_1=1}^{K} c_{1,0}(k_1)y(k-k_1) = \sum_{k_1=1}^{K} c_{0,1}(k_1)u(k-k_1)$$
$$+ \sum_{m=2}^{M}\sum_{p=0}^{m}\sum_{k_1,\,k_m=1}^{K}\left[c_{p,m-p}(k_1,\cdots,k_m)\prod_{i=1}^{p}y(k-k_i)\prod_{i=p+1}^{m}u(k-k_i)\right] \tag{4.5}$$

Applying the normalized Discrete Time Fourier Transform to (4.5) yields:

$$Y(j\omega) = L(j\omega)\sum_{k_1=1}^{K} DF\left[c_{0,1}(k_1)u(k-k_1)\right]\Delta t$$
$$+ L(j\omega)\sum_{m=2}^{M}\sum_{p=0}^{m}\sum_{k_1,\,k_m=1}^{K} DF\left[c_{p,m-p}(k_1,\cdots,k_m)\prod_{i=1}^{p}y(k-k_i)\prod_{i=p+1}^{m}u(k-k_i)\right]\Delta t \tag{4.6}$$

where

$$L(j\omega) = \left[1 - \sum_{k_1=1}^{K} c_{1,0}(k_1) \exp(-jk_1\omega\Delta t) \right]^{-1} \tag{4.7}$$

Denote

$$C_{p,m-p}(\omega_1,\ldots,\omega_m) = \sum_{k_1,\,k_m=1}^{K} c_{p,m-p}(k_1,\cdots,k_m) \exp\left(-j(k_1\omega_1 + \cdots + k_m\omega_m)\Delta t\right) \tag{4.8}$$

According to Lemma 3.2, (4.6) can be written as

$$
\begin{aligned}
Y(j\omega) = Y_1(j\omega) + \sum_{m=2}^{M} \frac{L(j\omega)}{\sqrt{m}\,(2\pi)^{m-1}} \sum_{p=0}^{m} \int_{\omega_1+\cdots+\omega_m=\omega} C_{p,m-p}(\omega_1,\ldots,\omega_m) \\
\times \prod_{i=1}^{p} Y(j\omega_i) \prod_{i=p+1}^{m} U(j\omega_i)\,d\sigma_\omega = \sum_{m=1}^{M} \widehat{Y}_m(j\omega)
\end{aligned}
\tag{4.9}
$$

where $\omega_i, \omega \in [-\pi/\Delta t, \pi/\Delta t]$, $i = 1,\ldots,n$, thus Proposition 4.1 is proven.

The new decomposition of the output frequency response of nonlinear systems given by (4.1) will, hereafter, be referred to as the Nonlinear Output Characteristic Spectra (NOCS) model with $\widehat{Y}_m(j\omega)$ being called the m th order NOCS function.

For example, consider the NARX model

$$y(k) = c_{0,1}(1)u(k-1) + c_{1,0}(1)y(k-1) + c_{1,0}(2)y(k-2) + c_{3,0}(1,1,1)y^3(k-1) \tag{4.10}$$

The NOCS model with $M = 3$ is obtained from Proposition 4.1 as

$$Y(j\omega) = \widehat{Y}_1(j\omega) + \widehat{Y}_3(j\omega) \tag{4.11}$$

where

$$\widehat{Y}_1(j\omega) = L(j\omega)c_{0,1}(1)\exp(-j\omega\Delta t)U(j\omega) \tag{4.12}$$

$$\widehat{Y}_3(j\omega) = c_{3,0}(1,1,1)\exp(-j\omega\Delta t)\frac{L(j\omega)}{\sqrt{3}(2\pi)^2}\int_{\omega_1+\cdots+\omega_3=\omega}\prod_{i=1}^{3}Y(j\omega_i)\,d\sigma_\omega \tag{4.13}$$

and $L(j\omega) = \left[1 - c_{1,0}(1)\exp(-j\omega\Delta t) - c_{1,0}(2)\exp(-j2\omega\Delta t)\right]^{-1}$.

The NOCS model of nonlinear system (2.6) introduced in Proposition 4.1 is an important basis for the derivation of a new criterion for the analysis of the convergence of the Volterra series representation of nonlinear systems.

4.3 The Generalized Output Bound Characteristic Function (GOBCF)

based convergence analysis

4.3.1 A sufficient condition of the convergence

In order to evaluate the convergence of the Volterra series representation of a nonlinear system, a sufficient condition as described in the following Lemma can be applied.

Lemma 4.1: *If there exists an integer* N^* *such that for all* ω ,

$$\left| Y_n \left(\mathrm{j}\omega \right) \right| < \left| Y_{n-1} \left(\mathrm{j}\omega \right) \right| \tag{4.14}$$

for all $n > N^*$ *, then the Volterra series representation of a nonlinear system is convergent* [97].

In practice, the use of Lemma 4.1 can be implemented by introducing a pre-specified threshold ρ and evaluating whether there exists a N^* such that when $\bar{N} \geq N^*$

$$\eta_N = \frac{\left| Y\left(\mathrm{j}\omega \right) - \sum_{n=1}^{\bar{N}} Y_n \left(\mathrm{j}\omega \right) \right|}{\left| Y\left(\mathrm{j}\omega \right) \right|} \times 100\% \leq \rho \quad \text{for all} \quad \omega \tag{4.15}$$

This approach will be applied later on to validate the new convergence criterion proposed in the present study.

In order to study the issue of convergence using equation (4.14), $Y_n \left(\mathrm{j}\omega \right), n = 1, 2, ...$ can be evaluated by using the GALEs for the NARX model of nonlinear systems proposed in Chapter 3. In the following studies, a new convergence criterion will be derived and the results will be validated using (4.14).

4.3.2 The determination of the GOBCF

The new convergence criterion will be formulated from the NOCS model (4.1) of a NARX system. As the first step of the derivation, the Generalized Output Bound Characteristic Function (GOBCF) is defined and an important property of the GOBCF relevant to the bound on the output spectrum of the NARX model of nonlinear systems is revealed in Proposition 4.2 below.

Proposition 4.2: *The GOBCF of the NARX model (2.6) is defined as*

$$f_{BC}\left(x \right) = x - \bar{L}_{w_{\mathrm{lin}}} \bar{C}_{0,1} [\![u]\!] - \sum_{m=2}^{M} \sum_{p=0}^{m} \bar{L}_w \bar{C}_{p,m-p} x^p [\![u]\!]^{m-p} \tag{4.16}$$

where x *is the variable of the GOBCF,*

$$\bar{C}_{p,m-p} = \sup_{\substack{\omega_1,\ldots,\omega_p \in W \\ \omega_{p+1},\ldots,\omega_m \in W_0}} \left| C_{p,m-p}^{sym}(\omega_1,\ldots,\omega_m) \right| \tag{4.17}$$

with

$$\left| C_{p,m-p}^{sym}(\omega_1,\ldots,\omega_m) \right| = \left| \frac{1}{m!} \sum_{\substack{all\ possible \\ permutation\ of\ \omega_i}} C_{p,m-p}(\omega_1,\ldots,\omega_m) \right| \tag{4.18}$$

$$\bar{L}_{w_{lin}} = \sup_{\omega \in W_0} \left| L(j\omega) \right|, \ \bar{L}_w = \sup_{\omega \in W} \left| L(j\omega) \right| \tag{4.19}$$

W_0 *represents the input frequency range,* $W \subseteq \left[-\pi/\Delta t, \pi/\Delta t \right]$, *and*

$$\llbracket u \rrbracket = \max_{-\infty \leq k < +\infty,\ \omega \in W_0} \left\{ DF^{-1}\left[\left| U(j\omega) \right| \right], \left| U(j\omega) \right| \right\} \tag{4.20}$$

where $DF^{-1}[.]$ *represents the invers normalised Discrete Time Fourier Transform.*

One of the solutions to equation $f_{BC}(x) = 0$ *is*

$$\llbracket y \rrbracket = \sum_{n=1}^{+\infty} \bar{H}_n \llbracket u \rrbracket^n = \bar{H}_1 \llbracket u \rrbracket + \cdots + \bar{H}_n \llbracket u \rrbracket^n + \cdots \tag{4.21}$$

where

$$\begin{cases} \bar{H}_1 = \bar{L}_{w_{lin}} \bar{C}_{0,1} \\ \bar{H}_n = \bar{L}_w \left(\bar{C}_{0,n} + \sum_{m=2}^{M} \sum_{p=1}^{m} \left(\bar{C}_{p,m-p} \sum_{r_1,\ldots,r_p=1, \sum r_i = n-m+p}^{n-m+1} \prod_{i=1}^{p} \bar{H}_{r_i} \right) \right) \end{cases} \tag{4.22}$$

and $\llbracket y \rrbracket$ *is a bound on the output spectrum of the NARX model such that* $\llbracket y \rrbracket \geq \max_{\omega \in W} \left| Y(j\omega) \right|$.

Proof of Proposition 4.2: Introduce the symmetric function

$$C_{p,m-p}^{sym}(\omega_1,\ldots,\omega_m) = \frac{1}{m!} \sum_{\substack{all\ possible \\ permutation\ of\ \omega_i}} C_{p,m-p}(\omega_1,\ldots,\omega_m) \tag{4.23}$$

with respect to $\omega_1,\ldots,\omega_m$ and denote

$$\bar{C}_{p,m-p} = \sup_{\substack{\omega_1,\ldots,\omega_p \in W \\ \omega_{p+1},\ldots,\omega_m \in W_0}} \left| C_{p,m-p}(\omega_1,\ldots,\omega_m) \right| = \sup_{\substack{\omega_1,\ldots,\omega_p \in W \\ \omega_{p+1},\ldots,\omega_m \in W_0}} \left| C_{p,m-p}^{sym}(\omega_1,\ldots,\omega_m) \right| \tag{4.24}$$

and

$$\bar{L}_{w_{lin}} = \sup_{\omega \in W_0} \left| L(j\omega) \right|, \ \bar{L}_w = \sup_{\omega \in W} \left| L(j\omega) \right| \tag{4.25}$$

where $W = \left[-\omega_s, +\omega_s \right]$, ω_s represents the maximum output frequency satisfying $\omega_s = \pi/\Delta t$. It is known

from (2.15) that

$$\left|Y\left(j\omega\right)\right| \le \sum_{n=1}^{+\infty} \bar{H}_n \frac{1}{\sqrt{n}\left(2\pi\right)^{n-1}} \int_{\omega_1+\cdots+\omega_n=\omega} \prod_{i=1}^{n}\left|U\left(j\omega_i\right)\right| d\sigma_\omega = \sum_{n=1}^{+\infty} \bar{H}_n DF\left[\bar{u}^n\left(k\right)\right]\Delta t$$

$$= \sum_{n=1}^{+\infty} \bar{H}_n \Delta t \int_{-\pi/\Delta t}^{\pi/\Delta t} \bar{u}^n\left(k\right)\Delta t \exp\left(-j\omega k\Delta t\right) d\omega \le \sum_{n=1}^{+\infty} \bar{H}_n [\![u]\!]^{n-1}\left|U\left(j\omega\right)\right| \le \sum_{n=1}^{+\infty} \bar{H}_n [\![u]\!]^n = [\![y]\!]$$

(4.26)

where $\bar{u}\left(k\right) = DF^{-1}\left[\left|U\left(j\omega_i\right)\right|\right]$.

From the description of the m th order NOCS function $\hat{Y}_m\left(j\omega\right)$ given in (4.2), it is known that

$$\left|\hat{Y}_1\left(j\omega\right)\right| \le \bar{L}_{w_{lin}} \bar{C}_{0,1} [\![u]\!]$$

(4.27)

and

$$\left|\hat{Y}_m\left(j\omega\right)\right| \le \bar{L}_w \bar{C}_{p,m-p} \frac{1}{\sqrt{m}\left(2\pi\right)^{m-1}} \sum_{p=0}^{m} \int_{\omega_1+\cdots+\omega_m=\omega} \prod_{i=1}^{p}\left(\sum_{n=1}^{+\infty} \bar{H}_n [\![u]\!]^{n-1}\left|U\left(j\omega_i\right)\right|\right) \prod_{i=p+1}^{m}\left|U\left(j\omega_i\right)\right| d\sigma_\omega$$

$$\le \bar{L}_w \bar{C}_{p,m-p} \sum_{p=0}^{m} \prod_{i=1}^{p}\left(\sum_{n=1}^{+\infty} \bar{H}_n [\![u]\!]^n\right)[\![u]\!]^{m-p} = \sum_{p=0}^{m} \bar{L}_w \bar{C}_{p,m-p} [\![y]\!]^p [\![u]\!]^{m-p}$$

(4.28)

Consequently,

$$\left|Y\left(j\omega\right)\right| \le \sum_{m=1}^{M}\left|\hat{Y}_m\left(j\omega\right)\right| \le \bar{L}_{w_{lin}} \bar{C}_{0,1} [\![u]\!] + \sum_{m=2}^{M}\sum_{p=0}^{m} \bar{L}_w \bar{C}_{p,m-p} [\![y]\!]^p [\![u]\!]^{m-p} = \bar{L}_{w_{lin}} \bar{C}_{0,1} [\![u]\!]$$

$$+ \sum_{n=2}^{+\infty} \bar{L}_w\left(\bar{C}_{0,n} + \sum_{m=2}^{n}\sum_{p=1}^{m}\left(\bar{C}_{p,m-p} \sum_{\substack{r_1,\ldots,r_p=1,\\ \sum r_i=n-m+p}}^{n-m+1} \prod_{i=1}^{p} \bar{H}_{r_i}\right)\right)[\![u]\!]^n$$

(4.29)

Considering that

$$\begin{cases} \bar{H}_1 = \bar{L}_{w_{lin}} \bar{C}_{0,1} \\ \bar{H}_n = \bar{L}_w\left(\bar{C}_{0,n} + \sum_{m=2}^{n}\sum_{p=1}^{m}\left(\bar{C}_{p,m-p} \sum_{\substack{r_1,\ldots,r_p=1,\\ \sum r_i=n-m+p}}^{n-m+1} \prod_{i=1}^{p} \bar{H}_{r_i}\right)\right) \end{cases}$$

(4.30)

are the bound on the system GFRFs over all possible frequency ranges [13,103] such that

$$\bar{H}_n \ge \sup_{\omega_1,\ldots,\omega_n \in W}\left|H_n\left(\omega_1,\ldots,\omega_n\right)\right|$$

(4.31)

It is known that the right hand side of (4.29) equals to the right hand side of (4.26). Therefore

$$\bar{L}_{w_{lin}} \bar{C}_{0,1} [\![u]\!] + \sum_{m=2}^{M}\sum_{p=0}^{m} \bar{L}_w \bar{C}_{p,m-p} [\![y]\!]^p [\![u]\!]^{m-p} = \sum_{n=1}^{\infty} \bar{H}_n [\![u]\!]^n = [\![y]\!]$$

(4.32)

that is, $[\![y]\!]$ is a solution to $f_{BC}\left([\![y]\!]\right) = 0$. Thus Proposition 4.2 is proven.

Remark 4.1: Theoretically, the frequency range W contains all possible output frequencies, which can be obtained using the algorithm in [43] provided the sampling frequency $1/\Delta t$ with the NARX model is sufficiently high. However, in practice, if only the system nonlinearity up to $\hat{N}$ th order needs to be taken

into account considering the higher frequencies are neglectable, then

$$W \subseteq \left[-\widehat{N} \omega_{\max}, \widehat{N} \omega_{\max} \right] \qquad (4.33)$$

where $\omega_{\max}$ represents the maximum frequency of the system input, and $2 \widehat{N} \omega_{\max} \le 2\pi/\Delta t$.

Remark 4.2: The value of $\overline{L}_w$ can be obtained from (4.19). $\overline{C}_{p,m-p}$ is the supreme value of a multi-variable symmetric function which can be determined using many numerical optimization approaches [120]. However, in many cases as shown in the case studies, the determination of $\overline{C}_{p,m-p}$ can be reduced to an optimization problem for a single variable function.

In the following, the GOBCF will be used for the analysis of the convergence with the Volterra series representation of the NARX model of nonlinear systems.

4.3.3 Convergence analysis of the Volterra series representation of nonlinear systems

Proposition 4.2 implies that if there exist real positive solutions to equation $f_{BC}(x) = 0$, then the output spectrum of the NARX model (2.6) is bounded by one of such solutions which satisfies (4.21). Consequently, the NARX model (2.6) can be described, around zero equilibrium, by a convergent Volterra series representation. In the following, Lemma 4.2 is introduced to discuss the cases where $f_{BC}(x) = 0$ has or has no real positive solutions.

Lemma 4.2: *Depending on $[\![u]\!]$ and the values of $\overline{L}_w$, $\overline{C}_{0,1}$ and $\overline{C}_{p,m-p}$, $p = 0, \ldots, m$ and $m = 2, \ldots, M$, which are associated with the NARX model parameters, there exist only three cases for the solutions to the equation*

$$f_{BC}(x) = x - \overline{L}_{w_{\lin}} \overline{C}_{0,1} [\![u]\!] - \sum_{m=2}^{M} \sum_{p=0}^{m} \overline{L}_w \overline{C}_{p,m-p} x^p [\![u]\!]^{m-p} = 0 \qquad (4.34)$$

which are

(1) There are two real positive solutions $\overline{x}_{\min}$ and $\overline{x}_{\max}$ with $\overline{x}_{\max} > \overline{x}_{\min}$ or

(2) There is one real positive solution $\overline{x}_{one}$ or

(3) There is no real positive solution.

Proof of Lemma 4.2: Evaluating the first and second derivative of the GOBCF $f_{BC}(x)$ yields

$$f'_{BC}(x) = 1 - \sum_{m=2}^{M} \sum_{p=1}^{m} p \overline{L}_w \overline{C}_{p,m-p} x^{p-1} [\![u]\!]^{m-p} \qquad (4.35a)$$

$$f_{BC}''(x) = -\sum_{m=2}^{M}\sum_{p=2}^{m} p(p-1)\overline{L}_w\overline{C}_{p,m-p}x^{p-2}[\![u]\!]^{m-p} \tag{4.35b}$$
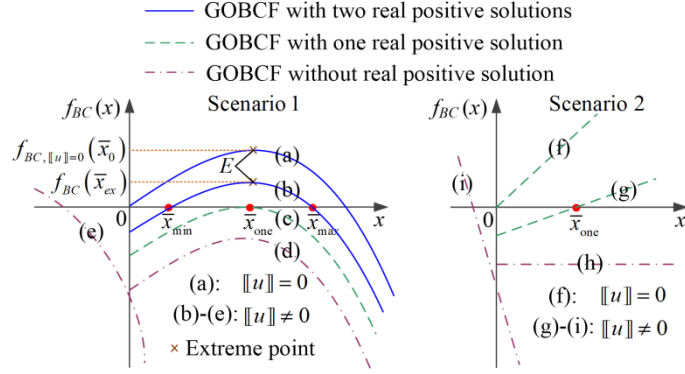

Fig.4.2 Illustration of the different situations of GOBCF with and without real positive solutions

It is known from (4.35b) that $f_{BC}''(x) \le 0$ when $x \ge 0$. Considering $f_{BC}(0) \le 0$ is always satisfied

since $\overline{L}_w, \overline{C}_{p,m-p}$, x and $[\![u]\!]$ are all positive, it is known that

(i)   When $f_{BC}'(0) > 0, f_{BC}''(x) < 0$, for $x \ge 0$, $f_{BC}(x)$ will increase first and then decrease. Therefore, there

exist cases (1)-(3) about the solutions to equation (4.34) which are illustrated in Fig.4.2 (a)-(d).

(ii)   When $f_{BC}'(0) > 0, f_{BC}''(x) = 0$, for $x \ge 0$, $f_{BC}(x)$ will monotonically increase. Therefore, cases (2) and

(3) exist about the solutions to equation (4.32) as illustrated in Fig.4.2 (f)-(g).

(iii)   When $f_{BC}'(0) \le 0$, for $x \ge 0$, equation (4.34) has no real positive solution. This is case (3) but in a

different situation as shown in Fig.4.2 (e), (h) and (i).

By combining (i), (ii) and (iii), the conclusions of Lemma 4.1 are reached.

Based on Lemma 4.2 and Proposition 4.2, a sufficient condition on the convergence of the Volterra series

representation of nonlinear systems can be derived. For the purpose of more quantitatively evaluating the

convergence issue, under the condition of $f_{BC}'(0) > 0, f_{BC}''(x) < 0$ for $x \ge 0$, the extreme point of the

GOBCF where $f_{BC}'(x) = 0$, is denoted as $E(\overline{x}_{ex}, f_{BC}(\overline{x}_{ex}))$ and $E(\overline{x}_0, f_{BC,[\![u]\!]=0}(\overline{x}_0))$ for the two cases of

$[\![u]\!] \ne 0$ and $[\![u]\!] = 0$, respectively as shown in Fig.4.2 where $\overline{x}_{ex}$ is the solution to

$$f_{BC}'(x) = 1 - \sum_{m=2}^{M}\sum_{p=1}^{m} p\overline{L}_w\overline{C}_{p,m-p}x^{p-1}[\![u]\!]^{m-p} = 0 \tag{4.36}$$

in which $[\![u]\!] \ne 0$ while $\overline{x}_0$ is the solution to

$$f_{BC,[\![u]\!]=0}'(x) = 1 - \sum_{m=2}^{M} m\overline{L}_w\overline{C}_{m,0}x^{m-1} = 0 \tag{4.37}$$

A sufficient criterion for the NARX model to be described by a convergent Volterra series model can,

consequently, be obtained as given in Proposition 4.3 below.

   Proposition 4.3: *If GOBCF $f_{BC}(x) = 0$ has real positive solutions, then, around zero equilibrium, the*

output response of the NARX model (2.6) can be described by a convergent Volterra series representation. In

addition, the extent to which this representation is convergent can be quantified by

$$\Gamma = \begin{cases} \dfrac{f_{BC}(\overline{x}_{ex})}{f_{BC,[\![u]\!]=0}(\overline{x}_0)} & f'_{BC}(0) > 0, \ f''_{BC}(x) < 0, \ x \geq 0 \\ f'_{BC}(0) & f'_{BC}(0) > 0, \ f''_{BC}(x) = 0, \ x \geq 0 \\ -1 & \text{Otherwise} \end{cases} \tag{4.38}$$

such that when $[\![u]\!]$, $\overline{L}_w$, or $\overline{C}_{p,m-p}$ in the GOBCF decreases, $\Gamma \to 1$, the convergence is enhanced; and

when $[\![u]\!]$, $\overline{L}_w$, or $\overline{C}_{p,m-p}$ increases, $\Gamma \to 0$, the convergence is weaken.

   Proof of Proposition 4.3: If equation $f_{BC}(x) = 0$ has real positive solutions, according to Proposition

4.2, the output bound $[\![y]\!]$ in (4.21) exists, which indicates the output response of the NARX model can be

represented by a convergent Volterra series. This proves the first part of Proposition 4.3.

   In order to quantify the extent of convergence, denote the GOBCF in the case of $[\![u]\!] = 0$ as $f_{BC,[\![u]\!]=0}(x)$,

which is case (a) and (f) in Fig.4.2. Then it can be observed that Γ defined in (4.38) has the following

properties:

   (i) $\Gamma \in [0,1]$ indicates the extreme point E is located in the first quadrant which is the cases of (1) and

(2) in Lemma 4.1, or the GOBCF monotonically increases which is the case of (2) in Lemma 4.1.

   (ii) $\Gamma < 0$ indicates the extreme point E is located in the fourth quadrant, or the GOBCF monotonically

decreases, which is case (3) in Lemma 4.1

   (iii) When $\Gamma \to 1$, the extreme point E or $f'_{BC}(0)$ moves upwards and away from case (c) and (h)

respectively in Fig.4.2, the boundary of the condition of convergency, so the convergence is enhanced. When

$\Gamma \to 0$, point E or $f'_{BC}(0)$ moves downwards and towards case (c) and (h), respectively, so the

convergence is weaken.

   These properties can be further analysed as follows.

   For $f'_{BC}(0) > 0, \ f''_{BC}(x) < 0, \ x \geq 0$, the extreme point $E\left(x_{ex}, f_{BC}(x_{ex})\right)$ of the GOBCF can be obtained by

solving equation (4.36) to find x_{ex} and then $f_{BC}(x_{ex})$ as

$$f_{BC}(x_{ex}) = x_{ex} - \overline{L}_{w_{\text{lin}}}\overline{C}_{0,1}[\![u]\!] - \sum_{m=2}^{M}\sum_{p=0}^{m}\overline{L}_w\overline{C}_{p,m-p}x_{ex}^{\ p}[\![u]\!]^{m-p} \tag{4.39}$$

Evaluating the first derivative with respect to $[\![u]\!]$ on both sides of (4.39) yields

$$\frac{df_{BC}\left(x_{ex},[\![u]\!]\right)}{d[\![u]\!]} = -\bar{L}_{w_{\text{lin}}}\bar{C}_{0,1} - \sum_{m=2}^{M}\sum_{p=1}^{m}(m-p)\bar{L}_{w}\bar{C}_{p,m-p}x_{ex}{}^{p}[\![u]\!]^{m-p-1}$$
$$+\left(1-\sum_{m=2}^{M}\sum_{p=1}^{m}p\bar{L}_{w}\bar{C}_{p,m-p}x_{ex}{}^{p-1}[\![u]\!]^{m-p}\right)\frac{dx_{ex}}{d[\![u]\!]} \tag{4.40}$$

Considering (4.36), (4.40) can be rewritten as

$$\frac{df_{BC}\left(x_{ex},[\![u]\!]\right)}{d[\![u]\!]} = -\bar{L}_{w_{\text{lin}}}\bar{C}_{0,1} - \sum_{m=2}^{M}\sum_{p=1}^{m}(m-p)\bar{L}_{w}\bar{C}_{p,m-p}x_{ex}{}^{p}[\![u]\!]^{m-p-1} < 0 \tag{4.41}$$

So $f_{BC}\left(x_{ex},[\![u]\!]\right)$ monotonically decreases with the increase of $[\![u]\!]$, that is, $\Gamma \to 0$ when $[\![u]\!]$ increases and $\Gamma \to 1$ when $[\![u]\!]$ decreases.

For $f'_{BC}(0) > 0$, $f''_{BC}(x)=0$, $x \geq 0$, the first derivate of the GOBCF is

$$f'_{BC}(x) = 1 - \sum_{m=2}^{M}\bar{L}_{w}\bar{C}_{1,m-1}[\![u]\!]^{m-1} = f'_{BC}(0) \tag{4.42}$$

which is the slope of the GOBCF independent of variable x, and $f'_{BC}(0)$ monotonically decreases with the increase of $[\![u]\!]$, that is, $\Gamma \to 0$ when $[\![u]\!]$ increases and $\Gamma \to 1$ when $[\![u]\!]$ decreases.

Considering that when the input bound $[\![u]\!]$ increases, the convergence of the Volterra series representation is weaken and when the input bound $[\![u]\!]$ decreases, the convergence is enhance, one can reach to the conclusion of the second part of Proposition 4.3 with regard to the effect of $[\![u]\!]$ on the convergence of the system Volterra series representation.

The analysis can readily be extended to reveal the similar effects of the system linear and nonlinear characteristic parameters $\bar{L}_{w}$ and $\bar{C}_{p,m-p}$ on the issue of convergency and indicate that Γ can be used to quantify the extent of convergence in the same way. Thus Proposition 4.3 is proven.

Corollary 4.1: The Volterra series representation of the NARX model (2.6) under harmonic input

$$u(k) = A\cos\left(\omega_{F}k\Delta t + \varphi\right) \tag{4.43}$$

is convergent if $\Gamma \in [0,1]$, where Γ is obtained from (4.38) using $f_{BC}(\bar{x}_{ex})$ and $f_{BC,[\![u]\!]=0}(\bar{x}_{0})$ or $f'_{BC}(0)$ obtained by solving equations (4.34) and (4.35) with $[\![u]\!] = A$,

$$\bar{C}_{p,m-p} = \sup_{\substack{\omega_{1},\ldots,\omega_{p}\in W_{H} \\ \omega_{p+1},\ldots,\omega_{m}=\pm\omega_{F}}}\left|\frac{1}{m!}\sum_{\substack{all\ possible \\ permutation\ of\ \omega_{i}}}C_{p,m-p}\left(\omega_{1},\ldots,\omega_{m}\right)\right| \tag{4.44}$$

$$\bar{L}_w = \sup_{\omega \in W_H} \left| 1 - \sum_{k_1=1}^{K} c_{1,0}(k_1) \exp(-jk_1 \omega \Delta t) \right|^{-1} \tag{4.45}$$

where $W_H = \left\{ \pm\beta\omega_F \, \middle| \, \leq \pi/\Delta t \, \middle| \, \beta \in Z^+, \beta \leq \hat{N}_H \right\}$ represents all possible output frequencies and $\hat{N}_H \leq \pi/(\Delta t \omega_F)$.

Proof of Corollary 4.1: The Corollary can be proven by using Proposition 4.3.

Proposition 4.3 provides an efficient criterion to assess the convergence of the Volterra series representation, which can also be applied to determine the convergence bound of a nonlinear system in terms of its parameters or inputs. The results are shown in Proposition 4.4 below.

Proposition 4.4: The convergence bound on the characteristic parameters or input of the NARX model (2.6) can be obtained by solving the simultaneous equations

$$\begin{cases} f_{BC}(\xi, x) = x - \bar{L}_{w_{\text{lin}}} \bar{C}_{0,1}\llbracket u \rrbracket - \sum_{m=2}^{M} \sum_{p=0}^{m} \bar{L}_w \bar{C}_{p,m-p} x^p \llbracket u \rrbracket^{m-p} = 0 \\ f'_{BC}(\xi, x) = 1 - \bar{L}_w \sum_{m=2}^{M} \sum_{p=1}^{m} p\bar{C}_{p,m-p} x^{p-1} \llbracket u \rrbracket^{m-p} = 0 \end{cases} \tag{4.46a}$$

under the condition of $f''_{BC}(x) < 0, x \geq 0$ and

$$f'_{BC}(\xi) = 1 - \bar{L}_w \sum_{m=2}^{M} \bar{C}_{1,m-1} \llbracket u \rrbracket^{m-1} = 0 \tag{4.46b}$$

under the condition of $f''_{BC}(x) = 0, x \geq 0$ for x and ξ where ξ, dependending on the need of analysis, can be $\bar{L}_w, \bar{C}_{p,m-p}$ or $\llbracket u \rrbracket$ representing the convergence bound on the system linear characteristic parameters, nonlinear characteristic parameters, or input.

Proof of Proposition 4.4: Proposition 4.4 can be obtained from Fig.4.2 by evaluating the conditions under which function $f_{BC}(x)$ is in situation (c) and (h).

In (4.44), $\bar{L}_{w_{\text{lin}}}$, $\bar{L}_w$ and $\bar{C}_{p,m-p}$ are dependent on the system linear characteristic parameters $c_{1,0}(k_1)$ and nonlinear characteristic parameters $c_{p,m-p}(k_1, \cdots, k_m), m \geq 2$ while $\llbracket u \rrbracket$ is determined by the magnitude of the system input.

4.3.4 The procedure for the new convergence analysis

A general procedure for analyzing the convergence of the Volterra series representation of the NARX model (2.6) is summarized in the following, where Propositions 4.3 and 4.4 are applied to assess the convergence and evaluate a convergence bound, respectively.

(A) The procedure for the analysis when the system is subject to a general input

If the system subject to a general input with spectrum $U(j\omega)$ given by

$$
\begin{aligned}
u(k) &= \frac{1}{2\pi} \int_{-\pi/\Delta t}^{\pi/\Delta t} \frac{U(j\omega)}{\Delta t} \exp(j\omega k \Delta t) d(\omega \Delta t) \\
&= \frac{1}{2\pi} \int_{-\pi/\Delta t}^{\pi/\Delta t} U(j\omega) \exp(j\omega k \Delta t) d\omega
\end{aligned}
\tag{4.47}
$$

the procedure of analysis can be summarised as follows:

Procedure of the convergence analysis

1: **Produce the system's NARX model:** Describe the system by a NARX model (2.6), such that all linear and nonlinear coefficients $c_{p,q}(.)$ can be determined. This can be achieved by using a data driven nonlinear system identification approach [11] or discretising a continuous time model of the system under study.

2: **Determine the system's output frequency range:** From the maximum input frequency ω_{max} and the maximum order $\hat{N}$ of the system nonlinearity being taken into account, find the output frequency range of interest $W \subseteq \left[-\hat{N}\omega_{max}, \hat{N}\omega_{max} \right]$ or $W \subseteq \left[-\pi/\Delta t, \pi/\Delta t \right]$.

3 **Evaluate the input bound:** Compute the inverse normalised Discrete Time Fourier Transform $DF^{-1}\left[\left| U(j\omega) \right| \right]$, then calculate the input bound $[\![u]\!] = \max_{-\infty \le k < +\infty, \omega \in W_0} \left\{ DF^{-1}\left[\left| U(j\omega) \right| \right], \left| U(j\omega) \right| \right\}$.

4 **Compute the coefficients bound:** Calculate $\bar{L}_{w_{lin}}$ and $\bar{L}_w$ according to (19) over the frequency range of $\omega \in W$ and determine the value of $\bar{C}_{p,m-p}$ from (4.8), (4.17), and the NARX model coefficients in these equations.

5: **Calculate the extreme point or slope of the GOBCF:** Compute the second derivative of the GOBCF $f_{BC}(x)$ using equation (4.35b) where

5.1: If $f'_{BC}(0) > 0$, $f''_{BC}(x) < 0$, $x \ge 0$, solve equations (4.36) and (4.37) to obtain the extreme point $E\left(\bar{x}_{ex}, f_{BC}(\bar{x}_{ex}) \right)$ and $E\left(\bar{x}_0, f_{BC,[\![u]\!]=0}(\bar{x}_0) \right)$ of the GOBCF in the cases of $[\![u]\!] \ne 0$ and $[\![u]\!] = 0$, respectively.

5.2: If $f'_{BC}(0) > 0$, $f''_{BC}(x) = 0$, $x \ge 0$, solve equation (4.35a) to obtain $f'_{BC}(0)$ of the GOBCF.

6: **Convergence assessment:** Determine Γ from (4.38) by using $f_{BC}(\bar{x}_{ex})$ and $f_{BC,[\![u]\!]=0}(\bar{x}_0)$ or

$f'_{BC}(0)$ obtained in Step 5. If $\Gamma \in [0,1]$, then it can be concluded that the Volterra series representation

of the nonlinear system is convergent.

7: **Evaluation of the parameter bound:** Determine the convergence bound on the system characteristic

parameters or input by solving equation (3.42).

(B) The procedure for the analysis when the system is subject to a harmonic input

If the input signal of the system is the harmonic input (4.39), the convergence of the system's Volterra

series representation can be analysed following Steps 1 to 7 above but, a $\hat{N}_H \leq \pi f_s / \omega_F$ is selected to

determine the frequency range of $\left\{ \beta \omega_F \leq \pi / \Delta t \mid \beta \in Z^+, \beta \leq \hat{N}_H \right\}$ in Step 2, and the input bound $\|u\| = A$

in Step 3. In Steps 4 and 5, $\bar{L}_{w_{\text{lin}}}$, $\bar{L}_w$ and $\bar{C}_{p,m-p}$ are determined over the frequency range of $\omega \in W_H$.

Steps 6 and 7 are the same as in the general input case.

In comparison with the convergence criteria recently proposed in [101-104], the newly proposed

convergent analysis has the following advantages:

(i) Because of the introduction of the GOBCF, the complex mathematical operations needed for evaluating

both the Hélie's and Xiao's criterion [101-103] are avoided. In addition, Proposition 4.3 can provide a more

rigorous and less conservative analysis than the analysis in Xiao's study [102,103].

(ii) In the Xiao's criterion [102,103], the coefficient bound $\bar{C}_{p,m-p}$ in (4.40) is given as the summation of

all absolute values of the model coefficients, producing over estimated results. In addition, the result is

dependent on the sampling frequency of the NARX model, so the analysis may fail if the sampling frequency

is inappropriately selected. On the contrary, the new criterion is independent of the sampling frequency as

explained in Appendix A.

(iii) It is worth pointing out that the convergence criterion under harmonic input proposed in previous

works [97,98,100,102,103] cannot be directly used for general inputs [104]. By using the new convergence

criterion, however, the convergence analysis problems can be resolved for both harmonic and general input

cases, and the analysis result is also more rigorous and much easier to be obtained than the analysis in [104].

Tab.4.1 provides a comprehensive comparison of the newly proposed convergent analysis with the existing

techniques. The conclusions are reached based on the case study results above and some studies in [103],

indicating the new analysis has advantages over all existing methods and, therefore, has potential to be more

widely used in the convergent analysis of the Volterra series representation of nonlinear systems.

Tab.4.1 Comparison of different criteria

Criterions	A	B	C	D	E
New criterion	+	+	+	+	+
Jing's criterion [104]	-	-	+	+	+
Xiao's criterion [102,103]	-	-	+	+	-
Hélie's criterion [101]	+	-	-	+	-
Peng's criterion [100]	+	+	-	-	-
Li's criterion [99]	+	-	+	-	-
Chatterjee's criterion [98]	+	+	-	-	-
Tomlinson's criterion [97]	+	+	-	-	-

Note: **A**: Independent (+) or dependent (-) of the sampling frequency; **B**: The convergence bound is less conservative (+) or more conservative (-); **C**: Can (+) or cannot (-) be used to compute the parameter convergence bound; **D**: Can (+) or cannot (-) deal with a general nonlinear system; **E**: Can (+) or cannot (-) deal with a general input signal.

In the next section, the Unplugged Van der Pol equation and a damped Duffing oscillator will be used in two case studies, respectively, to demonstrate the application of the newly proposed criterion to the analysis of the convergence of the Volterra series representation of nonlinear systems.

4.4 Case studies

4.4.1 Case 1- Unplugged Van der Pol equation

Consider the unplugged Van der Pol equation [115,121]

$$\ddot{y}(t) + c\dot{y}(t) + ky(t) + c_e y^2(t)\dot{y}(t) = u(t) \tag{4.48}$$

under harmonic input $u(t) = A\cos(\omega_F t)$ with the parameters

$$c = 50 \text{ Ns/m}, k = 10^4 \text{ N/m}, c_e = 2\times10^6 \text{ Ns/m}^3 \tag{4.49}$$

Model (4.48) can be discretized under a sampling frequency $1/\Delta t = 512$ Hz to produce a NARX model

$$\begin{aligned}y(k) &= c_{0,1}(1)u(k-1) + c_{1,0}(1)y(k-1) + c_{1,0}(2)y(k-2) \\ &+ c_{3,0}(1,1,1)y^3(k-1) + c_{3,0}(1,1,2)y^2(k-1)y(k-2)\end{aligned} \tag{4.50}$$

where

$$\begin{aligned}c_{0,1}(1) &= \Delta t^2 = 3.8147\times10^{-6}; c_{1,0}(1) = 2 - \Delta tc - \Delta t^2 k = 1.8642; c_{1,0}(2) = \Delta tc - 1 = -0.9023; \\ c_{3,0}(1,1,1) &= -\Delta tc_e = -5.8594\times10^3; c_{3,0}(1,1,2) = \Delta tc_e = 5.8594\times10^3\end{aligned} \tag{4.51}$$

To analyse the convergence of the Volterra series representation of system (4.48), Step 1-6 proposed in

Section 4.3.4 are followed as follows.

Step 1: The NARX model is derived and given in (4.50);

Step 2: Choose $\hat{N}_H = 5$ so the frequency range of interest is given as $W_H = \{\pm\omega_F, \pm 3\omega_F, \pm 5\omega_F\}$;

Step 3: Let $[\![u]\!] = A$;

Step 4: $\bar{L}_{w_{\text{lin}}}$ and $\bar{L}_w$ is obtained over $\omega \in W_H$. For the NARX model (4.50), $M = 3$ and $c_{p,m-p}(k_1,\cdots,k_m) = 0$ except $c_{3,0}(1,1,1)$ and $c_{3,0}(1,1,2)$ as shown in (4.51). Therefore, in this case, $\bar{C}_{p,m-p} = \bar{C}_{3,0}$ is a single variable function such that

$$
\begin{aligned}
\bar{C}_{3,0} &= \sup_{\substack{\omega_i \in W_H; \\ i=1,\ldots,m}} \left| \frac{1}{6} \sum_{\substack{\text{all possible} \\ \text{permutation} \\ \text{of } \omega_i}} c_{3,0}(1,1,1)\exp\left(-j(\omega_1 + \omega_2 + \omega_3)\Delta t\right) + c_{3,0}(1,1,2)\exp\left(-j(\omega_1 + \omega_2 + 2\omega_3)\Delta t\right) \right| \\
&= \sup_{\substack{\omega_i \in W_H; \\ i=1,\ldots,m}} \Delta t c_e \left| \frac{1}{3}\sum_{i=1}^{3}\left[1 - \exp\left(-j\omega_i\Delta t\right)\right] \right| = \sup_{\omega \in W_H} \Delta t c_e \left| 1 - \exp\left(-j\omega\Delta t\right) \right|
\end{aligned}
\tag{4.52}
$$

Step 5: Substituting $[\![u]\!]$, $\bar{L}_w$ and $\bar{C}_{p,m-p}$ in this specific case into (4.36) and (4,37) yields

$$
f'_{BC}(x) = f'_{BC,[\![u]\!]=0}(x) = 1 - 3\bar{L}_w\bar{C}_{3,0}x^2 = 0
\tag{4.53}
$$

producing $E(\bar{x}_{ex}, f_{BC}(\bar{x}_{ex}))$ and $E(\bar{x}_0, f_{BC,[\![u]\!]=0}(\bar{x}_0))$. In this case, $\bar{x}_{ex} = \bar{x}_0$ but the value of $f_{BC}(\bar{x}_{ex})$ and $f_{BC,[\![u]\!]=0}(\bar{x}_0)$ are different, as illustrated in Fig.4.2.

Step 6: Determine Γ from (4.36) by using $f_{BC}(\bar{x}_{ex})$ and $f_{BC,[\![u]\!]=0}(\bar{x}_0)$ obtained in Step 5.

Following Steps 1-6 above, the new criterion Γ was evaluated over the frequency range of $\omega_F \in [0, 300]$ rad/s for $A = 4$ N. The results are shown in Fig.4.3 where the results evaluated using the Xiao's criterion [102,103] are also provided for comparison. It can be observed in Fig.4.3 that at frequencies $\omega_{F,1} = 50$ rad/s and $\omega_{F,3} = 150$ rad/s, the new and Xiao's criterion all show the Volterra series representation is convergent. However, at the frequency of $\omega_{F,2} = 100$ rad/s, the new criterion indicates that the Volterra representation is convergent, while the Xiao's criterion claim it is divergent.

In order to validate the conclusion of the new criterion, the nonlinear output spectra up to the 5th order were calculated by using the ALEs over the frequency range of $\omega_F \in [0, 300]$ rad/s. The results are shown in Fig.4.4, indicating that $\left|Y_1(j\omega_{F,2})\right| > \left|Y_3(j\omega_{F,2})\right| > \left|Y_5(j\omega_{F,2})\right|$ where $\omega_{F,2} = 100$ rad/s. This observation from Fig.4.4 confirms that the conclusion from the new criterion is correct.
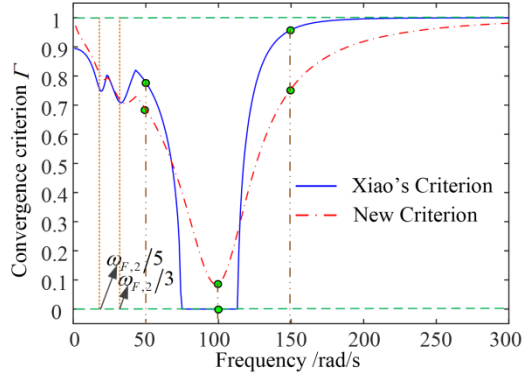
**Fig.4.3** Convergence analysis for nonlinear system (4.50)
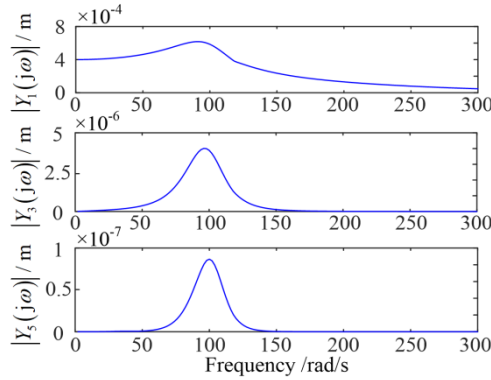
Fig.4.4 The nonlinear output spectra of system (4.50)

In addition, the values of the nonlinear output spectra up to 5th order at frequency $\omega_{F,2} = 100$ rad/s are shown in Tab.4.2. It is known from the convergence analysis using Lemma 1 that if the threshold ρ is taken as $\rho = 10^{-3}$, then Tab.4.2 implies the output frequency response can be convergent from $N = 5$ as

$$\left| Y_1 \left(j\omega_{F,2} \right) \right| > \left| Y_3 \left(j\omega_{F,2} \right) \right| > \left| Y_5 \left(j\omega_{F,2} \right) \right| \tag{4.52}$$

and $\eta_5 = 0.1738 \times 10^{-3} < 10^{-3}$.

Tab.4.2 Evaluated nonlinear output spectra

|	$\omega_{F,2} = 100$ rad/s	relative error η_N
$\left\| Y_1 \left(j\omega_{F,2} \right) \right\|$	5.8533×10^{-4} m	$\eta_1 = 0.9767 \times 10^{-2}$
$\left\| Y_3 \left(j\omega_{F,2} \right) \right\|$	3.8892×10^{-6} m	$\eta_3 = 0.2815 \times 10^{-3}$
$\left\| Y_5 \left(j\omega_{F,2} \right) \right\|$	8.6722×10^{-8} m	$\eta_5 = 0.1738 \times 10^{-3}$

It is worth noting that, by using the GALEs, the validation can be conducted by evaluating the output spectra up to an arbitrarily high order. For example, it has also been observed that $\left| Y_1 \left(j\omega_{F,2} \right) \right| > \left| Y_3 \left(j\omega_{F,2} \right) \right| > \cdots > \left| Y_{13} \left(j\omega_{F,2} \right) \right|$ but the details are omitted here.

In the following, the effects of input magnitude and nonlinear parameters on the convergence of the Volterra series representation will be discussed; the effect of sampling frequency on the convergence analysis will be evaluated; and the convergence boundary of the parameter and input amplitude of the unplugged Van der Pol system (4.50) will be investigated.

(A) Effect of the input magnitude and nonlinear parameters

It is obvious that if all system parameters are fixed, the output bound $\llbracket y \rrbracket$ will increase with the input magnitude. The criterion Γ is expected to decrease with the increase of the input magnitude, weakening the convergence of the system's Volterra series representation. The convergence criterion Γ under different input magnitudes of $A = \begin{bmatrix} 2, 4, 6 \end{bmatrix} \text{N}$ is shown in Fig.4.5. Clearly, the results are consistent with the expectation.

Moreover, the effects of different nonlinear parameter of $c_e = \begin{bmatrix} 1 \times 10^6, 2 \times 10^6, 3 \times 10^6 \end{bmatrix} \text{Ns/m}^3$ on the results of the new criterion Γ are shown in Fig.4.6, which is again as expected.
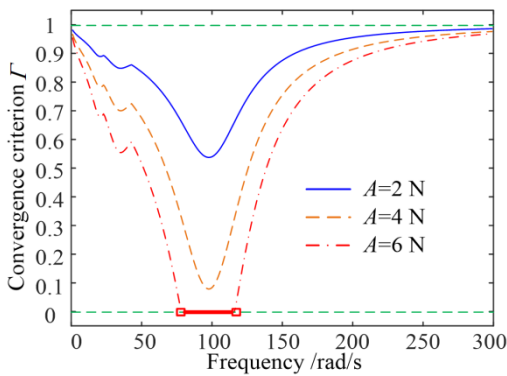
|	
Fig.4.5 The effect of input magnitude on Volterra series convergence	**Fig.4.6** The effect of nonlinear parameter on Volterra series convergence
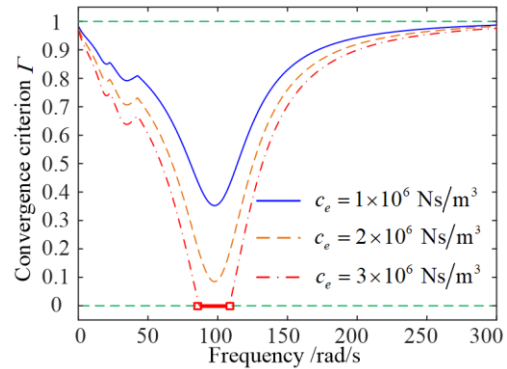
In Figs.4.5 and 4.6, the thick red line represents the Volterra series may not convergent with $\Gamma < 0$ and the two red squares represent $\Gamma = 0$ where the Volterra series is convergent according to the new criterion.

(B) Effect of the sampling frequency

The new convergence criterion Γ under three different sampling frequencies of $1/\Delta t = \begin{bmatrix} 512, 1024, 2048 \end{bmatrix} \text{Hz}$ is evaluated. The results are shown in Fig.4.7. Fig.4.8 shows the results evaluated by using the Xiao's criterion [102,103]. These results are all obtained when $A = 4 \text{ N}$ and using $\hat{N}_H = 5$.

A comparison of Fig.4.7 and Fig.4.8 indicates that the new criterion is not sensitive to the sampling

frequency while the Xiao's criterion [102,103] is, and may therefore fail to determine the convergence of the Volterra series representation of a NARX model if an inappropriate sampling frequency is used.

(C) The convergence boundary

In the case of the NARX model (4.48), equation (4.44) in Proposition 4.4 becomes

$$\begin{cases} f_{BC}\left(\xi, x\right) = x - \bar{L}_{w_{\text{lin}}} \bar{C}_{0,1} A - \bar{L}_w \bar{C}_{3,0} x^3 = 0 \\ f'_{BC}\left(\xi, x\right) = 1 - 3\bar{L}_w \bar{C}_{3,0} x^2 = 0 \end{cases} \tag{4.55}$$
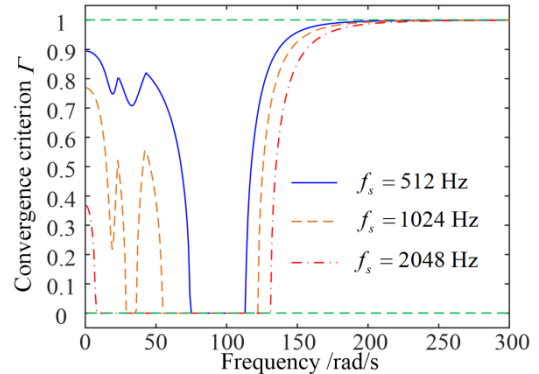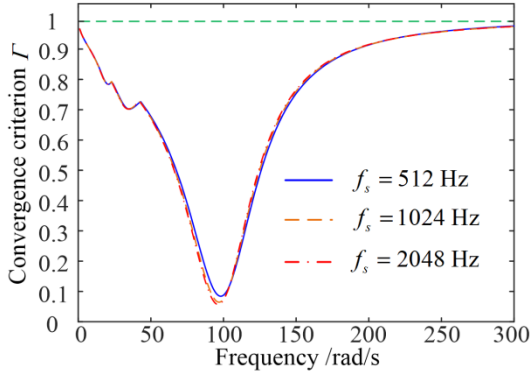
Fig.4.7 The effect of sampling frequency on new criterion   **Fig.4.8** The effect of sampling frequency on Xiao's criterion

By taking $\xi = A$ in (4.55), the convergence boundary of the input magnitude is calculated for $\omega_F \in [0, 300]$ rad/s when $c_e = 2 \times 10^6$ Ns/m^3. The results are shown in Fig.4.9. Moreover, by taking $\xi = c_e$ in (4.55), the convergence boundary of the nonlinear parameter c_e is also evaluated for $\omega_F \in [0, 300]$ rad/s in the case of $A = 4$. The results are shown in Fig.4.10.
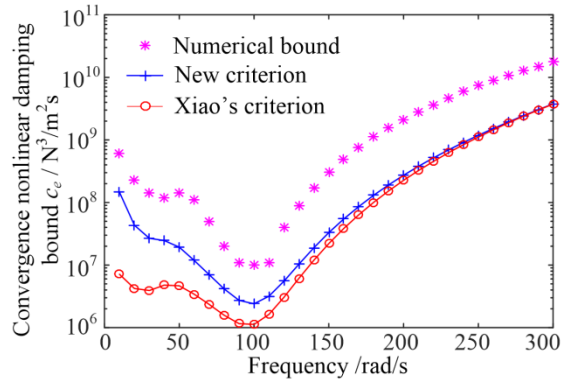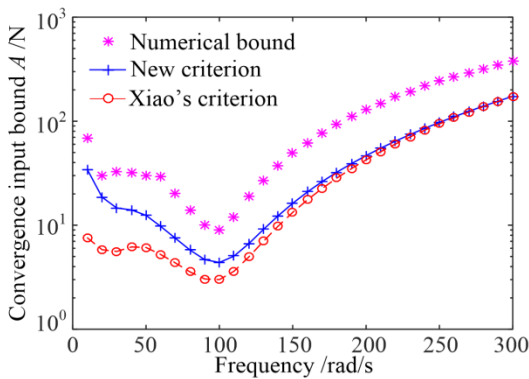

Fig.4.9 The convergence boundary of the input magnitude   **Fig.4.10** The convergence boundary of nonlinear parameter

In Figs.4.9 and 4.10, a numerical boundary is also provided and referred to as the "true" convergence boundary to justify the accuracy of the boundary determined using the new criterion. The numerical boundary is obtained based on Lemma 4.1 in Section 4.3.1, by finding a boundary for A or c_e such that when A or c_e is below this boundary.

$$\left|Y_1\left(j\omega_F\right)\right| > \left|Y_3\left(j\omega_F\right)\right| > \cdots > \left|Y_{13}\left(j\omega_F\right)\right| \tag{4.56}$$

with $\eta_{13} < 10^{-6}$, and $Y_n\left(j\omega_F\right)$, $n = 1,\ldots,13$ are calculated by using the GALEs of system (4.50).

The results in Figs.4.9 and 4.10 indicate that the new criterion provides a more accurate convergence boundary than the Xiao's criterion [102,103].

4.4.2 Case 2- Duffing oscillator with cubic damping

The Duffing oscillator with cubic damping can be described as

$$\ddot{y}(t) + c\dot{y}(t) + ky(t) + k_3 y^3(t) + c_3 \dot{y}^3(t) = u(t) \tag{4.57}$$

When

$$c = 50 \text{ Ns/m}, k = 10^4 \text{ N/m},$$
$$k_3 = 5\times10^8 \text{ N}^3/\text{m}^3, c_3 = 3\times10^2 \text{ N}^3\text{s}^3/\text{m}^3 \tag{4.58}$$

and the sampling frequency is $1/\Delta t = 512 \text{ Hz}$, system (4.57) can be discretized as

$$y(k) = c_{0,1}(1)u(k-1) + c_{1,0}(1)y(k-1) + c_{1,0}(2)y(k-2) + c_{3,0}(1,1,1)y^3(k-1)$$
$$+ c_{3,0}(1,1,2)y^2(k-1)y(k-2) + c_{3,0}(1,2,2)y(k-1)y^2(k-2) + c_{3,0}(2,2,2)y^3(k-2) \tag{4.59}$$

where

$$c_{0,1}(1) = \Delta t^2 = 3.8147\times10^{-6}; c_{1,0}(1) = 2 - \Delta tc - \Delta t^2 k = 1.8642;$$
$$c_{1,0}(2) = \Delta tc - 1 = -0.9023; c_{3,0}(1,1,1) = -k_3\Delta t^2 - c_3/\Delta t = -1.555\times10^5;$$
$$c_{3,0}(1,1,2) = 3c_3/\Delta t = 4.608\times10^5; c_{3,0}(1,2,2) = -3c_3/\Delta t = -4.608\times10^5; \tag{4.60}$$
$$c_{3,0}(2,2,2) = c_3/\Delta t = 1.536\times10^5$$

In this case study, the signal

$$u(k) = \frac{A}{\pi}\frac{\sin\left(150(k-\tau_0)\right) - \sin\left(50(k-\tau_0)\right)}{k-\tau_0}; \begin{cases} k \in [0, 2\tau_0] \\ \tau_0\Delta t = 3\sec \end{cases} \tag{4.61}$$

is applied as the system input. Fig.4.11 shows the signal in two cases of $A = 0.06$ and $A = 0.18$ in the time and the frequency domain, respectively.

The input frequency range is $\omega \in [50, 150] \text{ rad/s}$. In Step 2 of the analysis procedure, the output frequency range of interest is taken as $W = \left[-\hat{N}\omega_{\max}, \hat{N}\omega_{\max}\right]$ where $\hat{N} = 2$. In Step 3, it is determined that $[\![u]\!] = 1.9316$ and $[\![u]\!] = 5.7947$ in the two cases of $A = 0.06$ and $A = 0.18$, respectively.

In Step 4, $\bar{L}_w = 0.0188$ and in this case study, only $c_{3,0}(.)$ in the NARX model (4.59) is involved, so that $\bar{C}_{p,m-p} = \bar{C}_{3,0}$ is calculated as

$$\bar{C}_{3,0} = \sup_{\substack{\omega_i \in W; \\ i=1,\dots,m}} \left| \begin{array}{l} -k_3\Delta t^2 - \dfrac{1}{6} \displaystyle\sum_{\substack{all\ possible \\ permutation\ of\ \omega_i}} \dfrac{c_3}{\Delta t} \left\{ \left[1 - \exp\left(-j(\omega_1 + \omega_2 + \omega_3)\Delta t\right) \right] \right. \\ \left. + 3\left[\exp\left(-j\omega_3\Delta t\right) - \exp\left(-j(\omega_2 + \omega_3)\Delta t\right) \right] \right\} \end{array} \right|$$

$$= \sup_{\substack{\omega_i \in W; \\ i=1,\dots,m}} \left| -k_3\Delta t^2 - \dfrac{c_3}{\Delta t} \prod_{i=1}^{3}\left[1 - \exp\left(-j\omega_i\Delta t\right) \right] \right| = \sup_{\omega \in W} \left| -k_3\Delta t^2 - \dfrac{c_3}{\Delta t}\left[1 - \exp\left(-j\omega\Delta t\right) \right]^3 \right| \qquad (4.62)$$
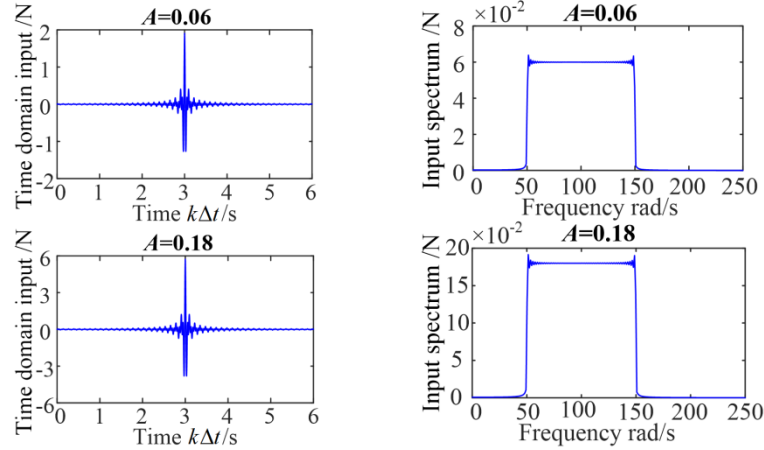
(a) Input signal in the time domain   (b) Input signal in the frequency domain

Fig.4.11 The input signal used in case study 2

Then in Steps 5 and 6, the criterion Γ is calculated as

$$\Gamma_{A=0.06} = 0.5177 \in (0,1] \quad \text{and} \quad \Gamma_{A=0.18} = -0.4468 < 0 \qquad (4.63)$$

indicating that the Volterra series representation of system (4.57) is convergent when $A = 0.06$ while divergent when $A = 0.18$.

The nonlinear output spectra up to the 13th order were calculated by using the GALEs over the frequency range of $\omega \in [50, 150]$ rad/s and the results up to the fifth order of nonlinearity are provided in Fig.4.12.

The results show that the Volterra series representation of system (4.59) can be convergent at $A = 0.06$ as

$$\left| Y_1(j\omega) \right| > \left| Y_3(j\omega) \right| > \cdots > \left| Y_{13}(j\omega) \right| \qquad (4.64)$$

while divergent at $A = 0.18$ because, in this case

$$\left| Y_1(j\omega) \right| > \left| Y_9(j\omega) \right| > \left| Y_7(j\omega) \right| > \cdots > \left| Y_5(j\omega) \right| > \left| Y_3(j\omega) \right| > \cdots \qquad (4.65)$$

Moreover, the convergence boundary of the system input can be obtained by solving equation (4.46) in the specific case of system (4.57), which is,

$$\begin{cases} f_{BC}(\xi, x) = x - \bar{L}_{w_{\text{lin}}}\bar{C}_{0,1}[\![u]\!] - \bar{L}_w\bar{C}_{3,0}x^3 = 0 \\ f'_{BC}(\xi, x) = 1 - 3\bar{L}_w\bar{C}_{3,0}x^2 = 0 \end{cases} \qquad (4.66)$$

for $[\![u]\!]$, yielding $[\![u]\!] = 3.992$ and the corresponding boundary on parameter A of the input signal (4.61)

is 0.124. This boundary is between $A = 0.06$ and $A = 0.18$, which further confirms the effectiveness of the proposed new convergence analysis.


(a) Input magnitude $A = 0.06$ (b) Input magnitude $A = 0.18$
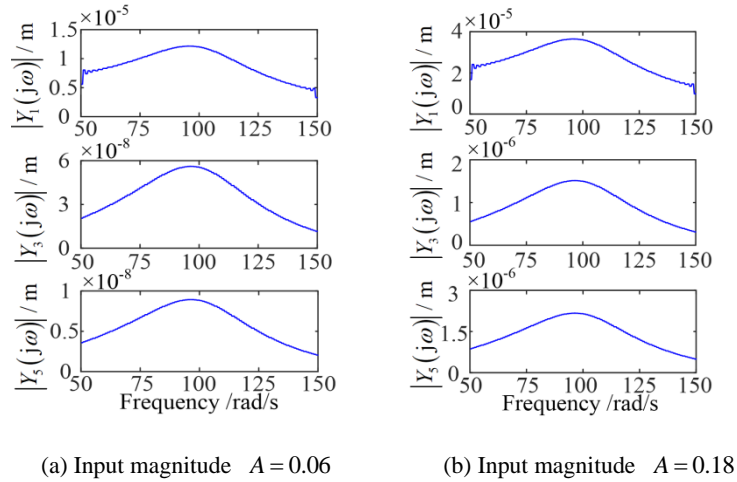
Fig.4.12 The nonlinear output spectra up to the 5th order

4.5 Conclusions

Based on the Volterra series representation of nonlinear systems, many theories and methods including e.g., the GFRFs, the NOFRFs and the OFRF, have been developed for the analysis and design of nonlinear systems in the frequency domain, and some of these theories and methods have been successfully applied to address the nonlinear system analysis and design problems in engineering practice. The fundamental assumption with these nonlinear system theories and methods is that the system under study can be represented by a convergent Volterra series. Generally, the assessment of the convergence issue with a general nonlinear system can only be conducted via numerical analyses to see whether the higher order terms of the Volterra series are degressive. In addition, some analytical methods are available, which can be used to study the convergence problem of the Volterra series representation of relatively simple nonlinear systems.

In the present study, a new convergence analysis for the Volterra series representation of nonlinear systems has been studied. In the analysis, a frequency domain representation of the NARX model, known as the Nonlinear Output Characteristic Spectra (NOCS) model, has been proposed. The Generalized Output Bound Characteristic Function (GOBCF) of NARX models is then defined to represent the bound characteristics of the NARX models. Moreover, a new criterion for the analysis of the convergence of the Volterra series representation is derived based on the GOBCF, producing a novel sufficient condition for a convergent Volterra series representation of the NARX model of nonlinear systems. Compared to existing approaches, the new criterion can provide a more rigorous and less conservative analysis result and is

applicable to nonlinear systems subject to both harmonic and general input excitations. Two case studies have been used to demonstrate the effectiveness of the new analysis and its advantages over available methods. The results achieved have provided an important basis for the application of the frequency domain theories and methods of nonlinear systems to address the analysis and design problems with a wide range of engineering systems. Similar results of the present study can be derived for the convergence analysis of the Volterra series representation of NDE models.

Chapter 5. The effects of both linear and nonlinear characteristic parameters on the output response of nonlinear systems

5.1 Introduction

It has been shown in previous chapters, that the NOFRFs and OFRF of nonlinear systems can be accurately evaluated by using the GALEs, under the convergence condition determined by the GOBCF of the system. However, in the OFRF based analysis and design of nonlinear systems, almost all currently available results require that a nonlinear differential equation-based physical model of the system is available in which the physical parameters that can be used for the system analysis and design are the coefficients in the differential equation model. In order to address this issue, the NARX-M-for-D of nonlinear systems has been proposed in Chapter 2. On the other hand, it is well known that the output frequency responses of nonlinear systems are affected by both the linear and nonlinear characteristic parameters of the system. The OFRF shows an analytical relationship between the output spectra of nonlinear systems and the system's nonlinear characteristic parameters and this relationship is only valid under the condition that the system linear characteristic parameters are fixed. There are still no results that can systematically relate the output frequency response of nonlinear systems to both the system linear and nonlinear characteristic parameters so as to facilitate the analysis and design of the effects of all parameters on the systen output frequency responses.

In this chapter, the OFRF of the NARX-M-for-D in terms of all parameters of concern is defined. A general OFRF-based approach to the frequency domain design of nonlinear systems described by the NARX-M-for-D is then proposed, which allows a systematic OFRF-based design that, for the first time, can take the effect of both the system linear and nonlinear characteristics on the design into account. Moreover, a new concept known as the Associated Output Frequency Response Function (AOFRF) is introduced based on the NARX model of nonlinear systems, which indicates that the output frequency response of nonlinear systems can be represented by a polynomial function of both the system linear and nonlinear characteristic parameters. Effective algorithms are then derived to determine the structure and coefficients of the AOFRF

based representation for the system output frequency response.

Finally, the case studies are used to demonstrate the effectiveness of the proposed new design approach in addressing the challenges with the design of both the linear and nonlinear characteristic parameters of a wide class of nonlinear systems. The structure of this chapter is illustrated as below.
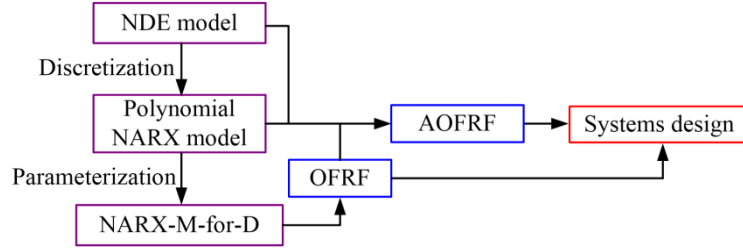

Fig.5.1 The contents of Chapter 5

5.2 The OFRF based design of NARX-M-for-D

5.2.1 The OFRF of the NARX-M-for-D

The OFRF of nonlinear systems is determined based on a nonlinear differential equation model [56], where a polynomial relationship between the system output frequency response and system parameters which defines the system nonlinearities is derived. In this relationship, the coefficients of the polynomial are dependent on the system linear characteristic parameters, and the order of the polynomial is determined by the highest order in the system's Volterra series representation.

For the NARX-M-for-D (2.11), the OFRF concept can be introduced as described in Proposition 5.1 below.

Proposition 5.1. *Assume* $\theta_{p,q}^{(k_1,\cdots,k_{p+q})}(\xi) \in \theta(\xi)$ *can be represented by a polynomial function of the system design parameters* $\xi_1,\ldots,\xi_S$ *up to the* n_ξ *th order such that*

$$\theta_{p,q}^{(k_1,\cdots,k_{p+q})}(\xi) = \sum_{(r_1,\cdots,r_S)\in R_S} \beta_{(r_1,\cdots,r_S)}\xi_1^{r_1}\cdots\xi_S^{r_S} \tag{5.1}$$

where R_S *is a set of* S *-dimensional nonnegative integer vectors which contains the exponents of* $\xi_1^{r_1}\xi_2^{r_2}\cdots\xi_S^{r_S}$ *, and* $r_1,\cdots,r_S \leq n_\xi$ *,* $\beta_{(r_1,\cdots,r_S)}$ *are constants.*

The output frequency response $Y(j\omega)$ *of the NARX-M-for-D can be written into a poynomial function of* $\xi = [\xi_1,\ldots,\xi_S]$ *as*

$$Y(j\omega) = \sum_{(j_1,\cdots,j_S)\in J} \lambda_{(j_1,\cdots,j_S)}(j\omega)\xi_1^{j_1}\cdots\xi_S^{j_S} \tag{5.2}$$

where $\lambda_{(j_1,\cdots,j_S)}(j\omega)$ are the functions of frequency variable ω and are dependent on $\theta_{1,0}^{(k_1)}(\xi)$ and

$\theta_{0,1}^{(k_1)}(\xi)$ *which are the linear characteristic parameters of system (2.11).* **J** *denotes the integer vectors.*

(5.2) is the OFRF of the NARX-M-for-D (2.11).

Proof of Proposition 5.1. Equation (5.2) can be directly achieved by substituting (5.1) into the OFRF

representation (2.31) of the corresponding NARX model.

For example, the OFRF of the NARX-M-for-D (2.8) with coefficients of (2.11) can be written as

$$Y(j\omega) = \lambda_{(0)}(j\omega) + \lambda_{(1)}(j\omega)k_{n3} + \lambda_{(2)}(j\omega)k_{n3}^2 + \cdots \tag{5.3}$$

where $\lambda_{(j)}(j\omega)$, $j = 0,1,\ldots$ are the functions of ω and dependent on the system linear parameters c_l

and k_l.

Also, it can be shown that the OFRF of the NARX-M-for-D (2.8) given by (5.3) is the same as the OFRF

that can be determined from the differential equation model (2.3) of the system given by (2.37). This implies

that, instead of using a physically meaningful differential equation model, the NARX-M-for-D of a nonlinear

system can equally be used to perform the OFRF-based system analysis and design.

It is worth noting that, given an appropriate order of the system nonlinearity that needs to be taken into

account, the OFRF of the NARX-M-for-D is a unique polynomial form representation for the system's output

spectrum [56]. The increase of the system design parameters may increase the complexity of the OFRF. But,

different from numerical approximation or curve fitting, there is no overfitting issue because of the OFRF's

uniqueness.

5.2.2 The determination of the OFRF of NARX-M-for-D

Assume that the coefficients of system (2.11) can be expressed as a polynomial function of the system

design parameters, these coefficients can be written into a matrix form as:

$$\theta_{p,q}^{(k_1,\cdots,k_{p+q})}(\xi) = \xi_{p,q}^{(k_1,\cdots,k_{p+q})}\beta_{p,q}^{(k_1,\cdots,k_{p+q})} \tag{5.4}$$

where $p + q > 0$, $\xi_{p,q}^{(k_1,\cdots,k_{p+q})}$ is the vector composed of the monomials of the form of $\xi_1^{r_1}\cdots\xi_S^{r_S}$ and

$\beta_{p,q}^{(k_1,\cdots,k_{p+q})}$ is a constant vector of a corresponding dimension.

Based on the results in Chapter 2, Section 2.3.4, a recursive algorithm for determining the structure of the

OFRFs of system (2.11) can be derived and described in the following proposition.

Proposition 5.2. *For system (2.11), given $H_1(j\omega)$ and the input spectrum $U(j\omega)$, the nth order*

output spectra of nonlinear system (2.11) can be expressed as:

$$Y_n(j\omega) = \boldsymbol{\Xi}_n \boldsymbol{Y}_n(j\omega) \tag{5.5}$$

and the output spectra of system (2.11) can be expressed as:

$$Y(j\omega) = \sum_{n=1}^{N} \boldsymbol{\Xi}_n \boldsymbol{Y}_n(j\omega) \tag{5.6}$$

In (5.5) and (5.6), $\boldsymbol{\Xi}_n$ is the vector whose components are the monomials of the system design parameters of interest that have contribution to the n th order nonlinear output of the system, $\boldsymbol{Y}_n(j\omega)$ is the vector with corresponding dimensions whose components are dependent only on $H_1(j\omega)$ and the frequency variable ω.

Proof of Proposition 5.2. The GFRFs of system (2.11) can be determined recursively from the parameters of the system time domain model (2.11) as:

$$\left[1 - \sum_{k_1=1}^{K} \theta_{1,0}^{(k_1)}(\xi)\exp\left(-j(\omega_1 + \cdots + \omega_n)k_1\Delta t\right)\right]H_n(\omega_1,\cdots,\omega_n) = \sum_{k_1,k_n=1}^{K} \theta_{0,n}^{(k_1,\cdots,k_n)}(\xi)\exp\left(-j(\omega_1 k_1 + \cdots + \omega_n k_n)\Delta t\right)$$
$$+ \sum_{q=1}^{n-1}\sum_{p=1}^{n-q}\sum_{k_1,k_n=1}^{K}\left[\theta_{p,q}^{(k_1,\cdots,k_{p+q})}(\xi)H_{n-q,p}(\omega_1,\cdots,\omega_{n-q})\exp\left(j(\omega_{n-q+1}k_{p+1} + \cdots + \omega_n k_{p+q})\Delta t\right)\right] \tag{5.7}$$
$$+ \sum_{p=2}^{n}\sum_{k_1,k_p=0}^{K}\left[\overline{\theta}_{p,0}^{(k_1,\cdots,k_p)}(\xi)H_{n,p}(\omega_1,\cdots,\omega_n)\right]$$

with

$$\begin{cases} H_{n,p}(\omega_1,\cdots,\omega_n) = \sum_{i=1}^{n-(p-1)} H_i(\omega_1,\cdots,\omega_i)H_{n-i,p-1}(\omega_{i+1},\cdots,\omega_n)\exp\left(-j\left(\sum_{l=1}^{i}\omega_l\right)k_p\Delta t\right) \\ H_{n,1}(\omega_1,\cdots,\omega_n) = H_n(\omega_1,\cdots,\omega_n)\exp\left(-j(\omega_1 + \cdots + \omega_n)k_1\Delta t\right) \end{cases}$$

It can be seen that given linear coefficients $\theta_{0,1}^{(\cdot)}(\xi)$ and $\theta_{1,0}^{(\cdot)}(\xi)$, the n th order GFRFs of the system (2.11) can be written as [56]:

$$H_n(\omega_1,\cdots,\omega_n) = \sum_{(v_1,\cdots,v_{sN})\in V} h_{(v_1,\cdots,v_{sN})}\theta_1^{v_1}\cdots\theta_{sN}^{v_{sN}} = \boldsymbol{\Theta}_n \boldsymbol{h}_n(\omega_1,\cdots,\omega_n) \tag{5.8}$$

where V represents a sN -dimensional nonnegative integer vectors which contains the exponents of $\theta_1^{v_1}\cdots\theta_{sN}^{v_{sN}}$ and $h_{(v_1,\cdots,v_{sN})}$ are constants, and $\theta_1,\ldots,\theta_{sN} \in \left[\theta_{p,q}^{(k_1,\cdots,k_n)}(\xi)\middle| p+q\geq 2\right]$.

Substituting (5.4) into (5.7), yields:

$$H_n(\omega_1,\cdots,\omega_n) = \sum_{i=1}^{N'} h_{n:i}(\omega_1,\cdots,\omega_n)\xi_{(n:i)}\boldsymbol{\beta}_{(n:i)} = \boldsymbol{\Xi}_n \boldsymbol{H}_n(\omega_1,\cdots,\omega_n) \tag{5.9}$$

where $h_{n:i}(\omega_1,\cdots,\omega_n)$ are the i th element of $\boldsymbol{h}_n(\omega_1,\cdots,\omega_n)$, $\boldsymbol{\Xi}_n$ is composed of $\xi_{(n:i)}$, $i=1,\ldots,N'$, and N' is the maximum dimension of vector $\boldsymbol{\Theta}_n$.

Substituting (5.9) into (5.7), yields:

$$
\begin{aligned}
Y(j\omega) &= \sum_{n=1}^{N} Y_n(j\omega) = \sum_{n=1}^{N} \frac{1}{\sqrt{n}(2\pi)^{n-1}} \int_{\omega_1+\cdots+\omega_n=\omega} \boldsymbol{\Xi}_n \boldsymbol{H}_n(\omega_1,\cdots,\omega_n) \prod_{i=1}^{n} U(j\omega_i) d\sigma_\omega \\
&= \sum_{n=1}^{N} \boldsymbol{\Xi}_n \boldsymbol{Y}_n(j\omega)
\end{aligned}
\tag{5.10}
$$

where

$$
\boldsymbol{Y}_n(j\omega) = \frac{1}{\sqrt{n}(2\pi)^{n-1}} \int_{\omega_1+\cdots+\omega_n=\omega} \boldsymbol{H}_n(\omega_1,\cdots,\omega_n) \prod_{i=1}^{n} U(j\omega_i) d\sigma_\omega
\tag{5.11}
$$

Therefore, Proposition 5.2 is proven.

Proposition 5.3. *The vector $\boldsymbol{\Xi}_n$ introduced in Proposition 5.2 can be determined recursively using an algorithm as follows:*

$$
\boldsymbol{\Xi}_n = \left[\bigcup_{k_1,\ldots,k_n=1}^{K} \boldsymbol{\xi}_{0,n}^{(k_1,\cdots,k_n)} \right] \cup \left[\bigcup_{q=1}^{n-1}\bigcup_{p=1}^{n-q}\bigcup_{k_1,\ldots,k_n=1}^{K} \left(\boldsymbol{\xi}_{p,q}^{(k_1,\cdots,k_{p+q})} \otimes \boldsymbol{\Xi}_{n-q,p} \right) \right] \cup \left[\bigcup_{p=2}^{n}\bigcup_{k_1,\ldots,k_n=1}^{K} \left(\boldsymbol{\xi}_{p,0}^{(k_1,\cdots,k_p)} \otimes \boldsymbol{\Xi}_{n,p} \right) \right]
\tag{5.12}
$$

where the symbol "$\otimes$" is the Kronecker product with $\bar{\bar{\boldsymbol{\Xi}}}_1 = [1]$

$$
\boldsymbol{\Xi}_{n,p} = \bigcup_{i=1}^{n-p+1} \left(\boldsymbol{\Xi}_i \otimes \boldsymbol{\Xi}_{n-i,p-1} \right) \quad and \quad \boldsymbol{\Xi}_{n,1} = \boldsymbol{\Xi}_n
\tag{5.13}
$$

Proof of Proposition 5.3. In (5.7), the nth order GFRFs' coefficient vector $\boldsymbol{\Theta}_n$ can be determined by using the algorithm proposed in Peng et al [74]:

$$
\boldsymbol{\Theta}_n = \left[\bigcup_{k_1,\ldots,k_n=1}^{K} \theta_{0,n}^{(k_1,\cdots,k_n)}(\boldsymbol{\xi}) \right] \cup \left[\bigcup_{q=1}^{n-1}\bigcup_{p=1}^{n-q}\bigcup_{k_1,\ldots,k_n=1}^{K} \left(\theta_{p,q}^{(k_1,\cdots,k_{p+q})}(\boldsymbol{\xi}) \otimes \boldsymbol{\Theta}_{n-q,p} \right) \right] \cup \left[\bigcup_{p=2}^{n}\bigcup_{k_1,\ldots,k_n=1}^{K} \left(\bar{\theta}_{p,0}^{(k_1,\cdots,k_p)}(\boldsymbol{\xi}) \otimes \boldsymbol{\Theta}_{n,p} \right) \right]
\tag{5.14}
$$

where $\boldsymbol{\Theta}_{n,p} = \bigcup_{i=1}^{n-p+1} \left(\boldsymbol{\Theta}_i \otimes \boldsymbol{\Theta}_{n-i,p-1} \right)$ and $\boldsymbol{\Theta}_{n,1} = \boldsymbol{\Theta}_n$.

By substituting (5.4) into (5.14), $\boldsymbol{\Xi}_2$ can be obtained and satisfies Proposition 5.3. Moreover, by using the mathematical induction and assuming Proposition 5.3 holds for $\boldsymbol{\Xi}_n$, it can be obtained that

$$
\boldsymbol{\Xi}_{n+1} = \left[\bigcup_{k_1,\ldots,k_{n+1}=1}^{K} \boldsymbol{\xi}_{0,n+1}^{(k_1,\cdots,k_{n+1})} \right] \cup \left[\bigcup_{q=1}^{n}\bigcup_{p=1}^{n+1-q}\bigcup_{k_1,\ldots,k_{n+1}=1}^{K} \left(\boldsymbol{\xi}_{p,q}^{(k_1,\cdots,k_{p+q})} \otimes \boldsymbol{\Xi}_{n+1-q,p} \right) \right] \cup \left[\bigcup_{p=2}^{n+1}\bigcup_{k_1,\ldots,k_{n+1}=1}^{K} \left(\boldsymbol{\xi}_{p,0}^{(k_1,\cdots,k_p)} \otimes \boldsymbol{\Xi}_{n+1,p} \right) \right]
\tag{5.15}
$$

where, according to (5.7), $\boldsymbol{\Xi}_{n+1,p}$ can be obtained as:

$$
\begin{cases}
\boldsymbol{\Xi}_{n+1,p} = \bigcup_{i=1}^{n+1-p+1} \left(\boldsymbol{\Xi}_i \otimes \boldsymbol{\Xi}_{n+1-i,p-1} \right) \\
\boldsymbol{\Xi}_{n+1,1} = \boldsymbol{\Xi}_{n+1}
\end{cases}
\tag{5.16}
$$

Therefore, Proposition 5.3 is proven.

Proposition 5.3 provides an efficient algorithm for the determination of the monomials that need to be included in the OFRF representation for the output spectrum $Y(j\omega)$ of the more general NARX-M-for-D (2.11). Although the OFRF structure is theoretically related to the system model and can be determined in an analytical way, Proposition 5.3 provides an algorithm which can readily be implemented using computer codes to automatically produce all the monomials in the OFRF.

According to Proposition 5.3, the OFRF of the output spectra of the NARX-M-for-D (2.11) can, like (2.31), be represented by polynomial function of the design parameters $\xi_1, \cdots, \xi_S$.

The coefficients of the OFRF of the NARX-M- for-D (2.11) are generally dependent on the frequency variable ω, the system input, as well as the system linear characteristic parameters. When all of these are fixed, these coefficients are constants and can be numerically evaluated as described in Proposition 5.3 below.

Proposition 5.4. *Assume that the coefficients $\lambda_{(j_1,\ldots,j_S)}(j\omega)$ in the OFRF (5.2) are independent of the system design parameters $\xi_1, \cdots, \xi_S \in \boldsymbol{\xi}$. Given the monomial vector*

$$\boldsymbol{\Xi} = \left[1, \boldsymbol{\Xi}_2, \cdots, \boldsymbol{\Xi}_N\right] = \left[\xi_1^{j_1} \cdots \xi_S^{j_S} \Big| (j_1, \ldots, j_S) \in \boldsymbol{J}\right] \subseteq \left[\bigcup_{j_1=0}^{m_1} \cdots \bigcup_{j_S=0}^{m_S} \xi_1^{j_1} \cdots \xi_S^{j_S}\right] \tag{5.17}$$

where m_i is the maximum power of $\xi_i, i = 1, \ldots, S$ that has been determined by using Proposition 5.2, denote

$$\boldsymbol{\Xi}_{(j)} = \left[1, \boldsymbol{\Xi}_{2,(j)}, \cdots, \boldsymbol{\Xi}_{N,(j)}\right] = \left[\boldsymbol{\Xi}_{(j)}(1), \cdots, \boldsymbol{\Xi}_{(j)}(\bar{M})\right] \tag{5.18}$$

as the vector $\boldsymbol{\Xi}$ evaluated at the j th set of the system design parameters $\xi_i(j), i = 1, \ldots, S$, $\bar{M}$ as the total number of designs that have been initially tried. Then the OFRF representation of the system output spectrum under the j th set of initial design can be written as

$$Y_{(j)}(j\omega) = \left[\boldsymbol{\Xi}_{(j)}(1), \cdots, \boldsymbol{\Xi}_{(j)}(\bar{M})\right] \times \boldsymbol{\Lambda}_{\bar{M}\times 1} = \left[\boldsymbol{\Xi}_{(j)}(1)/l_1, \cdots, \boldsymbol{\Xi}_{(j)}(\bar{M})/l_M\right] \times \tilde{\boldsymbol{\Lambda}}_{\bar{M}\times 1} \tag{5.19}$$

where $\boldsymbol{\Lambda}_{\bar{M}\times 1}$ is a $\bar{M}$ dimensional vector whose components are the coefficients of the OFRF (5.2) and

$$\boldsymbol{L} = \left[l_1, \ldots, l_{\bar{M}}\right]; l_i > 0, i = 1, \ldots, \bar{M} \tag{5.20}$$

is a constant vector, and

$$\tilde{\boldsymbol{\Lambda}}_{\bar{M}\times 1} = \left[l_1 \boldsymbol{\Lambda}_{\bar{M}\times 1}(1), \ldots, l_{\bar{M}} \boldsymbol{\Lambda}_{\bar{M}\times 1}(\bar{M})\right]^{\mathrm{T}} \tag{5.21}$$

are the coefficients in the representation of (5.19). Moreover, the coefficients in (5.19) can be determined as

$$\tilde{\Lambda}_{\bar{M}\times1} = \left(\tilde{\boldsymbol{P}}_{\bar{N}\times\bar{M}}^{\mathrm{T}} \tilde{\boldsymbol{P}}_{\bar{N}\times\bar{M}} \right)^{-1} \tilde{\boldsymbol{P}}_{\bar{N}\times\bar{M}}^{\mathrm{T}} \bar{\boldsymbol{X}}_{\bar{N}\times1} \tag{5.22}$$

where

$$\tilde{\boldsymbol{P}}_{\bar{N}\times\bar{M}} = \begin{bmatrix} \boldsymbol{\Xi}_{(1)}(1)/l_1 & \cdots & \boldsymbol{\Xi}_{(1)}(\bar{M})/l_{\bar{M}} \\ \vdots & \ddots & \vdots \\ \boldsymbol{\Xi}_{(\bar{N})}(1)/l_1 & \cdots & \boldsymbol{\Xi}_{(\bar{N})}(\bar{M})/l_{\bar{M}} \end{bmatrix}_{\bar{N}\times\bar{M}} \tag{5.23}$$

and

$$\bar{\boldsymbol{X}}_{\bar{N}\times1} = \left[X_{(1)}(\mathrm{j}\omega),\ldots,X_{(\bar{N})}(\mathrm{j}\omega) \right]^{\mathrm{T}} \tag{5.24}$$

is a vector the components of which are the system output frequency responses under $\bar{N} \geq \bar{M}$ *different pilot designs.*

Proof of Proposition 5.4. Proposition 5.4 can be proved by using the traditional Least Square (LS) algorithm.

Remark 5.1: The LS algorithm is a very basic method that can be applied as shown in Proposition 5.3 to determine coefficients of the OFRF using the system response data generated from a number of prototype designs. The introduction of the constant vector $\boldsymbol{L}$ in (25) is to ensure the numerical stability of the LS solution (5.22). When $\boldsymbol{L} = [1,\ldots,1]$, (5.22) produces the coefficients of the OFRF (5.2), that is

$$\tilde{\Lambda}_{\bar{M}\times1} = \Lambda_{\bar{M}\times1} \tag{5.25}$$

Otherwise, the coefficient vector $\tilde{\Lambda}_{\bar{M}\times1}$ evaluated from (5.22) is different from the coefficient vector of the original OFRF (5.2). This is needed in many practical cases to circumvent the problems numerically induced by significant difference between the values of different design parameters.

Remark 5.2: In general, the maximum order N of the system nonlinearity is pre-determined. The error of a nonlinear system's OFRF representation is induced by the truncation error associated with the Nth order Volterra series representation of the system. The increase of the order N will reduce the error of the representation. In practice, up to 3th or 5th order system nonlinearity is often sufficient to use in an OFRF representation for the output frequency response of nonlinear systems [56,93].

5.2.3 The OFRF based design of nonlinear systems

The OFRF provides an analytical representation of the output spectrum of nonlinear systems. When the OFRF of a NARX-M-for-D has been determined using the algorithm derived above. The problem of the system design can be described as a constrained optimization problem and formulated as follows.

Find the values of the system physical parameters of interest for the design:

$$\xi_0 = [\xi_1, \ldots, \xi_S]$$
(5.26a)

to solve the optimization problem

$$\underset{\{\xi_1, \ldots, \xi_S\}}{\text{MIN}} \left| \sum_{(j_1, \ldots, j_S) \in \mathbf{J}} \lambda_{(j_1, \ldots, j_S)} (j\omega) \xi_1^{j_1} \cdots \xi_S^{j_S} - Y_0(j\omega) \right|; \ \omega \in \Omega$$
(5.26b)

under the constraint:

$$g_i(\xi_1, \cdots, \xi_S) \leq 0; \ i = 1, \ldots, m$$
(5.26c)

In (5.26), Ω is the frequency range over which the design is considered, $Y_0(j\omega)$ is a desired system output spectrum and $g_i(\xi_1, \cdots, \xi_S)$, $i = 1, \ldots, m$ are the functions associated with the design constraints.

The approach to the solution to the design problem (5.26) can be summarized in a procedure of five steps as follows.

Procedure of the OFRF based Design

1: **System modelling:** Establish a NARX-M-for-D for the nonlinear system by either discretizing an available differential equation model of the system or using a nonlinear system identification method.

2: **Identify model coefficients:**

(i) **Nonlinear coefficients:** Identify the NARX-N-for-D coefficients which define the system nonlinearity and find the relationship between the coefficients and system design parameters $\theta_{p,q}^{(k_1, \cdots, k_{p+q})}(\xi) \in \theta(\xi)$ where $p + q > 1$.

(ii) **Linear coefficients:** Identify the coefficients of the NARX-M-for-D which define the system linear characteristics and the relationship between these coefficients and system design parameters $\theta_{1,0}^{(k_1)}(\xi)$ and $\theta_{0,1}^{(k_1)}(\xi)$

3: **Determine the design constraints:** Determine the system linear characteristic parameters $\theta_{1,0}^{(k_1)}(\xi)$ and $\theta_{0,1}^{(k_1)}(\xi)$ as required by the design for the FRF of the linear part of the system

$$H_1(j\omega) = \frac{\sum_{k_1=1}^{K} \theta_{0,1}^{(k_1)}(\xi) \exp(-j\omega k_1 \Delta t)}{1 - \sum_{k_1=1}^{K} \theta_{1,0}^{(k_1)}(\xi) \exp(-j\omega k_1 \Delta t)}$$
(5.27)

and establish a constraint for the design given by (5.26c) such that $H_1(j\omega)$ is independent from the

variation of the system design parameters $\xi_1, \cdots, \xi_S$.

4:   **Formulation of the design problem:** Determine the OFRF of the NARX-M-for-D using the algorithm in Section III and formulate the optimization design problem (5.26).

5:   **Optimal design:** Solve the optimization design problem (5.26) to find a solution to the design.

A case study of the OFRF based design of the NARX-M-for-D will be shown in details in Section 5.4.

Remark 5.3: The specific form of the design constraint (5.26c) is determined by the practical requirements for the design. However, it is worth pointing out that the design constraint (5.26c) also has to make sure that the OFRF coefficients $\lambda_{(j_1,\ldots,j_S)}(j\omega)$ are independent of the design parameters $\xi_1,\ldots,\xi_S \in \boldsymbol{\xi}$. This is required by the method used to evaluate the OFRF coefficients in Section 5.2.2.

In the following studies, the issue mentioned in Remark 5.3 is resolved based on a newly proposed concept known as the Associated Output Frequency Response Function (AOFRF) of nonlinear systems, which allows both the system linear and the nonlinear characteristic parameters to be taken into account in the system analysis and design.

5.3 The Associated Output Frequency Response Function (AOFRF)

5.3.1 Explicit relationships between the GFRFs and the parameters of the NARX model

In order to facilitate derivations, the *combination* operator " $\oplus$ " of matrix manipulations are firstly defined as bellow:

Considering a m dimensional vector $\boldsymbol{B}_1$ and a n dimensional vector $\boldsymbol{B}_2$, the operation of combination is defined as

$$\boldsymbol{B}_1 \oplus \boldsymbol{B}_2 = \left[\boldsymbol{B}_1(1),\ldots,\boldsymbol{B}_1(m), \boldsymbol{B}_2(1),\ldots,\boldsymbol{B}_2(n) \right]_{1\times(m+n)} \tag{5.28}$$

and $\overset{N}{\underset{i=1}{\oplus}} \boldsymbol{B}_i = \boldsymbol{B}_1 \oplus \boldsymbol{B}_2 \oplus \cdots \oplus \boldsymbol{B}_N$.

Denote, in equation (2.18),

$$L_n(\omega_1,\cdots,\omega_n) = 1 - \sum_{k_1=1}^{K} c_{1,0}(k_1)\exp\left(-j(\omega_1 + \cdots + \omega_n)k_1\Delta t\right) \tag{5.29}$$

$$H_1^{\ n}(\omega_1,\ldots,\omega_n) = H_1(\omega_1)\cdots H_1(\omega_n) \tag{5.30}$$

Then, the first order GFRF of system (2.6) can be determined by taking $n=1$ in (2.18) as

$$H_1(\omega) = \frac{\sum\limits_{k_1=1}^{K} c_{0,1}(k_1)\exp(-j\omega k_1 \Delta t)}{1 - \sum\limits_{k_1=1}^{K} c_{1,0}(k_1)\exp(-j\omega k_1 \Delta t)} \tag{5.31}$$

The second order GFRF of the system can be obtained by taking $n = 2$ in (2.18) to yield

$$\begin{cases} L_2(\omega_1, \omega_2) H_2(\omega_1, \omega_2) = \sum\limits_{k_1,k_2=1}^{K} c_{0,2}(k_1, k_2)\exp(-j(\omega_1 k_1 + \omega_2 k_2)\Delta t) \\ \quad + \sum\limits_{k_1,k_2=1}^{K} c_{1,1}(k_1, k_2) H_{1,1}(\omega_1)\exp(-j\omega_2 k_2 \Delta t) + \sum\limits_{k_1,k_2=1}^{K} c_{2,0}(k_1, k_2) H_{2,2}(\omega_1, \omega_2) \\ H_{2,2}(\omega_1, \omega_2) = H_1(\omega_1) H_{1,1}(\omega_2)\exp(-j\omega_1 k_2 \Delta t) \\ H_{1,1}(\omega_2) = H_1(\omega_2)\exp(-j\omega_2 k_1 \Delta t) \end{cases} \tag{5.32}$$

and consequently,

$$\begin{aligned} H_2(\omega_1, \omega_2) &= \left[L_{(2:0)}(\omega_1, \omega_2) \circ \Phi_{H(2:0)}(\omega_1, \omega_2) \right] C^{\mathrm{T}}_{(2:0)} \\ &\quad + H_1(\omega_1) \left[L_{(2:1)}(\omega_1, \omega_2) \circ \Phi_{H(2:1)}(\omega_1, \omega_2) \right] C^{\mathrm{T}}_{(2:1)} \\ &\quad + H_1^2(\omega_1, \omega_2) \left[L_{(2:2)}(\omega_1, \omega_2) \circ \Phi_{H(2:2)}(\omega_1, \omega_2) \right] C^{\mathrm{T}}_{(2:2)} \end{aligned} \tag{5.33}$$

where "$\circ$" represents the Hadamard product; $\Phi_{H(2:r)}(\omega_1, \omega_2)$ for $r = 0,1,2$ are the vectors of the functions

of frequency variables ω_1, ω_2

$$\begin{cases} L_{(2:0)}(\omega_1, \omega_2) = L_2^{-1}(\omega_1, \omega_2) \left[\bigoplus\limits_{k_1,k_2=1}^{K} 1 \right] \\ L_{(2:1)}(\omega_1, \omega_2) = L_2^{-1}(\omega_1, \omega_2) \left[\bigoplus\limits_{k_1,k_2=1}^{K} L_{([1,1]:1)}(\omega_1) \right] \\ L_{(2:2)}(\omega_1, \omega_2) = L_2^{-1}(\omega_1, \omega_2) \left[\bigoplus\limits_{k_1,k_2=1}^{K} L_{([2,2]:2)}(\omega_1, \omega_2) \right] \end{cases} \tag{5.34}$$

with

$$\begin{cases} L_{([2,2]:r)}(\omega_1, \omega_2) = L_{(1:R)}(\omega_1) \otimes L_{([1,1]:r-R)}(\omega_2) \\ L_{([1,1]:r)}(\omega_2) = L_{(1:r)}(\omega_2) \end{cases} ; \begin{cases} L_{(1:1)}(.) = [1] \\ L_{(1:0)}(.) = L_{(1:r)}(.) = [\mathrm{NULL}] \text{ for } r > 1 \end{cases} \tag{5.35}$$

and

$$\begin{cases} C_{(2:0)}(k_1, k_2) = \left[\bigoplus\limits_{k_1,k_2=1}^{K} c_{0,2}(k_1, k_2) \right] \\ C_{(2:1)}(k_1, k_2) = \left[\bigoplus\limits_{k_1,k_2=1}^{K} c_{1,1}(k_1, k_2) \right] \\ C_{(2:2)}(k_1, k_2) = \left[\bigoplus\limits_{k_1,k_2=1}^{K} c_{2,0}(k_1, k_2) \right] \end{cases} \tag{5.36}$$

where "$\otimes$" represents the Kronecker product.

By following the same procedure, the explicit relationship between the nth order GFRF of system (2.6)

and the system parameters can be obtained. The results are summarized in Proposition 5.4 as follows.

Proposition 5.5. *The* n *th order GFRF of the NARX model (2.6) with* $n \geq 1$ *can be described, in terms of the system first order GFRF and linear and nonlinear characteristic parameters, as*

$$H_n(\omega_1,\ldots,\omega_n) = \sum_{r=0}^{n} H_1^r(\omega_1,\ldots,\omega_r) \Big[L_{(n:r)}(\omega_1,\ldots,\omega_n) \circ \Phi_{H(n:r)}(\omega_1,\ldots,\omega_n) \Big] C^{\mathrm{T}}_{(n:r)} \tag{5.37}$$

where $\Phi_{H(n:r)}(\omega_1,\cdots,\omega_n), r = 0,\ldots,n$ *are the functions of frequency variables* $\omega_1, \cdots, \omega_n$ *;*

$$\begin{cases} L_{(n:r)}(\omega_1,\ldots,\omega_n) = L_n^{-1}(\omega_1,\ldots,\omega_n) \Bigg[\bigoplus_{k_1,\ldots,k_n=1}^{K} \delta \oplus \bigoplus_{q=1}^{n-1} \bigoplus_{p=1}^{n-q} \bigoplus_{k_1,\ldots,k_{p+q}=1}^{K} L_{([n-q,p]:r)}(\omega_1,\cdots,\omega_{n-q}) \\ \quad \oplus \bigoplus_{p=2}^{n} \bigoplus_{k_1,\ldots,k_p=1}^{K} L_{([n,p]:r)}(\omega_1,\cdots,\omega_n) \Bigg] \\ \delta = \begin{cases} [1] & r = 0 \\ [\text{NULL}] & r > 0 \end{cases} \end{cases} \tag{5.38}$$

with

$$\begin{cases} L_{([n,p]:r)}(\omega_1,\cdots,\omega_n) = \bigoplus_{i=1}^{n-p+1} \bigoplus_{R=0}^{r} L_{(i:R)}(\omega_1,\cdots,\omega_i) \otimes L_{([n-i,p-1]:r-R)}(\omega_{i+1},\cdots,\omega_n) \\ L_{([n,1]:r)}(\omega_1,\cdots,\omega_n) = L_{(n:r)}(\omega_1,\cdots,\omega_n) \\ L_{(1:1)}(\omega_1) = [1] \\ L_{(1:0)}(\omega_1) = L_{(n:r)}(.) = [\text{NULL}] \text{ for } r > n \end{cases} \tag{5.39}$$

are only related to the system linear characteristic parameters and

$$C_{(n:r)} = \begin{bmatrix} \bigoplus_{k_1,\ldots,k_n=1}^{K} c_{0,n}(k_1,\ldots,k_n) \delta \oplus \bigoplus_{q=1}^{n-1} \bigoplus_{p=1}^{n-q} \bigoplus_{k_1,\ldots,k_{p+q}=1}^{K} \Big(c_{p,q}(k_1,\ldots,k_{p+q}) \otimes C_{([n-q,p]:r)} \Big) \\ \oplus \bigoplus_{p=2}^{n} \bigoplus_{k_1,\ldots,k_p=1}^{K} \Big(c_{p,0}(k_1,\ldots,k_p) \otimes C_{([n,p]:r)} \Big) \end{bmatrix} \tag{5.40}$$

with

$$\begin{cases} C_{([n,p]:r)} = \bigoplus_{i=1}^{n-p+1} \bigoplus_{R=0}^{r} C_{(i:R)} \otimes C_{([n-i,p-1]:r-R)} \\ C_{([n,1]:r)} = C_{(n:r)} \end{cases}; \begin{cases} C_{(1:1)} = [1] \\ C_{(1:0)} = C_{(n:r)} = [\text{NULL}] \text{ for } r > n \end{cases} \tag{5.41}$$

are determined by the system nonlinear characteristic parameters.

Proof of Proposition 5.5. In the GFRF algorithm (2.18), $H_{n,p}(\omega_1,\cdots,\omega_n)$ can be rewritten as [52]

$$H_{n,p}(\omega_1,\cdots,\omega_n) = \sum_{\substack{r_1,\cdots,r_p=1 \\ \sum r_i=n}}^{n-(p-1)} \prod_{i=1}^{p} H_{r_i}(\omega_{X+1},\cdots,\omega_{X+r_i}) \exp\Big(-\mathrm{j}\big(\omega_{X+1}+\cdots+\omega_{X+r_i}\big)k_{p+1-i}\Delta t\Big) \tag{5.42}$$

where $X = \sum_{x=1}^{i-1} r_x$ and $\sum r_i = \sum_{i=1}^{p} r_i = n$, $f_s = 1/\Delta t$ is the smpling frequency.

It can be proven that Proposition 5.5 holds for $n = 1, 2$. Assuming this holds for the $n-1$ th order GFRF,

$$H_{n-1,p}(\omega_1,\cdots,\omega_{n-1}) = \sum_{i=1}^{n-1-(p-1)} H_i(\omega_1,\cdots,\omega_i) H_{n-1-i,p-1}(\omega_{i+1},\cdots,\omega_{n-1}) \exp\Bigg(-\mathrm{j}\Bigg(\sum_{l=1}^{i}\omega_l\Bigg)k_p\Delta t\Bigg) \tag{5.43}$$

can be rearranged by substituting (5.42) into (5.43) as

$$H_{n-1,p}(\omega_1,\cdots,\omega_{n-1}) = \sum_{\substack{r_1,\cdots,r_p=1 \\ \sum r_i=n-1}}^{n-1-(p-1)} \prod_{i=1}^{p} \sum_{R_i=0}^{r_i} H_1^{R_i}(\omega_1,\ldots,\omega_{R_i}) \left[L_{(r_i:R_i)}(\omega_1,\ldots,\omega_{r_i}) \circ \Phi_{H(r_i:R_i)}(\omega_1,\ldots,\omega_{r_i}) \right] C^{\mathrm{T}}_{(r_i:R_i)}$$

$$= \sum_{r=0}^{n-1} H_1^r(\omega_1,\ldots,\omega_{n-1}) \left[L_{([n-1,p]:r)}(\omega_1,\ldots,\omega_{n-1}) \circ \Phi_{H([n-1,p]:r)}(\omega_1,\ldots,\omega_n) \right] C^{\mathrm{T}}_{([n-1,p]:r)} \tag{5.44}$$

where $L_{([n-1,p]:r)}(\omega_1,\ldots,\omega_{n-1})$ and $C_{([n-1,p]:r)}$ can be calculated using algorithms (5.39) and (5.40) as

Proposition 5.5 holds for $n-1$ th order GFRF.

Substituting (5.44) into the recursive algorithm (2.18), the n th order GFRFs can be obtained as:

$$L_n(\omega_1,\ldots,\omega_n)H_n(\omega_1,\cdots,\omega_n) = \sum_{k_1,k_n=1}^{K} c_{0,n}(k_1,\cdots,k_n)\exp\left(-\mathrm{j}(\omega_1 k_1 +\cdots+\omega_n k_n)\Delta t\right)$$

$$+\sum_{q=1}^{n-1}\sum_{p=1}^{n-q}\sum_{k_1,k_{p+q}=1}^{K} \left\{ c_{p,q}(k_1,\cdots,k_{p+q})\sum_{r=0}^{n-q} H_1^r(\omega_1,\ldots,\omega_r) \left[L_{([n-q,p]:r)}(\omega_1,\ldots,\omega_{n-1}) \right. \right.$$

$$\left. \left. \circ \Phi_{H([n-q,p]:r)}(\omega_1,\ldots,\omega_{n-1}) \right] C^{\mathrm{T}}_{([n-1,p]:r)} \exp\left(-\mathrm{j}(\omega_{n-q+1}k_{p+1}+\cdots+\omega_n k_{p+q})\Delta t\right) \right\}$$

$$+\sum_{p=2}^{n}\sum_{k_1,k_p=1}^{K}\left[c_{p,0}(k_1,\cdots,k_p)H_{n,p}(\omega_1,\cdots,\omega_n)\right] \tag{5.45}$$

where

$$H_{n,p}(\omega_1,\cdots,\omega_n) = \sum_{i=1}^{n-(p-1)} H_i(\omega_1,\cdots,\omega_i)H_{n-i,p-1}(\omega_{i+1},\cdots,\omega_n)\exp\left(-\mathrm{j}\left(\sum_{l=1}^{i}\omega_l\right)k_p\Delta t\right)$$

$$= \sum_{i=1}^{n-(p-1)} \sum_{R_1=0}^{i} H_1^{R_1}(\omega_1,\ldots,\omega_i)\left[L_{(i:R_1)}(\omega_1,\ldots,\omega_i) \circ \Phi_{H(i:R_1)}(\omega_1,\ldots,\omega_i)\right] C^{\mathrm{T}}_{(i:R_1)}$$

$$\times \sum_{R_2=0}^{n-i} H_1^{R_2}(\omega_{i+1},\ldots,\omega_n)\left[L_{([n-i,p]:R_2)}(\omega_{i+1},\ldots,\omega_n) \circ \Phi_{H([n-i,p]:R_2)}(\omega_{i+1},\ldots,\omega_n)\right] C^{\mathrm{T}}_{([n-i,p]:R_2)}$$

$$\times \exp\left(-\mathrm{j}\left(\sum_{l=1}^{i}\omega_l\right)k_p\Delta t\right) = \sum_{r=0}^{n} H_1^r(\omega_1,\ldots,\omega_n)\left[L_{([n,p]:r)}(\omega_1,\ldots,\omega_n) \circ \Phi_{H([n,p]:r)}(\omega_1,\ldots,\omega_n)\right] C^{\mathrm{T}}_{([n,p]:r)} \tag{5.46}$$

with $r=R_1+R_2$,

$$\begin{cases} L_{([n,p]:r)}(\omega_1,\cdots,\omega_n) = \overset{n-p+1}{\underset{i=1}{\oplus}}\overset{r}{\underset{R=0}{\oplus}} L_{(i:R)}(\omega_1,\cdots,\omega_i)\otimes L_{([n-i,p-1]:r-R)}(\omega_{i+1},\cdots,\omega_n) \\ C_{([n,p]:r)} = \overset{n-p+1}{\underset{i=1}{\oplus}}\overset{r}{\underset{R=0}{\oplus}} C_{(i:R)}\otimes C_{([n-i,p-1]:r-R)} \end{cases} \tag{5.47}$$

Equation (5.45) can be easily rearranged as:

$$H_n(\omega_1,\ldots,\omega_n) = \sum_{r=0}^{n} H_1^r(\omega_1,\ldots,\omega_r)\left[L_{(n:r)}(\omega_1,\ldots,\omega_n) \circ \Phi_{H(n:r)}(\omega_1,\ldots,\omega_n)\right] C^{\mathrm{T}}_{(n:r)} \tag{5.48}$$

so Proposition 5.5 is proved.

Equation (5.37) reveals an important relationship between the GFRFs and the system linear and nonlinear characteristic parameters. Compared with the algorithm (2.18) for calculating GFRFs, the relationship (5.37) explicitly decouples the effects of the system linear and nonlinear characteristic parameters on the GFRFs, which can facilitate a separate analysis and design of the system linear and nonlinear characteristic parameters. Moreover, the order of the first order GFRF $H_1(.)$ that affects the GFRF is also explicit in

(5.37), making the effect of the system linear characteristic parameters on the GFRFs more easily be investigated.

Remark 5.4. When the system linear characteristic parameters are fixed in (5.37), the n th order GFRF can be directly written as a polynomial function of the nonlinear characteristic parameters [74]:

$$H_n\left(\omega_1,\ldots,\omega_n\right)=\sum_{r=0}^{n}\boldsymbol{\Psi}_{(n:r)}^{L}\left(\omega_1,\ldots,\omega_n\right)\boldsymbol{C}_{(n:r)}^{\mathrm{T}}$$ (5.49)

where

$$\boldsymbol{\Psi}_{(n:r)}^{L}\left(\omega_1,\ldots,\omega_n\right)=H_1^{r}\left(\omega_1,\ldots,\omega_r\right)\left[\boldsymbol{L}_{(n:r)}\left(\omega_1,\ldots,\omega_n\right)\circ\boldsymbol{\Phi}_{H(n:r)}\left(\omega_1,\ldots,\omega_n\right)\right]$$ (5.50)

is a function of the frequency variables.

When the system nonlinear characteristic parameters are fixed, equation (5.37) can be written as

$$H_n\left(\omega_1,\ldots,\omega_n\right)=\sum_{r=0}^{n}H_1^{r}\left(\omega_1,\ldots,\omega_r\right)\boldsymbol{L}_{(n:r)}\left(\omega_1,\ldots,\omega_n\right)\boldsymbol{\Psi}_{(n:r)}^{NL}\left(\omega_1,\ldots,\omega_n\right)$$ (5.51)

where

$$\boldsymbol{\Psi}_{(n:r)}^{NL}\left(\omega_1,\ldots,\omega_n\right)=\boldsymbol{\Phi}_{H}^{\mathrm{T}}{}_{(n:r)}\left(\omega_1,\ldots,\omega_n\right)\circ\boldsymbol{C}_{(n:r)}^{\mathrm{T}}$$ (5.52)

is again a function of the frequency variables. Clearly, the two cases of equation (5.37) given by (5.49) and (5.51) can be used to separately study the effects of the system linear and nonlinear characteristic parameters on the GFRFs.

5.3.2 Two special cases

In the following, two special NARX models with the pure input and pure output nonlinearity, respectively, are used to illustrate the results of Proposition 5.5.

The NARX model with pure input nonlinearity can be written as:

$$y(t)=\sum_{m=1}^{M}\sum_{k_1,k_n=1}^{K}\left[c_{0,n}(k_1,\cdots,k_n)\prod_{i=1}^{m}u(t-k_i)\right]$$ (5.53)

The GFRFs of the system are given by

$$H_n(\omega_1,\cdots,\omega_n)=\sum_{k_1,k_n=1}^{K}c_{0,n}(k_1,\cdots,k_n)\exp\left(-\mathrm{j}\left(\omega_1 k_1+\cdots+\omega_n k_n\right)\Delta t\right),n=1,2,\ldots$$ (5.54)

From Proposition 5.5, it can readily be shown that

Corollary 5.1. *The n th order GFRF of nonlinear systems with pure input nonlinearity can be described as:*

$$H_n\left(\omega_1,\ldots,\omega_n\right)=\boldsymbol{\Phi}_{H(n:0)}\left(\omega_1,\ldots,\omega_n\right)\boldsymbol{C}_{(n:0)}^{\mathrm{T}}$$ (5.55)

where

$$C_{(n:0)} = \left[\bigoplus_{k_1,\dots,k_n=1}^{K} c_{0,n}(k_1,\cdots,k_n) \right] \tag{5.56}$$

The NARX model of pure output nonlinearity can be expressed as:

$$y(t) = \sum_{m=1}^{M}\sum_{p=1}^{m}\sum_{k_1,k_p=1}^{K}\left[c_{p,0}(k_1,\cdots,k_p)\prod_{i=1}^{p} y(t-k_i) \right] \tag{5.57}$$

The GFRFs of the system are given by:

$$H_n(\omega_1,\cdots,\omega_n) = L_n^{-1}(\omega_1,\dots,\omega_n)\sum_{p=2}^{n}\sum_{k_1,k_p=1}^{K}\left[c_{p,0}(k_1,\cdots,k_p)H_{n,p}(\omega_1,\cdots,\omega_n) \right] \tag{5.58}$$

Again, following Proposition 5.5, it can be shown that

Corollary 5.2. *The n th order GFRF of pure output nonlinear systems can be expressed as:*

$$H_n(\omega_1,\cdots,\omega_n) = H_1^{n}(\omega_1,\dots,\omega_n)\left[L_{(n:n)}(\omega_1,\dots,\omega_n) \circ \Phi_{H(n:n)}(\omega_1,\dots,\omega_n) \right]C^{\mathrm{T}}_{(n:n)} \tag{5.59}$$

where

$$L_{(n:n)}(\omega_1,\dots,\omega_n) = L_n^{-1}(\omega_1,\dots,\omega_n)\left[\bigoplus_{p=2}^{n}\bigoplus_{k_1,\dots,k_p=1}^{K} L_{([n,p]:n)}(\omega_1,\cdots,\omega_n) \right] \tag{5.60}$$

$$C_{(n:n)} = \left[\bigoplus_{p=2}^{n}\bigoplus_{k_1,\dots,k_p=1}^{K} c_{p,0}\left(k_1,\dots,k_p\right) \otimes C_{([n,p]:n)} \right] \tag{5.61}$$

for $n \geq 1$, and

$$\begin{cases} \begin{cases} L_{([n,p]:n)}(\omega_1,\cdots,\omega_n) = \bigoplus_{i=1}^{n-p+1} L_{(i:i)}(\omega_1,\cdots,\omega_i) \otimes L_{([n-i,p-1]:n-i)}(\omega_{i+1},\cdots,\omega_n) \\ L_{([n,1]:n)}(\omega_1,\cdots,\omega_n) = L_{(n:n)}(\omega_1,\cdots,\omega_n) \end{cases} \\ \begin{cases} L_{(1:1)}(\omega_1) = [1] \\ L_{(1:0)}(\omega_1) = [\mathrm{NULL}] \end{cases} \end{cases} \tag{5.62}$$

$$\begin{cases} C_{([n,p]:n)} = \bigoplus_{i=1}^{n-p+1} C_{(i:i)} \otimes C_{([n-i,p-1]:n-i)} \\ C_{([n,1]:n)} = C_{(n:n)} \end{cases}; \begin{cases} C_{(1:1)} = [1] \\ C_{(1:0)} = [\mathrm{NULL}] \end{cases} \tag{5.63}$$

Corollaries 5.1 and 5.2 are two special cases but also important in practice. This is because many nonlinear systems in practice can be described by a pure input nonlinearity system such as a Volterra model [122,123] or a pure output nonlinearity system [75,124]. In these cases, the simpler results in Corollaries 5.1 and 5.2 can be used to study the GFRFs of corresponding nonlinear systems.

5.3.3 The concept of the Associated Output Frequency Response Function (AOFRF)

The AOFRF concept is introduced from the derivation of a new representation for the output spectrum of nonlinear systems as described in Proposition 5.5 bellow. The objective is to facilitate the derivation of an

analytical relationship between the output frequency response and both the linear and nonlinear characteristic

parameters of the NARX model of nonlinear systems

Proposition 5.6. *The output spectrum of nonlinear system (2.6) can be described as*

$$
\begin{aligned}
Y(j\omega) &= \sum_{r=0}^{N}\sum_{n=r}^{N}\int_{\omega_1+\cdots+\omega_n=\omega} H_1^{\ r}\left(\omega_1,\ldots,\omega_r\right)\left[\boldsymbol{L}_{(n:r)}\left(\omega_1,\ldots,\omega_n\right)\circ\boldsymbol{\Phi}_{(n:r)}\left(\omega_1,\ldots,\omega_n\right)\right]\boldsymbol{C}^{\mathrm{T}}_{\ (n:r)}\,\mathrm{d}\sigma_\omega \\
&= \sum_{r=0}^{N}\tilde{Y}_r\left(j\omega\right)
\end{aligned}
\tag{5.64}
$$

where

$$
\tilde{Y}_r\left(j\omega\right) = \sum_{n=r}^{N}\int_{\omega_1+\cdots+\omega_n=\omega} H_1^{\ r}\left(\omega_1,\ldots,\omega_r\right)\left[\boldsymbol{L}_{(n:r)}\left(\omega_1,\ldots,\omega_n\right)\circ\boldsymbol{\Phi}_{(n:r)}\left(\omega_1,\ldots,\omega_n\right)\right]\boldsymbol{C}^{\mathrm{T}}_{\ (n:r)}\,\mathrm{d}\sigma_\omega
\tag{5.65}
$$

is referred to as the r th order Associated Output Response Function (AOFRF) and

$$
\boldsymbol{\Phi}_{(n:r)}\left(\omega_1,\ldots,\omega_n\right) = \frac{1}{\sqrt{n}\left(2\pi\right)^{n-1}}\boldsymbol{\Phi}_{H(n:r)}\left(\omega_1,\ldots,\omega_n\right)\prod_{j=1}^{n}U\left(j\omega_j\right)
\tag{5.66}
$$

Proof of Proposition 5.6. Considering (5.37), the *n* th order output frequency response $Y_n\left(j\omega\right)$ can be

written as:

$$
\begin{aligned}
Y_n\left(j\omega\right) &= \frac{1}{\sqrt{n}\left(2\pi\right)^{n-1}}\int_{\omega_1+\cdots+\omega_n=\omega}\sum_{r=0}^{n}H_1^{\ r}\left(\omega_1,\ldots,\omega_r\right) \\
&\quad\times\left[\boldsymbol{L}_{(n:r)}\left(\omega_1,\ldots,\omega_n\right)\circ\boldsymbol{\Phi}_{H(n:r)}\left(\omega_1,\ldots,\omega_n\right)\right]\boldsymbol{C}^{\mathrm{T}}_{\ (n:r)}\prod_{i=1}^{n}U\left(j\omega_i\right)\mathrm{d}\sigma_\omega \\
&= \sum_{r=0}^{n}\int_{\omega_1+\cdots+\omega_n=\omega}\frac{1}{\sqrt{n}\left(2\pi\right)^{n-1}}H_1^{\ r}\left(\omega_1,\ldots,\omega_r\right) \\
&\quad\times\left[\boldsymbol{L}_{(n:r)}\left(\omega_1,\ldots,\omega_n\right)\circ\boldsymbol{\Phi}_{H(n:r)}\left(\omega_1,\ldots,\omega_n\right)\right]\boldsymbol{C}^{\mathrm{T}}_{\ (n:r)}\prod_{i=1}^{n}U\left(j\omega_i\right)\mathrm{d}\sigma_\omega
\end{aligned}
\tag{5.67}
$$

Substituting (5.67) into (2.14) for $Y_n\left(j\omega\right)$ yields:

$$
\begin{aligned}
Y\left(j\omega\right) &= \sum_{n=1}^{N}Y_n\left(j\omega\right) = \sum_{n=1}^{N}\sum_{r=0}^{n}\int_{\omega_1+\cdots+\omega_n=\omega}\frac{1}{\sqrt{n}\left(2\pi\right)^{n-1}}H_1^{\ r}\left(\omega_1,\ldots,\omega_r\right) \\
&\quad\times\left[\boldsymbol{L}_{(n:r)}\left(\omega_1,\ldots,\omega_n\right)\circ\boldsymbol{\Phi}_{H(n:r)}\left(\omega_1,\ldots,\omega_n\right)\right]\boldsymbol{C}^{\mathrm{T}}_{\ (n:r)}\prod_{i=1}^{n}U\left(j\omega_i\right)\mathrm{d}\sigma_\omega \\
&= \sum_{r=0}^{N}\sum_{n=r}^{N}\int_{\omega_1+\cdots+\omega_n=\omega}\frac{1}{\sqrt{n}\left(2\pi\right)^{n-1}}H_1^{\ r}\left(\omega_1,\ldots,\omega_r\right) \\
&\quad\times\left[\boldsymbol{L}_{(n:r)}\left(\omega_1,\ldots,\omega_n\right)\circ\boldsymbol{\Phi}_{H(n:r)}\left(\omega_1,\ldots,\omega_n\right)\right]\boldsymbol{C}^{\mathrm{T}}_{\ (n:r)}\prod_{i=1}^{n}U\left(j\omega_i\right)\mathrm{d}\sigma_\omega
\end{aligned}
\tag{5.68}
$$

Denote $\boldsymbol{\Phi}_{(n:r)}\left(\omega_1,\ldots,\omega_n\right)$ as given by (5.66) and define $\tilde{Y}_r\left(j\omega\right)$ as giben by (5.65), then (5.68) can be

rearranged as (5.64), so Proposition 5.6 is proven.

Given the system linear characteristic parameters and input spectrum, the AOFRF (5.67) can be written as

$$\tilde{Y}_r\left(\mathrm{j}\omega\right)=\sum_{n=r}^{N}\boldsymbol{\Gamma}_{(n:r)}\left(\omega_1,\ldots,\omega_n\right)\boldsymbol{C}^{\mathrm{T}}{}_{(n:r)} \tag{5.69}$$

where

$$\boldsymbol{\Gamma}_{(n:r)}\left(\omega_1,\ldots,\omega_n\right)=\int_{\omega_1+\cdots+\omega_n=\omega}H_1^r\left(\omega_1,\ldots,\omega_r\right)\left[\boldsymbol{L}_{(n:r)}\left(\omega_1,\ldots,\omega_n\right)\circ\boldsymbol{\Phi}_{(n:r)}\left(\omega_1,\ldots,\omega_n\right)\right]\mathrm{d}\sigma_\omega \tag{5.70}$$

is only dependent on the system linear characteristic parameters. Therefore,

$$Y\left(\mathrm{j}\omega\right)=\sum_{r=0}^{N}\sum_{n=r}^{N}\boldsymbol{\Gamma}_{(n:r)}\left(\omega_1,\ldots,\omega_n\right)\boldsymbol{C}^{\mathrm{T}}{}_{(n:r)}=\sum_{n=1}^{N}\boldsymbol{\Gamma}_{n}\left(\omega_1,\ldots,\omega_n\right)\boldsymbol{C}^{\mathrm{T}}{}_{n} \tag{5.71}$$

with

$$\boldsymbol{\Gamma}_{n}\left(\omega_1,\ldots,\omega_n\right)=\bigcup_{r=0}^{N}\boldsymbol{\Gamma}_{(n:r)}\left(\omega_1,\ldots,\omega_n\right)\quad\text{and}\quad\boldsymbol{C}_{n}=\bigcup_{r=0}^{N}\boldsymbol{C}_{(n:r)} \tag{5.72}$$

which is just the OFRF of the system (2.6), a polynomial function of the system nonlinear characteristic parameters.

The introduction of the AOFRF concept is to facilitate the derivation of the relationship between $Y\left(\mathrm{j}\omega\right)$ and both the system linear and nonlinear characteristic parameters when the system linear and nonlinear characteristic parameters are all of interests for the system analysis and design. More details will be discussed in the next section.

5.3.4 The AOFRF in terms of the system linear and nonlinear characteristic parameters

In this section, the AOFRF of system (2.6) is expanded as a polynomial function in terms of both the system linear and nonlinear characteristic parameters. In order to achieve this, a polynomial expansion of $H_1^r\left(\omega_1,\ldots,\omega_r\right)$ and $\boldsymbol{L}_{(n:r)}\left(\omega_1,\ldots,\omega_n\right)$ in terms of the system linear characteristic parameters is first considered. Then, based on the polynomial expansion, a polynomial representation of the AOFRF in terms of the system linear and nonlinear characteristic parameters is obtained.

Lemma 5.1. *If there exist a set of constants* $\boldsymbol{C}_z=\left[c_z\left(k\right)\middle|k=1,\ldots,K\right]$ *such that*

$$\sum_{k=1}^{K}\left|c_{1,0}\left(k\right)-c_z\left(k\right)\right|<1 \tag{5.73}$$

the terms relevant to the system linear characteristic parameters in the AOFRF, $H_1^r\left(\omega_1,\ldots,\omega_r\right)$ *and elements in* $\boldsymbol{L}_{(n:r)}\left(\omega_1,\ldots,\omega_n\right)$, *can be written in to a polynomial form as:*

$$H_1^r\left(\omega_1,\ldots,\omega_r\right)=\sum_{l=0}^{r\times n_L}\sum_{\substack{\tau_1+\cdots+\tau_K=l\\ \upsilon_1+\cdots+\upsilon_K=r}}\varphi_{\left[\substack{\tau_1,\cdots,\tau_K\\ \upsilon_1,\cdots,\upsilon_K}\right]}\prod_{k_\upsilon=1}^{K}c_{0,1}^{\upsilon_{k_\upsilon}}\left(k_\upsilon\right)\prod_{k_\tau=1}^{K}c_{1,0}^{\tau_{k_\tau}}\left(k_\tau\right) \tag{5.74}$$

$$EL\left[\boldsymbol{L}_{(n:r)}\right] = \sum_{l=0}^{(n-1)\times n_L} \sum_{\tau_1+\cdots+\tau_K=l} \tilde{\varphi}_{\tau_1,\cdots,\tau_K} \prod_{k=1}^{K} c_{1,0}{}^{\tau_k}(k) \tag{5.75}$$

where $EL[.]$ is defined as an operator for extracting the element of a vector. For example, in (5.75), $EL\left[\boldsymbol{L}_{(n:r)}\right]$ represents an element belongs to the vector $\boldsymbol{L}_{(n:r)}(\omega_1,\ldots,\omega_n)$; n_L is the maximum order of $H_1(.)$ that is expanded into a polynomial in terms of $c_{1,0}(.)$; $\varphi_{\left[\begin{smallmatrix}\tau_1,\cdots,\tau_K\\ \upsilon_1,\cdots,\upsilon_K\end{smallmatrix}\right]}$ and $\tilde{\varphi}_{\tau_1,\cdots,\tau_K}$ are the frequency related coefficients, and τ_i, υ_i for $i=1,\ldots,K$ are positive integers.

Proof of Lemma 5.1. See Appendix B

It is worth noticing that the first order GFRF $H_1(\omega_i)$ and $L_i^{-1}(\omega_1,\cdots,\omega_i)$ for $i=1,\ldots,n$ can be expanded into a polynomial of the same order n_L. It is known from (5.65) and the definition of $\boldsymbol{C}_{(n:r)}$ in (5.40) that, the AOFRF is a polynomial function of the system nonlinear characteristic parameters if $H_1^r(\omega_1,\ldots,\omega_r)$ and $\boldsymbol{L}_{(n:r)}(\omega_1,\ldots,\omega_n)$ are fixed. Lemma 5.1 shows both $H_1^r(\omega_1,\ldots,\omega_r)$ and $\boldsymbol{L}_{(n:r)}(\omega_1,\ldots,\omega_n)$ can be represented by a polynomial function of the system linear characteristic parameters. These imply that the AOFRF can be expanded as a polynomial function of both the system linear and nonlinear characteristic parameters as shown in Proposition 5.7.

Proposition 5.7. *The r th order AOFRF (5.65) of the NARX model (2.6) can be expressed as a polynomial function in terms of both system linear and nonlinear characteristic parameters*

$$\tilde{Y}_r(\mathrm{j}\omega) = \sum_{(j_1,\cdots,j_{rN})\in J_{rN}} \tilde{\lambda}_{j_1,\cdots,j_{rN}}(\mathrm{j}\omega)\theta_1^{j_1}\cdots\theta_{rN}^{j_{rN}} = \Lambda_r\boldsymbol{\Theta}_r^{\mathrm{T}} \tag{5.76}$$

under the convergence condition (5.73), where Λ_r is the vector of the coefficients $\tilde{\lambda}_{j_1,\cdots,j_{rN}}(\mathrm{j}\omega)$, $\boldsymbol{\Theta}_r$ is the vector of the monomials of (5.76), $\boldsymbol{J}_{rN}$ is the set of all available index $j_1,\ldots,j_{rN}$; $\tilde{\lambda}_{j_1,\cdots,j_{rN}}(\mathrm{j}\omega)$ is the function only related to the frequency variables, and $\theta_1,\ldots,\theta_{rN}$ belongs to

$$\boldsymbol{C}_r = \boldsymbol{C}_r^r \bigcup \boldsymbol{C}_{r+1}^r \bigcup\cdots\bigcup \boldsymbol{C}_N^r \tag{5.77}$$

where, for $r \le n \le N$, $n \ge 1$

$$\boldsymbol{C}_n^r = \begin{cases} c_{0,n}(k_1,\cdots,k_n) & \begin{cases} k_i=1,\ldots,K; i=1,\ldots,n \\ r=0 \end{cases} \\ c_{p,q}(k_1,\cdots,k_{p+q}) & \begin{cases} k_i=1,\ldots,K; i=1,\ldots,p+q \\ q=1,\ldots,n-r; p+q<n; r\ge1 \end{cases} \\ c_{p,0}(k_1,\cdots,k_p) & \begin{cases} k_i=1,\ldots,K; i=1,\ldots,p \\ p=1,\ldots,n; r\ge1 \end{cases} \end{cases}, c_{0,0}(.)=0 \tag{5.78}$$

Proof of Proposition 5.7. For any $r \leq n \leq N$, when $r = 0$, it is obvious that

$$C_n^0 = \left\{ c_{0,n}(k_1, \cdots, k_n) \quad k_i = 1, \ldots, K; i = 1, \ldots, n \right\} \tag{5.79}$$

When $r = 1$, according to Proposition 5.5, it is also known that $H_1^1(.)$ can be extracted from all

$H_{n-q,p}(.)$ for $n - q \geq 1$ and $p + q \leq n$, which means

$$C_n^1 = \begin{cases} c_{p,q}(k_1, \cdots, k_{p+q}) & \begin{cases} k_i = 1, \ldots, K; i = 1, \ldots, p+q \\ q = 1, \ldots, n-1; \ p+q \leq n \end{cases} \\ c_{p,0}(k_1, \cdots, k_p) & \begin{cases} k_i = 1, \ldots, K; i = 1, \ldots, p \\ p = 1, \ldots, n \end{cases} \end{cases} \tag{5.80}$$

Similarly, for the r th order, $r \geq 1$, $H_1^r(.)$ can be extracted from all $H_{n-q,p}(.)$ for $n - q \geq r$ and

$p + q \leq n$,

$$C_n^r = \begin{cases} c_{p,q}(k_1, \cdots, k_{p+q}) & \begin{cases} k_i = 1, \ldots, K; i = 1, \ldots, p+q \\ q = 1, \ldots, n-r; \ p+q \leq n \end{cases} \\ c_{p,0}(k_1, \cdots, k_p) & \begin{cases} k_i = 1, \ldots, K; i = 1, \ldots, p \\ p = 1, \ldots, n \end{cases} \end{cases} \tag{5.81}$$

Therefore, (5.77) and (5.78) can be obtained according to Proposition 5.6 and then the Proposition 5.7 is

proven.

Substituting (5.76) into (5.64) for $\tilde{Y}_r(j\omega)$ yields the AOFRF based representation of the output frequency

response of nonlinear systems which will be discussed in details next.

5.3.5 The AOFRF based representation of the output frequency response of nonlinear

systems

(A) The structure of the representation

According to Propositions 5.6 and 5.7, an AOFRF based representation for the output frequency response

of nonlinear system (2.6) can be obtained as

$$Y(j\omega) = \sum_{r=0}^{N} \tilde{Y}_r(j\omega) = \sum_{r=0}^{N} \Lambda_r \Theta_r^{\mathrm{T}} \tag{5.82}$$

The determination of the structure of (5.82) is concerned with determining the components in Θ_r^{T} for

$r = 0, \ldots, N$, which are the monomials in the polynomial representation of the r th order AOFRF. This can

be achieved by using the algorithm in Proposition 5.8 as follows.

Proposition 5.8. *The monomials in the r th order AOFRF can be determined as*

$$\boldsymbol{\Theta}_r = \bigcup_{n=r}^{N} \left[\boldsymbol{\Theta}_{(n:r)}^{L} \otimes \boldsymbol{\Theta}_{(n:r)}^{NL} \right] \tag{5.83}$$

where

$$\boldsymbol{\Theta}_r = \left[\theta_1^{j_1} \cdots \theta_{rN}^{j_{rN}} \big| \left(j_1, \ldots, j_{rN} \right) \in \boldsymbol{J}_{rN} \right] \tag{5.84}$$

and $\boldsymbol{\Theta}_{(n:r)}^{L}$ represents a vector only consisting of system linear characteristic parameters and $\boldsymbol{\Theta}_{(n:r)}^{NL}$ is a vector only consisting of system nonlinear characteristic parameters. $\boldsymbol{\Theta}_{(n:r)}^{L}$ and $\boldsymbol{\Theta}_{(n:r)}^{NL}$ can be obtained as bellow.

Denote $\boldsymbol{\theta}_H$ and $\boldsymbol{\theta}_L$ are the vectors of the monomials in the Taylor series representation of $H_1(\omega_i)$ and $L_i^{-1}(\omega_1, \cdots, \omega_i)$ for $i = 1, \ldots, n$, respectively. Then,

$$\boldsymbol{\Theta}_{(n:r)}^{L} = [\boldsymbol{\theta}_H]^r \otimes \bigcup_{i=1}^{n-1} [\boldsymbol{\theta}_L]^i \tag{5.85}$$

where $[\boldsymbol{\theta}_H]^r = \underbrace{\boldsymbol{\theta}_H \otimes \cdots \otimes \boldsymbol{\theta}_H}_{r}$ and $[\boldsymbol{\theta}_L]^i = \underbrace{\boldsymbol{\theta}_L \otimes \cdots \otimes \boldsymbol{\theta}_L}_{i}$.

$$\boldsymbol{\Theta}_{(n:r)}^{NL} = \left[\bigcup_{k_1, \ldots, k_n = 1}^{K} c_{0,n}(k_1, \cdots, k_n) \right] \cup \left[\bigcup_{q=1}^{n-1} \bigcup_{p=1}^{n-q} \bigcup_{k_1, \ldots, k_n = 1}^{K} \left(c_{p,q}(k_1, \cdots, k_{p+q}) \otimes \boldsymbol{\Theta}_{([n-q,p]:r)}^{NL} \right) \right]$$
$$\cup \left[\bigcup_{p=2}^{n} \bigcup_{k_1, \ldots, k_n = 1}^{K} \left(c_{p,0}(k_1, \cdots, k_p) \otimes \boldsymbol{\Theta}_{([n,p]:r)}^{NL} \right) \right] \tag{5.86}$$

where

$$\begin{cases} \boldsymbol{\Theta}_{([n,p]:r)}^{NL} = \bigcup_{i=1}^{n-p+1} \bigcup_{R=0}^{r} \boldsymbol{\Theta}_{(i:R)}^{NL} \otimes \boldsymbol{\Theta}_{([n-i,p-1]:r-R)}^{NL} \\ \boldsymbol{\Theta}_{([n,1]:r)}^{NL} = \boldsymbol{\Theta}_{(n:r)}^{NL} \end{cases}; \begin{cases} \boldsymbol{\Theta}_{(1:1)}^{NL} = [1] \\ \boldsymbol{\Theta}_{(1:0)}^{NL} = \boldsymbol{\Theta}_{(n:r)}^{NL} = [\text{NULL}] \ for \ r > n \end{cases} \tag{5.87}$$

Proof of Proposition 5.8. Omitted as (5.85) can be directly obtained according to Proposition 5.7, and (5.86) can be derived from Proposition 5.5 and Proposition 5.6.

When $\boldsymbol{\Theta}_r^{\mathrm{T}}, r = 0, \ldots, N$ have been obtained, the system output frequency response can further be described as

$$Y(j\omega) = \sum_{r=0}^{N} \boldsymbol{\Lambda}_r \boldsymbol{\Theta}_r^{\mathrm{T}} = [\boldsymbol{\Lambda}_0, \cdots, \boldsymbol{\Lambda}_N][\boldsymbol{\Theta}_0, \cdots, \boldsymbol{\Theta}_N]^{\mathrm{T}} = \boldsymbol{\Lambda}\boldsymbol{\Theta}^{\mathrm{T}} = \sum_{(j_1, \cdots, j_S) \in J_S} \lambda_{j_1, \cdots, j_S}(j\omega) \theta_1^{j_1} \cdots \theta_S^{j_S} \tag{5.88}$$

where $\boldsymbol{J}_S$ is the set of all available indices $j_1, \ldots, j_S$. The vector

$$\boldsymbol{\Theta} = [\boldsymbol{\Theta}_0, \cdots, \boldsymbol{\Theta}_N] = \left[\theta_1^{j_1} \cdots \theta_S^{j_S} \big| (j_1, \ldots, j_S) \in \boldsymbol{J}_S \right] \tag{5.89}$$

consists of all the monomials in the polynomial form representation of the system output frequency response,

and vector

$$\boldsymbol{\Lambda} = \left[\Lambda_0, \cdots, \Lambda_N \right] = \left[\lambda_{j_1, \cdots, j_S} \left(j\omega \right) \middle| \left(j_1, \ldots, j_S \right) \in \boldsymbol{J}_S \right] \tag{5.90}$$

consists of all the coefficients in the polynomial representation.

Proposition 5.8 exploits the fact that the AOFRF enables a separate consideration of the effect of linear and nonlinear characteristic parameters on the system output frequency response and provides an algorithm that can be implemented by using computer codes to automatically produce all the monomials in the polynomial form representation of the system output spectrum (5.88).

(B) Determination of the coefficients

The coefficients in the AOFRF based representation of the output spectrum (5.88) can be evaluated by using a LS method [74] as described in Proposition 5.9.

Proposition 5.9. *Denote* $\boldsymbol{\Theta}$ *in (5.88) evaluated at the* j *th set of the system parameters* $\theta_i(j), i = 1, \ldots, S$ *as*

$$\boldsymbol{\Theta}_{(j)} = \left[\boldsymbol{\Theta}_{(j)}(1), \cdots, \boldsymbol{\Theta}_{(j)}(\bar{M}) \right] \tag{5.91}$$

where $\bar{M}$ *is the dimension of vector* $\boldsymbol{\Theta}$ *and the output spectrum of the system when the system parameters take the values of* $\theta_i(j), i = 1, \ldots, S$ *as* $Y_{(j)}(j\omega)$. *Then* $Y_{(j)}(j\omega)$ *can be represented as*

$$Y_{(j)}(j\omega) = \left[\boldsymbol{\Theta}_{(j)}(1), \cdots, \boldsymbol{\Theta}_{(j)}(\bar{M}) \right] \boldsymbol{\Lambda} = \left[\boldsymbol{\Theta}_{(j)}(1)\middle/l_1, \cdots, \boldsymbol{\Theta}_{(j)}(\bar{M})\middle/l_{\bar{M}} \right] \boldsymbol{\Lambda}^* \tag{5.92}$$

where

$$\left[l_1, \ldots, l_{\bar{M}} \right] = \boldsymbol{L}; l_i \neq 0, i = 1, \ldots, \bar{M} \tag{5.93}$$

is a constant vector and

$$\boldsymbol{\Lambda}^* = \left[l_1 \Lambda(1), \ldots, l_{\bar{M}} \Lambda(\bar{M}) \right]^{\mathrm{T}} \tag{5.94}$$

Consequently, $\boldsymbol{\Lambda}^*$ *can be determined as*

$$\boldsymbol{\Lambda}^* = \left(\boldsymbol{P}^{\mathrm{T}} \boldsymbol{P} \right)^{-1} \boldsymbol{P}^{\mathrm{T}} \bar{\boldsymbol{Y}} \tag{5.95}$$

where

$$\boldsymbol{P} = \begin{bmatrix} \boldsymbol{\Theta}_{(1)}(1)\middle/l_1 & \cdots & \boldsymbol{\Theta}_{(1)}(\bar{M})\middle/l_{\bar{M}} \\ \vdots & \ddots & \vdots \\ \boldsymbol{\Theta}_{(\bar{N})}(1)\middle/l_1 & \cdots & \boldsymbol{\Theta}_{(\bar{N})}(\bar{M})\middle/l_{\bar{M}} \end{bmatrix}_{\bar{N} \times \bar{M}} \tag{5.96}$$

$$\bar{Y} = \left[Y_{(1)}\left(j\omega \right),\dots,Y_{(\bar{N})}\left(j\omega \right) \right]^{\mathrm{T}}$$ (5.97)

and $\bar{N} \geq \bar{M}$.

Proof of Proposition 5.9. Proposition 5.9 can be proved by using the traditional Least Square (LS) algorithm [56].

The introduction of L in (5.93) is to address possible numerical problems arising from a possibly significant difference between the magnitudes of the system parameters [125] so that more reliable values of the coefficients in the polynomial representation of the system output spectrum can be determined.

It is worth noting that the AOFRF based representation of the output spectra of system (2.6) is a polynomial function of both the system linear and nonlinear characteristic parameters. However, these parameters often do not have a clear physical meaning because the NARX model is either obtained from the input and output data of a practical system using a nonlinear system identification method or by discretising a nonlinear differential equation. In order to relate these parameters to the physical meaningful parameters of the system represented by the NARX model, the NARX-M-for-D can be applied.

5.4 Case studies

5.4.1 Case study 1 - The OFRF based design of the vibration isolation system

In this case study, the design of the vibration isolation system shown in Fig.5.2 is considered where $M_0 = 1\,\mathrm{kg}$. $k_1 = \xi_1$ and $c_1 = \xi_2$ are the parameters of the spring and damper in the system. The isolator in the system is a piece of damping material which cannot be described by an analytical physical model but whose NARX-M-for-D has been determined under the sampling frequency $f_s = 512\,\mathrm{Hz}$ as

$$f_{iso}\left(k \right) = a_1 \xi_3 y\left(k \right) + a_2 \xi_3 y^3\left(k \right) + a_3 \xi_3 y^3\left(k-1 \right)$$ (5.98)

by using nonlinear system identification techniques described in [27].

In (5.98), $f_{iso}\left(k \right)$ is the damping force produced by the isolator in the system, ξ_3 is the parameter of the isolator to be used for the system design, and

$$a_1 = 4 \times 10^{-3}, a_2 = 10^4, a_3 = -0.75 \times 10^4$$ (5.99)

are constants.
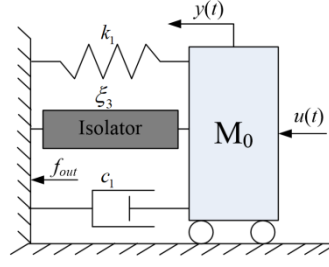
Fig.5.2 The vibration isolation system to design in Case study 1

According to the basic physical principle, the system in Fig.5.2 can be described as:

$$\begin{cases} u(t) = M_0 \ddot{y}(t) + c_1 \dot{y}(t) + k_1 y(t) + f_{iso}(t) \\ f_{out}(t) = c_1 \dot{y}(t) + k_1 y(t) + f_{iso}(t) \end{cases} \tag{5.100}$$

From (5.98) to (5.100), the NARX-M-for-D of the isolation system can be obtained as:

$$\bar{\theta}_{0,1}^{(1)}(\xi) u(k-1) + \bar{\theta}_{1,0}^{(2)}(\xi) y(k-2) + \bar{\theta}_{1,0}^{(1)}(\xi) y(k-1) + \bar{\theta}_{3,0}^{(1,1,1)}(\xi) y^3(k-1)$$
$$+ \bar{\theta}_{3,0}^{(2,2,2)}(\xi) y^3(k-2) + \bar{\theta}_{1,0}^{(0)}(\xi) y(k) = 0 \tag{5.101}$$

where

$$f_{out}(k-1) = \tilde{\theta}_{1,0}^{(1)}(\xi) y(k-1) + \tilde{\theta}_{1,0}^{(2)}(\xi) y(k-2) + \tilde{\theta}_{3,0}^{(1,1,1)}(\xi) y^3(k-1) + \tilde{\theta}_{3,0}^{(2,2,2)}(\xi) y^3(k-2) \tag{5.102}$$

with $\xi = [\xi_1, \xi_2, \xi_3]$, and the details of the coefficients are given as follows

$$\bar{\theta}_{0,1}^{(1)}(\xi) = 0.381 \times 10^{-5}; \ \bar{\theta}_{1,0}^{(0)}(\xi) = -1;$$
$$\bar{\theta}_{1,0}^{(1)}(\xi) = 2 - 0.195 \times 10^{-2} \xi_2 - 0.381 \times 10^{-5} \xi_1 - 0.153 \times 10^{-9} \xi_3;$$
$$\bar{\theta}_{1,0}^{(2)}(\xi) = 0.195 \times 10^{-2} \xi_2 - 1; \ \bar{\theta}_{3,0}^{(1,1,1)}(\xi) = -0.038 \xi_3;$$
$$\bar{\theta}_{3,0}^{(2,2,2)}(\xi) = 0.029 \xi_3; \ \text{else} \ \bar{\theta}_{p,q}^{(k_1, k_2, \cdots, k_{p+q})}(\xi) = 0$$

and

$$\tilde{\theta}_{1,0}^{(1)}(\xi) = 0.512 \times 10^3 \xi_2 + \xi_1 + 4 \times 10^{-3} \xi_3;$$
$$\tilde{\theta}_{1,0}^{(2)}(\xi) = -0.512 \times 10^3 \xi_2; \ \tilde{\theta}_{3,0}^{(1,1,1)}(\xi) = 10^4 \xi_3;$$
$$\tilde{\theta}_{3,0}^{(3,3,3)}(\xi) = 0.75 \times 10^4 \xi_3; \ \text{else} \ \tilde{\theta}_{p,q}^{(k_1, k_2, \cdots, k_{p+q})}(\xi) = 0$$

In the following, the design of parameters ξ of the vibration isolation system when the system is subject to the multi-tone input

$$u(t) = 6\cos(\omega_F t) + 4\cos^3(\omega_F t) \tag{5.103}$$

where $\omega_F = 100 \ \text{rad/s}$ is considered. The design objective is to achieve a desired force transmissibility at the frequency ω_F as defined by

$$T(j\omega) = \frac{F_{out}(j\omega)}{U(j\omega)} \tag{5.104}$$

where $U(j\omega)$ and $F_{out}(j\omega)$ is the spectrum of the input and output forces of the system, respectively.

From the NARX-M-for-D (5.101), the results in Steps 1 and 2 of the proposed general design approach in Section 5.2.3 are obtained, which are the NARX-M-for-D (5.101) and the relationship between the system design parameters ξ and the linear and nonlinear characteristic parameters of the system. In Step 3, three constraints on the design parameters ξ are introduced as

$$\begin{cases} g_1(\xi): \xi_1 - 4 \times 10^{-3}\xi_3 - 10^4 = 0 \\ g_2(\xi): \xi_2 - 30 = 0 \\ g_3(\xi): \xi_1 - 6 \times 10^4 \le 0 \end{cases} \tag{5.105}$$

to ensure that the FRF of the system at the driving frequency $\omega_F = 100\,\text{rad/s}$ is as specified in the following

$$\begin{aligned} H_1(j\omega_F) &= \frac{\bar{\theta}_{0,1}^{(1)}(\xi)\exp(-j\omega_F\Delta t)}{1 - \bar{\theta}_{1,0}^{(1)}(\xi)\exp(-j\omega_F\Delta t) - \bar{\theta}_{1,0}^{(2)}(\xi)\exp(-2j\omega_F\Delta t)} \\ &= 3.469 \times 10^{-5} - 3.320 \times 10^{-4}\text{i} \end{aligned} \tag{5.106}$$

and $g_3(\xi)$ is a constraint on the maximum value of the stiffiness of the spring.

Moreover, in Step 4, the OFRF representation of the force transmissibility $T(j\omega_F)$ of the system is determined. In this case, $N = 11$

$$\Xi = \bigcup_{n=1}^{N}\Xi_n = \left[1, \xi_3, \xi_3^2, \xi_3^3, \xi_3^4, \xi_3^5\right] \tag{5.107}$$

and the OFRF was determined from the system output responses to input (5.102) when the design parameters ξ_3 changes over the range of $\{0.01, 0.8, 2, 3, 4, 5\}$ as

$$\begin{aligned} T(j\omega_F) &= (-2.456 + 1.443\text{i}) + (1.383 - 4.098\text{i})l_\xi^{-1}\xi_3 + (-0.846 + 3.293\text{i})l_\xi^{-2}\xi_3^2 \\ &\quad + (0.285 - 1.244\text{i})l_\xi^{-3}\xi_3^3 + (-0.047 + 0.220\text{i})l_\xi^{-4}\xi_3^4 + (0.306 \times 10^{-3} - 0.015\text{i})l_\xi^{-5}\xi_3^5 \end{aligned} \tag{5.108}$$

where $l_\xi = 10^6$

Based on the results of Steps 1-4 above, in Step 5, the design issue in this case study can be described as an optimal design probem as follows.

Find

$$\xi_0 = [\xi_1, \xi_2, \xi_3] \tag{5.109a}$$

to solve the optimization problem

$$\underset{\{\xi_1, \xi_2, \xi_3\}}{\text{MIN}}\left|T(j\omega_F) - 1.5\right| \tag{5.109b}$$

under the constraint

$$\begin{cases} g_1(\boldsymbol{\xi}) : \xi_1 - 4\times10^{-3}\xi_3 - 10^4 = 0 \\ g_2(\boldsymbol{\xi}) : \xi_2 - 30 = 0 \\ g_3(\boldsymbol{\xi}) : \xi_1 - 6\times10^4 \le 0 \end{cases} \tag{5.109c}$$

where

$$\left| T(\mathrm{j}\omega_F) \right| = \sqrt{\mathrm{Re}^2\left[T(\mathrm{j}\omega_F)\right] + \mathrm{Im}^2\left[T(\mathrm{j}\omega_F)\right]} \tag{5.110}$$

and

$$\begin{cases} \mathrm{Re}\left[T(\mathrm{j}\omega_F)\right] = -2.456 + 1.383 l_\xi^{-1}\xi_3 - 0.846 l_\xi^{-2}\xi_3^2 + 0.285 l_\xi^{-3}\xi_3^3 \\ \qquad - 0.047 l_\xi^{-4}\xi_3^4 + 0.306\times10^{-3} l_\xi^{-5}\xi_3^5 \\ \mathrm{Im}\left[T(\mathrm{j}\omega_F)\right] = 1.443 - 4.098 l_\xi^{-1}\xi_3 + 3.293 l_\xi^{-2}\xi_3^2 - 1.244 l_\xi^{-3}\xi_3^3 \\ \qquad + 0.220 l_\xi^{-4}\xi_3^4 - 0.015 l_\xi^{-5}\xi_3^5 \end{cases} \tag{5.111}$$

Considering the constraints of $g_1(\boldsymbol{\xi})$ and $g_3(\boldsymbol{\xi})$, it can be obtained that

$$\xi_3 = \frac{\xi_1 - 10^4}{4\times10^{-3}} \le 12.5\times10^6 \tag{5.112}$$

Under the constraint of (5.112), inequality (5.109c) can be solved to yield

$$2.3\times10^6 \le \xi_3 \le 12.5\times10^6 \tag{5.113}$$

Consequently, from (5.112) and (5.113), it can be obtained that

$$1.92\times10^4 \le \xi_1 \le 6\times10^4 \tag{5.114}$$

Therefore, the feasible solutions to the design problem in the case study are:

$$\begin{cases} 2.3\times10^6 \le \xi_3 \le 12.5\times10^6 \\ \xi_2 = 30 \\ 1.92\times10^4 \le \xi_1 \le 6\times10^4 \end{cases} \tag{5.115}$$

If ξ_3 is designed as $\xi_3 = 2.3\times10^6$, the corresponding $\xi_1 = k_1$ and $\xi_2 = c_1$ can be obtained as $\xi_1 = k_1 = 1.92\times10^4$ N/m, $\xi_2 = c_1 = 30$ N/ms^{-1}. The time history of the output force and the corresponding transmissibility are shown in Fig.5.3, where a comparison with the result in the case of $\xi_1 = k_1 = 1.92\times10^4$ N/m, $\xi_2 = c_1 = 30$ N/ms^{-1} and $\xi_3 = 0$ can also be observed.
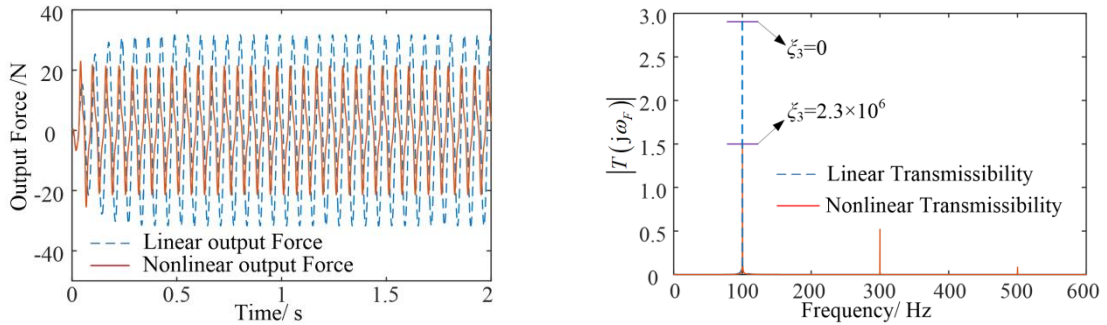
(a) Time history of the output force   (b) The force transmissibility

Fig.5.3 A comparison of the system performances under the linear and nonlinear designs

From Fig.5.3, it can be observed that under the design, the transmissibility at the base frequency of

$\omega_F = 100 \, \text{rad/s}$ has reached 1.5 as required. But, compared to the case of $\xi_3 = 0$ where no material-based

nonlinear isolator is introduced, the optimal design induces additional components at super harmonic

frequencies, $\omega = 3\omega_F$ and $\omega = 5\omega_F$. However, the time history of the system response shown in Fig.5.3 (a)

indicates that the optimal design has an overall better performance in vibration isolation. In order to confirm

this observation, the concept of power transmissibility $E(\omega_F)$ introduced in [126]

$$E(\omega_F) = \frac{\int_0^{T_0} |f_{out}(t)|^2 \, \mathrm{d}t}{\int_0^{T_0} |u(t)|^2 \, \mathrm{d}t} = \sum_{p=1}^{\infty} \left| T(\mathrm{j}\omega) \right|_{\omega = p\omega_F} \Big|^2 , \quad T_0 = \frac{2\pi}{\omega_F} \tag{5.116}$$

was used to evaluate the vibration isolation performance of the system in the two cases. The results are

$$E(\omega_F) = 8.457 \tag{5.117}$$

when no material-based isolator is used and

$$E(\omega_F) = 2.559 \tag{5.118}$$

when the isolator is applied. Clearly, the optimal nonlinear design has achieved an overall better performance

than the linear solution.

It is worth pointing out that because the optimisation problem is formulated using the OFRF which is a

polynomial function of the design parameters, the numerical costs associated with the new design are

normally less than the costs associated with a completely numerical simulation based method. In the case

study above, for example, the overall computation on a standard PC running MATLAB codes only took 30

sec to complete.

5.4.2 Case study 2 - The AOFRF based representation of the output spectrum of a

Duffing nonlinear system

Consider the Duffing equation with nonlinear damping

$$\ddot{y}(t) + c_l \dot{y}(t) + k_l y(t) + k_{n3} y(t)^3 + c_{n3} \dot{y}(t)^3 = u(t) \tag{5.119}$$

where $c_{n1} = 80 \, \text{N/ms}^{-1}$ and $c_{n3} = 200 \, \text{N/m}^3\text{s}^{-3}$.

Approximating the first and the second derivatives in (5.119) as:

$$\dot{y}(t) = \frac{y(k) - y(k-1)}{\Delta t}, \, \ddot{y}(t) = \frac{y(k+1) - 2y(k) + y(k-1)}{\Delta t^2} \tag{5.120}$$

and substituting (5.120) into (5.119) with $\Delta t = 1/256 \, \text{s}$ yields an NARX model of system (5.119) as

$$
\begin{aligned}
y(k) &= c_{0,1}(1)u(k-1) + c_{1,0}(1)y(k-1) + c_{1,0}(2)y(k-2) + c_{3,0}(1,1,1)y^3(k-1) \\
&+ c_{3,0}(1,1,2)y^2(k-1)y(k-2) + c_{3,0}(1,2,2)y(k-1)y^2(k-2) + c_{3,0}(2,2,2)y^3(k-2)
\end{aligned}
\tag{5.121}
$$

where

$$
c_{0,1}(1) = 1.526 \times 10^{-5};\ c_{1,0}(2) = -0.687;\ c_{3,0}(1,1,2) = 1.024 \times 10^5;
$$
$$
c_{3,0}(1,2,2) = -1.024 \times 10^5;\ c_{3,0}(2,2,2) = 0.512 \times 10^5;
\tag{5.122a}
$$

$$
c_{3,0}(1,1,1) = -\left(1.526 \times 10^{-5} k_{n3} + 0.512 \times 10^5\right);\ c_{1,0}(1) = -\left(1.526 \times 10^{-5} k_l - 1.687\right);\ \text{else } c_{p,q}(.) = 0 \tag{5.122b}
$$

The objective now is to investigate how the physical parameters k_l, k_{n3} of system (5.119) affect the system output frequency response when the values of the two parameters vary over the range of

$$
k_l \in [0.5, 1.4] \times 10^4 \text{ N/m} \quad \text{and} \quad k_{n3} \in [0, 1] \times 10^9 \text{ N/m}^3 \tag{5.123}
$$

Denote $c_L = c_{1,0}(1)$ and $c_{NL} = c_{3,0}(1,1,1)$. It is known from the relationship between k_l and k_{n3} and $c_{1,0}(1)$ and $c_{3,0}(1,1,1)$ that

$$
\begin{cases}
c_L = c_{1,0}(1) \in [1.473, 1.611] \\
c_{NL} = c_{3,0}(1,1,1) \in [0.512, 0.665] \times 10^5
\end{cases}
\tag{5.124}
$$

Take $N = 5$, then the AOFRF based representation for the output spectrum of the system can be determined by the following steps.

Step 1: Determine a polynomial representation of $H_1(\omega_i)$ and $L_i^{-1}(\omega_1, \cdots, \omega_i)$ for $i = 1, \ldots, n$ in terms of the system linear characteristic parameter of concern, which is $c_L = c_{1,0}(1)$, in this case.

For NARX model (5.121), over the range of values of parameters $c_{1,0}(1)$ and $c_{3,0}(1,1,1)$ given by (123), it can be shown that the convergent condition (5.73) is satisfied by chosen, for example, $c_z(1) = (1.473 + 1.611)/2 = 1.542$ and $c_z(2) = c_{1,0}(2) = -0.687$. Therefore, $H_1(\omega)$ can be expanded into a convergent polynomial function of c_L whose second order approximation can be written as

$$
H_1(\omega) \approx \varphi_0(j\omega) + \varphi_1(j\omega)c_L + \varphi_2(j\omega)c_L^2 \tag{5.125}
$$

Moreover, $L_i^{-1}(.)$ for $i = 1, \ldots, n$ can also be approximately expanded into a polynomial function of c_L of the same form as (5.125).

Step 2: Determine the structure of the AOFRF based representation of the system output frequency response.

According to Proposition 3, the monomial vector associated with the AOFRF based representation can be written as

$$\boldsymbol{\Theta} = \bigcup_{r=1}^{N} \left[\boldsymbol{\Theta}_{(r:r)}^{L} \otimes \boldsymbol{\Theta}_{(r:r)}^{NL} \right] = \left[\boldsymbol{\Theta}_{(1:1)}^{L} \otimes \boldsymbol{\Theta}_{(1:1)}^{NL} \right] \cup \left[\boldsymbol{\Theta}_{(3:3)}^{L} \otimes \boldsymbol{\Theta}_{(3:3)}^{NL} \right] \cup \left[\boldsymbol{\Theta}_{(5:5)}^{L} \otimes \boldsymbol{\Theta}_{(5:5)}^{NL} \right] \tag{5.126}$$

In this case, it is known from Step 1 that $\boldsymbol{\theta}_H = \boldsymbol{\theta}_L = \left[1, c_L, c_L^{2} \right]$ and, from Proposition 5.8, it is known

that

$$\begin{cases} \boldsymbol{\Theta}_{(1:1)}^{L} = \boldsymbol{\theta}_H = \left[1, c_L, c_L^{2} \right] \\ \boldsymbol{\Theta}_{(1:1)}^{NL} = [1] \end{cases} \tag{5.127a}$$

$$\begin{cases} \boldsymbol{\Theta}_{(3:3)}^{L} = \left[\boldsymbol{\theta}_H \right]^{3} \otimes \bigcup_{i=1}^{2} \left[\boldsymbol{\theta}_L \right]^{i} = \left[1, c_L, c_L^{2}, \ldots, c_L^{10} \right] \\ \boldsymbol{\Theta}_{(3:3)}^{NL} = \left[c_{NL} \right] \end{cases} \tag{5.127b}$$

and

$$\begin{cases} \boldsymbol{\Theta}_{(5:5)}^{L} = \left[\boldsymbol{\theta}_H \right]^{5} \otimes \bigcup_{i=1}^{4} \left[\boldsymbol{\theta}_L \right]^{i} = \left[1, c_L, c_L^{2}, \ldots, c_L^{18} \right] \\ \boldsymbol{\Theta}_{(5:5)}^{NL} = \left[c_{NL}^{2} \right] \end{cases} \tag{5.127c}$$

Consequently, substituting (5.127) into (5.126) yields the structure of the AOFRF based representation of

the output spectrum of system (5.121) as:

$$Y(j\omega) \approx \lambda_{0,0}(j\omega) + \lambda_{1,0}(j\omega)c_L + \lambda_{2,0}(j\omega)c_L^{2} + c_{NL}\sum_{I_1=0}^{10}\lambda_{I_1,1}(j\omega)c_L^{I_1} + c_{NL}^{2}\sum_{I_2=0}^{18}\lambda_{I_2,1}(j\omega)c_L^{I_2} \tag{5.128}$$

Step 3: Determination of the coefficients in the poly-nomial representation of $Y(j\omega)$.

Equation (5.128) can be rewritten as

$$Y(j\omega) \approx \tilde{\lambda}_{0,0}(j\omega) + \tilde{\lambda}_{1,0}(j\omega)\frac{c_L}{l_L} + \tilde{\lambda}_{2,0}(j\omega)\frac{c_L^{2}}{l_L^{2}} + \frac{c_{NL}}{l_{NL}}\sum_{I_1=0}^{10}\tilde{\lambda}_{I_1,1}(j\omega)\frac{c_L^{I_1}}{l_L^{I_1}} + \frac{c_{NL}^{2}}{l_{NL}^{2}}\sum_{I_2=0}^{18}\tilde{\lambda}_{I_2,1}(j\omega)\frac{c_L^{I_2}}{l_L^{I_2}} \tag{5.129}$$

where $\lambda_{i,j}(j\omega) = \tilde{\lambda}_{i,j}(j\omega)/l_L^{i}l_{NL}^{j}$, $i,j = 0,1,\ldots$ with $l_L = 1$ and $l_{NL} = 10^{4}$ are introduced as weights to

transform the frequency dependent polynomial coefficients from $\lambda_{i,j}(j\omega)$ in (5.128) to $\tilde{\lambda}_{i,j}(j\omega)$ in

(5.129). The objective is to circumvent possible numerical issues with evaluation of these coefficients [127].

Now consider the situation where the system input is $u(t) = 3\cos(\omega t)$ with $\omega = 110\,\text{rad/s}$. The

coefficients $\lambda_{i,j}(j\omega), i,j = 0,1,\ldots$ in (5.129) were evaluated from the system output frequency responses to

this input when the system linear and nonlinear characteristic parameters c_L and c_{NL} vary over the

following range of values

$$\begin{cases} c_L/l_L = [1.54 : 0.003 : 1.57] \\ c_{NL}/l_{NL} = [5.80 : 0.05 : 6.30] \end{cases} \tag{5.130}$$

The result is a specific case of (5.129), which is a polynomial function of the system parameters c_L and c_{NL} containing 33 terms which are omitted here due to space limitation. A comparison of the system output spectrum evaluated using (5.129) thus determined and the result determined from the simulated system output response is shown in Fig.5.4.
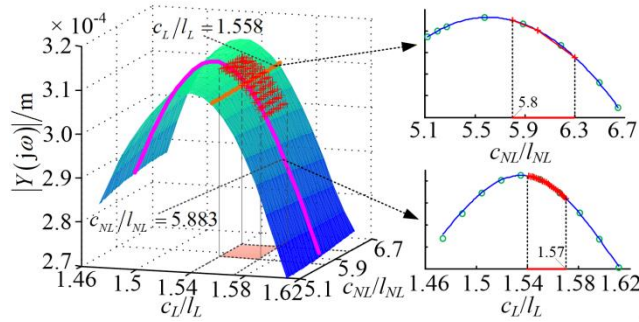
Fig.5.4. A comparison of the simulated system output spectrum with the result evaluated using the AOFRF based representation.

Circle: Simulated results; Surface: Results evaluated using the AOFRF based representation; Cross: Data of the output spectra used to determine the AOFRF based representation.

It is worth noting that, if the system linear characteristic parameters are fixed, then the AOFRF based representation (5.129) will become the OFRF of the system, which is a 2nd order polynomial function of the system nonlinear characteristic parameter c_{NL}. If the system nonlinear characteristic parameters are fixed, the AOFRF based representation (5.129) becomes a 18th order polynomial function of the system linear characteristic parameter c_L. These results are also illustrated in Fig.5.4.

Fig.5.4 clearly indicates that the AOFRF based representation for the system output spectrum is valid over a wide range of values of the system linear and nonlinear characteristic parameters, including the values which are outside the parameter ranges (5.130), over which the polynomial representation was determined. This is because the AOFRF based representation is capable to capture inherent system dynamics rather than simply fit the data.

Now consider another case where a random band limited signal over the frequency range of $\omega \in [50, 200]$ rad/s with magnitude varying over $[-30, 30]$ N is applied as input to system (5.121). The AOFRF based representation for the system output spectrum was determined over the same range of the values of the system parameters c_L and c_{NL} as in (5.130). Fig.5.5 shows a comparison of simulated output spectra of system (5.121) to this random input with the results evaluated using the AOFRF based representation under three different sets of values of c_L and c_{NL}, indicating that the AOFRF based

representation can also accurately describe the system output spectra to a random input.
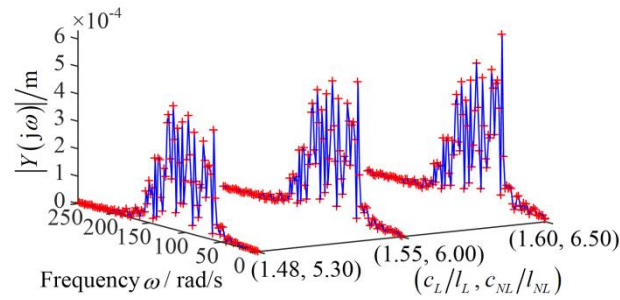
Fig.5.5. The output spectrum and its AOFRF based representation under a random input

Line: Simulation results; Cross: The AOFRF based representation.

It is worth noting that many terms in the AOFRF based representation of nonlinear system output spectra as determined in the case study above are often redundant. An optimal selection of the terms (monomials) in the polynomial representation will be investigated in future studies.

5.5 Conclusions

Traditional nonlinear system designs are basically based on the time domain response analysis, which is often difficult to reveal the relationship between the system performance and the parameters that can be used to perform the design. Motivated by the wide engineering applications of the FRF-based linear system frequency domain analysis and design, the OFRF concept was proposed in order to extend the effective linear system approach to the nonlinear case. However, the method requires to know a differential equation-based physical model of the system where the physical parameters that can be used for the analysis and design are the coefficients in the model.

Considering that it is difficult even impossible to find a differential equation model for complex engineering systems and the need to extend the physical model-based system design approach to address more complicated complex system designs. The NARX-M-for-D is introduced to resolve this problem, and a new OFRF-based methodology is developed that can be applied to the design of nonlinear systems described by a NARX-M-for-D. The methodology consists of a five step procedure including novel algorithm and technique for determining the structure and evaluating the coefficients of the OFRF of a NARX-M-for-D and can be applied to design a general class of nonlinear systems in the frequency domain.

Moreover, noting the OFRF only shows a polynomial relationship between the system's output spectrum and nonlinear characteristic parameters, and it can't explicitly reveal the effect of system linear characteristic parameters on output spectra, a new concept known as the AOFRF of nonlinear systems, has been proposed.

The AOFRF enables an explicit separation of the system linear and nonlinear characteristic parameters in the representation of the system output spectrum and, consequently, facilitates the derivation of a polynomial representation in terms of both the system linear and nonlinear characteristic parameters.

Two case studies have been used to demonstrate how to determine the OFRF for aa` NARX-M-for-D and how to derive an AOFRF based representation for the output spectrum of an nonlinear system, respectively. The results show that the new design method, for the first time, transforms a complicated dynamic loading oriented engineering design into a much simpler polynomial-based optimal design problem, and the new AOFRF based representation has potential to be used for the analysis and design of nonlinear systems in a wide range of applications.

Chapter 6. Nonlinear damping based semi-active building isolation system

6.1 Introduction

Many buildings in Japan currently have a base-isolation system with a low stiffness that is designed to shift the natural frequency of the buildings below the frequencies of the ground motion due to earthquakes. However, the ground motion observed during the 2011 Tohoku earthquake contained strong long-period waves that lasted for a record length of three minutes. To provide a novel and better solution against the long-period waves while maintaining the performance of the standard isolation range, the exploitation of the characteristics of nonlinear damping is proposed in this chapter. This is motivated by previous studies at Sheffield, which have demonstrated that nonlinear damping can achieve desired performance over both low and high frequency regions and the optimal nonlinear damping force can be realized by closed loop controlled semi-active dampers. Simulation results have shown a very good vibration isolation performance on a building model with identified parameters and have indicated that nonlinear damping can achieve low acceleration transmissibilities around the structural natural frequency as well as the higher ground motion frequencies that have been frequently observed during most earthquakes in Japan. In addition, physical building model based laboratory experiments are also conducted, The results demonstrate the advantages of the proposed nonlinear damping technologies over both traditional linear damping and more advanced Linear-Quadratic Gaussian (LQG) feedback control which have been used in practice to address building isolation system design and implementation problems. In comparison with the tuned-mass damper and other active control methods, the proposed solution offers a more pragmatic, low-cost, robust and effective alternative that can be readily installed into the base-isolation system of most buildings. The studies can be summarized in a diagram as follows.
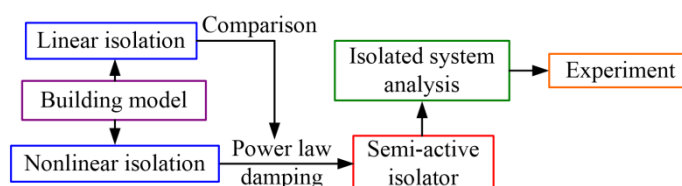
Fig.6.1 The contents of Chapter 6

6.2 Semi-active Damping System for the Sosokan Building

6.2.1 The Sosokan Building and its model representation

Sosokan, a symbolic nine-storey tower located in the Yagami campus of Keio University, was completed in 2000. Its isolation layer under B2F floor, is composed of sixty-five laminated rubber bearings, one set of twelve passive hydraulic dampers and four semi-active dampers oriented horizontally in the east-west direction, and another identical set of passive and semi-active dampers in the north-south direction. The lateral dynamics of the building subject to the horizontal ground acceleration as shown in Fig. 6.2 can be modelled by a system of mass-spring-damper in series given by

$$M\ddot{x} + C\dot{x} + Kx = Eu + F\ddot{z} \tag{6.1}$$

where u represents the force of the semi-active damper,

$$x = \left[x_1, x_2, x_3, \ldots, x_{10} \right]^{\mathrm{T}} \tag{6.2}$$

$$M = \mathrm{diag}\left[m_1, m_2, m_3, \ldots, m_{10} \right] \tag{6.3}$$

$$C = \begin{bmatrix} c_1 + c_2 & -c_2 & \cdots & 0 & 0 \\ -c_2 & c_2 + c_3 & & & 0 \\ \vdots & & \ddots & & \vdots \\ 0 & & & c_9 + c_{10} & -c_{10} \\ 0 & 0 & \cdots & -c_{10} & c_{10} \end{bmatrix} \tag{6.4}$$

$$K = \begin{bmatrix} k_1 + k_2 & -k_2 & \cdots & 0 & 0 \\ -k_2 & k_2 + k_3 & & & 0 \\ \vdots & & \ddots & & \vdots \\ 0 & & & k_9 + k_{10} & -k_{10} \\ 0 & 0 & \cdots & -k_{10} & k_{10} \end{bmatrix} \tag{6.5}$$

$$E = \left[1, 0, 0, \ldots, 0 \right]^{\mathrm{T}} \tag{6.6}$$

and

$$F = \left[-m_1, -m_2, -m_3, \ldots, -m_{10} \right]^{\mathrm{T}} \tag{6.7}$$

x_i for $i = 1, 2, \ldots, 10$ are the horizontal displacement of each floor relative to ground while m_i, c_i and k_i for $i = 1, 2, \ldots, 10$ are the mass, damping constant and spring stiffness respectively with values given in Tab.6.1.
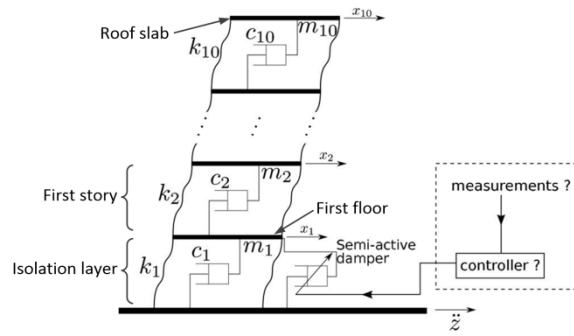
Fig.6.2. A model of a multi-storey building with built-in semi-active dampers in the isolation layer

Tab.6.1. Parameters of the Sosokan Building in the east-west direction [128]

Floor	Mass 10^6 kg	Stiffness 10^6 Nm^{-1}	Damping 10^6 Nsm^{-1}
B2F	$m_1 = 4.9814$	$k_1 = 66.836$	$c_1 = 9.996$
B1F	$m_2 = 3.4382$	$k_2 = 2273.6$	$c_2 = 18.306$
1F	$m_3 = 2.4906$	$k_3 = 2763.6$	$c_3 = 22.252$
2F	$m_4 = 1.8264$	$k_4 = 1979.6$	$c_4 = 15.940$
3F	$m_5 = 2.0331$	$k_5 = 1803.2$	$c_5 = 14.520$
4F	$m_6 = 2.0500$	$k_6 = 1813.0$	$c_6 = 14.598$
5F	$m_7 = 2.0369$	$k_7 = 1568.0$	$c_7 = 12.625$
6F	$m_8 = 2.0371$	$k_8 = 1381.8$	$c_8 = 11.126$
7F	$m_9 = 2.0664$	$k_9 = 1156.4$	$c_9 = 9.3110$
RF	$m_{10} = 2.4999$	$k_{10} = 999.60$	$c_{10} = 8.0487$

Under the influence of the horizontal ground acceleration $\ddot{z}$, the performance of the base-isolation system is determined by the total stiffness of the laminated rubber bearings k_1 , the linear damping provided by the passive dampers c_1 and the force provided by all of the semi-active dampers u .

Assuming that the building is at a large distance from the epicenter, the ground input $\ddot{z}$ can be modelled by a sinusoidal signal given by

$$\ddot{z} = A\sin\left(2\pi ft\right) \tag{6.8}$$

where A and f are excitation magnitude and frequency in ms^{-2} and Hz respectively [129]. The vibration isolation performance can then be measured by the ratio of the magnitude of the output spectrum evaluated at the excitation frequency f to the excitation magnitude A known as the absolute acceleration

transmissibility

$$T(f) = \frac{\left| F\left\{ \ddot{x}_i(t) + \ddot{z}(t) \right\} \right|_{\omega = 2\pi f}}{A}$$

(6.9)

where $F\{.\}$ is the Fourier transform operation and $\ddot{x}_i(t)$, $i = 1, 2, \ldots, 10$ are the acceleration response of each floor of the building. With all system parameters held constants, $T(f)$ is dependent on the semi-active damper force u. Their relationship will be further explored below.

6.2.2 Semi-active damping system for the Sosokan Building

Semi-active dampers are gaining popularity in vibration control as they could offer some benefits of active control systems [130], without consuming a high level of energy or compromising the structural stability [131]. Controlled by electromagnetic valves which could move to several different positions, semi-active dampers are currently used in the isolation layer of the Sosokan Building with an output force

$$u = -C_l v$$

(6.10)

where $v = \dot{x}_1$ and the linear damping coefficient can have four choices which are $C_l = C_{p1} \left(3.33 \text{ MNsm}^{-1} \right)$, $C_{p2} \left(6.68 \text{ MNsm}^{-1} \right)$, $C_{p3} \left(31.4 \text{ MNsm}^{-1} \right)$ or $C_{p4} \left(58.8 \text{ MNsm}^{-1} \right)$. These linear relationships between the output force u and the velocity v are depicted in Fig.6.2 (a). To alter the damping coefficient, an electronic signal is sent to the electromagnetic valves to modify their positions. The relationship between the actual values of the damping coefficient $C_o(t)$ and the electrical signal $C_s(t)$ can be modelled by a first order system given by

$$\frac{L\left[C_o(t) \right]}{L\left[C_s(t) \right]} = \frac{1}{Ts + 1}$$

(6.11)

where $T = 0.1\,\text{s}$, an empirically-determined parameter based on tests on the semi-active dampers and $L[.]$ is the Laplace operation [112].

Substituting Eqs. (6.8) and (6.10) into (6.1), the building model becomes a purely linear system when C_l is kept constant at one of the four values. The acceleration transmissibility curves from the ground input to the isolation layer for different C_l are presented by the black lines in Fig.6.3 with the effect of an increasing C_l indicated by blue arrows. The first mode of vibration occurs at about 0.25 Hz where a higher damping coefficient $C_l = C_{p4}$ provides a much lower transmissibility, which would be essential for tackling the

long-period waves. On the contrary, when the frequency is higher, the transmissibility curve of the system where $C_l = C_{p4}$ indicated by the black dash-dotted line is well above that of a system with $C_l = C_{p1}$ indicated by the black solid line. It is clear that none of a single semi-active damper setting could produce satisfactory isolation over the whole frequency range.
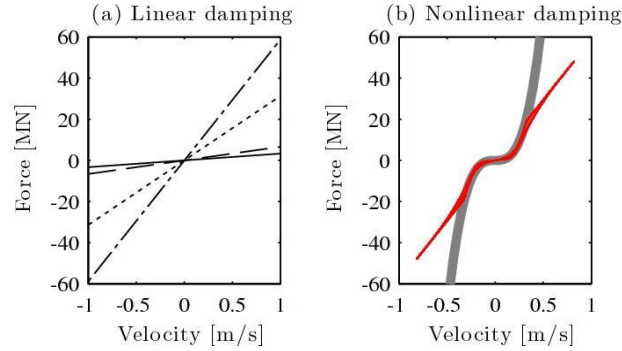
Fig.6.3. Force-velocity relationship of semi-active damper.

(a) Four linear damping settings where $u = -C_l v$, $C_l = C_{p1}$ (solid), C_{p2} (dashed), C_{p3} (dotted) and C_{p4}

(dot-dashed). (b) Desired nonlinear damping (thick grey) where $u = -C_n v^3$ and that implemented by semi-active

dampers under closed-loop control (red solid)

If only one damper setting is chosen for each excitation frequency, the lowest possible transmissibility, referred to as the optimal transmissibility line hereafter, can be achieved by selecting $C_l = C_{p4}$ when $f < 0.35\,\text{Hz}$ and $C_l = C_{p1}$ when $f > 0.35\,\text{Hz}$, as shown in Fig.6.4. Fig.6.4 shows the transmissibility in both the linear and log scale. In order to more clearly reveal the transmissibility over the whole range of frequency, the magnitude will be presented in dB ($10\log_{10}\left(T\left(f\right)\right)$) in figures hereafter.

(a) The linear scale transmissibility   (b) The DB scale transmissibility
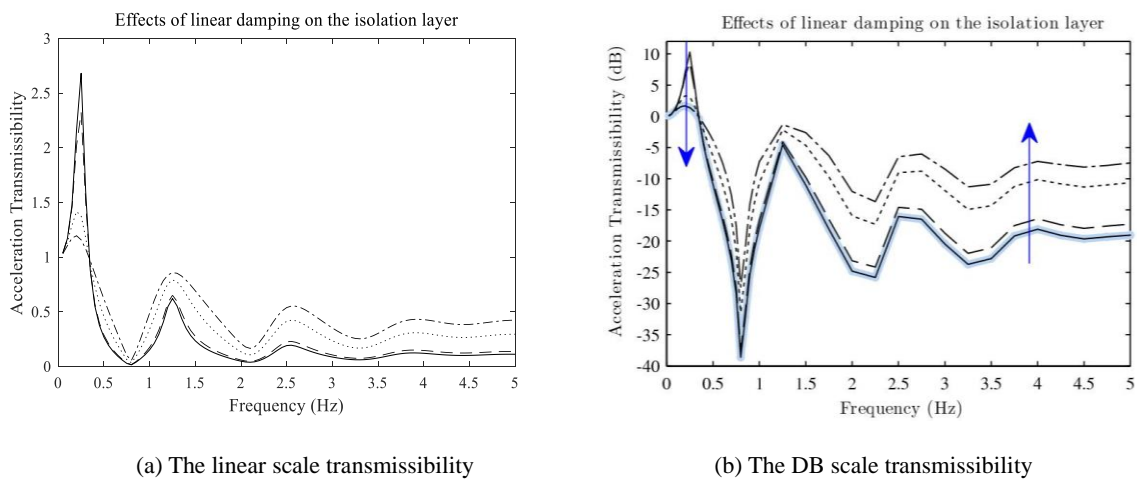
Fig.6.4. Acceleration transmissibility from ground input to the isolation layer where $u = -C_l v$, $C_l = C_{p1}$ (solid), C_{p2}

(dashed), C_{p3} (dotted) and C_{p4} (dot-dashed). The optimal transmissibility line is notated by the thick pale blue line.

Although it is not practical to implement an adaptive semi-active control system that switches between the

two damping coefficients purely depending on the excitation frequency, this optimal transmissibility line, indicated by the thick pale blue line in Fig.6.4 (b), sets a benchmark for other types of control methods based on this particular fluid viscous damper.

6.3 Nonlinear Damping Based Semi-active Building Vibration Isolation

The semi-active damper is considered as passive components that form an integral part of the system, where the semi-active damper together with its controller described in [132] relies on the local measurements without depending on signals from other parts of the building as illustrated in Fig.6.5.

As discussed in [75], a nonlinear viscous damper has significant advantages over a conventional passive viscous damper, especially in the high frequency region. The focus of this study is to realize such a cubic damping force in the base-isolation system of the Sosokan Building using controlled semi-active fluid viscous dampers as depicted in Fig.6.5.

The idea of implementing a closed-loop controller to reshape the force-velocity relationship of a semi-active damper was first developed for electrorheological dampers [133,134]. This simple yet effective closed-loop control approach is now applied to the Sosokan Building aiming to transform the output force of the semi-active dampers from four possible linear functions as shown in Fig.6.3 (a) into a cubic function

$$u_d = -C_n v^3 \tag{6.12}$$

as depicted by the thick grey line in Fig.6.3 (b), where C_n is the cubic damping coefficient.
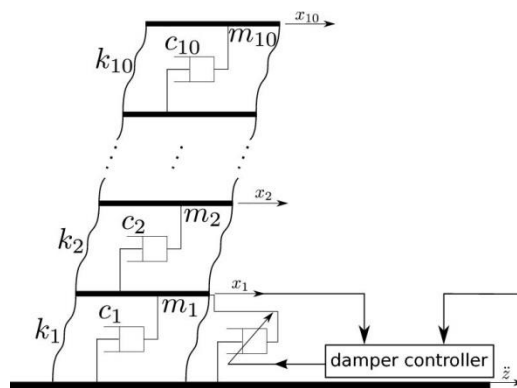
Fig.6.5. Nonlinear damping implementation using semi-active dampers

The PI controller given by

$$r(t) = K_p e(t) + K_i \int_0^t e(\tau) \mathrm{d}\tau \tag{6.13}$$

is used to control the damping force to achieve the designed cubic damping characteristics in Eq. (6.12) where

$$e(t) = \text{sgn}(u_m)(u_d - u_m) \tag{6.14}$$

$r(t)$ is the control signal of the same unit as $C_{p1}, C_{p2}, C_{p3}, C_{p4}$ and u_d/v (MNsm^{-1}), u_m is the measured damping force, and K_p and K_i are the proportional and integral gain (sm^{-1}) of the PI controller, respectively.

As the semi-active dampers are resistive devices, the sign adjustment in Eq. (6.14) is required to ensure that the output force is minimized when u_d and u_m have opposite signs and the sign of $u_d - u_m$ does not agree with u_d. See [133] for more details.

Unlike electrorheological dampers, which accept a continuous current or a voltage signal, the fluid viscous dampers in the Sosokan Building may only have one of four settings. The control signal $r(t)$ is therefore discretized as

$$C_s(t) = \begin{cases} C_{p1}, & \text{for } r(t) \le (C_{p1} + C_{p2})/2 \\ C_{p2}, & \text{for } (C_{p1} + C_{p2})/2 < r(t) \le (C_{p2} + C_{p3})/2 \\ C_{p3}, & \text{for } (C_{p2} + C_{p3})/2 < r(t) \le (C_{p3} + C_{p4})/2 \\ C_{p4}, & \text{for } r(t) > (C_{p3} + C_{p4})/2 \end{cases} \tag{6.15}$$

The combination of this controller and the semi-active damper, as shown in Fig.6.6, becomes one integral unit that exhibits passive damping behaviour illustrated by the red line in Fig.6.3 (b) which resembles the nonlinear damping function described by (6.12).
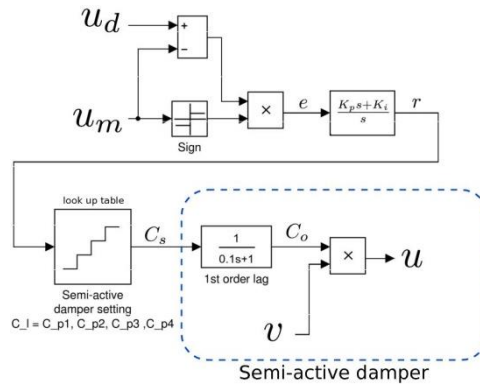
Fig.6.6. Closed-loop semi-active damper control

Unlike any active design approach, the semi-active dampers remain as passive components during the design process. The closed-loop control method only requires local force and velocity measurements, which offers significant practical advantages over other control strategies that rely on feedback signals from sensors located on different floors of the building.

6.4 Simulation Studies

A nonlinearly damped base-isolation system implemented by semi-active fluid viscous dampers as proposed in Section 6.3 has been incorporated into the Sosokan Building modelled in MATLAB/Simulink. The performances of the nonlinear vibration isolation system under harmonic loading are provided in Figs.6.7–6.10.

6.4.1 Objectives of Nonlinear damping design

In the Sosokan Building, the vibration isolation performance is limited by the four available linear settings of the semi-active dampers. As discussed in Section 6.2, the best possible isolation results when the building is under a single-tone sinusoidal excitation can be achieved by selecting $C_l = C_{p4}$ in the low frequency range and $C_l = C_{p1}$ in the high frequency range. This produces the optimal transmissibility line that the implementation of nonlinear damping aims to achieve. For the purpose of comparison, this optimal line as well as the transmissibilities given by the semi-active damper at its highest damping setting $C_l = C_{p4}$ is included in Figs. 6.7–6.10.

6.4.2 Effects of nonlinear damping coefficient

In Fig.6.7, the system is excited by ground acceleration $\ddot{z} = A\sin(2\pi ft)$ with $A = 1\,\mathrm{ms}^{-2}$, the amplitude of which is almost the same as the amplitude recorded in an actual earthquake [128].

Two values for nonlinear damping coefficients are chosen to show their effects on the isolation performance between the ground and the isolation layer. In order to enable the cubic damper to achieve the same transmissibility as the linear damper with coefficient $C_l = C_{p4}$ at the resonant frequency, the cubic damping coefficient is designed as $C_n = 0.588 \times 10^9\,\mathrm{Ns}^3\mathrm{m}^{-3}$ to produce the nonlinear damping force $u = -C_n v^3$. In this case, the system produces a transmissibility curve, shown by the black solid line, that is almost identical to the optimal transmissibility line indicated by the thick pale blue line. When the nonlinear damping coefficient is increased to a higher value such as $2.94 \times 10^9\,\mathrm{Ns}^3\mathrm{m}^{-3}$, a small increase in the acceleration transmissibilities around mid-frequency range from about 0.5 Hz to 3 Hz is observed. This implies an optimal solution to the damping coefficient C_n can achieve the desired damping characteristics as indicated by the pale blue line in Figs.6.7–6.10.
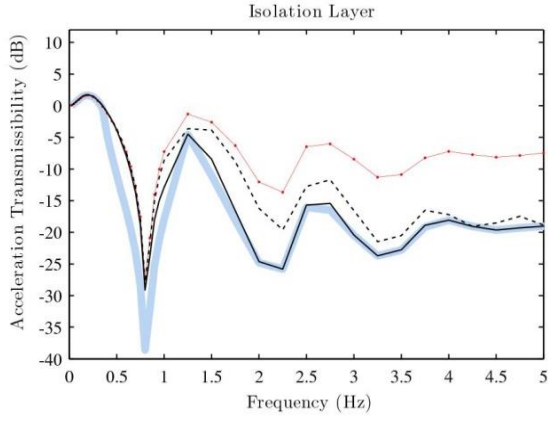
Fig. 6.7. Acceleration transmissibility from ground input $A = 1 \, \mathrm{ms^{-2}}$ to the isolation layer where $u = -C_n v^3$, $C_n = 0.588 \times 10^9 \, \mathrm{Ns^3 m^{-3}}$ (black solid), $C_n = 2.94 \times 10^9 \, \mathrm{Ns^3 m^{-3}}$ (black dotted) are implemented by semi-active dampers and $u = -C_{p4} v$ (red dotted).
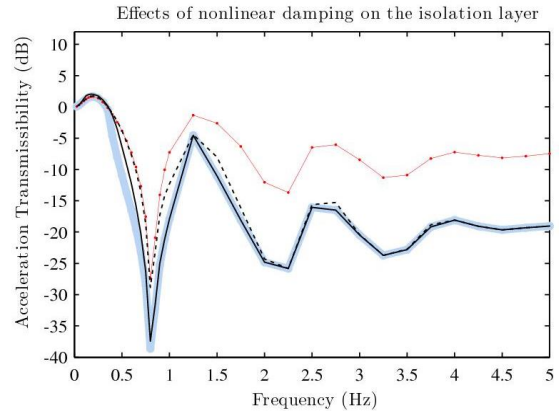
Fig. 6.8. Acceleration transmissibility from ground input $A = 2 \, \mathrm{ms^{-2}}$ to the isolation layer where $u = -C_n v^3$, $C_n = 0.588 \times 10^9 \, \mathrm{Ns^3 m^{-3}}$ (black solid), $C_n = 2.94 \times 10^9 \, \mathrm{Ns^3 m^{-3}}$ (black dotted) are implemented by semi-active dampers and $u = -C_{p4} v$ (red dotted).

6.4.3 Effects of ground excitation magnitude

As the system contains nonlinear elements, the relationships between the ground input and the acceleration outputs are dependent on the excitation magnitude. Fig.6.8 shows the transmissibility curves resulting from a larger input magnitude of $A = 2 \, \mathrm{ms^{-2}}$. When the nonlinear damping coefficient is $0.588 \times 10^9 \, \mathrm{Ns^3 m^{-3}}$, the transmissibility curve still lies very close to the optimal line. Even when C_n is raised to $2.94 \times 10^9 \, \mathrm{Ns^3 m^{-3}}$, the transmissibilities are well below the result generated with a linear system where $C_l = C_{p4}$ over high frequencies. Therefore, the optimal solution has a sufficient robustness with respect to the changes in loading conditions. It is worth noting that the different magnitudes of $A = 1 \, \mathrm{ms^{-2}}$ and $A = 2 \, \mathrm{ms^{-2}}$ are two cases recorded in an earthquake [128,135], demonstrating the nonlinear damping based semi-active damper has a sufficient robustness with respect to the changes in loading conditions.

6.4.4 Isolation performance on higher floors

The base-isolation system is designed to reduce acceleration on all floors during earthquakes. Figs.6.9 and 6.10 show the performance of the implemented nonlinearly damper on 3F and 7F for two excitation amplitudes. For both floors, the transmissibilities of the proposed system almost coincide with the optimal lines over the whole frequency range when $A = 1 \, \mathrm{ms^{-2}}$. However, the performance is less ideal in the mid-frequency region when $A = 2 \, \mathrm{ms^{-2}}$.
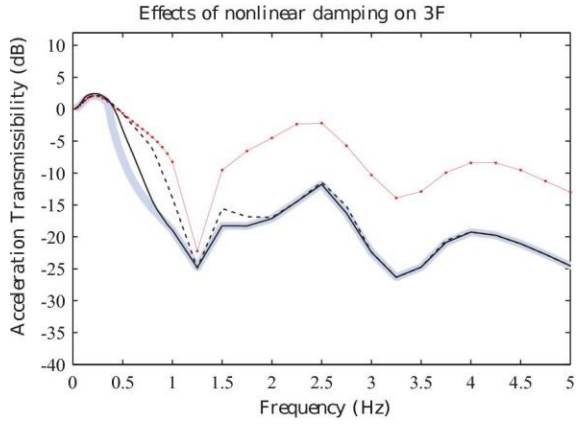
Fig. 6.9. Acceleration transmissibility from ground input $A = 1\,\mathrm{ms}^{-2}$ (black solid) and $A = 2\,\mathrm{ms}^{-2}$ (black dotted) to 3F where $u = -C_n v^3$, $C_n = 0.588 \times 10^9\,\mathrm{Ns}^3\mathrm{m}^{-3}$ (black solid) is implemented by semi-active dampers and $u = -C_{p4} v$ (red dotted).
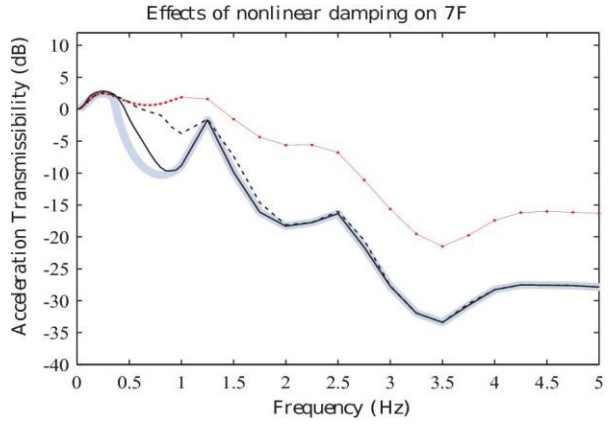
Fig. 6.10. Acceleration transmissibility from ground input $A = 1\,\mathrm{ms}^{-2}$ (black solid) and $A = 2\,\mathrm{ms}^{-2}$ (black dotted) to 7F where $u = -C_n v^3$, $C_n = 0.588 \times 10^9\,\mathrm{Ns}^3\mathrm{m}^{-3}$ (black solid) is implemented by semi-active dampers and $u = -C_{p4} v$ (red dotted).

To resolve this issue, it is possible to design C_n for a specific range of A to achieve the optimal line over the required frequency range by using the nonlinear design method described in [56,126].

6.4.5 Isolation performance in terms of the roof drift

The roof drift of the building is also an important criterion to assess the building isolation performance [136]. Denote the roof drift as

$$R(f) = \left| F\{x_r(t) + z(t)\}\big|_{\omega=2\pi f} \right| \tag{6.16}$$

where $x_r(t)$ represents the displacement of the roof floor of the building, and $z(t)$ is the ground displacement.

The roof drifts of the Sosokan Building in different cases were simulated and the results are shown in Fig.6.11. The results indicate that when the same isolation performance at the resonant frequency is achieved, the cubic damper $C_n = 0.588 \times 10^9\,\mathrm{Ns}^3\mathrm{m}^{-3}$ can produce a better performance in terms of roof drift than a linear damper with $C_l = C_{p4}$ in both the cases of $A = 1\,\mathrm{ms}^{-2}$ and $A = 2\,\mathrm{ms}^{-2}$.

6.4.6 Isolation performance in terms of harmonics and a comparison with the performance under LQG control

The presence of harmonics is inevitable in a system containing any kinds of nonlinearities. The introduction of cubic damping creates odd harmonics in the output signals. Using the concept of energy

transmissibility to include the effects of all super-harmonics in previous studies at Sheffield [137], it has been analytically shown that the magnitudes of these harmonics are small compare to the size of the fundamental harmonic. Additionally, the study has also shown that nonlinear damping can suppress the undesired harmonics and jumps caused by stiffness nonlinearity. As the building itself may already contain some stiffness nonlinearities, the introduction of nonlinear damping would therefore enhance the overall system stability.
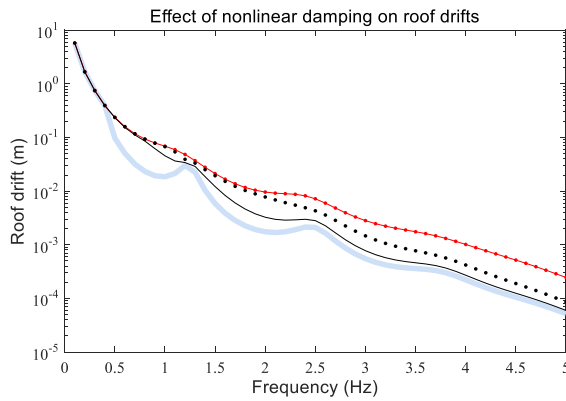
Fig. 6.11. Roof drifts under the ground displacement amplitude $A = 1\,\mathrm{ms}^{-2}$ (black solid) and $A = 2\,\mathrm{ms}^{-2}$ (black dotted), respectively when the nonlinear damping $u = -C_n v^3$, $C_n = 0.588 \times 10^9\,\mathrm{Ns^3 m^{-3}}$ is implemented by the semi-active dampers and the linear damping $u = -C_{p4} v$ (red dotted) is applied.
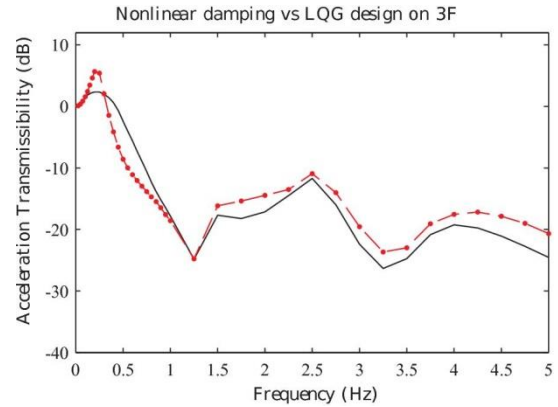
Fig. 6.12. Acceleration transmissibility from ground input $A = 1\,\mathrm{ms}^{-2}$ to 3F, where the semi-active dampers are controlled by the passive nonlinearly damping method (black solid) and the LQG method (red dashed).

Fig.6.12 shows a comparison of the acceleration transmissibility to 3F of the proposed nonlinear damped system against the LQG design in [128]. It can be observed from Fig.6.12 that the nonlinear damped system delivers better performance over both the resonant higher frequency regions hence offers a more effective alternative to the LQG design approach. It is worth pointing out that although an optimal solution can be found by minimizing the cost function provided by [128], the dampers often cannot deliver the designed optimal performance in reality [138,139]. Moreover, it is noticeable that the nonlinear damping design only relies on local sensors in the isolation layer whereas any implementation based on an active control law (such as the LQG approach) would require sensors on other floors. When considering the practical aspects of the design, the reliability and quality of the sensor communication, be it wired or wireless, must also be taken into account.

In summary, the simulation results above have demonstrated the advantages of a nonlinearly damped

semi-active base-isolation system. First, the acceleration transmissibilities achieved by the proposed system is very close to the optimal lines where only one damping coefficient can be chosen for each excitation frequency. Second, although the performance of a nonlinear design is dependent on the input magnitude, the results have shown sufficient robustness to the loading. Third, instead of optimizing the acceleration of one particular floor, the results indicate strong isolation performance across all floors.

In order to confirm some important points reached by the numerical simulation, laboratory experimental work has been conducted. The details are introduced in the next section.

6.5 Experimental Validation

To validate the performance of the proposed passive nonlinearly damped building isolation system, a scaled physical model of the Sosokan Building has been built, as shown in Fig.6.13, in a laboratory at Keio University. The schematic of the semi-active damper in Fig.6.14 shows two solenoid valves (with orifice diameters of 3 and 5 mm, respectively) which can be controlled to create four different damping coefficients that could facilitate the implementation of the power law nonlinear damping.
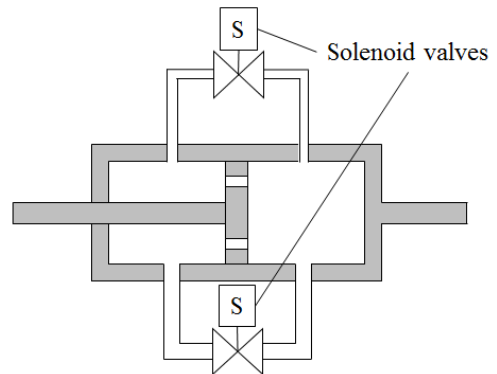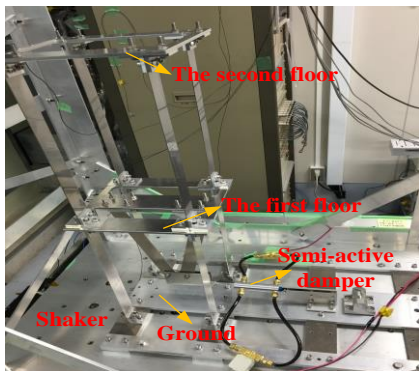
Fig. 6.13. The laboratory physical model of Sosokan Building   **Fig. 6.14.** Schematic illustration of a semi-active damper

For base-isolated buildings, a 2-DOF model is often used to model the dynamic properties [140,141].
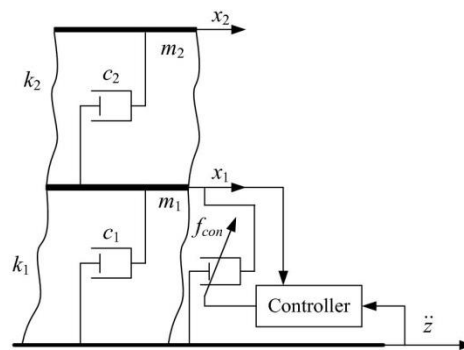
Fig.6.15. The 2-DOF representation of the physical model

The equation of motion for the 2-DOF system in Fig. 6.15 can be described as follows.

$$M\ddot{x} + C\dot{x} + Kx = Ef_{con} + F\ddot{z} \tag{6.17}$$

where f_{con} represents the controlled damping force.

$$x = \left[x_1,\, x_2\right]^T;\ M = \begin{bmatrix} m_1 & 0 \\ 0 & m_2 \end{bmatrix};\ C = \begin{bmatrix} c_1 + c_2 & -c_2 \\ -c_2 & c_2 \end{bmatrix};$$

$$K = \begin{bmatrix} k_1 + k_2 & -k_2 \\ -k_2 & k_2 \end{bmatrix};\ E = \left[1, 0\right]^T;\ F = \left[-m_1, -m_2\right]^T$$

with

$$m_1 = 3.264\ \text{kg};\ m_2 = 1.589\ \text{kg};\ k_1 = 249.9\ \text{N/m};$$

$$k_2 = 1968\ \text{N/m};\ c_1 = 0.1294\ \text{Ns/m}\ \ \text{and}\ \ c_2 = 1.019\ \text{Ns/m}$$

The first and second natural frequencies of the building model system are 1.134 Hz and 6.877 Hz, respectively.

A semi-active linear damper with the damping coefficient being able to be switched over four different values is fitted on the ground floor of the test rig, which is the same as the situation with the Sosokan Building.

The four damping coefficients are

$$C_{p1} = 30.8\ \text{Ns/m}; C_{p2} = 40.1\ \text{Ns/m}; C_{p3} = 44.5\ \text{Ns/m}; C_{p4} = 84.8\ \text{Ns/m} \tag{6.18}$$

The experiments were conducted when the sweep sine wave

$$\ddot{z}(t) = 0.6\sin(2\pi f t)\ \text{m/s}^2 \tag{6.19}$$

with $f \in [0, 15]\ \text{Hz}$ was applied as the loadings to the model.

In the experiments, the cubic damping coefficient was chosen as $C_n = 3000\ \text{Ns}^3/\text{m}^3$. In this case, the cubic damping characteristic and the force-velocity relationships of the semi-active damper under the four damping coefficients given in (6.18) are shown in Fig.6.16 where the maximum velocity across the damper is $0.2\ \text{m/s}$. In order to compare the performance of the proposed nonlinearly damped system with the performance that can be achieved by the LQG based feedback control and traditional linear damping, an equivalent linear damping was chosen as $C_{p4} = 84.8\ \text{Ns/m}$ such that the three different techniques can achieve a similar transmissibility over the resonant frequency range as shown in Fig.6.16.
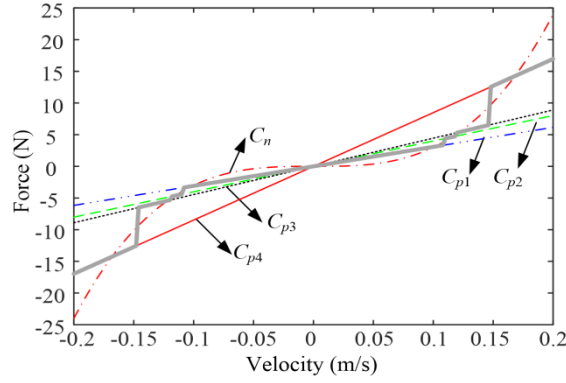
Fig.6.16. Force-velocity relationship of $C_n = 3000 \ \text{Ns}^3/\text{m}^3$ and the real damping force (thick grey line)

With respect to the LQG clipped semi-active control, the adopted cost functional is chosen following the standard requirement in earthquake engineering [142]. The functional is the sum of squared floor accelerations and squared control force with an empirically-tuned weight coefficient of $10 \ \text{kg}^{-2}$ as given by

$$J = E\left\{\int_0^\infty \left[\left(\ddot{x}_0(t) + \ddot{x}_1(t)\right)^2 + \left(\ddot{x}_0(t) + \ddot{x}_2(t)\right)^2 + Ru^2(t)\right]dt\right\} \tag{6.20}$$

where $E\{.\}$ denotes the mathematical expectation, $\ddot{x}_0(t), \ddot{x}_1(t)$ and $\ddot{x}_2(t)$ are the accelerations on the ground, the first, and the second floor, respectively, $R = 10 \ \text{kg}^{-2}$, and $u(t)$ is the semi-active control force.

In (6.20), the term $E\left\{\int_0^\infty \left[\left(\ddot{x}_0(t) + \ddot{x}_1(t)\right)^2 + \left(\ddot{x}_0(t) + \ddot{x}_2(t)\right)^2\right]dt\right\}$ in the cost functional is introduced to minimise the absolute accelerations on each floor so as to reduce possible damage to contents and non-structural components in a building structure. The additional term $E\int_0^\infty \left\{Ru^2(t)\right\}dt$ is used to penalise the excessive control action that could take by the semi-active controller. The weighting value $R = 10 \ \text{kg}^{-2}$ was empirically tuned in order for the LQG clipped semi-active control to achieve the same transmissibility at the first resonant frequency as the transmissibility that can be achieved by the proposed cubic damping with coefficient $3000 \ \text{Ns}^3/\text{m}^3$ and its equivalent linear damping with coefficient $84.8 \ \text{Ns}/\text{m}$. This is to facilitate an effective comparison between the three different building isolation techniques.

In determination of a Kalman filter gain, noise intensities are assigned $2.6 \times 10^{-4} \ \text{m}^2/\text{s}^2$ for system noise and $2.99 \times 10^{-4} \ \text{m}^2/\text{s}^4$, $1.62 \times 10^{-4} \ \text{m}^2/\text{s}^4$, and $9.30 \times 10^{-4} \ \text{m}^2/\text{s}^4$ for noise of accelerometers at the table, lower floor, and upper floor, respectively.

In the laboratory studies, due to the limitation of the software system and also for the simplicity of implementation, instead of using the PI control in (6.15), a straightforward look-up table-based feedforward

control was applied to determine the damping coefficient from its four available choices based on the measured velocity across the damper as follows:

$$C_s(t) = \begin{cases} C_{p1}, & \text{for } u_d/v \le (C_{p1}+C_{p2})/2 \\ C_{p2}, & \text{for } (C_{p1}+C_{p2})/2 < u_d/v \le (C_{p2}+C_{p3})/2 \\ C_{p3}, & \text{for } (C_{p2}+C_{p3})/2 < u_d/v \le (C_{p3}+C_{p4})/2 \\ C_{p4}, & \text{for } u_d/v > (C_{p3}+C_{p4})/2 \end{cases} \tag{6.21}$$

$$u_m = -C_s(t)v \tag{6.22}$$

where u_d and u_m are the desired and measured damping force, respectively, and v is the velocity across the damper. In the experiments, v is estimated by a Kalman filter using the measured acceleration data $\ddot{z}, \ddot{x}_1$ and $\ddot{x}_2$. The implemented cubic damping characteristic is shown by the grey line in Fig.6.16. Consequently, a qualitative demonstration of the performance of the proposed nonlinearly damped system is expected from the experimental studies.

Remark 6.1: Eq. (6.15) shows how a PI feedback control can be implemented by using the semi-active damping system currently used in the Sosokan Building to achieve a desired damping characteristic. Eq. (6.21) shows a simpler feed forward control solution used in the experimental study. Both implementations are based on traditional control system designs. Generally speaking, Eq. (6.15) is an ideal solution if the implementation is not constrained by hardware and software limitations. This is because a PI based close loop control can achieve the desired damping force better than an open loop method.

(a) The transmissibility of the 1st floor   (b) The transmissibility of the 2nd floor
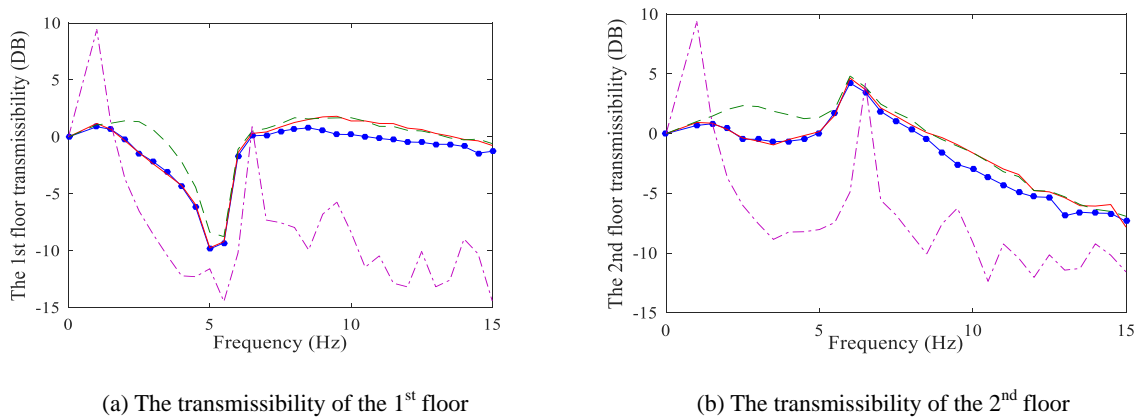
Fig.6.17. Comparison of the transmissibilities: Cubic damper (Blue dot line); LQG (Red line); Linear damper (Green dash line); No damper (Purple dash-dot line)

Fig.6.17 shows the main results from the experimental studies. The results indicate that the proposed nonlinear damping always gives the best performance. Over both the resonant frequency and the high frequency ranges, the nonlinear damping produces a lower transmissibility compared to that with the LQG

method; while the transmissibility with the equivalent linear damping increases significantly beyond the resonant frequency range of the system. All of these are consistent with the conclusions reached in Section 6.4 from simulation studies.
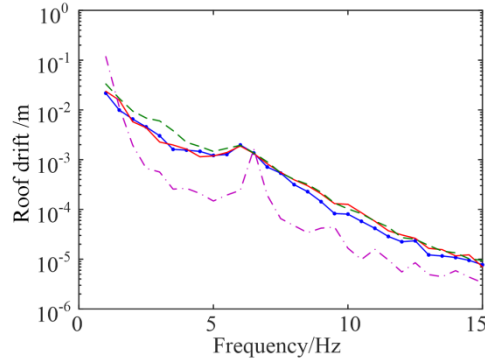
Fig. 6.18. Comparison of the roof drifts: Cubic damper (Blue dot line); LQG (Red line); Linear damper (Green dash line); No damper (Purple dash-dot line)

The roof drifts of the 2DOF physical building model controlled by the three different methods are shown in Fig.6.18, which further confirms the conclusion reached by simulation that the nonlinear damping method outperforms the other two approaches.

(a) Cubic damping   (b) LQG
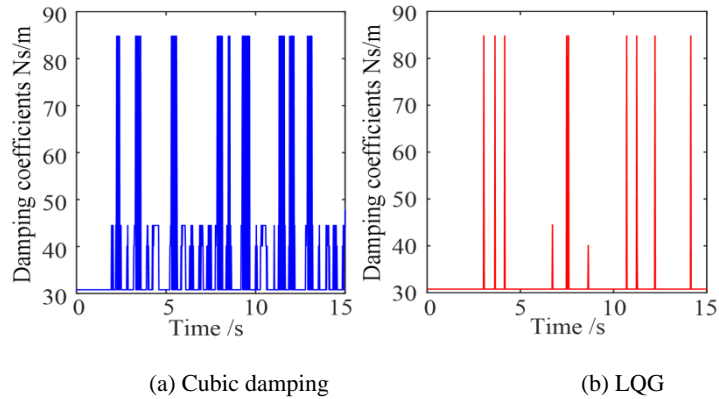
Fig.6.19. Situations with switching over four damping coefficients at $f = 1.0$ Hz

(a) Cubic damping   (b) LQG
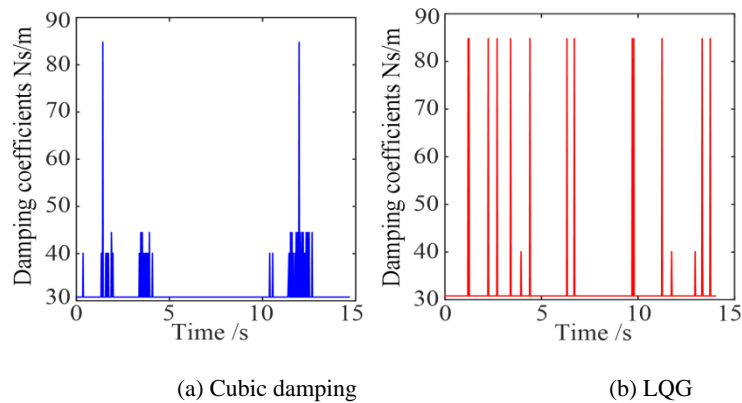
Fig.6.20. Situations with switching over four damping coefficients at $f = 13.0$ Hz

In order to explain the superior performance of nonlinear damping over LQG, the situations with switching over the four different damping coefficients under the nonlinear damping and LQG are shown in Figs.6.19 and 6.20 for the cases when the system is working at the resonant frequency ($f \approx 1.0$ Hz) and high frequency ($f = 13$ Hz), respectively.

From Figs.6.19 and 6.20, it can be observed that over the resonant frequency range, the nonlinear damping approach select, the maximum damping coefficient for most of the time while the LQG method only occasionally use the maximum damping coefficient. On the other hand, over the higher frequency, the nonlinear damping method uses smaller damping coefficients while LQG still opts for the maximum damping intermittently.

It is worth noting that the minimum damping coefficient that both nonlinear damping and LQG approach can use in the experiment is $C_{p1} = 30.8$ Ns/m . If the minimum realisable damping coefficient is very small, it is expected that the nonlinear damping would achieve almost the same transmissibility as that shown in purple dash-dot line in Fig. 6.17 over the range of higher frequencies while still suppressing the vibration well over the resonance, showing an ideal performance over almost all ranges of frequencies.
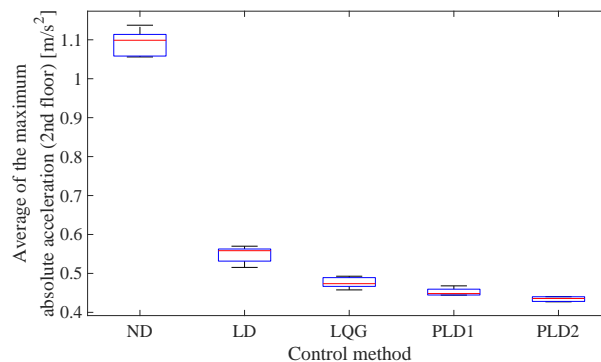
Fig.6.21. An experimental comparison of the base isolation performances when the building model (Fig.6.12) is subject to a simulated near-fault ground motion in the four cases of   (i) No Damping (ND), (ii) Linear Damping (LD), (iii) LQG, (iv) Two different cubic damping (denoted as PLD1 and PLD2, respectively)

In the present study, the great potential of a base-isolation system with nonlinear damping implemented by using a semi-active damper has been demonstrated when the ground motion can be assumed to be a single-tone sinusoidal wave, which is often the case when the building is located far away from the epicenter. The scenarios considered in this study are the earthquake ground motions which have either dominant frequency in the isolated range or a dominant frequency in the non-isolated range of the system. The results indicate the proposed nonlinear damping solution guarantees that the base isolation system works well in both cases. For the cases of near-fault ground motions as well as the cases where the ground motion contains

energy in both frequency ranges, the proposed cubic damping solution is also expected to perform better than linear solutions according to the analyses and results in [143-145]. One of these results is, for example, shown in Fig.6.21 [145]. However, a more comprehensive principle needs to be followed to perform the nonlinear damping design, which will be investigated in a future study.

6.6 Conclusions

In March 2011, the most powerful earthquake ever recorded in Japan occurred approximately 70 kilometres east of the Oshika Peninsula. The measured ground motion contained long-period waves with unprecedented intensity and duration. However, the building regulations in Japan currently do not cover the profile of the long-period waves observed in 2011. Engineers are therefore motivated to improve the current seismic protection technologies.

Ideally, dampers used for system isolation should have high damping coefficients when the excitation frequency is low and have low damping coefficients when the excitation frequency is high. As it is impossible to predict the frequency spectrum of future earthquakes, changing dampers according to the input frequency is not a practical solution.

The idea of applying nonlinear damping to vibration isolation problem has been explored in previous studies. It has been proven that nonlinear damping in a vibration isolation system can offer sufficient isolation around the resonance without affecting the high frequency performance. In this Chapter, the realization of the desired nonlinear damping force has been implemented using a semi-active damper, which can be readily achieved in practice. The Sosokan Building model based numerical simulation studies and experimental studies on a scaled physical model have demonstrated the performance of the new technique and the advantages of the technique over traditional solutions

The proposed nonlinear damping isolation system provides a good isolation against long-period waves as well as ground motions in the frequency spectrum which have been observed during most earthquakes. The controller only requires force and velocity measurements that are local to the semi-active dampers. This is a major practical advantage over other solutions as local measurements are much less susceptible to noise and interference. Instead of treating the semi-active dampers as actuators during the design process, the proposed approach guarantees robustness and stability, which is essential during earthquakes.

Other advantages of the proposed method can be highlighted by comparing with some existing solutions. The nonlinear damping based semi-active dampers can be easily installed in the isolation layer of most buildings without requiring a major redesign. Active actuators can be readily installed but the requirement of

a large power supply may have more safety implications. Therefore, in terms of costs, practicality and performance, the proposed nonlinearly damping solution is a better all-round alternative.

Chapter 7. Conclusions

Traditional nonlinear system designs are basically based on the time domain response analysis, which is often difficult to reveal the relationship between the system performance and the parameters that can be used to perform the design. Motivated by the wide engineering applications of the FRF-based linear system frequency domain analysis and design, the frequency analysis approaches, i.e. the GFRFs, the NOFRFs and OFRF, etc., were proposed in order to extend the effective linear system approaches to the nonlinear case. However, there are many issues need to be addressed to facilitate the engineering application of these approaches.

In order to address the problems with many existing nonlinear system analyses, the present research work has first proposed a new concept known as the GALEs and developed effective methods for the determination of the GALEs of the NDE and NARX models of nonlinear systems, respectively. The GALEs can transform the analysis of the NDE or NARX model of nonlinear systems to the analysis of a series of linear differential or linear difference equations so as to significantly facilitate nonlinear system analyses including, for example, the evaluation of time domain responses of complicated nonlinear systems, the determination of the NOFRFs for nonlinear system frequency analysis, and the identification of the physically meaningful differential equation model of nonlinear systems.

Considering that the convergence of the Volterra series representation of nonlinear systems is the basis of the frequency domain analysis and design of nonlinear systems, in the present study, a new convergence analysis for the Volterra series representation of nonlinear systems has been proposed. A frequency domain representation of the NARX model of nonlinear systems, known as the Nonlinear Output Characteristic Spectra (NOCS) model, has been derived. The Generalized Output Bound Characteristic Function (GOBCF) is then defined to represent the bound characteristics of the NARX models. Moreover, a new criterion for the analysis of the convergence of the Volterra series representation of nonlinear systems is derived based on the GOBCF, producing a novel sufficient condition for a convergent Volterra series representation of the NARX model of nonlinear systems. Compared to existing approaches, the new criterion provides a more rigorous and less conservative analysis result and is applicable to nonlinear systems subject to either harmonic or general inputs.

Moreover, consider that it is difficult even impossible to find a differential equation model for complex engineering systems and the need to extend the physical model-based nonlinear system analysis and design

approach to more complicated systems, a new model known as the NARX-M-for-D is proposed, which can be derived from a nonlinear differential equation model of a system but, more importantly, can also be determined from the system input output data through a nonlinear system identification process. A new OFRF-based methodology is then developed that can be applied to the design of nonlinear systems described by a NARX-M-for-D. Further, in order to address the issue that the OFRF only shows a polynomial relationship between the system's output spectrum and nonlinear characteristic parameters, but can't explicitly reveal the effect of system linear characteristic parameters on output spectra, a concept known as the AOFRF of nonlinear systems has been proposed. The AOFRF enables an explicit separation of the system linear and nonlinear characteristic parameters in the representation of the system output spectrum and, consequently, facilitates the derivation of a polynomial representation in terms of both the system linear and nonlinear characteristic parameters.

Finally, the idea of applying nonlinear damping to vibration isolation problems is explored, where the realization of the desired nonlinear damping force has been implemented using a semi-active damper, which can be readily achieved in practice. The Sosokan Building model based numerical simulation studies and experimental studies on a scaled physical building model have demonstrated the performance of the new technique and the advantages of the technique over traditional solutions. The significance and advantages of the nonlinear base-isolation systems have been discussed, which are expected to have potential to be applied in many engineering practices in the near future.

7.1 Main contributions of the present research

This research study has made many significant contributions in the field of nonlinear system frequency analysis and design. The main points of these contributions are summarized as below.

(1) A new method that can accurately evaluate the system Volterra series representation, known as the GALEs, was proposed. By using an efficient algorithm, the system GALEs can be automatically determined, such that the Volterra series representation of the nonlinear system output can be evaluated up to an arbitrarily high order by solving a series of linear equations.

(2) A new convergence criterion for the Volterra series representation of nonlinear systems was derived based on the GOBCF of the system NARX model. The new convergence criterion is independent of sampling frequency with the NARX model, applicable to nonlinear systems under general inputs, and does not require carrying out complex mathematical computations.

(3) The OFRF of NARX-M-for-D of nonlinear systems was determined. The AOFRF concept is proposed

and the AOFRF based representation of the output spectrum of nonlinear systems was defined as an extension of the OFRF. Based on the AOFRF, the system output spectrum can represented by a polynomial function of both the system linear and nonlinear characteristic parameters. By using the AOFRF representation, it is possible to design a nonlinear system in a systematical way by considering the effects of both the system linear and nonlinear parameters on the system performance.

(4) A desired nonlinear damping is implemented by using a semi-active control method for the base isolation of buildings. The results indicate that it is possible to apply the newly proposed nonlinear system design in practice to address challenges in earthquake engineering.

7.2 Future works

Although, in the present study, significant progress has been made and many results have been achieved in the analysis and design of nonlinear systems in the frequency domain, there are still many further works to develop. These works include the identification of physically meaningful data driven models of nonlinear systems, determination of a reduced order OFRF/AOFRF representation of the system output frequency response, application of the GALEs in the system analysis, identification and design, convergence analyses of the Volterra series representation of continuous time nonlinear systems, and the extension of what has been achieved to MIMO nonlinear systems, etc.. More detailed discussion of these possible future works are as follows:

(1) The techniques for the determination of the NARX-M-for-D for nonlinear systems needs to be further developed by taking into account the physical relationship in a data driven NARX model. The NDE model is a "white box model" while a data driven NARX model is a "black box model". The NARX-M-for-D is a "gray box model" making it possible to describe, in a physically meaningful way, a large class of nonlinear systems. The frequency analysis and design of nonlinear systems can then be applied based on the NARX-M-for-D. In developing the NARX-M-for-D identification, design of the experiments for training data collection is important and more efficient identification algorithm will be developed in the future works.

(2) It has been observed that, can be seen that, although a polynomial representation of the output frequency response in terms of the system linear and nonlinear parameters provides a convenient way for the analysis and design of nonlinear systems, the order of the OFRF/AOFRF polynomial can be significantly high. This may induce numerical errors and limit the application of the OFRF/AOFRF based approaches in practice. Therefore, it is significant to developmore effective algorithm to

produce the OFRF/AOFRF of a reduced order to address possible numerical error issues with current techniques.

(3) The GALEs provides an efficient approach to the analysis of nonlinear systems by using linear system methods. The method has great potential for a much wider range of nonlinear system studies. It is therefore necessary to further explore the application of the GALEs and associated methods.

(4) In the present study, a new convergence analysis of the NARX model of nonlinear systems has been established. How to apply the same idea to extend the convergence analysis to the NDE models of nonlinear systems can be a related research topic in the next step.

(5) All the results obtained in this study are based on SISO nonlinear systems while in practice, many systems, for example, the building system discussed in Chapter 6, are MIMO systems. The newly proposed frequency domain analysis and design approaches will be extended to MIMO cases in future works to address more general and complex engineering problems.

The aforementioned are a only a few possible future works that could be conducted based on the present state of this research. More opportunities and innovative developments include engineering system condition monitoring, optimal design, identification and control, etc., which could all be addressed under the framework that has been established in the present study.

Appendices

Appendix A. Sampling frequency independence

The normalized convergence criterion in Proposition 4.3 is independent of sampling frequency. This is because when the sampling frequency $1/\Delta t$ is sufficiently large, the GOBCF of the nonlinear system can be written as

$$f_{BC}(x) = x - \bar{L}_{w_{\text{lin}}} \bar{C}_{0,1} [\![u]\!] - \sum_{m=2}^{M} \sum_{p=0}^{m} \left(x^p [\![u]\!]^{m-p} \lim_{\Delta t \to 0} \bar{L}_w \bar{C}_{p,m-p} \right) \tag{A1}$$

Noting that for any physical system, the NARX model with $\Delta t \to 0$ is in fact the NDE model of the system due to the relationship of

$$\dot{y}(k) = \frac{y(k) - y(k-1)}{\Delta t}, \quad \ddot{y}(k) = \frac{y(k+1) - 2y(k) + y(k-1)}{\Delta t^2} \tag{A2}$$

Therefore, $\lim_{\Delta t \to 0} \bar{L}_w \bar{C}_{p,m-p}$ is a constant and independent of the sampling time Δt, when all frequency variables are bounded.

Consequently, the GOBCF of the NARX model is independent of sampling frequency, indicating that the new convergence criterion in Proposition 4.3 is also independent of sampling frequency.

Appendix B. Proof of Lemma 5.1

The linear frequency response function $H_1(\omega_i), i = 1, \ldots, n$ is

$$H_1(\omega_i) = \sum_{k=1}^{K} c_{0,1}(k) \exp(-j\omega_i k \Delta t) \frac{1}{1 - \sum_{k=1}^{K} c_{1,0}(k) \exp(-j\omega_i k \Delta t)} \tag{B1}$$

and

$$L_n^{-1}(\omega_1, \cdots, \omega_n) = \frac{1}{1 - \sum_{k=1}^{K} c_{1,0}(k) \exp(-j(\omega_1 + \cdots + \omega_n) k \Delta t)} \tag{B2}$$

Denote $C_c(j\omega) = \sum_{k=1}^{K} c_{1,0}(k) \exp(-j\omega k \Delta t)$, by employing the n_e th order Taylor expansion at the point of

$C_z(j\omega) = \sum_{k=1}^{K} c_z(k) \exp(-j\omega k \Delta t)$, there is

$$f\left[C_c\left(\mathrm{j}\omega\right)\right] = \frac{1}{1-C_c\left(\mathrm{j}\omega\right)} = \frac{f\left[C_z\left(\mathrm{j}\omega\right)\right]}{0!} + \frac{f'\left[C_z\left(\mathrm{j}\omega\right)\right]}{1!}\left[C_c\left(\mathrm{j}\omega\right)-C_z\left(\mathrm{j}\omega\right)\right] +$$

$$\frac{f''\left[C_z\left(\mathrm{j}\omega\right)\right]}{2!}\left[C_c\left(\mathrm{j}\omega\right)-C_z\left(\mathrm{j}\omega\right)\right]^2 + \cdots + \frac{f^{(n_e)}\left[C_z\left(\mathrm{j}\omega\right)\right]}{n_e!}\left[C_c\left(\mathrm{j}\omega\right)-C_z\left(\mathrm{j}\omega\right)\right]^{n_e} + \cdots \tag{B3}$$

with the convergence radius of $\rho = \left|C_c\left(\mathrm{j}\omega\right)-C_z\left(\mathrm{j}\omega\right)\right| < 1$, where $f^{(i)}[.]$ is the i th order derivation of the function $f[.]$.

Based on the Euler's formula, notice that

$$\left|\exp\left(-\mathrm{j}\omega k\Delta t\right)\right| = \left|\cos\left(\omega k\Delta t\right) + \mathrm{j}\sin\left(\omega k\Delta t\right)\right| = 1 \tag{B4}$$

and

$$\rho = \left|C_c\left(\mathrm{j}\omega\right)-C_z\left(\mathrm{j}\omega\right)\right| = \left|\sum_{k=1}^{K}c_{1,0}\left(k\right)\exp\left(-\mathrm{j}\omega k\Delta t\right) - \sum_{k=1}^{K}c_z\left(k\right)\exp\left(-\mathrm{j}\omega k\Delta t\right)\right|$$

$$\leq \sum_{k=1}^{K}\left|c_{1,0}\left(k\right)-c_z\left(k\right)\right|\left|\exp\left(-\mathrm{j}\omega k\Delta t\right)\right| = \sum_{k=1}^{K}\left|c_{1,0}\left(k\right)-c_z\left(k\right)\right| \tag{B5}$$

which indicates that $H_1(.)$ and $L_n^{-1}\left(\omega_1,\cdots,\omega_n\right)$ can be expressed by a convergent Taylor series when

$$\sum_{k=1}^{K}\left|c_{1,0}\left(k\right)-c_z\left(k\right)\right| < 1 \tag{B6}$$

and obviously, (B6) is a sufficient condition for that $H_1(.)$ and $L_n^{-1}\left(\omega_1,\cdots,\omega_n\right)$ can be written into a convergent Taylor series.

Assuming the expansion order of (B3) is $n_e = n_L$ and (B6) is satisfied, (B1) can be written as:

$$H_1\left(\omega_i\right) = \left[\sum_{k_\upsilon=1}^{K}c_{0,1}\left(k_\upsilon\right)\exp\left(-\mathrm{j}\omega_i k_\upsilon\Delta t\right)\right]\left[a_0 + a_1\sum_{k_\tau=1}^{K}\left[c_{1,0}\left(k_\tau\right)-c_z\left(k_\tau\right)\right]\exp\left(-\mathrm{j}\omega_i k_\tau\Delta t\right)\right.$$

$$\left. + a_2\left(\sum_{k_\tau=1}^{K}\left[c_{1,0}\left(k_\tau\right)-c_z\left(k_\tau\right)\right]\exp\left(-\mathrm{j}\omega_i k_\tau\Delta t\right)\right)^2 + \cdots + a_{n_L}\left(\sum_{k_\tau=1}^{K}\left[c_{1,0}\left(k_\tau\right)-c_z\left(k_\tau\right)\right]\exp\left(-\mathrm{j}\omega_i k_\tau\Delta t\right)\right)^{n_L}\right] \tag{B7}$$

$$= \sum_{l=0}^{n_L}\sum_{\substack{\tau_1+\cdots+\tau_K=l \\ \upsilon_1+\cdots+\upsilon_K=1}}\varphi_{\left[\substack{\tau_1,\cdots,\tau_K \\ \upsilon_1,\cdots,\upsilon_K}\right]}\prod_{k_\upsilon=1}^{K}c_{0,1}^{\upsilon_{k_\upsilon}}\left(k_\upsilon\right)\prod_{k_\tau=1}^{K}c_{1,0}^{\tau_{k_\tau}}\left(k_\tau\right)$$

where $a_i, i = 0,\ldots,n_L$ are constants.

Noticing that the sufficient convergence condition (B6) is independent to frequency variables, it is easy to know that there exists an integer n_L, let $H_1\left(\omega_i\right)$ for $i = 1,\ldots,n$ be expressed by the same order Taylor series of $n_e = n_L$, therefore,

$$H_1^r(.) = \sum_{l=0}^{r\times n_L}\sum_{\substack{\tau_1+\cdots+\tau_K=l \\ \upsilon_1+\cdots+\upsilon_K=r}}\varphi_{\left[\substack{\tau_1,\cdots,\tau_K \\ \upsilon_1,\cdots,\upsilon_K}\right]}\prod_{k_\upsilon=1}^{K}c_{0,1}^{\upsilon_{k_\upsilon}}\left(k_\upsilon\right)\prod_{k_\tau=1}^{K}c_{1,0}^{\tau_{k_\tau}}\left(k_\tau\right) \tag{B8}$$

Considering the order of the Taylor expansion is only related to $\left| c_{1,0}(k) - c_z(k) \right|$, and according to (B1)

and (B2), $L_n^{-1}(\omega_1, \cdots, \omega_n)$ can be expressed as:

$$
\begin{aligned}
L_n^{-1}(\omega_1, \cdots, \omega_n) &= \left[b_0 + b_1 \sum_{k=1}^{K} \left[c_{1,0}(k) - c_z(k) \right] \exp\left(-j\omega_i k \Delta t\right) + b_2 \left(\sum_{k=1}^{K} \left[c_{1,0}(k) - c_z(k) \right] \exp\left(-j\omega_i k \Delta t\right) \right)^2 \right. \\
&\quad \left. + \cdots + b_{n_L} \left(\sum_{k=1}^{K} \left[c_{1,0}(k) - c_z(k) \right] \exp\left(-j\omega_i k \Delta t\right) \right)^{n_L} \right] = \sum_{l=0}^{n_L} \sum_{\tau_1 + \cdots + \tau_K = l} \tilde{\varphi}_{[\tau_1, \cdots, \tau_K]} \prod_{k=1}^{K} c_{1,0}{}^{\tau_k}(k)
\end{aligned}
\tag{B9}
$$

where $\tilde{\varphi}_{[\tau_1, \cdots, \tau_K]}$ represents the function of frequecy variables.

According to (5.34),

$$
EL\left[\boldsymbol{L}_{(1:r)} \right] = 1
\tag{B10b}
$$

$$
EL\left[\boldsymbol{L}_{(2:r)} \right] = \sum_{l=0}^{n_L} \sum_{\tau_1 + \cdots + \tau_K = l} \tilde{\varphi}_{[\tau_1, \cdots, \tau_K]} \prod_{k=1}^{K} c_{1,0}{}^{\tau_k}(k)
\tag{B10a}
$$

Assuming (5.75) holds for $(n-1:r)$th term, for the $(n:r)$th term,

$$
EL\left[\boldsymbol{L}_{(n:r)} \right] = L_n^{-1}(\omega_1, \ldots, \omega_n) \left\{ \delta + \sum_{q=1}^{n-1} \sum_{p=1}^{n-q} EL\left[\boldsymbol{L}_{([n-q,p]:r)} \right] + \sum_{p=2}^{n} EL\left[\boldsymbol{L}_{([n,p]:r)} \right] \right\}
\tag{B11}
$$

where $\delta = \begin{cases} 1 & r = 0 \\ 0 & r > 0 \end{cases}$. According to (5.42),

$$
\begin{aligned}
EL\left[\boldsymbol{L}_{([n,p]:r)} \right] &= \sum_{i=1}^{n-p+1} EL\left[\boldsymbol{L}_{(i:R_1)}(\omega_1, \cdots, \omega_i) \otimes \boldsymbol{L}_{([n-i,p-1]:R_2)}(\omega_{i+1}, \cdots, \omega_n) \right] \\
&= \sum_{\substack{r_1, \cdots, r_p = 1 \\ \sum r_i = n}}^{n-p+1} \prod_{i=1}^{p} EL\left[\boldsymbol{L}_{(r_i : \bar{R}_i)}(\omega_{X+1}, \cdots, \omega_{X+r_i}) \right] \exp\left(-j\left(\omega_{X+1} + \cdots + \omega_{X+r_i} \right) k_{p+1-i} \Delta t \right) \\
&= \sum_{g=0}^{(n-p)} \sum_{l=0}^{g \times n_L} \sum_{\tau_1 + \cdots + \tau_K = l} \tilde{\varphi}_{[\tau_1, \cdots, \tau_K]} \prod_{k=1}^{K} c_{1,0}{}^{\tau_k}(k)
\end{aligned}
\tag{B12}
$$

where $r = \sum_{i=1}^{p} R_i$.

Substituting (B12) into (B11), yields:

$$
EL\left[\boldsymbol{L}_{(n:r)} \right] = \sum_{l=0}^{(n-1) \times n_L} \sum_{\tau_1 + \cdots + \tau_K = l} \tilde{\varphi}_{[\tau_1, \cdots, \tau_K]} \prod_{k=1}^{K} c_{1,0}{}^{\tau_k}(k)
\tag{B13}
$$

Then Lemma 5.1 is proven.

References

[1] Krstic, M., Kanellakopoulos, I., & Kokotovic, P. V. (1995). *Nonlinear and adaptive control design (Vol. 222)*. New York: Wiley.

[2] Vander Velde, W. E. (1968). *Multiple-input describing functions and nonlinear system design*. McGraw-Hill, New York.

[3] Jiang, B., Staroswiecki, M., & Cocquempot, V. (2006). Fault accommodation for nonlinear dynamic systems. *IEEE Transactions on Automatic Control, 51(9),* 1578-1583.

[4] Sastry, S. (2013). *Nonlinear systems: analysis, stability, and control (Vol. 10)*. Springer Science & Business Media.

[5] Vidyasagar, M. (2002). *Nonlinear systems analysis (Vol. 42)*. Siam.

[6] Jing, X., & Lang, Z. (2015). *Frequency domain analysis and design of nonlinear systems based on Volterra series expansion*. Springer International Publishing, Berlin Google Scholar.

[7] Nayfeh, A. H., & Balachandran, B. (2008). *Applied nonlinear dynamics: analytical, computational and experimental methods*. John Wiley & Sons.

[8] Tomlinson, G. R., & Worden, K. (2000). *Nonlinearity in structural dynamics: detection, identification and modelling*. CRC Press.

[9] Liu, L., Thomas, J. P., Dowell, E. H., Attar, P., & Hall, K. C. (2006). A comparison of classical and high dimensional harmonic balance approaches for a Duffing oscillator. *Journal of Computational Physics, 215(1),* 298-320.

[10] Peng, Z. K., Lang, Z. Q., Billings, S. A., & Tomlinson, G. R. (2008). Comparisons between harmonic balance and nonlinear output frequency response function in nonlinear system analysis. *Journal of Sound and Vibration, 311(1-2),* 56-73.

[11] Billings, S. A. (2013). *Nonlinear system identification: NARMAX methods in the time, frequency, and spatio-temporal domains*. John Wiley & Sons.

[12] Chua, L. O., & Oka, H. (1988). Normal forms for constrained nonlinear differential equations. I. Theory. *IEEE transactions on circuits and systems, 35(7),* 881-901.

[13] Peyton-Jones, J. C., & Billings, S. A. (1989). Recursive algorithm for computing the frequency response of a class of non-linear difference equation models. *International Journal of Control*, *50*, 1925-1940.

[14] Espinoza, M., Suykens, J. A., & De Moor, B. (2005). Kernel based partially linear models and nonlinear identification. *IEEE Transactions on Automatic Control*, *50(10),* 1602-1606.

[15] Vandersteen, G., Rolain, Y., & Schoukens, J. (1997). Non-parametric estimation of the frequency-response functions of the linear blocks of a Wiener-Hammerstein model. *Automatica, 33(7),* 1351-1355.

[16] Rijlaarsdam, D., Oomen, T., Nuij, P., Schoukens, J., & Steinbuch, M. (2012). Uniquely connecting frequency domain representations of given order polynomial Wiener–Hammerstein systems. *Automatica*, *48(9),* 2381-2384.

[17] Isidori, A. (2013). *Nonlinear control systems*. Springer Science & Business Media.

[18] Hwang, G. C., & Lin, S. C. (1992). A stability approach to fuzzy control design for nonlinear systems. *Fuzzy sets and Systems, 48(3),* 279-287.

[19] Barton, D. A., Burrow, S. G., & Clare, L. R. (2010). Energy harvesting from vibrations with a nonlinear oscillator. *Journal of Vibration and Acoustics, 132(2),* 021009.

[20] Carrella, A., Brennan, M. J., Waters, T. P., & Lopes Jr, V. (2012). Force and displacement transmissibility of a nonlinear isolator with high-static-low-dynamic-stiffness. *International Journal of Mechanical Sciences, 55(1),* 22-29.

[21] Schröck, J., Meurer, T., & Kugi, A. (2013). Motion planning for piezo-actuated flexible structures: Modeling, design, and experiment. *IEEE Transactions on Control Systems Technology, 21(3),* 807-819.

[22] Castanier, M. P., & Pierre, C. (2006). Modeling and analysis of mistuned bladed disk vibration: current status and emerging directions. *Journal of Propulsion and Power, 22(2),* 384-396.

[23] Chen, S., & Billings, S. A. (1989). Representations of non-linear systems: the NARMAX model. *International Journal of Control, 49(3),* 1013-1032.

[24] Li, P., Wei, H. L., Billings, S. A., Balikhin, M. A., & Boynton, R. (2013). Nonlinear model identification from multiple data sets using an orthogonal forward search algorithm. *Journal of Computational and Nonlinear Dynamics, 8(4),* 041001.

[25] Guo, Y. Z., Guo, L. Z., Billings, S. A., & Wei, H. L. (2015). An iterative orthogonal forward regression algorithm. *International Journal of Systems Science, 46(5),* 776-789.

[26] Giri, F. (2010). *Block-oriented nonlinear system identification (Vol. 1)*. E. W. Bai (Ed.). London: Springer.

[27] Wei, H. L., Lang, Z. Q., & Billings, S. A. (2008). Constructing an overall dynamical model for a system with changing design parameter properties. *International Journal of Modelling, Identification and Control, 5(2),* 93-104.

[28] Liu, H. P, Zhu, Y. P., Luo, Z., & Han, Q. K. (2017). PRESS-based EFOR algorithm for the dynamic parametrical modelling of nonlinear MDOF systems. *Frontiers of Mechanical Engineering, 3(11),* 1-11.

[29] Pavlov, A., van de Wouw, N., & Nijmeijer, H. (2007). Frequency response functions for nonlinear convergent systems. *IEEE Transactions on Automatic Control, 52(6),* 1159-1165.

[30] Garbuio, L., Lallart, M., Guyomar, D., Richard, C., & Audigier, D. (2009). Mechanical energy harvester with ultralow threshold rectification based on SSHI nonlinear technique. *IEEE Transactions on Industrial Electronics, 56(4),* 1048-1056.

[31] Jing, X. (2014). Nonlinear characteristic output spectrum for nonlinear analysis and design. *IEEE/ASME Transactions on Mechatronics, 19(1),* 171-183.

[32] Alma, M., Martinez, J. J., Landau, I. D., & Buche, G. (2012). Design and tuning of reduced order h-infinity

feedforward compensators for active vibration control. *IEEE Transactions on Control Systems Technology, 20(2),* 554-561.

[33] Moradi, M., & Fekih, A. (2015). A stability guaranteed robust fault tolerant control design for vehicle suspension systems subject to actuator faults and disturbances. *IEEE Transactions on Control Systems Technology, 23(3),* 1164-1171.

[34] Yao, M. H., Chen, Y. P., & Zhang, W. (2012). Nonlinear vibrations of blade with varying rotating speed. *Nonlinear Dynamics, 68(4),* 487-504.

[35] Pearson, R. K. (1999). *Discrete-time dynamic models.* Oxford University Press on Demand.

[36] George, D. A. (1959). *Continuous nonlinear systems.* Technical Report 335, MIT Research Laboratory of Electronics.

[37] Han, H. T., Ma, H. G., Xu, D. H., Wu, Z. W., Yang, D. D., & Jin, W. (2013). Non-parametric identification method of GFRFs for MIMO nonlinear system excited by multitone signal. *Journal of Sound and Vibration, 332(10),* 2562-2574.

[38] Zhang, H., & Billings, S. A. (1996). Gain bounds of higher-order nonlinear transfer functions. *International Journal of Control, 64(4),* 767-773.

[39] Yue, R., Billings, S. A., & Lang, Z. Q. (2005). An investigation into the characteristics of non-linear frequency response functions. Part 1: Understanding the higher dimensional frequency spaces. *International Journal of Control, 78(13),* 1031-1044.

[40] Yue, R., Billings, S. A., & Lang, Z. Q. (2005). An investigation into the characteristics of non-linear frequency response functions. Part 2: New analysis methods based on symbolic expansions and graphical techniques. *International Journal of Control, 78(14),* 1130-1149.

[41] Billings, S. A., & Peyton-Jones, J. C. (1990). Mapping non-linear integro-differential equations into the frequency domain. *International Journal of Control, 52(4),* 863-879.

[42] Jing, X. J., Lang, Z. Q., & Billings, S. A. (2009). Parametric characteristic analysis for generalized frequency response functions of nonlinear systems. *Circuits, Systems & Signal Processing, 28(5),* 699-733.

[43] Lang, Z. Q., & Billings, S. A. (1996). Output frequency characteristics of nonlinear systems. *International Journal of Control, 64(6),* 1049-1067.

[44] Wu, X., Lang, Z. Q., & Billings, S. A. (2006, December). Output frequencies of a class of nonlinear systems. *In Electronics, Circuits and Systems, 2006. ICECS'06. 13th IEEE International Conference on (pp. 744-747). IEEE.*

[45] Wu, X., Lang, Z. Q., & Billings, S. A. (2007). Analysis of output frequencies of nonlinear systems. *IEEE transactions on signal processing, 55(7),* 3239-3246.

[46] Wei, H. L., Lang, Z. Q., & Billings, S. A. (2007). An algorithm for determining the output frequency range of Volterra models with multiple inputs. *IEEE Transactions on Circuits and Systems II: Express Briefs, 54(6),* 532-536.

[47] Billings, S. A., & Li, L. M. (2000). Reconstruction of linear and non-linear continuous-time system models from input/output data using the kernel invariance algorithm. *Journal of sound and vibration, 233(5),* 877-896.

[48] Li, L. M., & Billings, S. A. (2001). Continuous time non-linear system identification in the frequency domain. *International Journal of Control, 74(11),* 1052-1061.

[49] Zhu, D., Billings, S. A., Balikhin, M., Wing, S., & Coca, D. (2006). Data derived continuous time model for the Dst dynamics. *Geophysical research letters, 33(4),* 1-11.

[50] Chatterjee, A., & Vyas, N. S. (2003). Non-linear parameter estimation with Volterra series using the method of recursive iteration through harmonic probing. *Journal of Sound and Vibration, 268(4),* 657-678.

[51] Chatterjee, A. (2010). Identification and parameter estimation of a bilinear oscillator using Volterra series with harmonic probing. *International Journal of Non-Linear Mechanics, 45(1),* 12-20.

[52] Jing, X. J., Lang, Z. Q., Billings, S. A., & Tomlinson, G. R. (2006). The parametric characteristic of frequency response functions for nonlinear systems. *International Journal of Control, 79(12),* 1552-1564.

[53] Jing, X. J., Lang, Z. Q., & Billings, S. A. (2008). Mapping from parametric characteristics to generalized frequency response functions of non-linear systems. *International Journal of Control, 81(7),* 1071-1088.

[54] Jing, X. J., Lang, Z. Q., & Billings, S. A. (2010). Output frequency properties of nonlinear systems. *International Journal of Non-Linear Mechanics, 45(7),* 681-690.

[55] Lang, Z. Q., & Billings, S. A. (2005). Energy transfer properties of non-linear systems in the frequency domain. *International Journal of Control, 78(5),* 345-362.

[56] Lang, Z. Q., Billings, S. A., Yue, R., & Li, J. (2007). Output frequency response function of nonlinear Volterra systems. *Automatica, 43(5),* 805-816.

[57] Nuij, P. W. J. M., Bosgra, O. H., & Steinbuch, M. (2006). Higher-order sinusoidal input describing functions for the analysis of non-linear systems with harmonic responses. *Mechanical Systems and Signal Processing, 20(8),* 1883-1904.

[58] Peng, Z. K., Lang, Z. Q., & Billings, S. A. (2007). Crack detection using nonlinear output frequency response functions. *Journal of Sound and Vibration, 301(3-5),* 777-788.

[59] Xia, X., Ni, W., & Sang, Y. (2017). A novel analysis method for fault diagnosis of hydro-turbine governing system. *Proceedings of the Institution of Mechanical Engineers, Part O: Journal of Risk and Reliability, 231(2),* 164-171.

[60] Peng, Z. K., Lang, Z. Q., & Billings, S. A. (2009). Analysis of locally nonlinear MDOF systems using nonlinear output frequency response functions. *Journal of Vibration and Acoustics, 131(5),* 051007.

[61] Zhao, X. Y., Lang, Z. Q., Park, G., Farrar, C. R., Todd, M. D., Mao, Z., & Worden, K. (2015). A new transmissibility analysis method for detection and location of damage via nonlinear features in mdof structural systems. IEEE/ASME transactions on mechatronics, 20(4), 1933-1947.

[62] Chu, F. L., Peng, Z. K., & Lang, Z. Q. (2008). An effective method for locating nonlinear components in periodic structures. *In Journal of Physics: Conference Series, 96 (1),* 12-16.

[63] Peng, Z. K., Lang, Z. Q., & Billings, S. A. (2007). Linear parameter estimation for multi-degree-of-freedom nonlinear systems using nonlinear output frequency-response functions. *Mechanical Systems and Signal Processing, 21(8),* 3108-3122.

[64] Peng, Z. K., Lang, Z. Q., & Billings, S. A. (2008). Nonlinear parameter estimation for multi-degree-of-freedom nonlinear systems using nonlinear output frequency-response functions. *Mechanical Systems and Signal Processing, 22(7),* 1582-1594.

[65] Feijoo, J. V., Worden, K., & Stanway, R. (2006). Analysis of time-invariant systems in the time and frequency domain by associated linear equations (ALEs). *Mechanical systems and signal processing, 20(4),* 896-919.

[66] Feijoo, J. V., Worden, K., & Stanway, R. (2004). System identification using associated linear equations. *Mechanical Systems and Signal Processing, 18(3),* 431-455.

[67] Zhang, H., Lang, Z. Q., & Zhu, Y. P. (2016, September). A comparative study on the evaluation of Nonlinear Output Frequency Response Functions (NOFRFs) of nonlinear systems. *In Automation and Computing (ICAC), 2016 22nd International Conference on (pp. 323-328).* IEEE.

[68] Bayma, R. S., & Lang, Z. Q. (2014). Fault diagnosis methodology based on nonlinear system modelling and frequency analysis. *IFAC Proceedings Volumes, 47(3),* 8278-8285.

[69] Guo, P. F., Lang, Z. Q., & Peng, Z. K. (2012). Analysis and design of the force and displacement transmissibility of nonlinear viscous damper based vibration isolation systems. *Nonlinear Dynamics, 67(4),* 2671-2687.

[70] Laalej, H., Lang, Z. Q., Daley, S., Zazas, I., Billings, S. A., & Tomlinson, G. R. (2012). Application of non-linear damping to vibration isolation: an experimental study. *Nonlinear Dynamics, 69(1-2),* 409-421.

[71] Rijlaarsdam, D., Nuij, P., Schoukens, J., & Steinbuch, M. (2011). Spectral analysis of block structured nonlinear systems and higher order sinusoidal input describing functions. *Automatica, 47(12),* 2684-2688.

[72] Rijlaarsdam, D., Nuij, P., Schoukens, J., & Steinbuch, M. (2012). Frequency domain based nonlinear feed forward control design for friction compensation. *Mechanical Systems and Signal Processing, 27(4),* 551-562.

[73] Rijlaarsdam, D. J., Setiadi, A. C., Nuij, P. W. J. M., Schoukens, J., & Steinbuch, M. (2013). Frequency domain‐based nonlinearity detection and compensation in Lur'e systems. *International Journal of Robust and Nonlinear Control, 23(10),* 1168-1182.

[74] Peng, Z. K., & Lang, Z. Q. (2008). The effects of nonlinearity on the output frequency response of a passive engine mount. *Journal of Sound and Vibration, 318(1-2),* 313-328.

[75] Lang, Z. Q., Jing, X. J., Billings, S. A., Tomlinson, G. R., & Peng, Z. K. (2009). Theoretical study of the effects of nonlinear viscous damping on vibration isolation of SDOF systems. *Journal of Sound and Vibration, 323(1-2),* 352-365.

[76] Peng, Z. K., Lang, Z. Q., Zhao, L., Billings, S. A., Tomlinson, G. R., & Guo, P. F. (2011). The force transmissibility of MDOF structures with a non-linear viscous damping device. *International Journal of Non-Linear Mechanics, 46(10),* 1305-1314.

[77] Lv, Q., & Yao, Z. (2015). Analysis of the effects of nonlinear viscous damping on vibration isolator. *Nonlinear Dynamics, 79(4),* 2325-2332.

[78] Jing, X. (2014). Nonlinear characteristic output spectrum for nonlinear analysis and design. *IEEE/ASME Transactions on Mechatronics, 19(1),* 171-183.

[79] Xiao, Z., & Jing, X. (2016). A Novel Characteristic Parameter Approach for Analysis and Design of Linear Components in Nonlinear Systems. *IEEE Trans. Signal Processing, 64(10),* 2528-2540.

[80] Xiao, Z., & Jing, X. (2016). Frequency-domain analysis and design of linear feedback of nonlinear systems and applications in vehicle suspensions. *IEEE/ASME transactions on mechatronics, 21(1),* 506-517.

[81] Pati, Y. C., Rezaiifar, R., & Krishnaprasad, P. S. (1993, November). Orthogonal matching pursuit: Recursive function approximation with applications to wavelet decomposition. In Proceedings of 27th Asilomar conference on signals, systems and computers (pp. 40-44). IEEE.

[82] Herzet, C., Drémeau, A., & Soussen, C. (2015). Relaxed recovery conditions for OMP/OLS by exploiting both coherence and decay. IEEE Transactions on Information Theory, 62(1), 459-470.

[83] Cui, M., & Prasad, S. (2016). Sparse representation-based classification: Orthogonal least squares or orthogonal matching pursuit?. Pattern Recognition Letters, 84, 120-126.

[84] Tropp, J. A. (2004). Greed is good: Algorithmic results for sparse approximation. IEEE Transactions on Information theory, 50(10), 2231-2242.

[85] Needell, D., & Tropp, J. A. (2010). CoSaMP: iterative signal recovery from incomplete and inaccurate samples. Communications of the ACM, 53(12), 93-100.

[86] Brunton, S. L., & Kutz, J. N. (2019). Data-driven science and engineering: Machine learning, dynamical systems, and control. Cambridge University Press.

[87] Casenave, C. (2011). Time-local formulation and identification of implicit Volterra models by use of diffusive representation. *Automatica, 47(10),* 2273-2278.

[88] Abbas, H. M., & Bayoumi, M. M. (2006). Volterra-system identification using adaptive real-coded genetic algorithm. *IEEE Transactions on Systems, Man, and Cybernetics-Part A: Systems and Humans, 36(4),* 671-684.

[89] Boaghe, O. M., & Billings, S. A. (2003). Subharmonic oscillation modeling and MISO Volterra series. *IEEE Transactions on Circuits and Systems I: Fundamental Theory and Applications, 50(7),* 877-884.

[90] Borys, A. (2010). Consideration of Volterra series with excitation and/or impulse responses in the form of Dirac Impulses. *IEEE Transactions on Circuits and Systems II: Express Briefs, 57(6),* 466-470.

[91] Gray, W. S., & Nabet, B. (1999). Volterra series analysis and synthesis of a neural network for velocity estimation. *IEEE Transactions on Systems, Man, and Cybernetics, Part B (Cybernetics), 29(2),* 190-197.

[92] Wang, X., & Mortazawi, A. (2016). Bandwidth Enhancement of RF Resonators Using Duffing Nonlinear Resonance for Wireless Power Applications. *IEEE Transactions on Microwave Theory and Techniques, 64(11),* 3695-3702.

[93] Peng, Z. K., Lang, Z. Q., Billings, S. A., & Tomlinson, G. R. (2008). Comparisons between harmonic balance and nonlinear output frequency response function in nonlinear system analysis. *Journal of Sound and Vibration, 311(1-2),* 56-73.

[94] Siu, T., & Schetzen, M. (1991). Convergence of Volterra series representation and BIBO stability of bilinear systems. *International journal of systems science, 22(12),* 2679-2684.

[95] Zhu, Y. P., & Lang, Z. Q. (2016). Analysis of output response of nonlinear systems using nonlinear output frequency response functions. *Control (CONTROL), 2016 UKACC 11th International Conference on (pp.1-6). IEEE,* 2016.

[96] Barrett, J. F. (1965). The Use of Volterra Series to Find Region of Stability of a Non-linear Differential Equation†. *International Journal of Control, 1(3),* 209-216.

[97] Tomlinson, G. R., Manson, G., & Lee, G. M. (1996). A simple criterion for establishing an upper limit to the harmonic excitation level of the Duffing oscillator using the Volterra series. *Journal of Sound and Vibration, 190(5),* 751-762.

[98] Chatterjee, A., & Vyas, N. S. (2000). Convergence analysis of Volterra series response of nonlinear systems subjected to harmonic excitation. *Journal of Sound and Vibration, 236(2),* 339-358.

[99] Li, L. M., & Billings, S. A. (2011). Analysis of nonlinear oscillators using Volterra series in the frequency domain. *Journal of Sound and Vibration, 330(2),* 337-355.

[100] Peng, Z. K., & Lang, Z. Q. (2007). On the convergence of the Volterra-series representation of the Duffing's oscillators subjected to harmonic excitations. *Journal of Sound and Vibration, 305(1),* 322-332.

[101] Hélie, T., & Laroche, B. (2011). Computation of convergence bounds for Volterra series of linear-analytic single-input systems. *IEEE Transactions on automatic control, 56(9),* 2062-2072.

[102] Xiao, Z., Jing, X., & Cheng, L. (2013). Parameterized convergence bounds for Volterra series expansion of NARX models. *IEEE Transactions on Signal Processing, 61(20),* 5026-5038.

[103] Xiao, Z., Jing, X., & Cheng, L. (2014). Estimation of parametric convergence bounds for Volterra series expansion of nonlinear systems. *Mechanical Systems and Signal Processing, 45(1),* 28-48.

[104] Jing, X., & Xiao, Z. (2017). On Convergence of Volterra Series Expansion of a Class of Nonlinear Systems. *Asian Journal of Control, 19(3),* 1–14.

[105] Schröck, J., Meurer, T., & Kugi, A. (2013). Motion planning for piezo-actuated flexible structures: Modeling, design, and experiment. *IEEE Transactions on Control Systems Technology, 21(3),* 807-819.

[106] Castanier, M. P., & Pierre, C. (2006). Modeling and analysis of mistuned bladed disk vibration: current status and emerging directions. *Journal of Propulsion and Power, 22(2),* 384-396.

[107] Chen, S., & Billings, S. A. (1989). Representations of non-linear systems: the NARMAX model. *International Journal of Control, 49(3),* 1013-1032.

[108] Bayma, R. S., Zhu, Y. P., & Lang, Z. (2018). The analysis of nonlinear systems in the frequency domain using

Nonlinear Output Frequency Response Functions. *Automatica*.

[109] Worden, K., Manson, G., & Tomlinson, G. R. (1997). A harmonic probing algorithm for the multi-input Volterra series. *Journal of Sound and Vibration, 201(1),* 67-84.

[110] Feijoo, J. V., Worden, K., & Stanway, R. (2005). Associated linear equations for Volterra operators. *Mechanical Systems and Signal Processing, 19(1),* 57-69.

[111] Jordan, D. W., & Smith, P. (2007). *Nonlinear ordinary differential equations*. Oxford Univ. Press, 153-154.

[112] Poularikas, A., 2000. *The Transforms and Applications: Handbook*. The Electrical Engineering Handbook Series. Taylor & Francis Group.

[113] Edwards, T. S. (2007). Effects of aliasing on numerical integration. *Mechanical systems and signal processing, 21(1),* 165-176.

[114] Swain, A. K., & Billings, S. A. (1998). Weighted complex orthogonal estimator for identifying linear and non-linear continuous time models from generalised frequency response functions. *Mechanical systems and signal processing, 12(2),* 269-292.

[115] Tang, B., & Brennan, M. J. (2012). A comparison of the effects of nonlinear damping on the free vibration of a single-degree-of-freedom system. *Journal of Vibration and Acoustics, 134(2),* 024501.

[116] Ma, H., Zeng, J., Lang, Z., Zhang, L., Guo, Y., & Wen, B. (2016). Analysis of the dynamic characteristics of a slant-cracked cantilever beam. *Mechanical Systems and Signal Processing, 75(1),* 261-279.

[117] Zeng, J., Ma, H., Zhang, W., & Wen, B. (2017). Dynamic characteristic analysis of cracked cantilever beams under different crack types. *Engineering Failure Analysis, 74(1),* 80-94.

[118] Zhang, W., Ma, H., Zeng, J., Wu, S., & Wen, B. (2017). Vibration responses analysis of an elastic-support cantilever beam with crack and offset boundary. *Mechanical Systems and Signal Processing*, *95(1)*, 205-218.

[119] Tehrani, M. G., & Elliott, S. J. (2014). Extending the dynamic range of an energy harvester using nonlinear damping. *Journal of Sound and Vibration*, *333(3),* 623-629.

[120] Boyd, S., & Vandenberghe, L. (2004). *Convex optimization*. Cambridge university press.

[121] Mickens, R. E. (2001). Analytical and numerical study of a non-standard finite difference scheme for the unplugged van der Pol equation. *Journal of sound and vibration*, *245(4),* 757-761.

[122] Maner, B. R., Doyle, F. J., Ogunnaike, B. A., & Pearson, R. K. (1996). Nonlinear model predictive control of a simulated multivariable polymerization reactor using second-order Volterra models. *Automatica, 32(9),* 1285-1301.

[123] Campello, R. J., Favier, G., & Do Amaral, W. C. (2004). Optimal expansions of discrete-time Volterra models using Laguerre functions. *Automatica, 40(5),* 815-822.

[124] Ibrahim, R. A. (2008). Recent advances in nonlinear passive vibration isolators. *Journal of sound and vibration, 314(3),* 371-452.

[125] Jing, X. J., Lang, Z. Q., & Billings, S. A. (2008). Output frequency response function-based analysis for nonlinear Volterra systems. *Mechanical systems and signal processing, 22(1),* 102-120.

[126] Ho, C., Lang, Z. Q., & Billings, S. A. (2014). Design of vibration isolators by exploiting the beneficial effects of stiffness and damping nonlinearities. *Journal of Sound and Vibration, 333(12),* 2489-2504.

[127] Zhu, Y., & Lang, Z. Q. (2017). Design of Nonlinear Systems in the Frequency Domain: An Output Frequency Response Function-Based Approach. *IEEE Transactions on Control Systems Technology*, 99(1), 1-11.

[128] Dan, M., & Kohiyama, M. (2013). System identification and control improvement of a semi-active-controlled base-isolated building using the records of the 2011 Great East Japan earthquake. *In 11th International Conference on Structural Safety and Reliability,* ICOSSAR 2013.

[129] Takewaki, I., & Tsujimoto, H. (2011). Scaling of design earthquake ground motions for tall buildings based on drift and input energy demands. *Earthquake and Structures, 2(2),* 171-187.

[130] Kar, I. N., Seto, K., & Doi, F. (2000). Multimode vibration control of a flexible structure using H/sub/spl infin//-based robust control. *IEEE/ASME transactions on Mechatronics, 5(1),* 23-31.

[131] Karnopp, D. (1990). Design principles for vibration control systems using semi-active dampers. *Journal of Dynamic Systems, Measurement, and Control, 112(3),* 448-455.

[132] Ho, C., Lang, Z. Q., Sapiński, B., & Billings, S. A. (2013). Vibration isolation using nonlinear damping implemented by a feedback-controlled MR damper. *Smart Materials and Structures, 22(10),* 105010.

[133] Sims, N. D., Stanway, R., Peel, D. J., Bullough, W. A., & Johnson, A. R. (1999). Controllable viscous damping: an experimental study of an electrorheological long-stroke damper under proportional feedback control. *Smart materials and structures, 8(5),* 601.

[134] Blanchini, F., Colaneri, P., Casagrande, D., Gardonio, P., & Miani, S. (2014). Switching gains for semiactive damping via nonconvex Lyapunov functions. *IEEE Transactions on Control Systems Technology, 22(2),* 721-728.

[135] Lang, Z. Q., Guo, P. F., & Takewaki, I. (2013). Output frequency response function based design of additional nonlinear viscous dampers for vibration control of multi-degree-of-freedom systems. *Journal of Sound and Vibration, 332(19),* 4461-4481.

[136] Miranda, E., & Reyes, C. J. (2002). Approximate lateral drift demands in multistory buildings with nonuniform stiffness. *Journal of Structural Engineering, 128(7),* 840-849.

[137] Ho, C., Lang, Z. Q., & Billings, S. A. (2014). A frequency domain analysis of the effects of nonlinear damping on the Duffing equation. *Mechanical Systems and Signal Processing, 45(1),* 49-67.

[138] Yu, M., Dong, X. M., Choi, S. B., & Liao, C. R. (2009). Human simulated intelligent control of vehicle suspension system with MR dampers. *Journal of Sound and Vibration, 319(3-5),* 753-767.

[139] Zhu, W. Q., Luo, M., & Dong, L. (2004). Semi-active control of wind excited building structures using MR/ER dampers. *Probabilistic engineering mechanics, 19(3),* 279-285.

[140] Fujita, K., Miura, T., Tsuji, M., & Takewaki, I. (2016). Experimental study on influence of hardening of isolator in multiple isolation building. *Frontiers in Built Environment, 2(1),* 12.

[141] Eem, S. H., Jung, H. J., & Koo, J. H. (2013). Seismic performance evaluation of an MR elastomer-based smart base

isolation system using real-time hybrid simulation. *Smart Materials and Structures, 22(5),* 055003.

[142] Christenson, R. E., Spencer Jr, B. F., Hori, N., & Seto, K. (2003). Coupled building control using acceleration feedback. *Computer-Aided Civil and Infrastructure Engineering, 18(1),* 4-18.

[143] Lang, Z. Q., Guo, P. F., & Takewaki, I. (2013). Output frequency response function based design of additional nonlinear viscous dampers for vibration control of multi-degree-of-freedom systems. *Journal of Sound and Vibration, 332(19),* 4461-4481.

[144] Guo, P. (2012). *Damping System Designs using Nonlinear Frequency Analysis Approach* (Doctoral dissertation, University of Sheffield).

[145] Chae, Y. (2011). *Seismic hazard mitigation of building structures using magneto-rheological dampers.* Lehigh University.